NORTHWESTERN UNIVERSITY

Comparison of Measured Crack Response in Diverse Structures to Dynamic Events and Weather Phenomena

A Thesis

Submitted to the Graduate School
In Partial Fulfillment of the Requirements

For the Degree

MASTER OF SCIENCE

Field of Civil Engineering

By

Laureen M. McKenna

EVANSTON, IL

March 2002

ACKNOWLEDGEMENTS

This thesis is mainly a result of the collaboration of several people, whom I would like to acknowledge. I would like to thank my advisor, Dr. Charles Dowding, who has offered his continuing guidance and expertise, and served as the main force in orchestrating this collaboration. Thank you to Dr. Cathy Aimone-Martin and Mary Alena Martell of New Mexico Institute of Mining and Technology for allowing me to utilize the data they collected for the Office of Surface Mining Comparative study of atypical structure response to surface coal mine blasting. I also would like to thank Dr. Aimone-Martin for arranging my company at two of the eleven sites evaluated. Thank you to Ken Eltschlager of the Office of Surface Mining for allowing Northwestern permission to do a complimentary study to Aimone-Martin's.

I would also like to thank the Infrastructure Technology Institute at Northwestern University for continuing funding of the Autonomous Crack Monitoring study. I would especially like to recognize Dan Marron, Dave Kosnik, and Cristin Dziekonski for their hard work and support on the electronic and programming side of the ACM project. Good luck to Mickey Snider who will take over the project as part of his Master's thesis.

Additionally, I would like to thank Dr. Richard Finno, Dr. Howard Reeves, and again Dr. Charles Dowding and Dr. Cathy Aimone-Martin, for their teaching and support during the year and a half I have been at Northwestern. I also would like to thank all of my fellow graduate students in the geotechnical engineering department for their advice, support, and friendship. Special thanks are extended to Jill Roboski and Katie Wierman for their friendship and endless encouragement over the last year and a half. I wish them luck in their ongoing pursuit for doctoral degrees.

Last, but not least, I want to thank my family for their love and support. Without their constant encouragement, I would not be where I am today. Thank you especially to my parents for believing in me and understanding my desire to explore the world.

ABSTRACT

This thesis consists of the data and analysis of structural responses for two different studies: the Office of Surface Mining (OSM) study of the velocity response of "atypical" residential structures and the Autonomous Crack Monitoring (ACM) study. The main basis of this thesis was to do additional analysis on a select four "atypical" structures instrumented during the OSM study conducted by Dr. Cathy Aimone-Martin at New Mexico Tech. In addition, crack response between these four structures and three ACM structures was compared in order to further expand the study of crack response on structures due to long term environmental phenomena and dynamic events.

The four OSM structures were instrumented with crack displacement sensors, in addition to the standard velocity transducers employed for the entire OSM study, in order to compare measured and predicted response of crack displacement for long term and dynamic events. Chapters 2 through 6 present the data and results associated with these comparisons. In Chapters 7 and 8, additional analyses conducted on two of the three ACM structures is presented. Chapter 7 describes the improved monitoring system of one of the ACM structures, were two different displacement sensors were instrumented and their responses compared. Chapter 8, describes the second ACM structure included in this thesis, which was instrumented in June of 2001. The third ACM structure is not discussed individually in this thesis; further details can be found in Seibert 2000. Finally, Chapter 9 provides a synthesis of the data with a comparison of all responses, in order to identify any common responses among the seven structures.

TABLE OF CONTENTS

TABLE OF CONTENTS (cont.)

TABLE OF CONTENTS (cont.)

LIST OF FIGURES

LIST OF FIGURES (cont.)

LIST OF FIGURES (cont.)

LIST OF FIGURES (cont.)

LIST OF FIGURES (cont.)

LIST OF TABLES

CHAPTER 1

INTRODUCTION

This thesis synthesizes the data and analyses of structural and crack response of seven different structures from two different studies: the Office of Surface Mining (OSM) "Comparative Study of the Structure Response to Coal Mine blasting – Non-traditional Residential Structure" and the Autonomous Crack Monitoring (ACM) study. The objective of the OSM study was to measure the structure response of atypical structures to surface coal mine, blast-induced, ground motions and air vibrations. Velocity transducers were installed to measure whole structure and midwall response in 33 structures at 11 sites. As part of a continuing effort to predict trends in the crack response of various structures, this thesis presents crack response to long term (weather and environmental) and short term (transient) effects of 4 of the 11 OSM structures. Displacements calcuated from the structures' motion response were compared to the crack displacements measured by these displacement sensors, in order to evaluate any correlations between the estimated and measured values.

The objective of the ongoing Autonomous Crack Monitoring (ACM) study is to compare crack changes produced by short term blasting or construction vibrations with those produced by long-term environmental effects (such as temperature and humidity) in an easy to understand fashion. The ACM study consists of 3 structures, at 3 different locations that are instrumented to

monitor crack response and ground. Data collected at these sites are remotely accessed via a phone line and converted accordingly to display over the internet.

This thesis, which presents and compares the crack response of seven, is organized into 10 chapters and four appendices. Chapter 2 presents typical response velocity OSM instrumentation and introduces crack response instrumentation with furrther detail described in each individual chapter. Chapters 3 through 6 presents the data and analyses associated with the 4 OSM structures, in chronological order of monitoring. Each chapter includes the following:

- description of the structure and the location of instrumentation,
- summary of measurements recorded for each blast detected during the respective monitoring periods and a representative comparison of time histories for at least one of the observed blasts,
- determination of dominant/natural frequencies of the structure,
- crack response to environmental long-term effects,
- crack response to household activities, where measured, and
- comparison of calculated displacements with measured crack displacements.

Chapters 7 through 8 present measurements from two of the three ACM structures. The structure in Chapter 7 was most similar to the those in the OSM study as it was subjected to ground motions from quarry blasting. Crack responses were measured with two different sensors at this structure. The structure in Chapter 8, and the third ACM structure mentioned in Chapter 9, involved measurements of crack response only to long term, weather and occupant events. A synthesis of the responses measured at all seven structures is presented in Chapter 9. Chapter 10 provides a summary of the study and conclusions. The three appendices contain figures and tables that support the data presented in this thesis.

CHAPTER 2

INSTRUMENTATION

This thesis presents crack response data collected in conjunction with the Office of Surface Mining (OSM) study of the velocity response of "atypical" residential structures, and Autonomous Crack Monitoring (ACM) studies. Measurement of ground, structural, and wall response with velocity transducers allows comparison of standard velocity–based calculation estimates with the measured crack response. Responses of three of the four OSM structures were measured during a three-day to one-week period, which is relatively short compared to the months to a year observational periods for other Autonomous Crack Monitoring (ACM) studies. The fourth OSM structure (in New Mexico) was monitored over a period of several weeks, which allowed measurement of response to an extreme weather event. Velocity transducers were not employed at any of the ACM structures, therefore, comparisons with velocity-based estimations of structural response were not feasible. This chapter includes descriptions of instrumentation, which were typically the same at all of the OSM sites. Differences in instrumentation found at the ACM structures are described in each structure's respective chapter.

Instrumentation

This chapter describes the common instruments employed to measure structural and wall response, as well as crack response. Emphasis is placed on the crack response instrumentation since velocity instrumentation for structural response is described in greater detail in Volume I of Aimone-Martin (2002). Instruments can be divided into three main categories based on the following measurements: 1) structural response using velocity transducers, 2) crack response using eddy current sensors, and 3) environmental changes using a dual temperature and humidity sensor.

Configuration of Velocity transducers

All four structures from the OSM study were fitted with velocity transducers to measure structural responses and were arrayed in the same basic configuration illustrated in Figure 2.1. (Outdoor velocity transducers are not included in this illustration, but were located at the same corner of the house outside, with the seismograph contained in a sealed container.) Two basic measurements were provided by the velocity transducers- ground excitation and structural response. Deployment for each will be discussed separately.

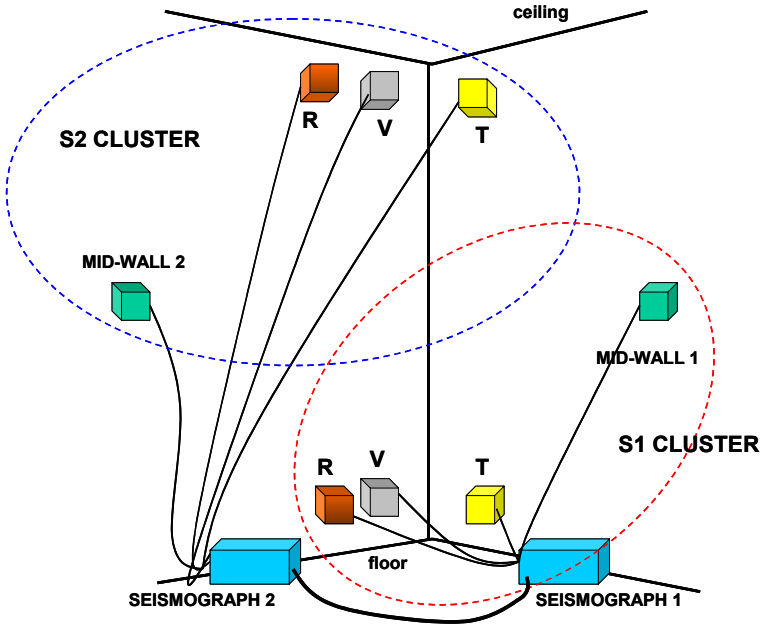

Figure 2.1 Typical indoor velocity transducer and seismograph set-up

Excitation ground motions were measured with standard three-axis Larcor velocity geophones in the radial (R), transverse (T), and vertical (V) directions. These excitation geophones were typically placed within three to ten feet of the structure corner and buried approximately 4 to 6 inches in the ground. In all cases, except the bungalow in Indiana (House 1), the arrow on the geophone, which indicates the radial direction pointed away from the blast, but along the long axis of the structure. At the bungalow in Indiana, the arrow pointed along the long axis of the structure, but towards the blast. The Larcor seismograph geophones report the first arriving radial component of ground motion as positive if moving in the direction of the arrow on the geophone cylinder. For other axes, positive motions are downward for the vertical and to the right (looking in the direction of the arrow).

A standard, Larcor seismograph air blast transducer was installed outside, adjacent to the three-axis ground geophones, attached three feet above the ground and pointed toward the location of blasting. The seismograph provided a resolution of 0.005 ips for ground motion and 0.02 millibars for the air overpressure. (For the first five blasts at the New Mexico structure, the ground motion time histories were twice as large, because the resolution on the machine was set incorrectly.) The seismograph, for all cases, was configured so that any ground motion equal to or greater than 0.02 ips, on any axis, would trigger data collection of excitation and response motions. The seismograph was further configured to record for the allotted time period defined for each structure (7 to 12 seconds), starting with the 0.5 seconds of ground motion that occurred before the seismograph was triggered.

Response motions were measured at the structure interior corners corresponding with the exterior three-axis geophones as shown in Figure 2.1, using two seismographs, each with four single axis velocity transducers. Each seismograph, S1 and S2, serviced three single-axis velocity transducers installed at the bottom and top corners of the structure and installed in the middle of the adjacent walls. Figure 2.2 shows a typical S1 cluster at the lower corner and Figure 2.3 shows a typical S2 cluster at the top corner. Of the three single axis transducers installed in the corners, one detected motion in the vertical direction (V), and two detected motion in the horizontal direction (R and T). Of the remaining midwall transducers, one was placed on the transverse wall, therefore detecting radial motion, and the other was placed on the radial wall, therefore detecting transverse motion.

Figure 2.2 Typical S1 cluster of transducers in the lower corner with S1 and S2 seismographs

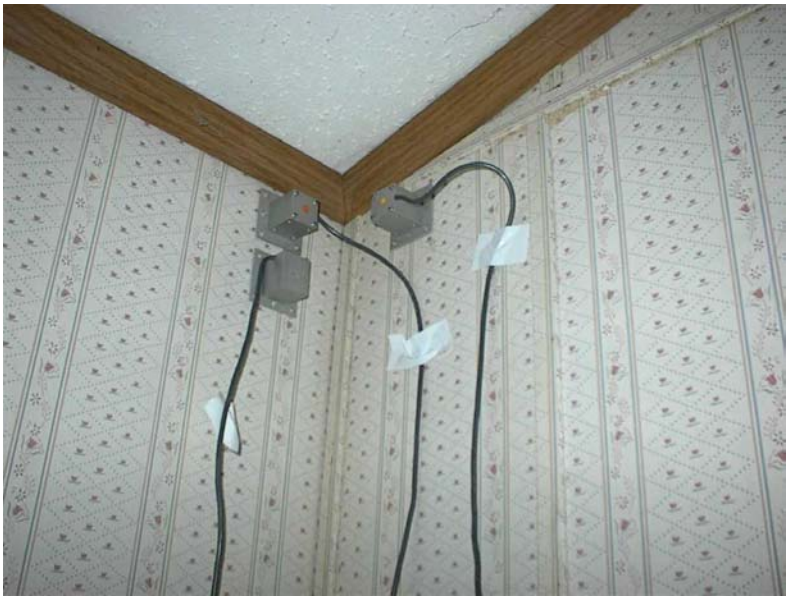

Figure 2.3 Upper corner velocity transducers connected to the S2 seismograph

All seismographs were connected with a common trigger cable. The interior seismographs were set on manual mode. When the exterior seismograph triggered an event, all three recording units turned on. The excitation threshold used at all sites was set to 0.2 ips (0.5 mm/sec), therefore, whenever the ground geophone detected this level of motion, the whole system was set to record a prescribed length of data. Data files for all three seismographs

contained 4 channels. The four channels on the exterior seismograph, G, were air pressure and radial, vertical, and transverse ground motion, corresponding to the acoustical, vertical, radial, and transverse labels, respectively, in the data files. The four channels on the S1 and S2 seismograph were vertical and radial motion of the structure, transverse or radial motion detected from the midwall, and transverse motion of the structure, which correspond with the acoustical, vertical, radial, and transverse labels, respectively, in the data files.

Concept of Comparative Crack Displacement

Crack displacements of typical wall cracks were measured using displacement sensors. The change in an existing crack width in response to structure motions is illustrated in Figure 2.4. The total crack width itself is not actually measured, but rather the change (or variation) in crack width. The change in crack width is hereafter referred to as the crack displacement. By measuring the crack displacement instead of the crack width, it is possible to install the sensor without disturbing the crack itself during installation and monitoring. Further details of this concept are available in Dowding and Seibert (2000) and at http://www.iti.northwestern.edu/acm.

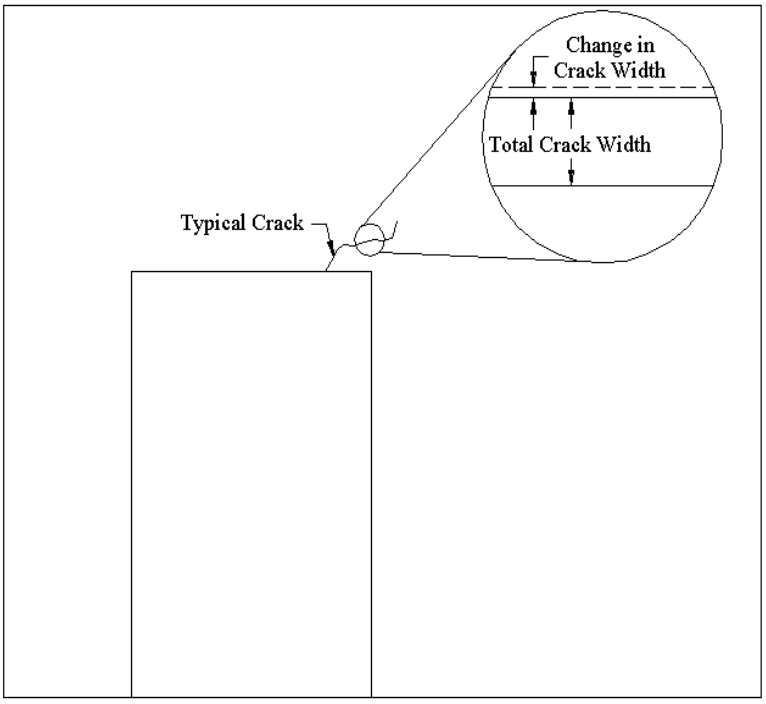

Figure 2.4 Definition of crack displacement (Siebert, 2000)

Changes in crack width occurred from many different phenomena that include both long-term (environmental) effects and short-term (dynamic or vibration) effects. As with the ACM studies, both long-term and short-term effects were measured simultaneously with the system deployed during this study. The instrumentation system for crack displacement measurement was linked with the triggering exterior seismograph so that measurements of crack responses were recorded simultaneously with structure and ground motions. In addition, crack displacement measurements were obtained on an hourly basis in order to monitor the long-term movement of the cracks.

The concept of measuring crack displacements from both long-term and short-term effects with the same sensor is not dependent on the type of sensor. (Dowding and Seibert, 2000) Therefore, any number of sensor types can be employed. To date, two have been employed in the typical ACM studies; an eddy current proximity sensor (Kaman SMU9000 2U), and a Linear Variable Differential Transformer (LVDT DC 750 Series) sensor. These transducers have differing attributes as described in Siebert (2000). However, only Kaman transducers were employed in the OSM study.

Measurement of long-term crack displacements may involve long-term drift and temperature responses. In order to track such effects, a sensor (the null) can be affixed to a non-cracked section of the wall. The response of the null sensor can then be subtracted from the crack sensor response in order to obtain the true crack displacement. This concept is described further in Siebert (2000) and Dowding and Seibert (2000). Additional study has shown that null sensor response is typically small. (Louis 2001) A null sensor was employed in two of the four OSM study structures for verification.

Instrumentation for Measurement of Crack Response

Data Acquisition System

The Data Acquisition System (DAS) in the OSM study, employed to record crack response, was similar to the Somat platform that was employed by Seibert (2000) and Louis (2000) in the ACM studies - the Somat 2100 Field Computer System which contained three signal-conditioning modules and three filter modules. A sampling rate of the system was 1000 samples per second was used. Two signal-conditioning layers, 12-bit analog to digital converters

(A/D), were designated for the crack displacement sensors. A third signal-conditioning layer, an 8-bit A/D converter, was designated to receive the trigger signal from the exterior seismograph. Time histories of vibratory crack response were the same length as those for the structural and ground motions. The pre-trigger recording time ranged from 0.1 to 0.5 seconds.

The DAS was also configured to record long-term crack measurements in addition to measurements during dynamic events. During the monitoring period, the DAS would record a single "burst" ($1/1000^{th}$ of a second) sample every hour during a running test. As a result, the single crack displacement measurements from these "hourly" readings generated long-term crack displacement time histories.

To download the recorded data, a field computer loaded with the Somat Test Control Software for Windows (WinTCS v2.0.1 software), was connected to the DAS and data was retrieved either daily or weekly during the monitoring period.

Crack Displacement Sensors

Kaman Displacement Measurement Sensor

The Kaman SMU-9000 2U, single channel, displacement measurement sensor is shown in Figure 2.5.

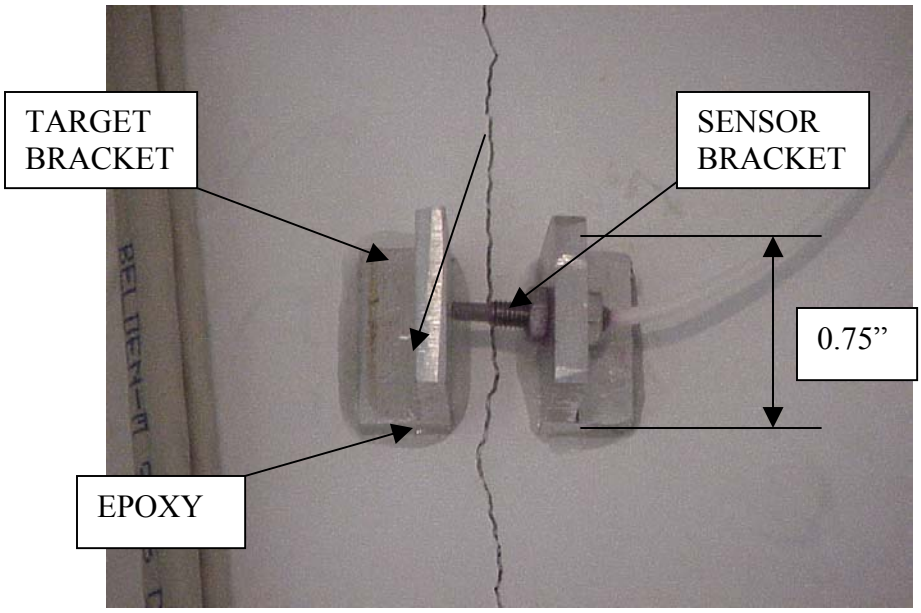

Figure 2.5 Kaman SMU-9000 2U eddy current displacement measuring sensor mounted across crack on an aluminum anchor block

The 9000 2U sensor has a displacement range of 20 mils (0.02 inches, or 508 micrometers), with a voltage range of 5 volts. According to the manufacturer, the sensor has a resolution of 0.1 micrometers and a frequency response of 10,000 Hertz. Each sensor is independently calibrated to convert from voltage to mils (0.001 inches).

The Kaman gauge senses changes in an eddy current, produced by changes in the distance between the sensor and the target. Two aluminum brackets are epoxyed on either side of the crack, at a distance of 0.25 in. (6 mm) apart. One of the brackets supports the sensor, and the other serves as the target for the eddy current produced by the sensor. The initial distance between the target and the sensor is set to approximately 10 mils (0.254 mm). The sensor is connected to the DAS and is powered by a separate 15-volt DC power supply.

LVDT Displacement Measurement Sensor

LVDTs (or Linear Variable Differential Transformers) have also been employed, in ACM studies. The sensors employed to date were the DC 750-050 and DC 750-125 LVDTs produced by MacroSensors. The 050's have a displacement range of ± 1.3 millimeters (± 3.17 millimeters for the 125's) with a voltage range of ±10 volts. Each sensor is deployed in the same configuration. The manufacturer does not give the sensor resolution or frequency response. However, the calculated resolution for the sensor based on an A/D converter system is 0.6 micrometers per A/D unit. The system used for these studies relies on A/D converters, therefore, 0.5 micrometers is the minimum resolution that the sensor is capable of producing with such a system. Each sensor has a constant factor to convert from voltage to displacement. The conversion factor for the 050 is 7.87 volts/millimeter and that for the 125 is 3.15 volts/millimeter. A photo of the 050 is shown in Figure 2.6. The body of the LVDT cannot be seen in this Figure directly because it is contained within an aluminum casing for mounting purposes (Seibert 2000).

A schematic drawing of the DC 750 Series LVDT is shown as Figure 2.7. The LVDT consists of two parts: a moveable magnetic core that is threaded onto a stainless steel screw and attached to the aluminum bracket; and a circular body with an cylindrical inner opening in which the core is able to translate parallel to the cylindrical axis. The core is centered within the body of the sensor, without contact, and moves relative to the body. This relative displacement

changes the magnetic field in the core, which in turn changes the output voltage. As with the Kaman gauge, the LVDT is connected to the DAS, and has its own 15-volt DC power supply.

Figure 2.6 LVDT displacement measurement sensor

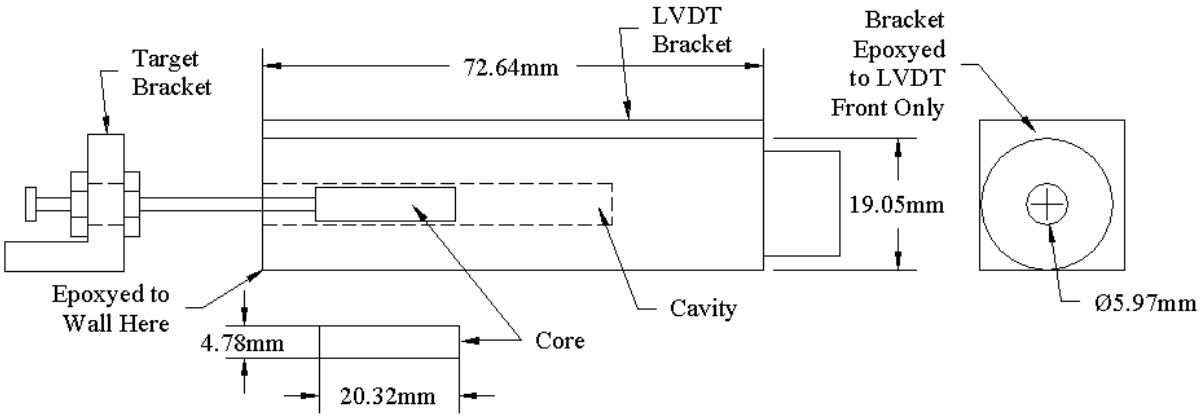

Figure 2.7 Schematic of DC 750 series LVDTs

Site specific considerations

In two of the OSM study structures, the one in Pennsylvania and New Mexico, only one Kaman sensor was employed. At the two sites in Indiana, two Kaman sensors were employed. One sensor was placed over a crack, while the other (the null) spanned an un-cracked surface area near the instrumented crack. At least two LVDTs were installed at all three of the ACM

study structures. In the Wisconsin structure, two Kaman sensors and two LVDT sensors were employed.

System resolutions are governed by either A/D resolution or sensor resolution; however, in these cases the two were similar. The sensor resolution for the Kaman sensor was 0.1 micrometers, while none was provided for the LVDT sensor. Since the dynamic response of the LVDT is similar to that of the Kaman, as shown in Chapter 7, it was assumed to be equal to that of the Kaman. A/D resolutions of all Kaman systems (OSM and Wisconsin) were between 0.065 and 0.083 micrometers/A/D division. For LVDTs, it was 0.62 for Minnesota (because the voltage range was set high) and 0.099 for Illinois. A/D resolution is the voltage range times the given conversion factor (micrometers/volts) divided by the A/D conversion rate (divisions/range or 2^{12} in all cases).

Measurement of Temperature and Humidity

A Supco DataLogger Temperature and Humidity (DLTH) sensor, shown as Figure 2.8, was used to record temperature and humidity every 10 minutes. At the Pennsylvania site and one of the houses in Indiana, the datalogger was installed indoors, and at New Mexico site and the other Indiana house, the datalogger was installed outdoors. Data were retrieved from the sensor by directly downloading the files from the sensor with the Supco software. These long-term weather data were then compared with the long-term crack response.

Figure 2.8 Supco temperature and humidity data logger

CHAPTER 3

DOUBLE-WIDE TRAILER - PENNSYLVANIA

The Pennsylvania structure, shown in Figure 3.1, is a double-wide trailer located approximately 1400 feet from surface coal mining in Kittanning, Pennsylvania. Data collected on-site from 19 to 24 May 2001 are summarized in Table 3.1. Four blasts with maximum charge weights/delay between 486 and 612 lbs (221 and 278 kg) produced ground motions of 0.07 to 0.32 inches per second (ips) (1.78 to 8.13 mm/sec), maximum structure responses of 0.19 to 0.42 ips (4.83 to 10.67 mm/sec), and maximum wall responses of 0.27 to 1.08 ips (6.86 to 27.43 mm/sec). In addition, a number of household activities were simulated in order to obtain comparative structure and crack responses. Weather data varied cyclically each day with inside temperatures ranging between 68 and 81 °F (20 to 27 °C) to and inside humidity ranging between 40 and 58%.

Figure 3.1 Pennsylvania double-wide trailer

Table 3.1 Summary of structural and crack response for Pennsylvania double-wide trailer

Time of blast	Distance (ft)	Charge Weight/ Delay (lb)	Scaled Distance ($ft/lb^{1/2}$)	Peak Particle Velocity (ips)			Structure response in S1 cluster (ips)		Structure response in S2 cluster (ips)		Midwall responses (ips)		Air Blast (dB)	Measured Crack Displacement above arch in kitchen (μin)
				Vertical	Radial	Transverse	Radial	Transverse	Radial	Transverse	Radial	Transverse		
5/22/2001 10:38	1437	612	58.1	0.07	0.24	0.14	0.31	0.11	0.42	0.20	0.98	0.27	117	36
5/22/2001 12:16	1458	486	66.1	0.10	0.19	0.24	0.22	0.13	0.30	0.30	0.90	0.45	119	31
5/23/2001 14:19	1483	612	59.9	0.07	0.32	0.17	0.33	0.14	0.27	0.21	0.47	0.36	119	36
5/24/2001 10:51	1390	504	61.9	0.12	0.20	0.17	0.22	0.09	0.19	0.20	1.08	0.54	122	27

Structure Description

Plan and elevation drawings are shown for the Pennsylvania double-wide trailer in Figures 3.2 and 3.3. The structure is approximately 24 feet wide and 48 feet long (7.3 x 14.6 m), seven feet (2.1 m) in height, with a basement space approximately ten feet (3 m) in height. The exterior of the structure is covered with vinyl siding. The interior walls are four inches thick (102 mm) and are paneled or covered with wallpaper. The interior "marriage" wall along the long axis of the structure is constructed of wood studs and gypsum drywall. This dividing wall, shown in Figure 3.2, is the only wall in which a crack was found upon preblast inspection.

Basement photographs given in Figure 3.4, show standard-sized, concrete masonry blocks and a concrete slab floor. As shown in Figure 3.4a, metal posts, spaced 12 feet (3.7 m) apart, connected to a central ceiling beam, provide support along the radial axis of the structure; while steel floor joists, shown in Figure 3.4b, support the structure along the transverse axis of the structure.

As shown in Figure 3.4c, a portion of the trailer floor beam has been removed. The location of this cut out is near the stairway to the basement, which is located near the bathroom. As shown in Figure 3.3, this area is near the crack in the center wall. It appears as though the pipe post to the left of the cut was installed to support the load carried by the severed beam. When structural elements are altered, adverse effects (such as differential settlement, cracks, etc.) are likely. The crack studied in this structure may be related in some way to the alteration of the foundation system.

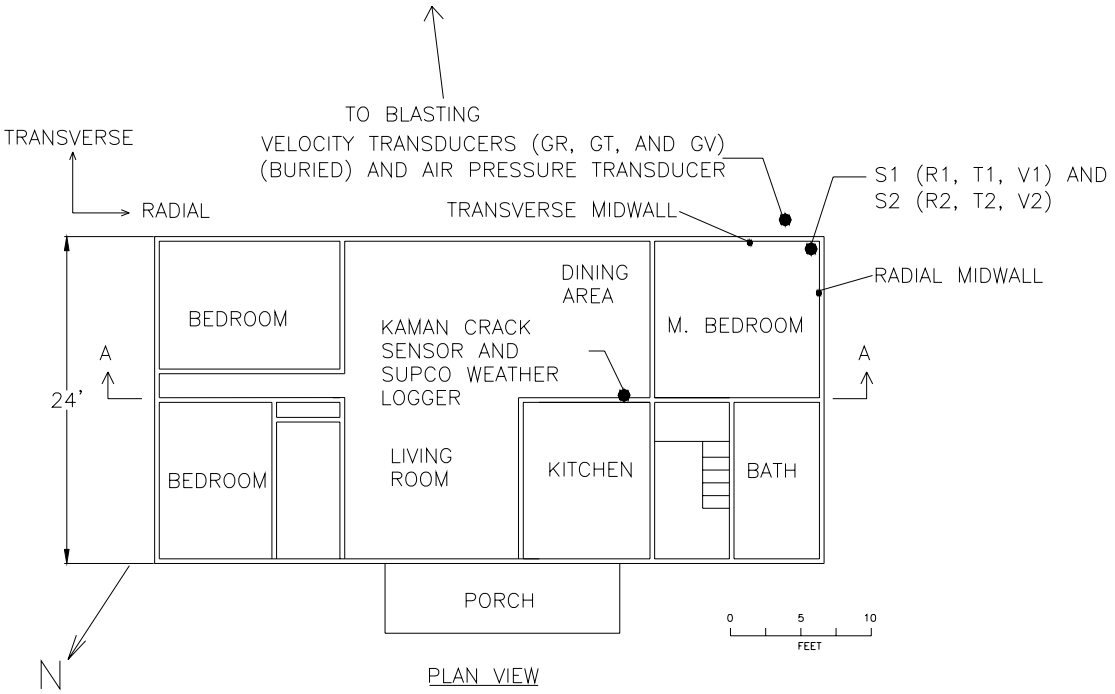

Figure 3.2 Plan view of the Pennsylvania trailer

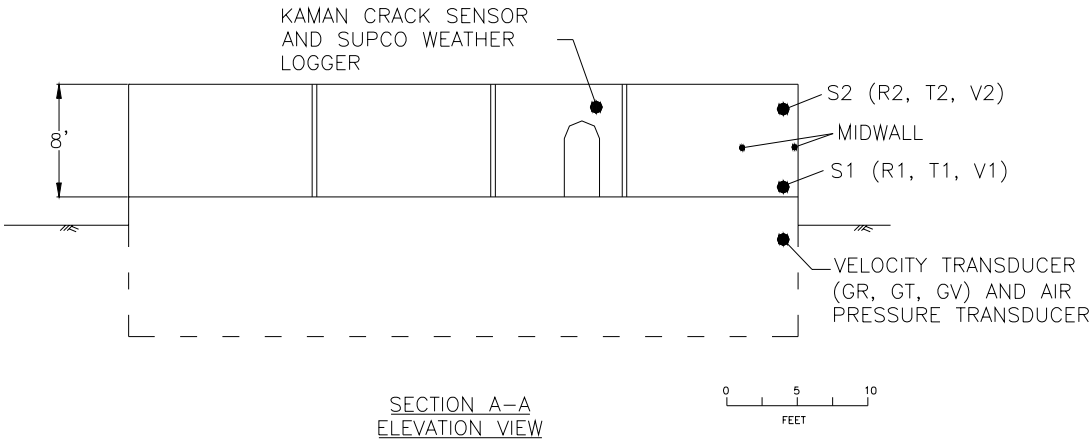

Figure 3.3 Elevation view of the Pennsylvania trailer

(a) Central ceiling beam spanning in the radial direction

(b) Steel floor joists in transverse direction

(c) Area of trailer floor beam with portion removed from stairway

Figure 3.4 Basement of double-wide trailer

Location of instrumentation

Locations of all instruments are shown in Figures 3.2 and 3.3. Eleven velocity transducers were installed on and outside of the southwest corner of the structure, closest to the mining activity. The crack displacement sensor was located above the archway of the interior wall in the kitchen of the structure, as shown in Figure 3.5. Further details on placement and description are given in Chapter 2.

Figure 3.5 shows the wall with the Kaman crack displacement sensor and the Supco temperature and humidity datalogger. The crack monitored is located approximately six inches (152 mm) from the ceiling and is vertically oriented as shown by the magnified inset in Figure 3.5. Its width was estimated from photographs to be approximately 700 micrometers (27,700 μin).

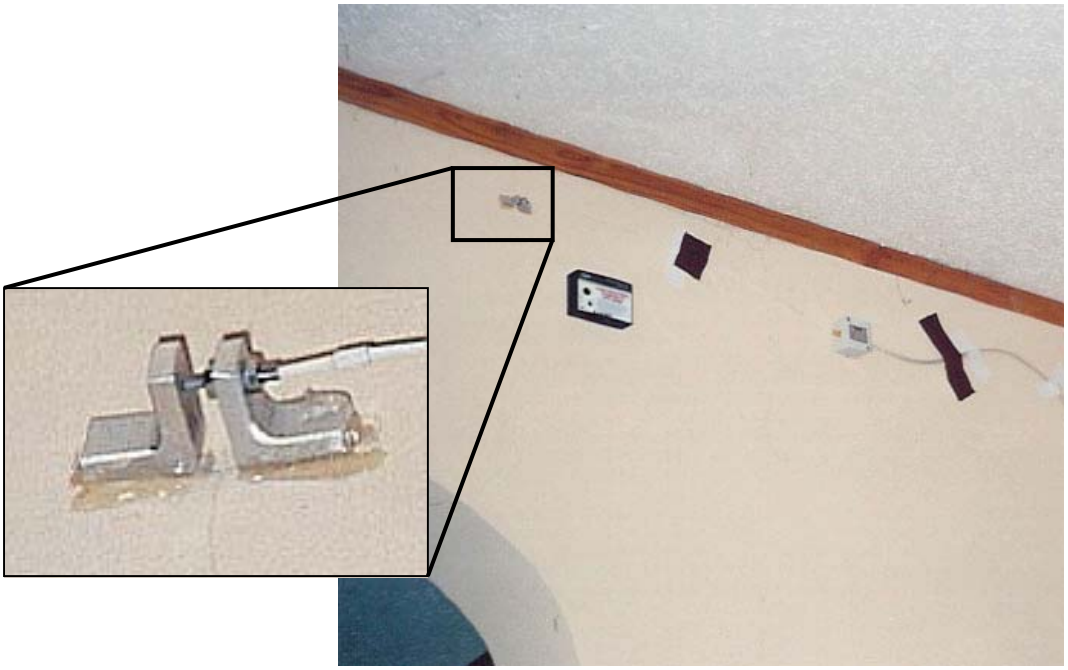

Figure 3.5 Kaman crack displacement sensor and Supco weather logger

For each blast, time histories were recorded for a total of 6.5 seconds. Time correlated (within 1/1000 second) time histories of dynamic crack displacement were also collected from the Kaman sensor for five seconds.

Transient Responses

Figure 3.6 shows radial velocity time histories of excitation ground motions and structure response, as well as crack response, associated with the blast on 22 May 2001 at 10:38. This blast was typical of the four blast events that were observed during the monitoring period. The top graph shows crack displacement, followed by the ground excitation, and the lower, S1, and upper, S2, structure corner response. The difference of the integrated lower and upper velocity responses follows, and is labeled as S1-S2 (R). This difference of integrated time histories represents an estimated relative displacement time history for the structure. Finally, the air blast response, in millibars, is shown. This blast produced a peak crack displacement of 0.91 μm (36.0 μin) and a peak ground motion, parallel to the wall direction, of 0.24 ips (6.1 mm/sec).

The radial responses shown are parallel to the plane of the wall containing the crack. Thus, they can be employed to predict displacements (or strain) and compare to the measured crack displacements.

In Figure 3.7, the time histories of all three components of ground motion (R, T, and V) along with the air blast response are compared to the crack response. In addition, the upper corner responses (S2) of the structure, both radial and transverse, are also shown. All time histories have a common time base. All significant structural response, including that from the air blast, occurred within the first three seconds.

As mentioned previously, structure response was used in order to compute relative displacements from transient events. To do this, in some instances, it is necessary to estimate a dominant frequency of the structure. Ground motions of a certain dominant frequency typically do not exhibit the same relative displacements in structures of differing dominant frequencies. (Dowding 1996) The dominant frequency of the structure was estimated two ways: 1) the zero-point-crossing frequency determination method and 2) Fourier Frequency Spectra (Dowding 1996). Where free response occurred, as shown in Figure 3.8, the zero-crossing method was employed on the S2 time histories. The inverse of twice the time between successive zero-crossings resulted in an estimated dominant/natural frequency of the structure. Estimations of dominant frequencies calculated from the S2 time histories (in both R and T directions) were averaged, therefore, giving the structure an estimated natural frequency of 8 Hz.

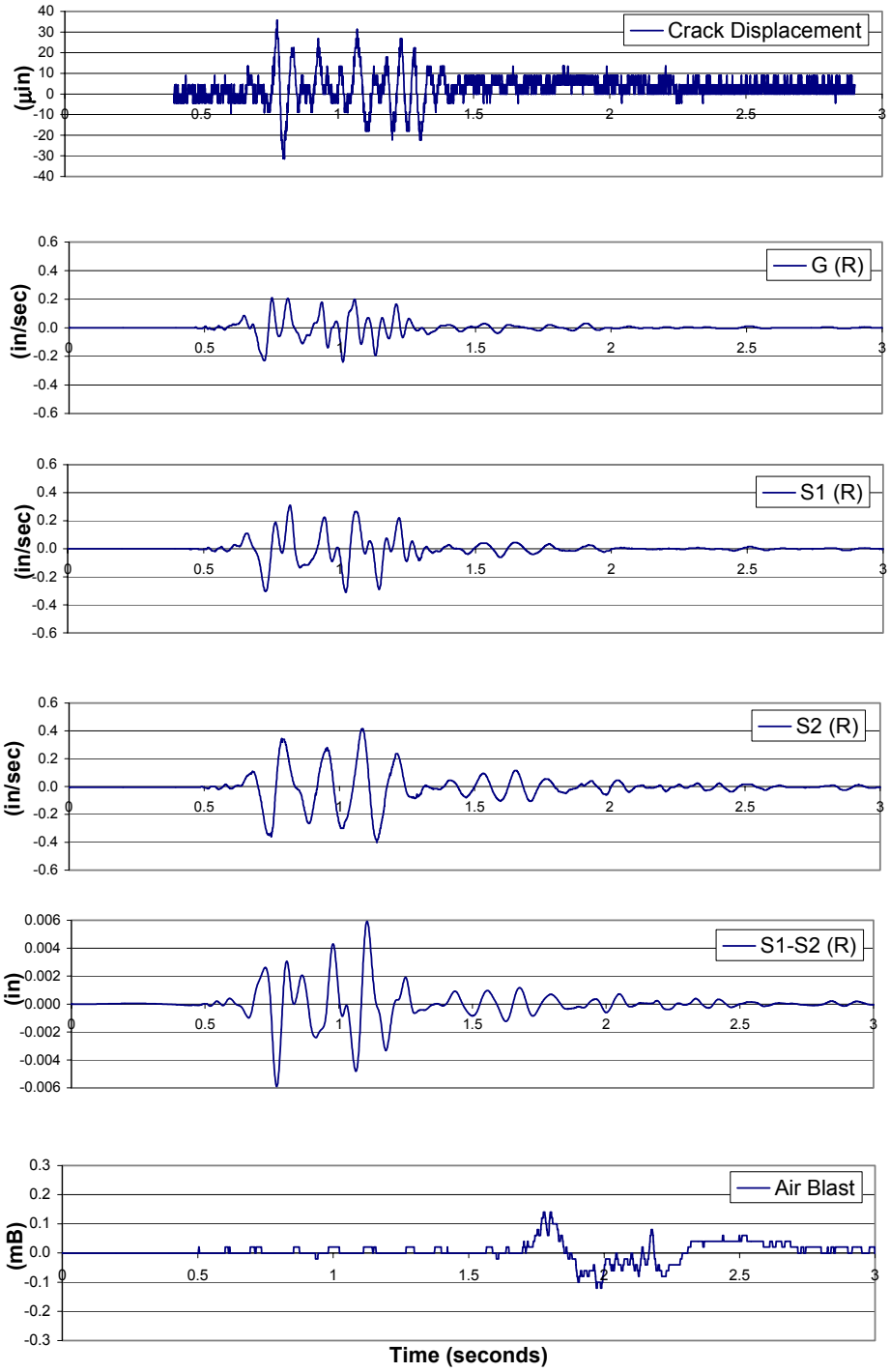

Figure 3.6 Time history of crack displacement on 22 May at 10:38 compared to ground excitation, S1 and S2 response, calculated relative displacement of structure (R1-R2), and air blast

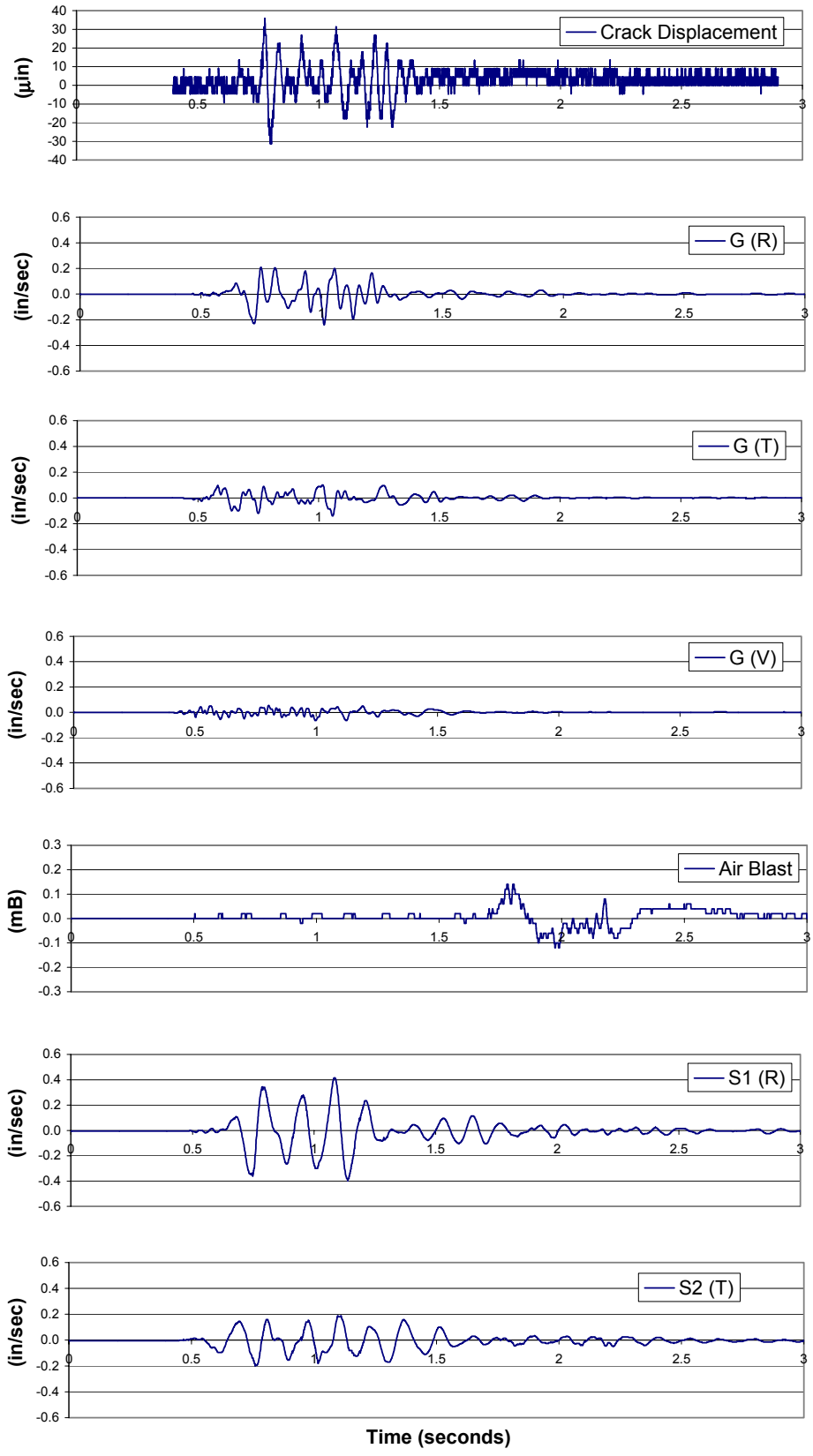

Figure 3.7 Time history of crack displacement on 22 May at 10:38 compared to ground excitation in the radial, transverse, and vertical directions, air blast response, and S2 radial and transverse structure response

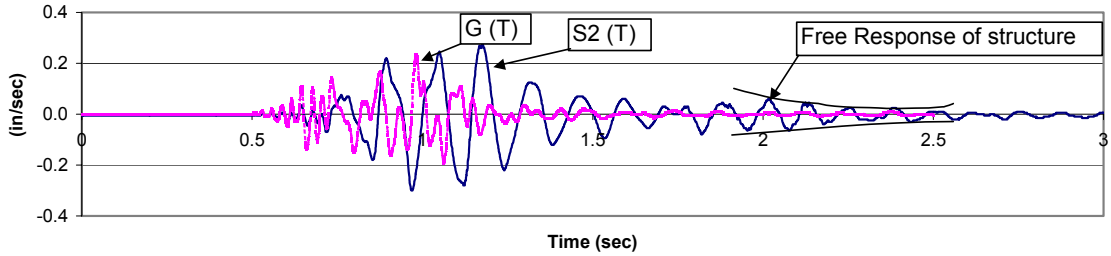

Figure 3.8 Free response of S2 velocity time history in Pennsylvania double-wide trailer

The Fourier frequency approach is most useful when there is little or no free response detected in the response time histories. To obtain dominant frequencies, Fourier Frequency Transforms (FFTs) can be determined using dedicated software such as White Seismograph Data Analysis (White Industrial Seismology, Inc. (1998) or NUVIB (Huang, 1994) for any of the velocity time histories. Only NUVIB can be employed to obtain FFT spectra for the crack displacement time histories, since White only analyzes data files recorded from the seismographs. The ratio of the FFT spectra of the structure response at S2 divided by the ground motion for the same component provides a means to determine the dominant frequency, as shown in Figure 3.9 for the event on 22 May at 12:16. Here the upper corner velocity (S2) Fourier spectrum (b) is divided by that of the ground velocity (c) to produce the ratio (a). False peaks may develop when small structural amplitudes are divided by much smaller ground motion amplitudes. To prevent large ratios of insignificant response and excitation, broad-frequency-band, low amplitude noise should be added to both the structural and ground motion amplitudes to eliminate these false transfer function peaks. (Dowding 1996) Alternatively these peaks can be filtered out by replacing any amplitude less than ten percent of the peak amplitude of a given FFT with ten percent of the peak amplitude. The second approach was followed in this study. FFTs produced for all structures can be found in Appendix A.

Dominant response frequencies estimated from ratios of these moderated FFT spectra of upper structure response and ground motion were approximately 8 to 10 Hz for all responses in the radial direction. As seen in Figure 3.9a, the dominant response frequency for the blast on 22 May at 12:16 was 10 Hz. For this case both the FFT and zero crossing methods yielded the same dominant frequency, 8 to 10 Hz.

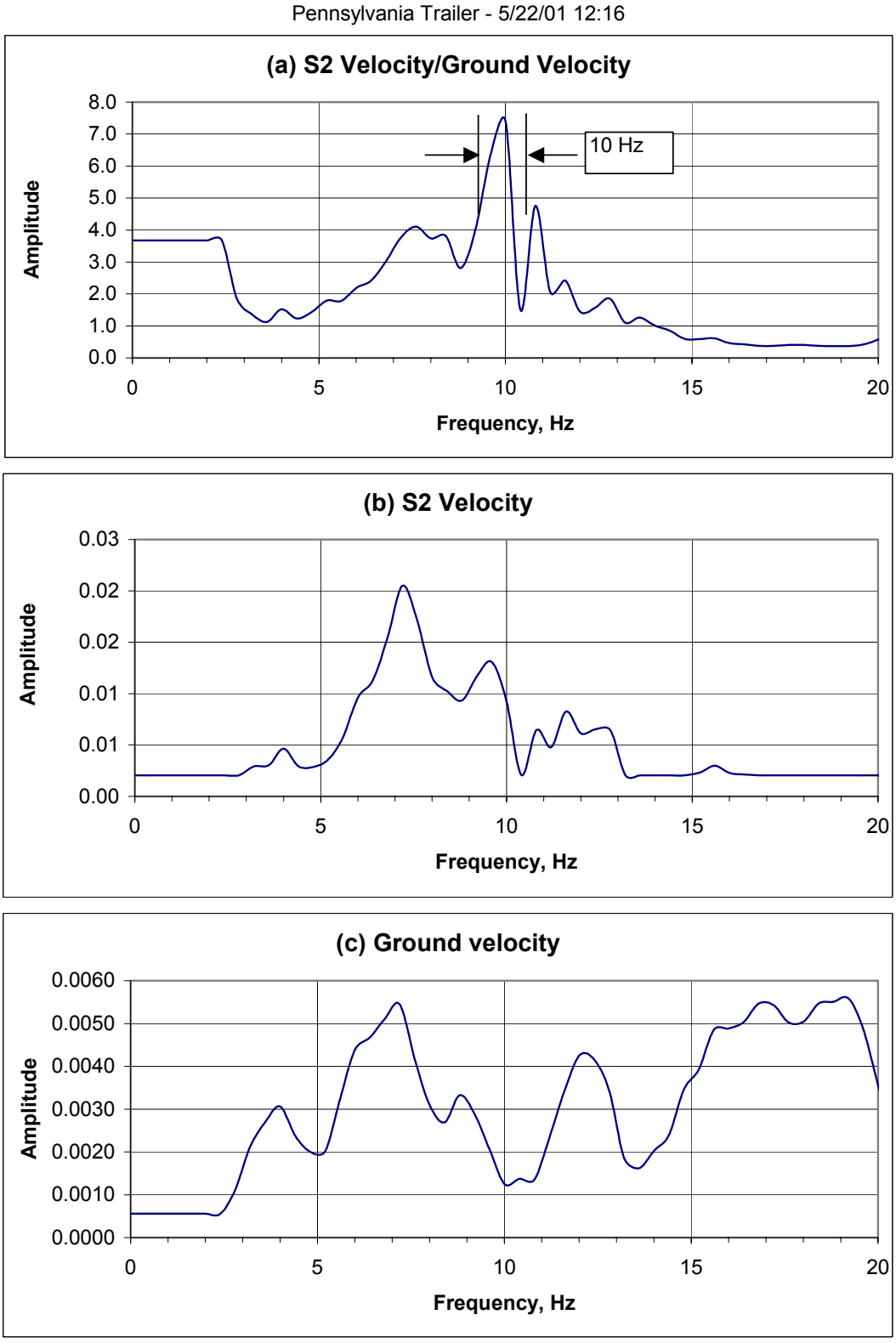

Figure 3.9 Spectra of ratio of S2 velocity FTT and ground velocity FFT, S2 FFT, and ground FFT

Single Degree of Freedom analyses were performed on all radial ground motions produced by the blast events. The Single Degree of Freedom model (SDOF) has been used to predict cracking potential of structures subjected to excitation motions in the ground. A spectrum curve is generated from a SDOF analysis that represents the response of structures (of varying natural frequencies) to the same ground motion. (Dowding 1996) Further detail on the background of the SDOF model can be found in Appendix B.

The SDOF response spectrum for the radial ground motion produced by the 22 May blast at 10:38 is displayed as Figure 3.10. A damping coefficient of 5% was assumed in determining the response spectra for all of the ground motions analyzed in this thesis, based on average values from previous studies. By calculating this coefficient from some of the time histories exhibiting free response, this assumption proved to be valid. The approximate dominant (natural) frequency of the Pennsylvania trailer was 8 Hertz (as determined above), therefore, the estimated displacement of the structure relative to this ground motion was 9600 μin (243 μm), as shown by the intersection of the vertical 8 Hertz line with the response spectrum.

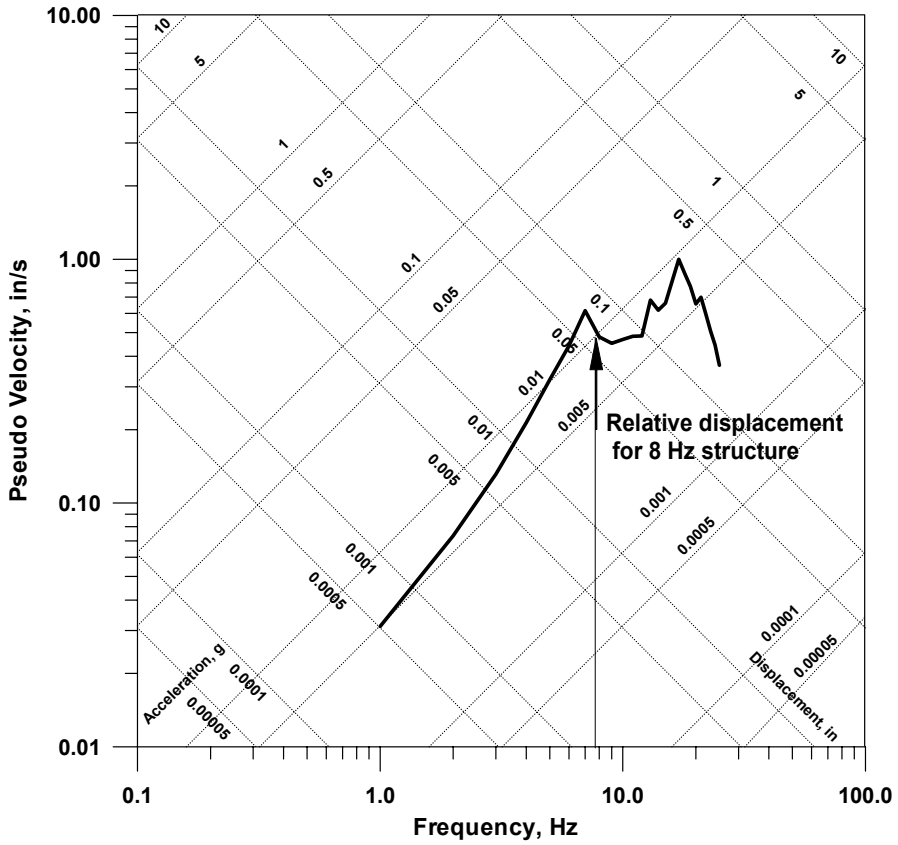

Figure 3.10 Single Degree of Freedom response spectrum of radial motion produced by blast on 5/22/2001 at 10:38, showing estimated relative displacement of an 8 Hz structure

Crack Response to Household and Blast Events

Table 3.2 presents the measured crack displacement corresponding to all dynamic events. Household activities such as closing doors and windows, hitting walls, jumping in the house, and dropping a chair, were performed to measure crack responses and compare them to responses from the blasts. Blast-induced displacements are included for comparison. Approximate distances between the location of the activity and the crack are also presented in the table.

Table 3.2 Summary of measured crack displacements associated with dynamic events

Activity	Description	Approximate distance from crack (feet)	Peak crack displacement (micro-inch)	Peak crack displacement (micrometers)	Approximate distance from radial midwall (feet)	Peak Radial Midwall Response (ips)
	gentle	10 to 11	8.9	0.23		0.62
bathroom door	hard		22.3	0.57	8	2.14
	moderate	5 to 6	8.9	0.23		0.34
	gentle		8.9	0.23		0.23
	harder		18.4	0.47		0.53
bedroom door	slam		97.7	2.48	12	1.46
	moderate	14	22.3	0.57		0.32
front screen door	hard		26.7	0.68		0.46
	gentle		4.4	0.11		0.07
front door	hard		6.9	0.18		0.35
kitchen door			26.8	0.68	30	0.34
jump	bedroom	10 to 11	58.4	1.48		0.42
vacuum hit wall	bedroom		22.5	0.57	5	0.11
chair fall back	dining room	5	49.2	1.25	15	0.09
hammer	bedroom wall	10 to 11	8.8	0.22	5	0.06
close window	bedroom S. wall	27	4.4	0.11	2	0.16
shot 1	5/22/2001 10:38	1450	35.9	0.91	1430	0.98
shot 2	5/22/2001 12:16	1560	31.3	0.79	1450	0.90
shot 3	5/23/2001 14:19	1500	36.3	0.92	1475	0.47
shot 4	5/24/2001 10:51	1400	26.6	0.68	1380	1.08

In many instances, the crack responded at a greater amplitude of displacement to the household activities than to the highest ground motions from blasting. Crack responses associated with the four blasts ranged between 0.68 and 0.92 micrometers (26.9 and 36.3 μin). The smallest response occurred when the window in the far bedroom was shut, which resulted in a peak crack displacement of 0.11 micrometers (4.3 μin); this event was approximately 30 feet (9.1 m) away from the instrumented crack. The largest response occurred when the master bedroom door (approximately 5 ft, or 1.5 m, from the crack in an adjacent room) was slammed shut; this resulted in a peak crack displacement of 2.48 micrometers (90.5 μin). Other responses greater than those associated with the blasts occurred when a person jumped in the middle of the master bedroom and when a chair was dropped in the dining room (another adjacent room).

Closing most of the doors in the structure resulted in peak crack displacements close to the crack displacement associated with the smallest intensity blast. Only when doors were closed gently did the crack displacements remain around 0.2 μm (7.9 μin).

Crack Response to Environmental Effects

Figure 3.11 compares the long-term action of weather indicators (temperature and humidity) with the long-term crack response. Temperature, crack displacement, and humidity were plotted with thin solid lines along the same time scale to illustrate interrelationships. Long-term crack displacement was measured hourly during the monitoring period and temperature and humidity were measured every 10 minutes. Sharp changes were observed in the temperature, crack displacement, and humidity throughout the monitoring period. At the time of monitoring, an air conditioning unit was functioning, which produced severe changes in temperature on a regular basis. In addition, rainfall was observed intermittently, producing concentrated periods of high humidity. Consequently, these conditions, more than likely, were the cause of sharp changes in crack displacement.

Average values of crack displacement (and temperature and humidity) were systemically calculated at every hourly measurement taken (and are shown in Figure 3.11 with diamond-constructed lines). These 24-hour "rolling" averages consisted of the measurements from 12 hours before and 12 hours after each hourly measurement. For example, at 12:00 p.m. on 22 May 2001, a 24-hour average crack displacement was calculated from the 24 measurements recorded between 12:00 a.m. on 22 May to 12:00 on 23 May. For the first and last 12 rolling averages computed, the first and last measurement recorded was counted more than once in the respective averages, in order to have 24 measurements included in every average. For this monitoring period, the 24-hour rolling averages of temperature remained relatively constant, but slightly mirrored those of displacement and humidity. The 24-hour averages of humidity increased gradually during most of the observed period, while slightly declining at the end. The 24-hour averages of crack displacement followed those of humidity, but lagged slightly behind.

Overall averages, shown with the thick solid lines in Figure 3.11, were computed for crack displacement, temperature, and humidity throughout the whole monitoring period. Hourly measurements from the first to last hour were included in these averages.

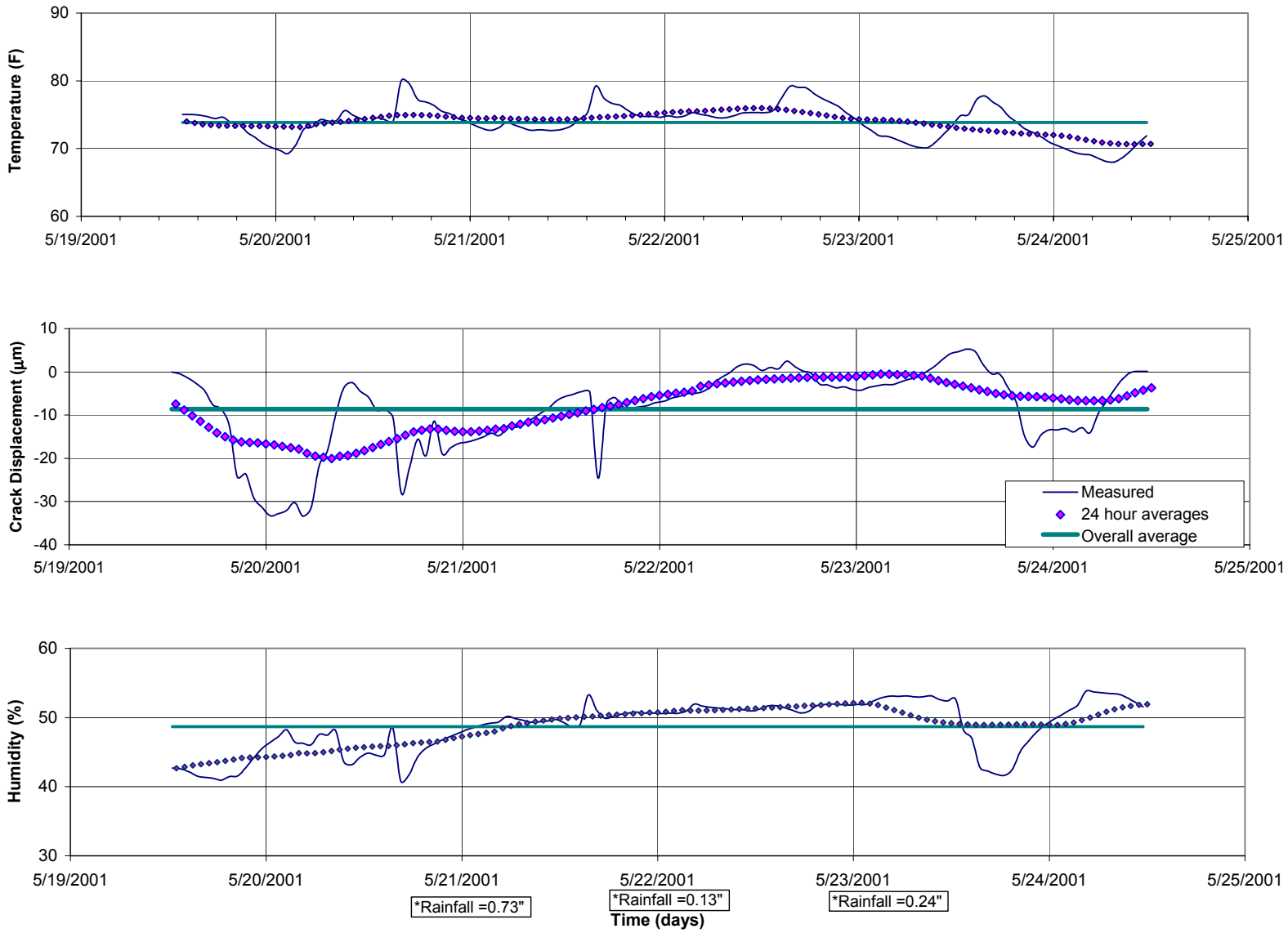

Figure 3.11 Long-term crack displacement and weather versus time

Collectively, the actual measurements, 24-hour averages, and overall averages were used to determine crack response to weather effects. Weather effects have three distinct contributors: 1) frontal movements that change overall temperature and humidity for periods of several days to several weeks, 2) daily responses to changes in average temperature and solar radiation, and 3) weather fronts that contain extremes of unusual weather or other environmental effects. Table 3.3 lists all of the average and maximum values for the frontal, daily, and weather effects. Values of crack response to typical and maximum ground motions associated with coal mine blasts are also included in this table, in order to compare the difference in magnitude between weather-induced and blast-induced crack response.

The first contributor, the frontal effect, is defined as the deviation of the peak 24-hour average value from the overall computed average. In between each instance when the 24-hour average line crossed the overall average line, the frontal effect was calculated at the peak 24-hour average value and taken as an absolute value. The average and maximum of the calculated frontal effects (for temperature, crack displacement in both μm and μin, and humidity) were included in Table 3.3.

The second contributor, the daily effect, is defined as the difference of the peak actual measurement from the 24-hour average. In between each instance when the actual measurement line crossed the overall average line, the daily effect was calculated (actual minus 24-hour average) and taken as an absolute value. The average and maximum of the calculated daily effects (for temperature, crack displacement in both μm and μin, and humidity) were also included in Table 3.3.

The third contributor, the weather effect, was defined as the difference in the peak actual measurement from the overall computed average. In between each instance when the actual measurement crossed the overall average line, the weather effect was calculated (actual minus overall average) and taken as an absolute value. The average and maximum of the calculated weather effects (for temperature, crack displacement in both μm and μin, and humidity) were also included in Table 3.3.

Table 3.3 Computed crack displacements due to long-term weather phenomena

	Temperature Change (DegF)	Crack Displacement (μin)	Crack Displacement (μm)	Humidity Change (%)
Frontal Effect				
Average deviation of 24 hr average from overall average	0.2	381	10	3
Max deviation of 24 hr average from overall average	0.4	451	11	4
Daily effect				
Average of deviations from 24 hr average trend	2	414	11	2
Max deviations from 24 hr average trend	4	639	16	5
Weather Effect				
Average deviations from overall average	3	419	11	4
Max deviations from overall average	5	962	24	7
Vibration Effects				
Typical Ground motion (PPV=0.10 ips)	-	12	0.3	-
Max ground motion (PPV=0.32 ips)	-	36	0.9	-

In Figure 3.12, the crack displacements due to different weather phenomena measured over the entire monitoring period are compared to those from the blasts. The magnitude of each dynamic response to a blast event corresponds to the absolute, maximum zero-to-peak displacement of the crack during the five seconds of resulting vibratory motion. In order to display the relatively, small responses associated with the blasts, the blast-induced responses (illustrated with vertical lines) are encircled and the two day period of blasting is magnified in Figure 3.12(b). The zero-to-peak values are shown originating from the overall average line in order to emphasis the large difference in magnitude (between long term and dynamic response) pictorially. The maximum dynamic crack displacement of 0.92 μm or 36.3 μin (associated with a peak radial ground motion of 0.32 ips from the blast on 23 May 2001 at 14:19) is small compared to the average and maximum crack displacements due to computed weather effects of 7 and 24 μm (277 and 948 μin), respectively. The maximum weather front is almost 25 times this particular crack response.

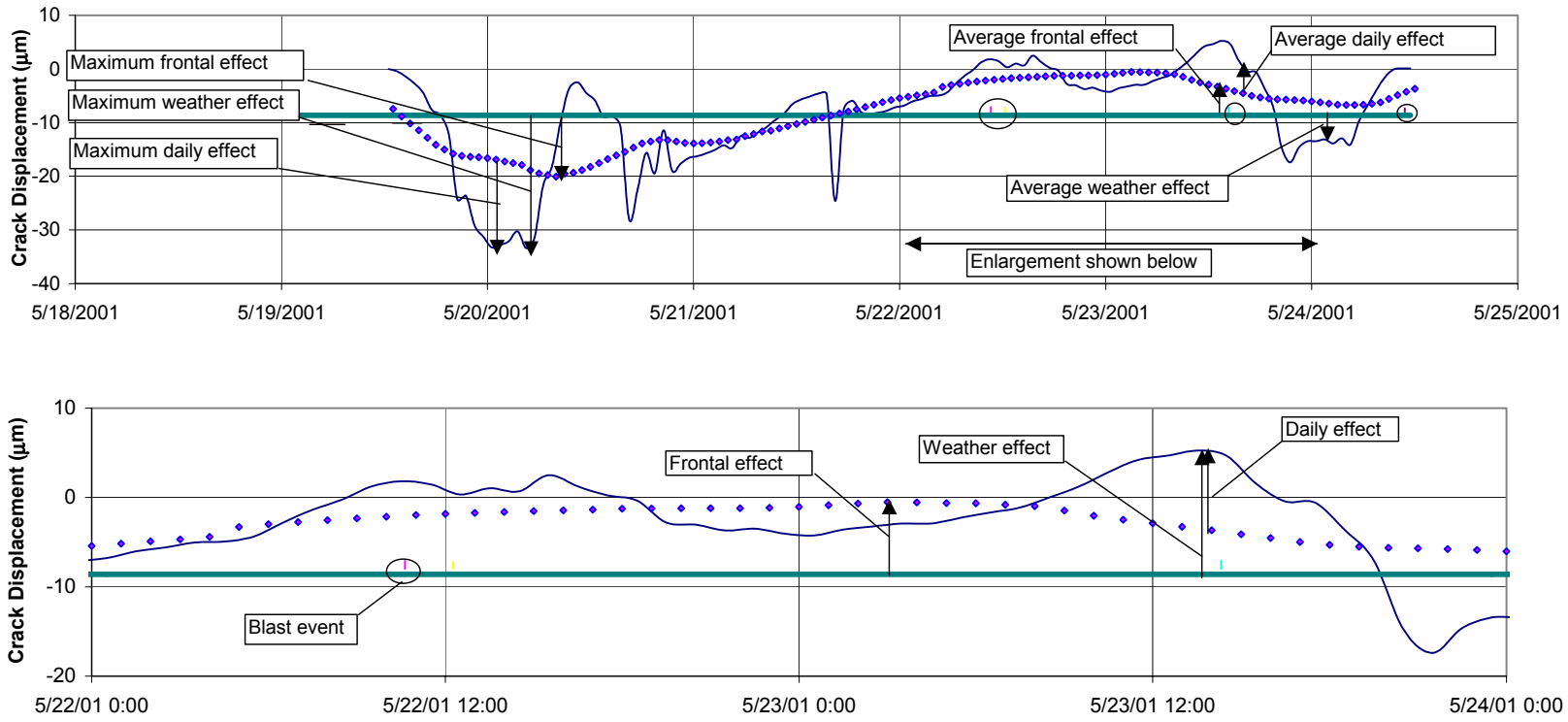

Figure 3.12 Typical crack displacements due to long-term phenomena and maximum zero to peak dynamic blast events

Comparison of computed displacements with measured crack displacements

The maximum measured crack displacement produced by each shot is compared in Table 3.4 to various computed wall displacements based on structure responses, and peak ground motion measured in the direction parallel to the cracked wall. Structure/wall displacements were computed using a number of methods such as the integration of velocity time histories, the Single Degree of Freedom response spectrum method, and estimation based on sinusoidal approximation. All computed displacements were based on structure and ground responses in the direction parallel to the wall containing the crack, since crack displacement was measured in the plane of the wall. All comparisons are presented graphically in Figures 3.13 and 3.14. Details pertaining to these methods to compute structural displacements are presented below.

Integration of time histories

Displacement time histories can be calculated by integrating velocity time histories. By subtracting perfectly time correlated (±0.001 sec) pairs of these integrated velocity time histories, a relative displacement time history was created. This was done for two different pairs - upper corner, S2, minus lower corner, S1, and S2 minus ground, G. The peak relative displacements were determined from these resulting time histories and used as a representative values of computed displacement. Comparisons between measured crack displacements and these $(S2\text{-}S1)_{max}$ and $(S2\text{-}G)_{max}$ displacements are presented graphically in Figure 3.13 (a) and (b), respectively.

Displacements were also estimated from the integrated ground velocity time histories, exclusively. The peak values from these time histories were used as representative values of computed displacement. The comparison between measured crack displacements and these G_{max} displacements are presented graphically in Figure 3.13 (c).

Table 3.4 Summary of computed and measured displacements

Date of Shot	Relative displacement, δ, of structure by method (μin)						Peak ground motion in the radial direction (μin/sec)	Measured crack displacement (μin)
	Integration of Velocities			δ from SDOF method	Approximation with $\delta = V/2\pi f$			
				From response spectra	Estimated from V and f at	Estimated from V and f at		
				for f_n of 8 Hz	G_{max}	$S1_{max}$		
				Average of $10 < f_n < 15$	$S2_{max}$	$S2_{max}$		
	$(S2\text{-}S1)_{max}$	$(S2\text{-}G)_{max}$	G_{max}	-	G_{max} and $S2_{max}$	$S1_{max}$ and $S2_{max}$		
5/22/01 10:38	5914	8403	4755	9557 7209	4607 8636 5607	913 7219 3949	0.24	36
5/22/01 12:16	3921	5747	3246	6784 4970	259 6301 3821	633 5191 3591	0.19	31
5/23/01 14:19	5317	6323	3320	7926 7380	2519 7148 1937	1058 5508 1422	0.32	36
5/24/01 10:51	2802	3967	2337	4639 4382	1685 2423 1823	1635 1210 1067	0.20	27

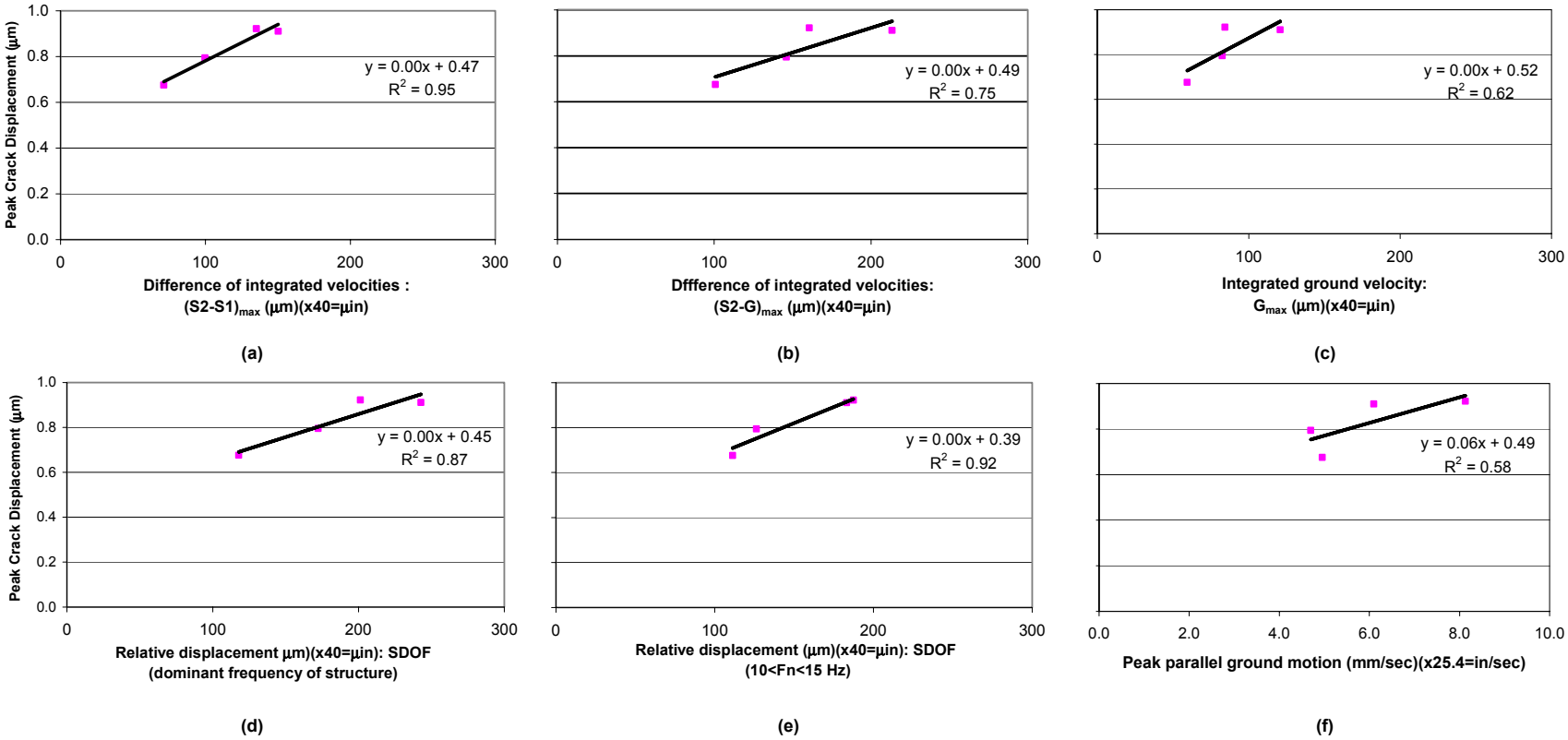

Figure 3.13 Correlations between measured crack displacement and computed displacements and peak radial ground motions

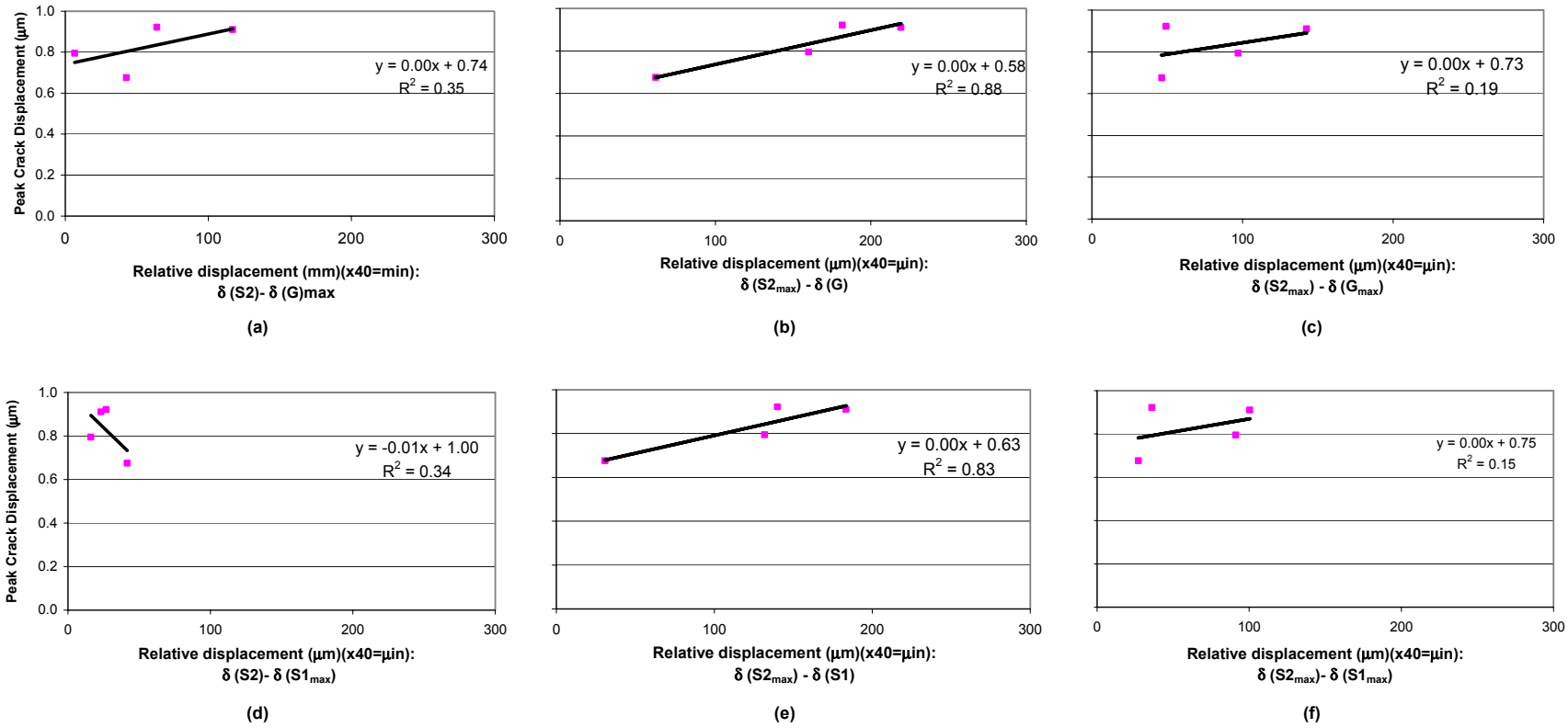

Figure 3.14 Correlations between measured crack displacement and computed relative displacements

Single degree of freedom response spectrum method

As described earlier in this chapter, by analyzing SDOF response spectra of blast-induced ground motions, relative displacements can be estimated for structures of different dominant frequencies. Two approaches were made in picking these estimated relative displacements. The first was to find the relative displacement associated with the estimated dominant frequency of the structure. These values were used as representative values of computed displacements, and are equated to peak displacements that the structure would experience. Comparisons between measured crack displacements and these computed displacements are presented graphically as Figure 3.13 (d).

The second approach to finding structure/wall displacements based on this method was to average a range of estimated displacements based on a range of dominant frequencies. As reported in previous studies, the 10 to 15 Hz range is the average range of dominant frequencies for one to two story structure walls. Therefore, estimated displacements for dominant frequencies between 10 and 15 Hz were averaged in order to find representative values of computed displacement for the structure wall. These values were desired since the crack was located on the wall, and were expected to have a stronger correlation with the measured displacements than those computed using the estimated dominant frequency of the structure. Comparisons between the measured crack displacements and these computed displacements are presented graphically as Figure 3.13 (e).

Estimation based on sinusoidal approximation

Relative displacements can be estimated visually from time histories by assuming that velocity time histories approximate sinusoidal waveforms. Displacement, δ, can be estimated using the following equation:

$$\delta = V/2\pi f,$$

where V is a given velocity in a time history and f is the dominant frequency of the velocity at the time it occurs. The frequency is determined by taking the inverse of twice the time between the zero-crossings enclosing the given velocity. Displacements approximated in this manner can be determined for both upper and lower bounds of the structure and subtracted in order to obtain various measures of relative displacement.

Approximated relative displacements have been produced from the following pairs of velocity time histories: 1) ground motion, G, and the upper corner, S2, at the time of peak G, 2) G and S2 at the time of peak S2, 3) peak G and peak S2, regardless of the time at which each occurs. For the two time-correlated pairs, (1) and (2), displacement is still computed at the same time, regardless of the magnitude of the velocity at that point in time, for either of the time histories. In other words, if the velocity on one of the time histories is 0.0 in/sec and the velocity on the other is 0.3 ips, then the displacement of the first time history would be considered zero, and the relative displacement would be equal to that computed from the second time history. These resulting values from $\delta(S2)-\delta(G_{max})$, $\delta(S2_{max})-\delta(G)$, and $\delta(S2_{max})-\delta(G_{max})$, were all used as representative values of computed displacements. Figure 3.15 displays the calculation of relative displacement using ground motion and S2 response, at the time of peak ground motion, for the blast on 22 May at 10:38. Comparisons between measured crack displacements and the computed displacements are presented graphically as Figure 3.14 (a), (b), and (c), respectively.

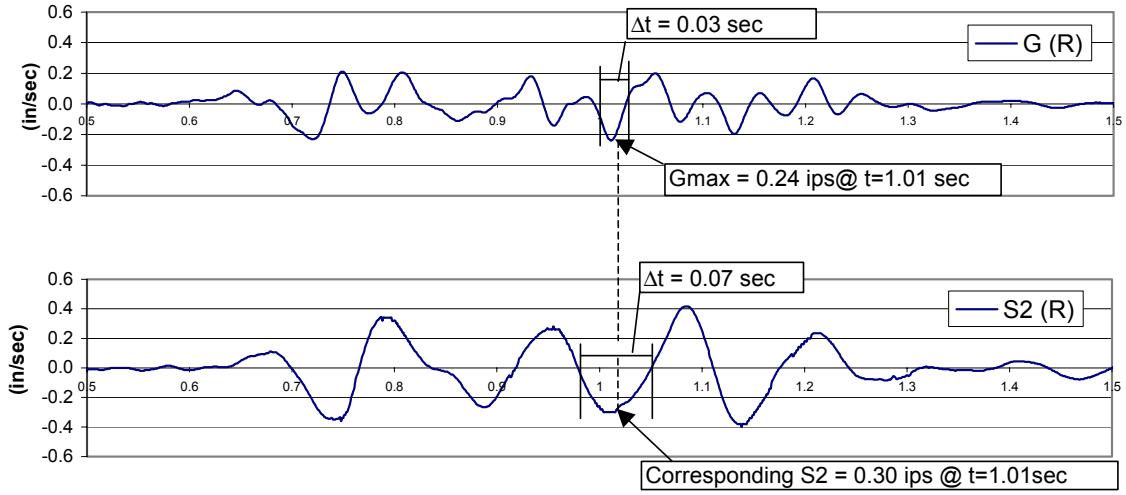

$$\text{Relative displacement} = \delta\,(S2) - \delta\,(G_{max})$$

$$\text{Relative displacement} = \frac{0.24\,\text{ips}}{2\pi * (1/2 * 0.03\,\text{sec})} - \frac{0.30\,\text{ips}}{2\pi * (1/2 * 0.07\,\text{sec})} = 4607\ \mu\text{in or } 117\ \mu\text{m}$$

Figure 3.15 Calculation of relative displacement using method of approximation

In addition, three more pairs were analyzed, where velocity in the lower corner, S1, was used in place of ground motion, G. (G and S1 at the time of peak G, G and S1 at the time of peak S1, and peak G and peak S1, regardless of the time at which each occurs) These resulting values from $\delta(S1)$-$\delta(G_{max})$, $\delta(S1_{max})$-$\delta(G)$, and $\delta(S1_{max})$-$\delta(G_{max})$, were also used as representative values of computed displacements. Comparisons between measured crack displacements and these computed displacements are presented graphically as Figure 3.14 (d), (e), and (f), respectively.

The last pair, in both sets of three is not as precise as the others, as it fails to take into account the necessity of simultaneity of the motions. Such values do not depict the displacement at a given time, but rather, a maximum possible displacement. Therefore, it would be expected that the first two pairs of both sets would yield better correlations with the measured displacements than would the last pairs.

Based on the data shown in Figures 3.13 and 3.14, the best correlation was produced between the measured displacements and the displacements from the difference of integrated velocities, S1-S2, as shown in Figure 3.13 (a). The trend line for this relationship exhibits a regression coefficient, R^2 =0.95. The estimated displacements from SDOF analyses also resulted in high regression coefficients, with the displacement representing the average range of wall frequencies having a tighter trendline, as expected (R^2 = 0.92), than the displacement corresponding with the estimated dominant frequency (R^2=0.87). These correlations were shown in Figure 3.13 (d) and (e), respectively. The lowest regression coefficients were seen from the approximated displacements computed at the times of G_{max} and $S1_{max}$, and also when no time correlation was involved in the computation (Figure 3.14 (a), (d), (c), and (e), respectively).

In this thesis, the square of the regression coefficient, R^2, was employed to describe the tightness of data to a best-fit trendline. Microsoft Excel defines the R^2 value as the square of the Pearson product moment correlation coefficient, which is the proportion of the variance in y, depending on the variance in x. The tightness of fit (of the data to the best-fit trendline) was also calculated with standard deviations, using the y- distances, as well as the perpendicular distances, of the data points from their respective trendline. Only one of these comparisons, R^2, was presented in this thesis, as the conclusions did not change with varying methods of calculating tightness of data about best-fit trendlines.

CHAPTER 4

ADOBE RANCH HOUSE – NEW MEXICO

The New Mexico structure, shown in Figure 4.1, is an adobe brick structure located approximately 5000 feet (1533 m) from surface coal mining in Farmington, New Mexico. Data collected onsite from 21 June to 26 July 2001 are summarized in Table 4.1. Nine blasts with maximum charge weights/delay between 300 and 13,047 lbs (136 and 5930 kg) produced ground motions of 0.01 to 0.16 ips (0.3 to 4.1 mm/sec), maximum structure response of 0.02 to 0.22 ips (0.5 to 5.6 mm/sec), and maximum wall response of 0.03 to 0.31 ips (0.8 to 7.9 mm/sec). Weather data varied cyclically each day with outside temperatures ranging between 52 and 103°F (11 to 39 °C) and outside humidity ranging between 10 and 92 %.

Figure 4.1 New Mexico adobe structure

Table 4.1 Summary of structural and crack response for New Mexico adobe structure

Time of Blast	Distance	Charge Weight/ Delay	Scaled Distance	Peak Particle Velocity (ips)			Structure response in S1 cluster (ips)		Structure response in S2 cluster (ips)		Midwall responses (ips)			Measured Crack Displacement under outdoor window frame
	(ft)	(lb)	($ft/lb^{1/2}$)	Vertical	Radial	Transverse	Radial	Transverse	Radial	Transverse	Radial	Transverse	Air Blast (dB)	(μin)
6/22/01 14:20	5333	13047	46.7	0.09	0.16	0.11	0.13	0.11	0.19	0.14	0.19	0.25	128	90.1
6/26/01 15:57	5186	1708	125.5	0.01	0.01	0.01	0.01	0.01	0.02	0.02	0.03	0.05	112	11.8
6/28/01 15:03	4816	300	278.1	0.03	0.04	0.05	0.05	0.06	0.06	0.06	0.06	0.06	100	23.6
7/3/01 13:48	4478	300	258.5	0.05	0.09	0.05	0.05	0.06	0.06	0.08	0.08	0.08	100	23.6
7/5/01 15:03	4941	9591	50.5	0.10	0.13	0.14	0.11	0.11	0.17	0.17	0.20	0.26	117	166.7
7/17/01 12:51	4606	11183	43.6	0.10	0.12	0.14	0.12	0.11	0.15	0.22	0.28	0.31	116	94.0
7/23/01 11:22	4621	300	266.8	0.05	0.07	0.06	0.07	0.07	0.09	0.08	0.13	0.08	110	37.9
7/26/01 11:04	5565	1200	160.6	0.04	0.11	0.07	0.11	0.08	0.13	0.09	0.17	0.09	106	54.8
7/26/01 14:55	4593	7455	53.2	0.07	0.07	0.11	0.06	0.09	0.08	0.17	0.19	0.17	120	90.9

Structure Description

As shown by plan and elevation drawings in Figures 4.2 and 4.3, the structure is approximately 32 feet wide and 70 feet long (9.7 x 21.3 m). The structure is a one-story residential unit, eleven to sixteen feet in height (3.3 to 4.9 m), with no basement space. The walls of the house are comprised of adobe laid brick, and are approximately 10 inches (254 mm) thick (both exterior and interior). Adobe is constructed from a mixture of clay and straw that is compacted into a mold. For this structure, the individual adobe bricks were approximately 6 in. x 3 in. by 12 in. (152 x 76 x 76 mm)

Location of Instrumentation

Locations of all instruments are shown in Figures 4.2 and 4.3. Eleven velocity transducers were installed on and outside of the southeast corner of the structure, closest to the mining. The crack displacement sensor was located on the exterior of the house, spanning a crack that formed a 45 ° angle from a window frame on the south wall of the house as shown in Figure 4.4. The width of the crack was approximated from the photograph as approximately 800 μm (31,600 μin). Further details on placement and description of the instrumentation are given in Chapter 2.

The sensor is located approximately three feet above ground surface on the exterior wall of the house, was placed outside in order to monitor crack displacement during extreme temperature and humidity swings typical of a desert environment. The Supco temperature and humidity sensor was placed adjacent to the Kaman sensor on the exterior wall to record weather changes.

For each blast, time histories were recorded for a total of 13 seconds. Time correlated (within 1/1000 second) time histories of dynamic crack displacement were also collected from the Kaman sensor for nine seconds.

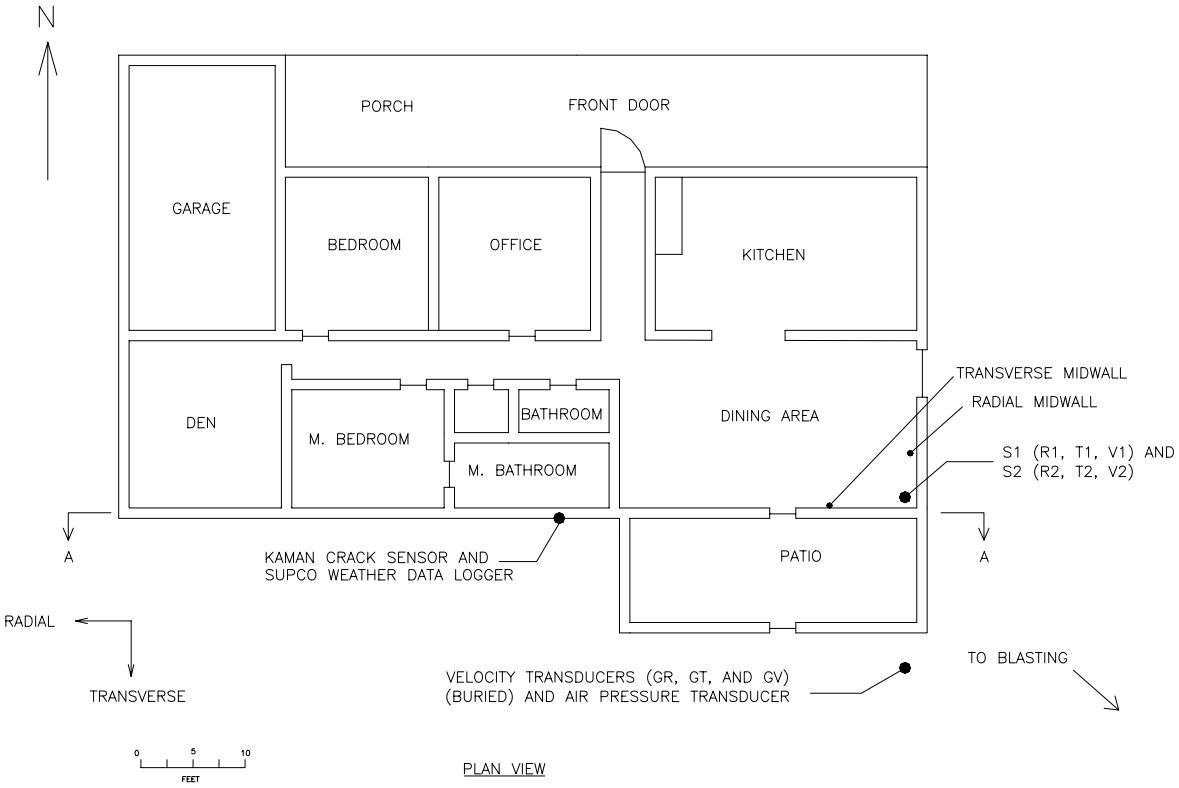

Figure 4.2 Plan view of New Mexico adobe

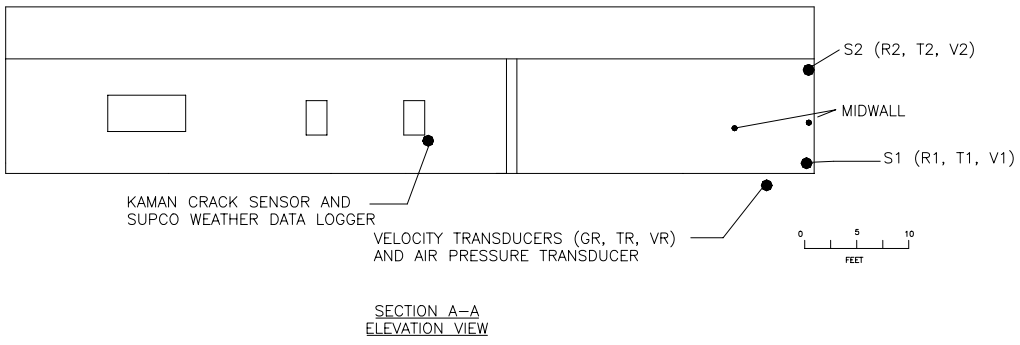

Figure 4.3 Elevation view of New Mexico adobe

Figure 4.4 Kaman crack displacement sensor

Transient Responses

Figure 4.5 shows the velocity time histories of excitation ground motions and structure response, as well as crack response, associated with the blast on 5 July 2001 at 15:03. The responses shown are radial since the plane of the wall containing the crack is radial. This blast produced a peak crack displacement of 4.2 μm (165.9 μin) and a peak radial ground motion of 0.13 ips (3.3 mm/sec). This blast produced the largest dynamic crack displacement during the monitoring period.

In Figure 4.6, the time histories of all three components of ground motion, along with the air blast response, are compared to crack response (for the same blast). In addition, the upper corner (S2) responses of the structure, both radial and transverse, are also shown. All significant structural response from this blast, as well as from the air blast, occurred within the first nine seconds. This also was the case for every each blast during the monitoring period.

Figure 4.7 shows the velocity time histories of excitation ground motions and structure response, as well as crack response, associated with the blast on 17 July 2001 at 12:51. This blast produced a crack response that was typical during the monitoring period.

In Figure 4.8, the time histories of all three components of ground motion, along with the air blast response, are compared to crack response (for the same blast). In addition, the upper corner (S2) responses of the structure, both radial and transverse, are also shown. This blast produced a peak crack displacement of 2.4 μm (94.8 μin) and a peak radial ground motion of 0.12 ips (3.0 mm/sec).

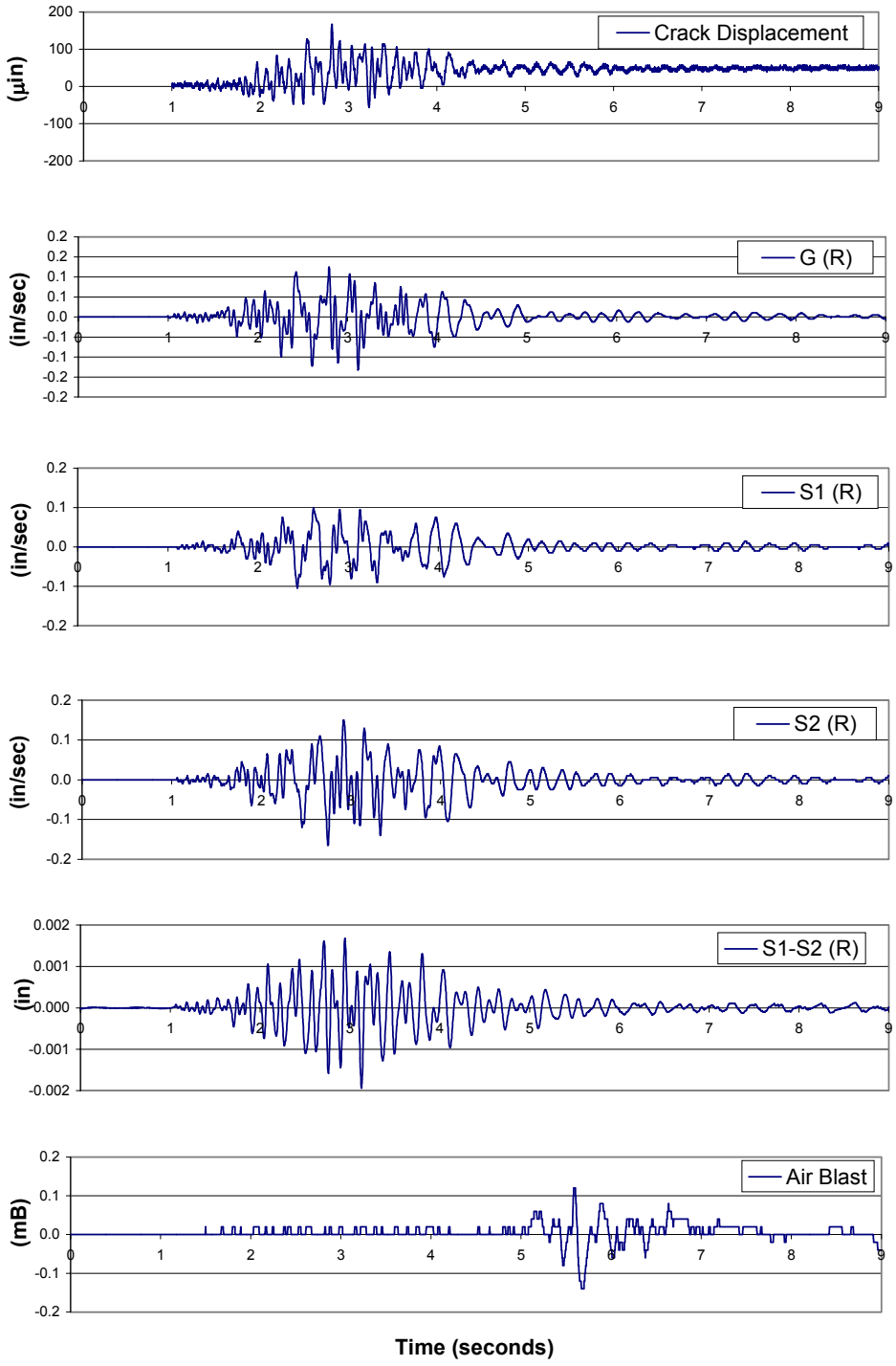

Figure 4.5 Time history of 5 July 2001 crack displacement compared to compared to ground excitation, S1 and S2 response, calculated relative displacement of structure (R1-R2), and air blast

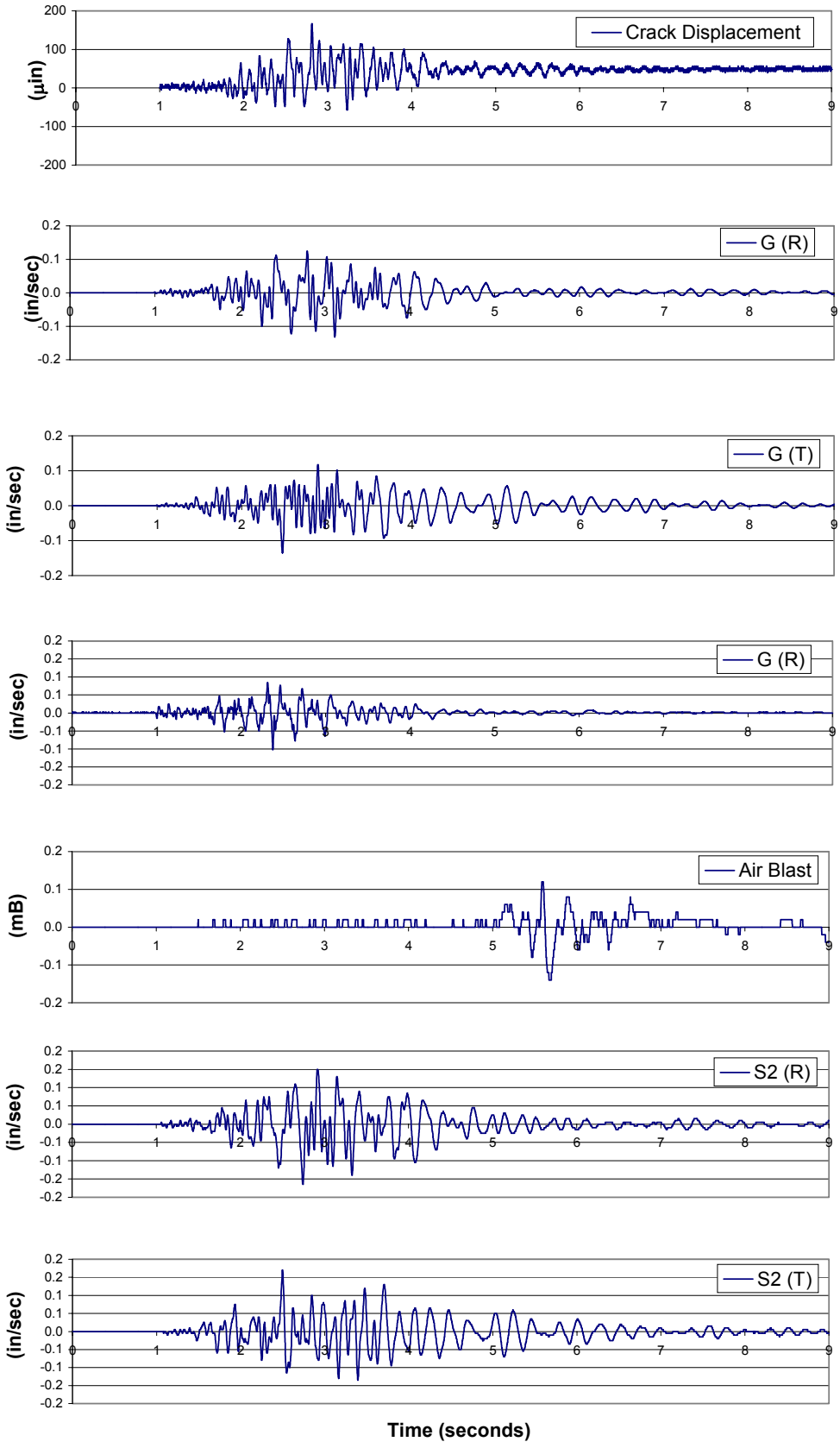

Figure 4.6 Time history of 5 July 2001 crack displacement compared ground excitation in the radial, transverse, and vertical directions, air blast response, and S2 radial and transverse structure responses

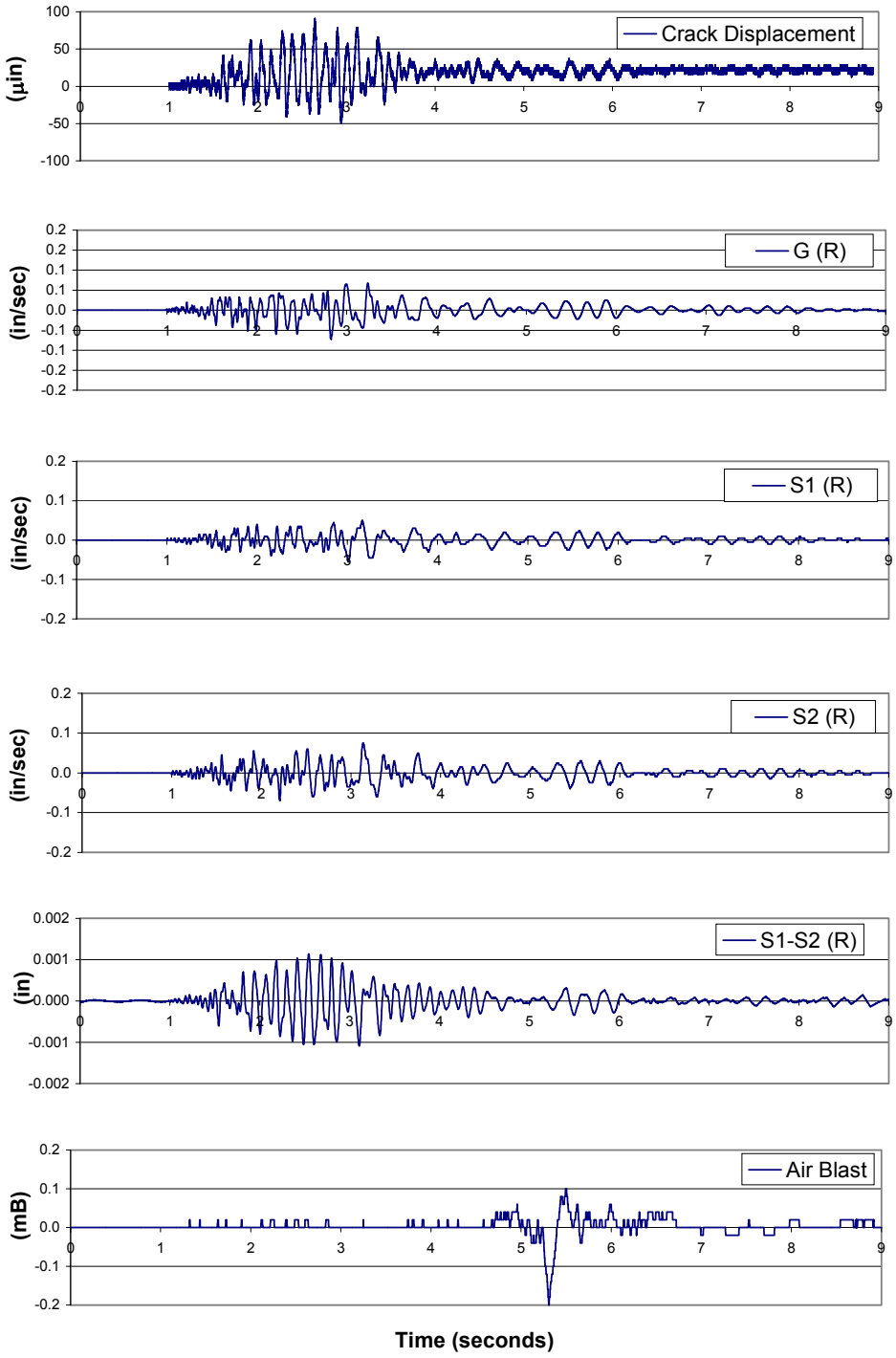

Figure 4.7 Time history of crack displacement at 17 July 2001 at 12:51 compared to compared to ground excitation, S1 and S2 response, calculated relative displacement of structure (R1-R2), and air blast

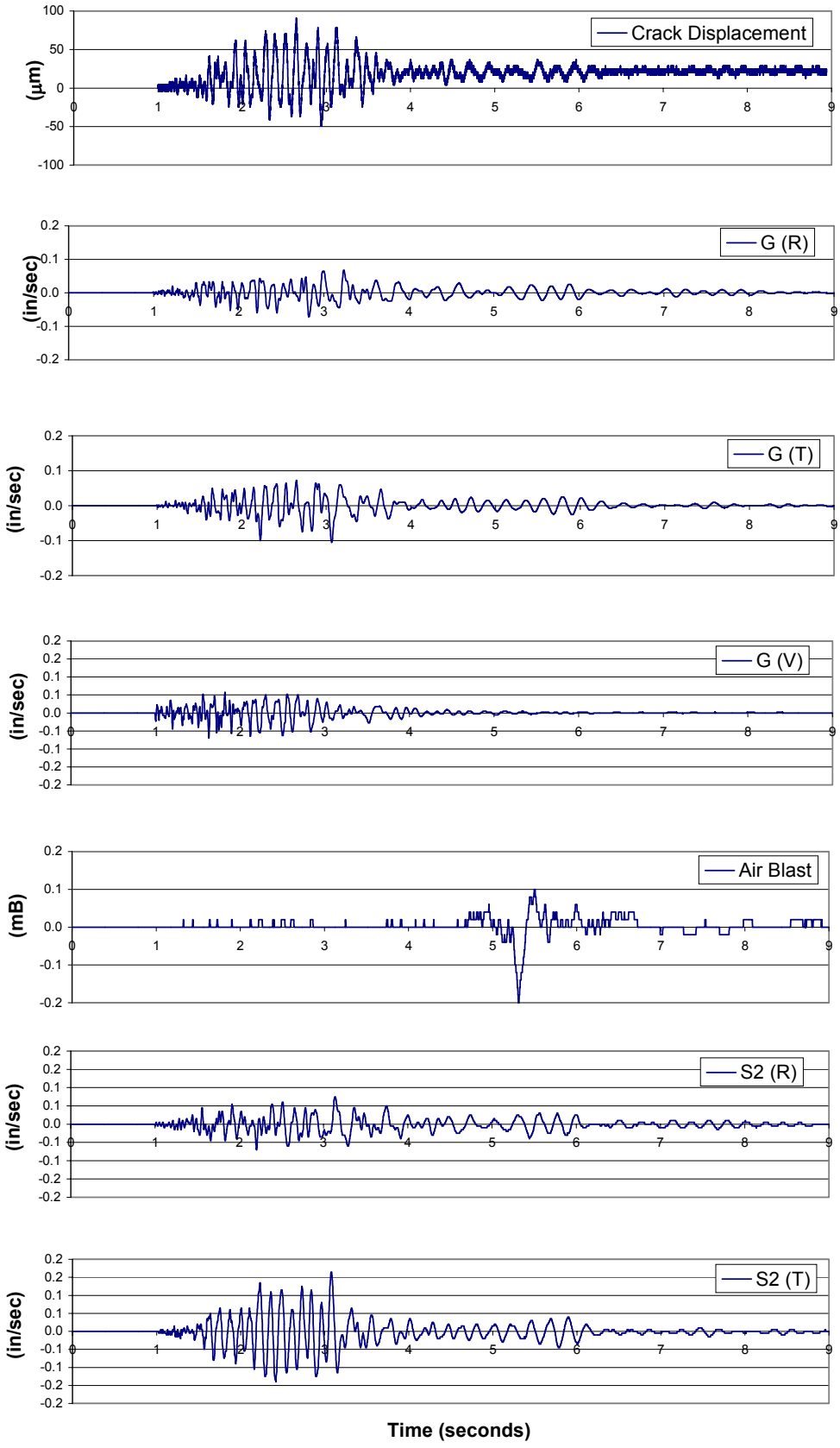

Figure 4.8 Time history of crack displacement on 17 July 2001 compared to ground excitation in the radial, transverse, and vertical directions, air blast response, and S2 radial and transverse structure responses

The dominant response frequencies of the structure required calculation of the FFT ratio because of the lack of free response in the S2 time histories. Ratios were calculated with radial crack response and excitation displacements in order to directly identify the response of the exterior wall in which it was located. It was necessary to employ crack rather than structural response because the upper and midwall velocity transducers were located far from the crack. Further details on the method of calculation for FFT ratios can be found in Chapter 3. Examples of the FFT crack displacement ratios for the 5 July and the 17 July events that correspond to the ground motions in Figures 4.5 and 4.7 are shown in Figures 4.9 and 4.10, respectively. The ground motion causing the greatest crack (and presumably wall) response, 5 July, produced high ratios at 8.5 and 14 Hz. For the 17 July event, high ratios were produced around 7.5 and 9 Hz. Examples of superstructure response FFT ratios are shown in Figures 4.11 and 4.12, respectively. The overall structure responds most to motion in the 5 Hz range. For the two events shown in Figures 4.11 and 4.12, the dominant frequencies were approximately 5.5 and 7 Hz, respectively. Higher dominant frequencies were observed with the crack to ground ratios than with the structure to ground ratios, as was expected, since the dominant frequencies of walls are typically higher than the dominant frequency of the structure.

The response spectra of radial ground motions from the 5 and 17 July 2001 (at 15:03 and 12:51, respectively) blasts are displayed as Figure 4.13. The estimated relative displacements of the structure, with a dominant frequency of 5 Hz, are 8200 μin (208 μm), and 9200 μin (234 μm), as shown in Figure 4.13. The estimated relative displacements of the wall, with a dominant frequency is 9 Hz, are shown in Figure 4.13, as 4500 μin (115 μm) and 6200 μin (157 μm).

The effect of the higher response frequency for the wall is illustrated on the response spectra of the radial ground motions in Figure 4.13. At 14 Hz, the dominant frequency of the wall, the response spectrum of the 17 July radial ground motion is significantly less than that of the 5 July ground motion. This difference corresponds to the difference in measured crack displacements as reported in Table 4.1. The effect of the lower response frequency for the overall structure is also illustrated in Figure 4.13. In the 5 Hz range, the 5 July ground motion also produces its largest response spectra amplitudes. This difference corresponds to the measurements of radial structural response reported in Table 4.1.

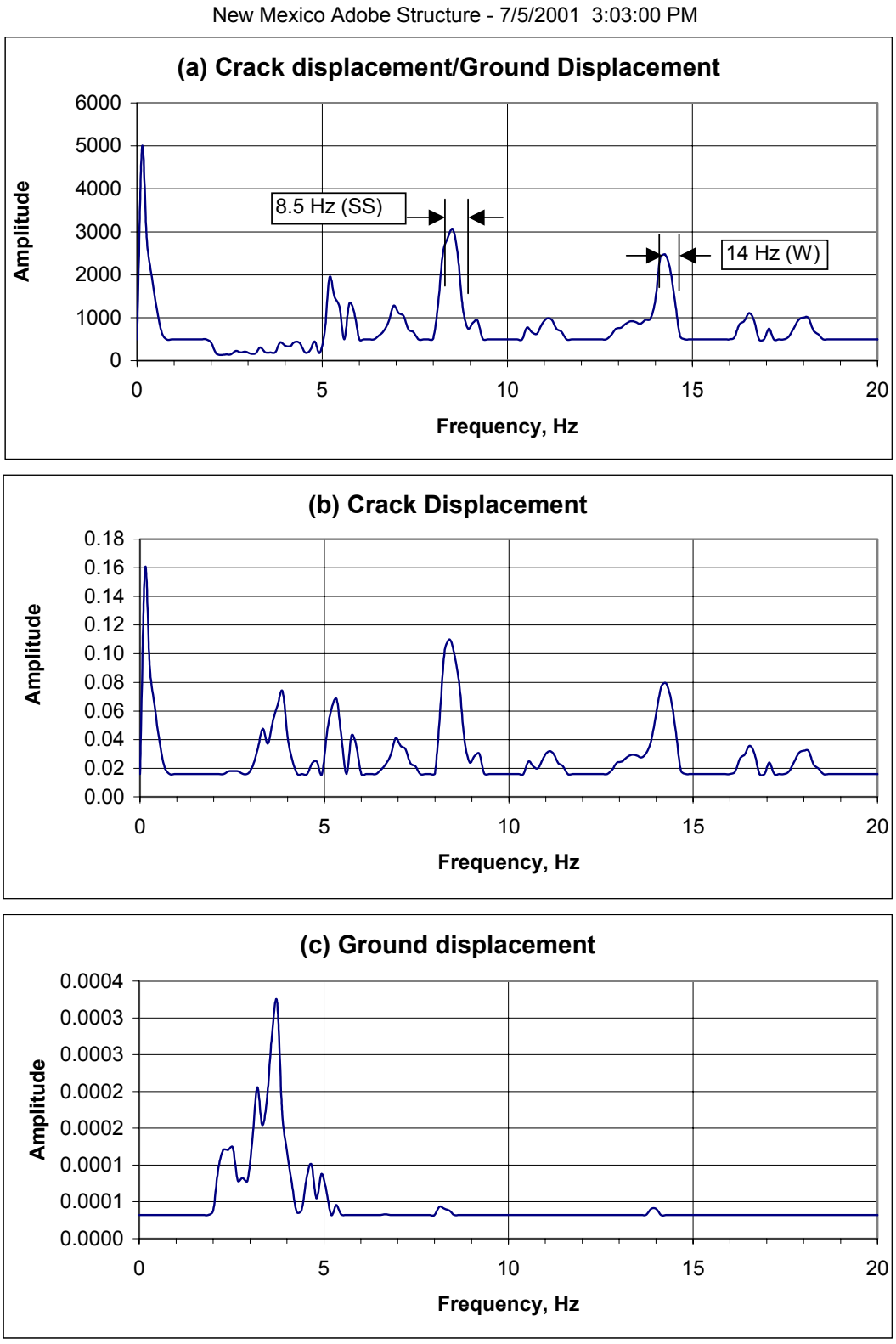

Figure 4.9 FFT Crack displacement ratio, crack displacement FFT, and ground displacement FFT for 5 July blast

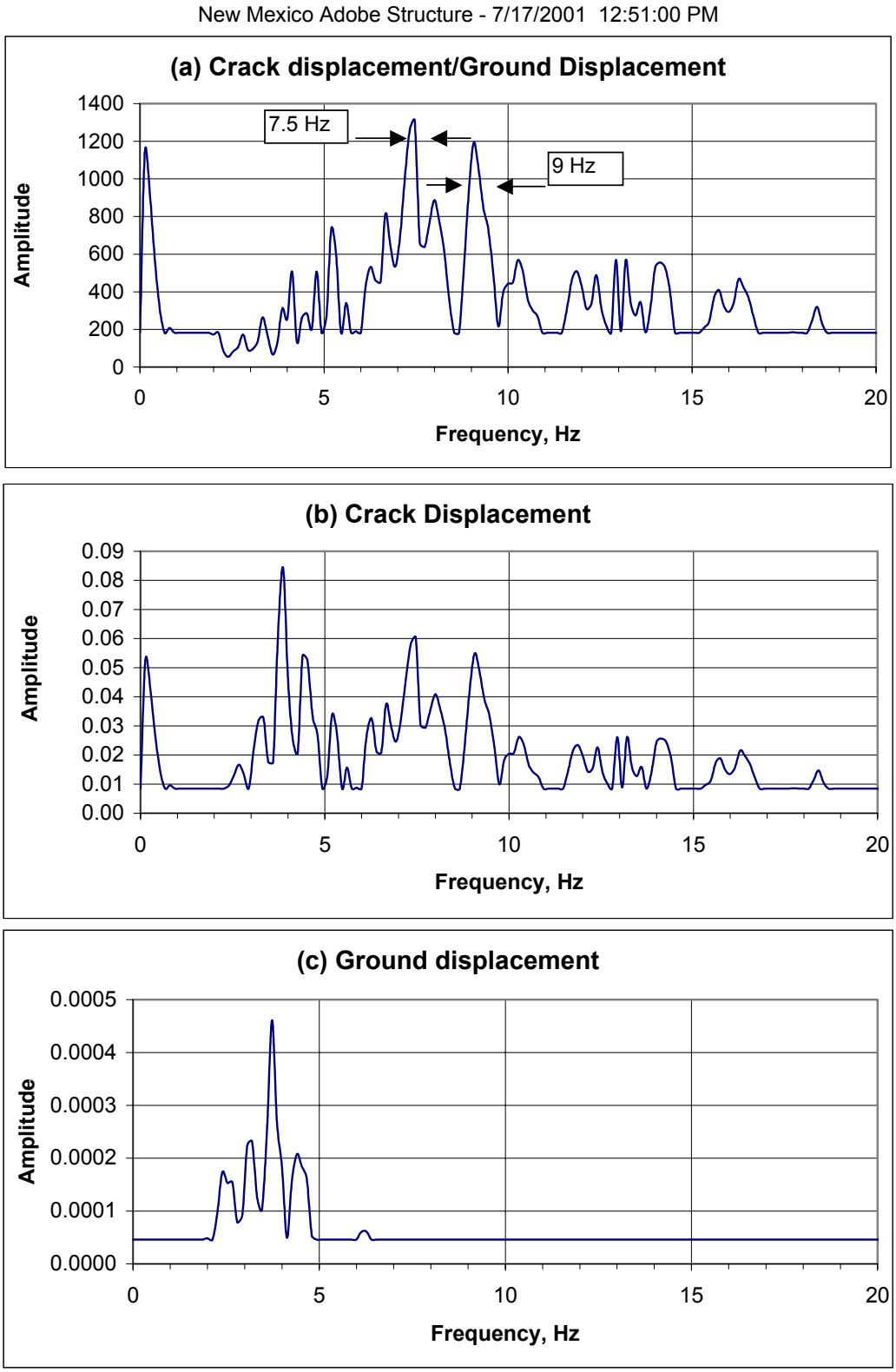

Figure 4.10 FFT crack displacement ratio, crack displacement FFT, and ground displacement FFT for 17 July blast

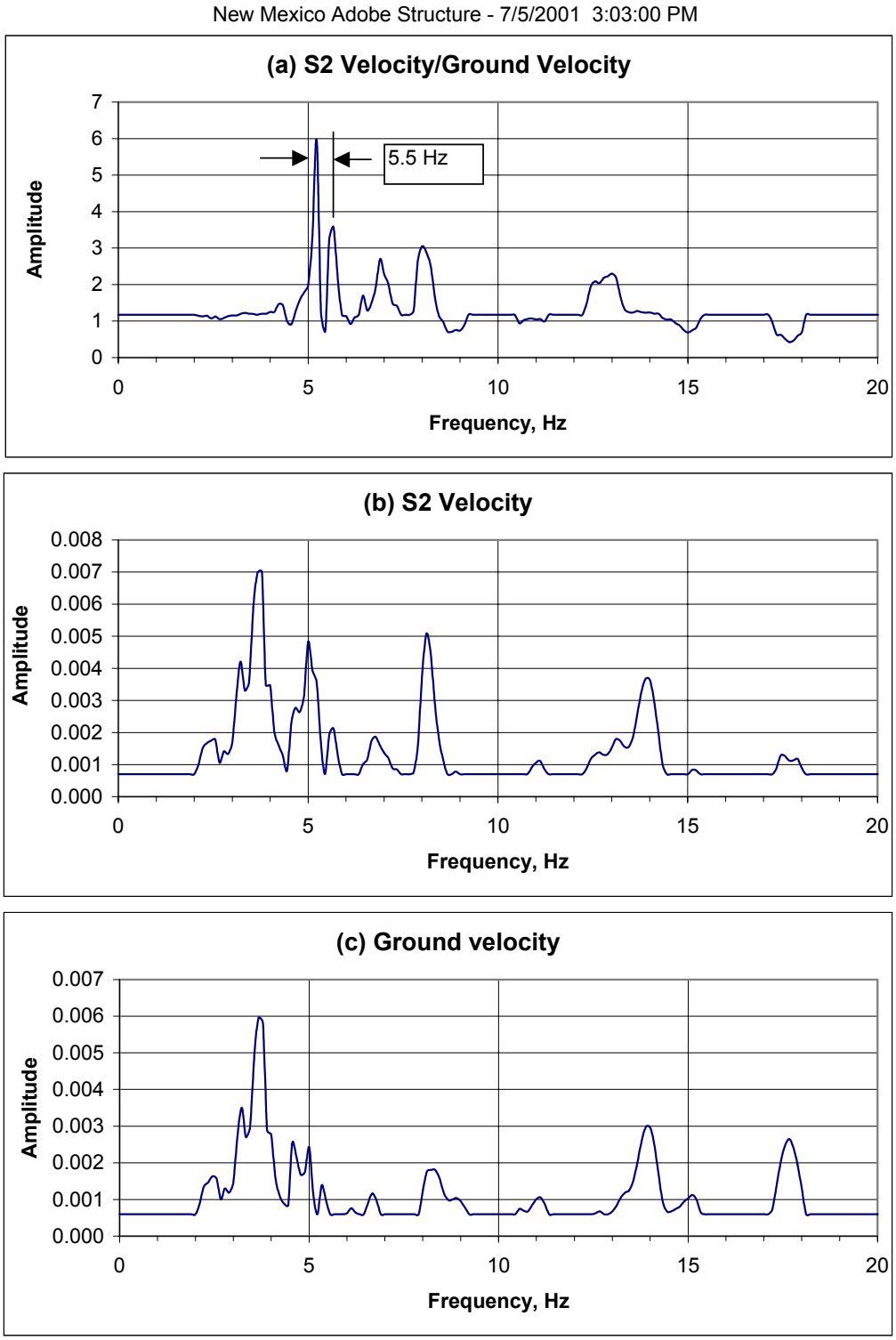

Figure 4.11 FFT superstructure response ratio, S2 response FFT, and ground motion FFT for 5 July blast

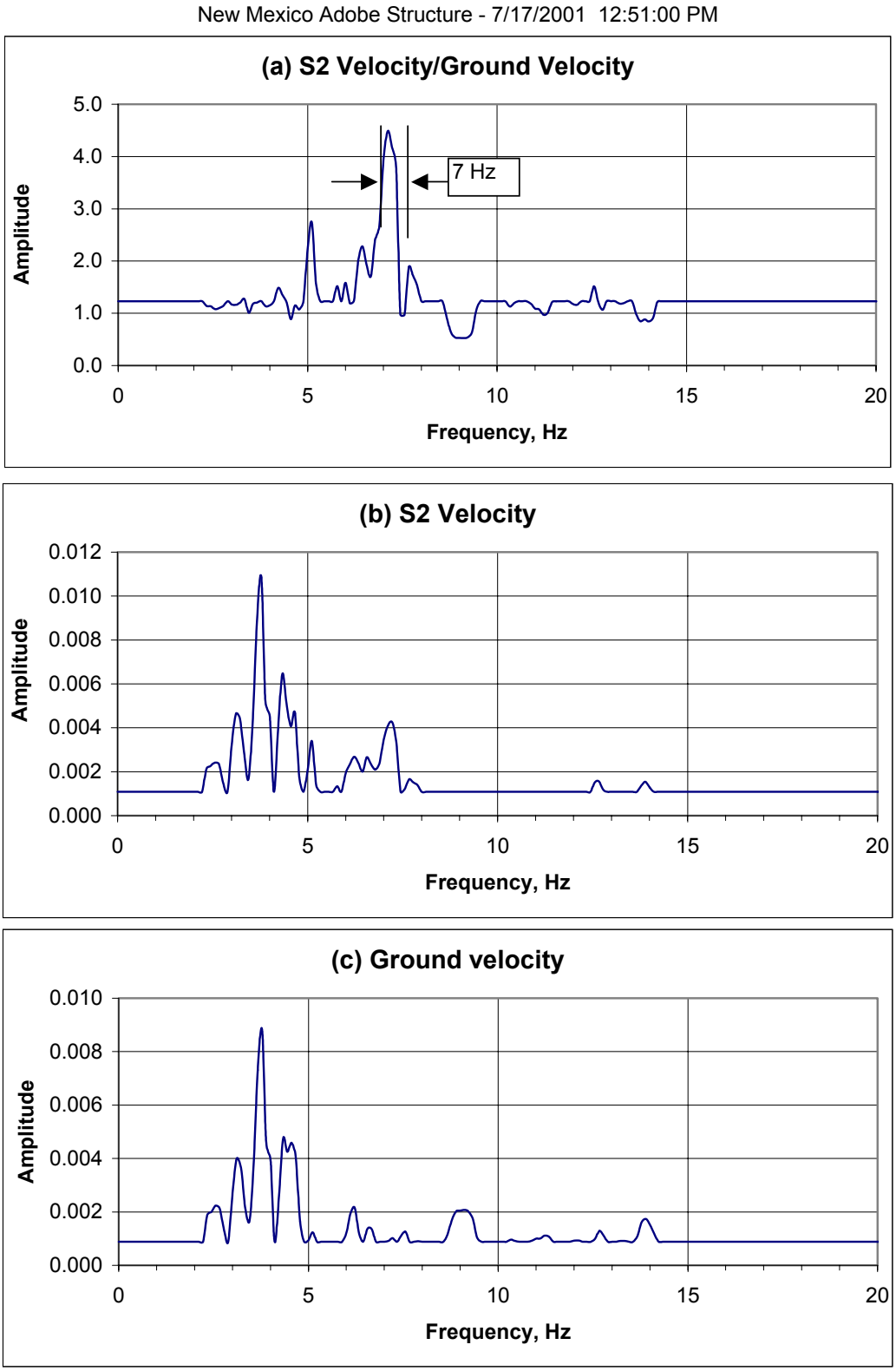

Figure 4.12 FFT superstructure response ratio, S2 response FFT, and ground motion FFT for 17 July blast

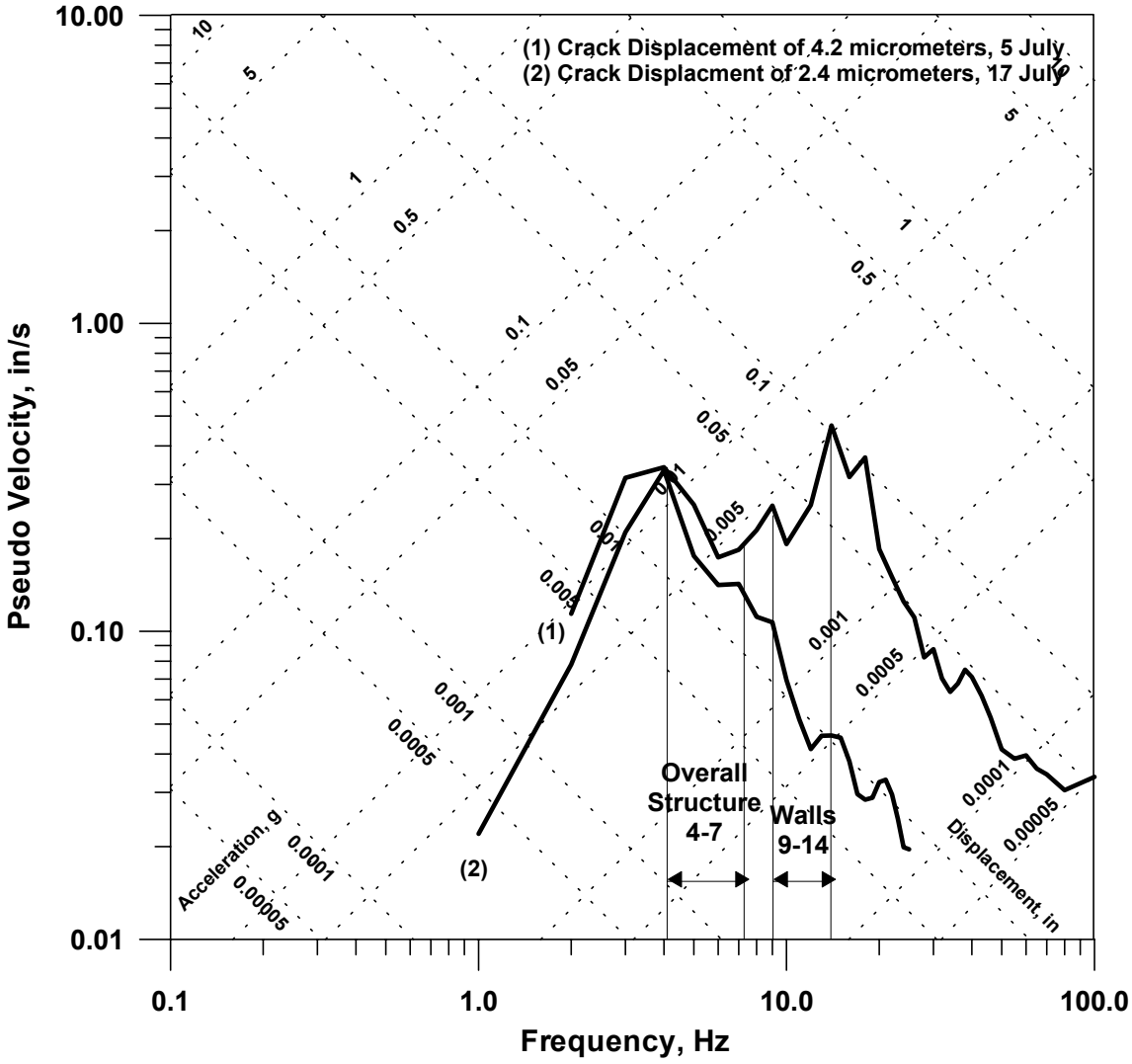

Figure 4.13 Single Degree of Freedom response spectrum of radial motion produced by maximum blast on 7/5/01 at 15:03 and an average blast on 7/17/01 at 12:51, showing estimated relative displacements for the superstructure and the wall

Crack Response to Environmental Effects

Figure 4.14 compares the long-term action of weather indicators (temperature and humidity) with the long-term crack response. 24-hour averages of temperature, crack displacement, and humidity were computed as they were in Chapter 3. Since the monitoring period covered a significant amount of time, actual patterns of temperature, crack displacement, and humidity were observed.

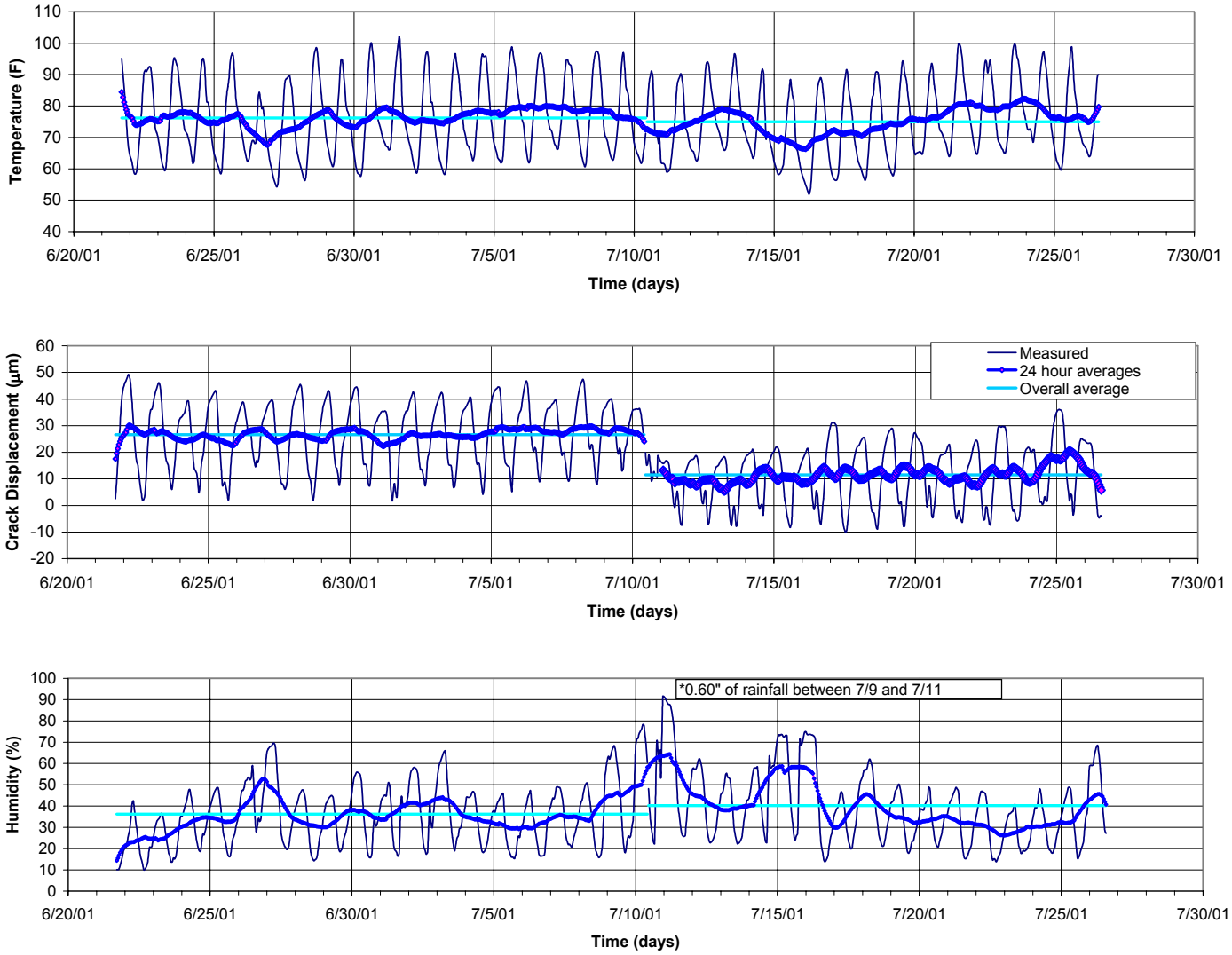

Figure 4.14 Long-term crack displacement and weather versus time

The 24-hour average temperature fluctuated mainly within the 70 to 80 degree range (21.1 to 26.7 C) during the monitoring period, dipping below and above twice, respectively. The temperature exhibited daily changes of 40 degrees Fahrenheit (4.4 °C) between the morning and evening hours. The 24-hour humidity was more variable. Typical daily changes in humidity were around 30%. Four significant increases in humidity, relative to the rest of the data, occurred during the monitoring period - the most significant occurring between 9 and 11 July. During the night of 11 July, the humidity changed almost 80%. According to NOAA climatological observation records for San Juan County, 0.60 in (15.2 mm) of rain was measured from 9 to 12 July 2001. This is a significant amount of rain for the region and explains the large change in humidity.

The effects of the unusual rain event are also reflected in the 24-hour average crack displacements. Around the time of the significant rainfall, the sensor experienced a permanent shift in readings of approximately 20 μm (790 μin). This change is probably not a response to changes in temperature and humidity, but more likely the result of direct wetting of the adobe or expansion of soil due to increased water content. This is a dramatic change that illustrates the importance of long-term monitoring to facilitate the observation of the effects of change in foundation conditions.

Table 4.2 lists all of the average and maximum values for the frontal, daily, and weather effects; an example of each type is displayed graphically in Figure 4.15. Because of the dramatic shift in crack displacement, effects were based upon two overall averages; before and after the significant rainfall. The temperature and humidity variations were not subdivided, as the shift was not as dramatic. Values of crack response to typical and maximum ground motions associated with coal mine blasts are also included in this table, in order to compare the difference in magnitude between weather-induced and blast-induced crack response.

Table 4.2 Computed crack displacements due to long-term weather phenomena

	Temperature Change (DegF)	Crack Displacement (μin)	Crack Displacement (μm)	Humidity Change (%)
Frontal Effect				
Average deviation of 24 hr average from overall average	3	118	3	8
Max deviation of 24 hr average from overall average	9	354	9	18
Daily effect				
Average of deviations from 24 hr average trend	15	669	17	16
Max deviations from 24 hr average trend	25	984	25	33
Weather Effect				
Average deviations from overall average	15	669	17	16
Max deviations from overall average	24	984	25	38
Vibration Effect				
Typical Ground motion (PPV=0.10 ips)	-	91	2.3	-
Max ground motion (PPV=0.13 ips)	-	165	4.2	-

In Figure 4.15, the crack displacements resulting from different weather phenomena measured over the entire monitoring period are compared to those resulting from blasts. Blast responses are circled on the figure, to locate the relatively small events. The maximum dynamic crack displacement of 4.2 μm or 166 μin (produced by ground motions associated with an average blast from the surface coal mine) is small compared to the average and maximum crack displacements daily and weather effects of 17 and 25 μm (672 and 988 μin). The average dynamic crack displacement experienced during blast events was less than 1/6 of the maximum daily and weather effect crack displacement.

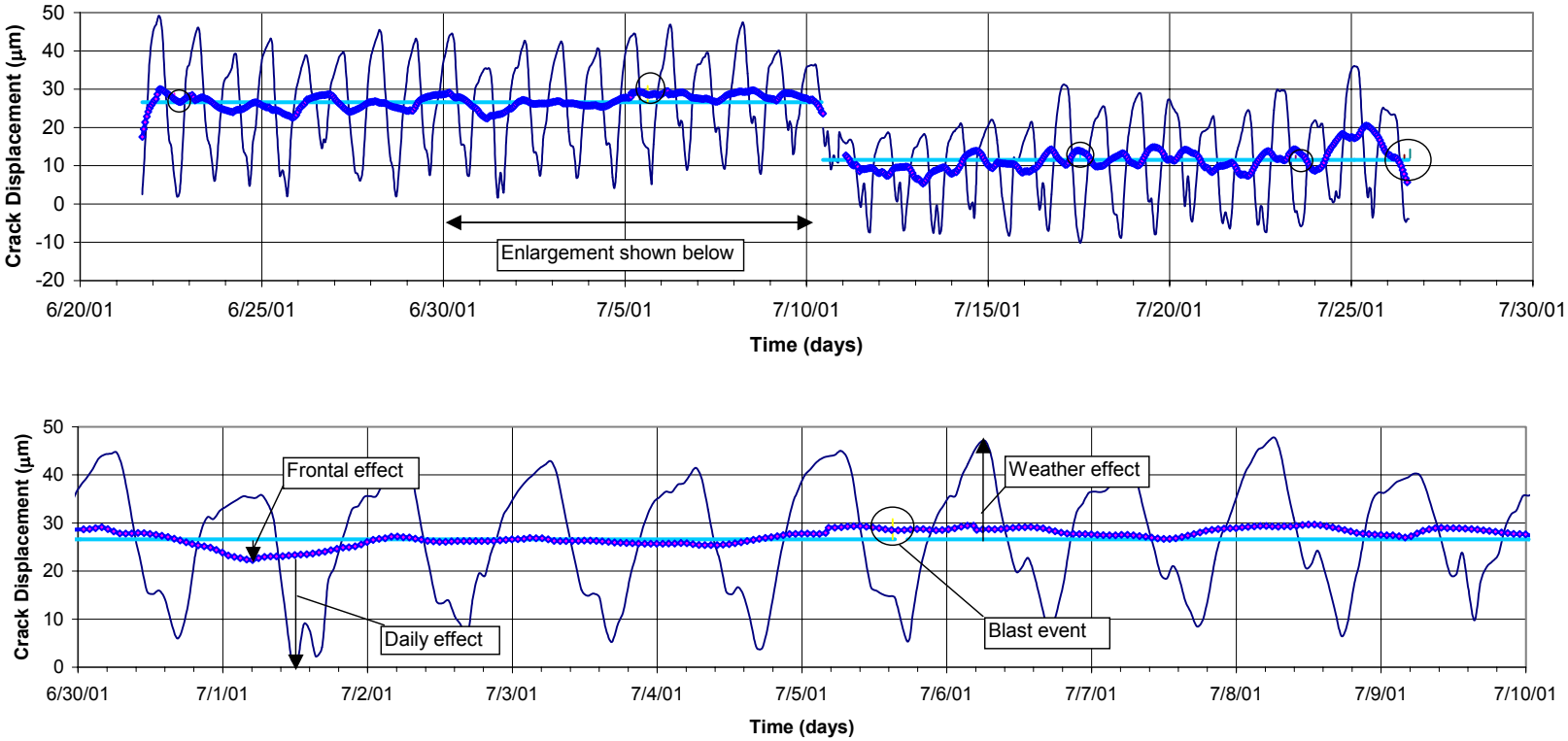

Figure 4.15 Typical crack displacements due to long-term phenomena and maximum zero to peak dynamic blast

Comparisons of computed displacements with measured crack displacement

The maximum measured crack displacement produced by each shot is compared in Table 4.3 to various computed wall displacements based on structure responses, and peak ground motion measured in the direction parallel to the cracked wall. All responses analyzed were those in the radial direction. All comparisons are presented graphically in Figures 4.16 and 4.17. Details of the methods used to compute displacements are presented in Chapter 3.

The best correlation found was that between the measured crack displacements and the approximated relative displacements, $\delta(S2)-\delta(S1_{max})$ (R^2=0.91). This comparison is shown in Figure 4.17 (d). Correlations between the measured crack displacements and the displacements from the difference of integrated velocities, S1-S2, as well as those correlations with the displacements estimated from response spectra for the 10 to 15 Hz wall frequency range, were also high (R^2=0.86 and R^2=0.81, respectively). These correlations are displayed in Figure 4.16 (a) and (e), respectively. A higher correlation was found with the average relative displacements from the SDOF, than with the relative displacements corresponding the dominant frequency of the structure. The correlation found with the estimated displacements for a 5 Hz dominant frequency was very poor, reinforcing the conclusion that the dominant frequency of structural components responsible for crack deformations are in the 10 to 15 Hz range.

Table 4.3 Summary of computed and measured displacements

Date of Shot	Relative displacement, δ, of structure by method (μin)						Peak ground motion in the radial direction (μin/sec)	Measured crack displacement (μin)
	Integration of Velocities			δ from SDOF method	Approximation with $\delta = V/2\pi f$			
	$(S2-S1)_{max}$	$(S2-G)_{max}$	G_{max}	From response spectra for f_n of 5 Hz Average of 10 <f_n<15 -	Estimated from V and f at G_{max} $S2_{max}$ G_{max} and $S2_{max}$	Estimated from V and f at $S1_{max}$ $S2_{max}$ $S1_{max}$ and $S2_{max}$		
6/22/01 14:20	1660	9890	4535	9802 3810	11410 7470 4358	572 1725 1290	0.24	90
6/26/01 15:57	170	715	320	505 388	446 396 11	171 189 165	0.19	13
6/28/01 15:03	420	3755	1710	3446 422	3482 3873 435	252 448 448	0.32	22
7/3/01 13:48	410	4900	2320	4260 630	4829 3854 362	62 62 62	0.20	22
7/5/01 15:03	1940	8730	3885	8207 3919	2091 6885 2322	205 2443 1728	0.24	167
7/17/01 12:51	1630	10900	5040	9193 3226	6875 7945 559	721 1900 134	0.19	94
7/23/01 11:22	900	6290	3150	5593 698	6131 5572 366	75 310 310	0.32	38
7/26/01 11:04	960	9470	3150	7703 673	9218 9417 928	928 928 928	0.20	55
7/26/01 14:55	1140	4280	3150	3721 2275	528 3728 1131	506 1191 848	0.20	91

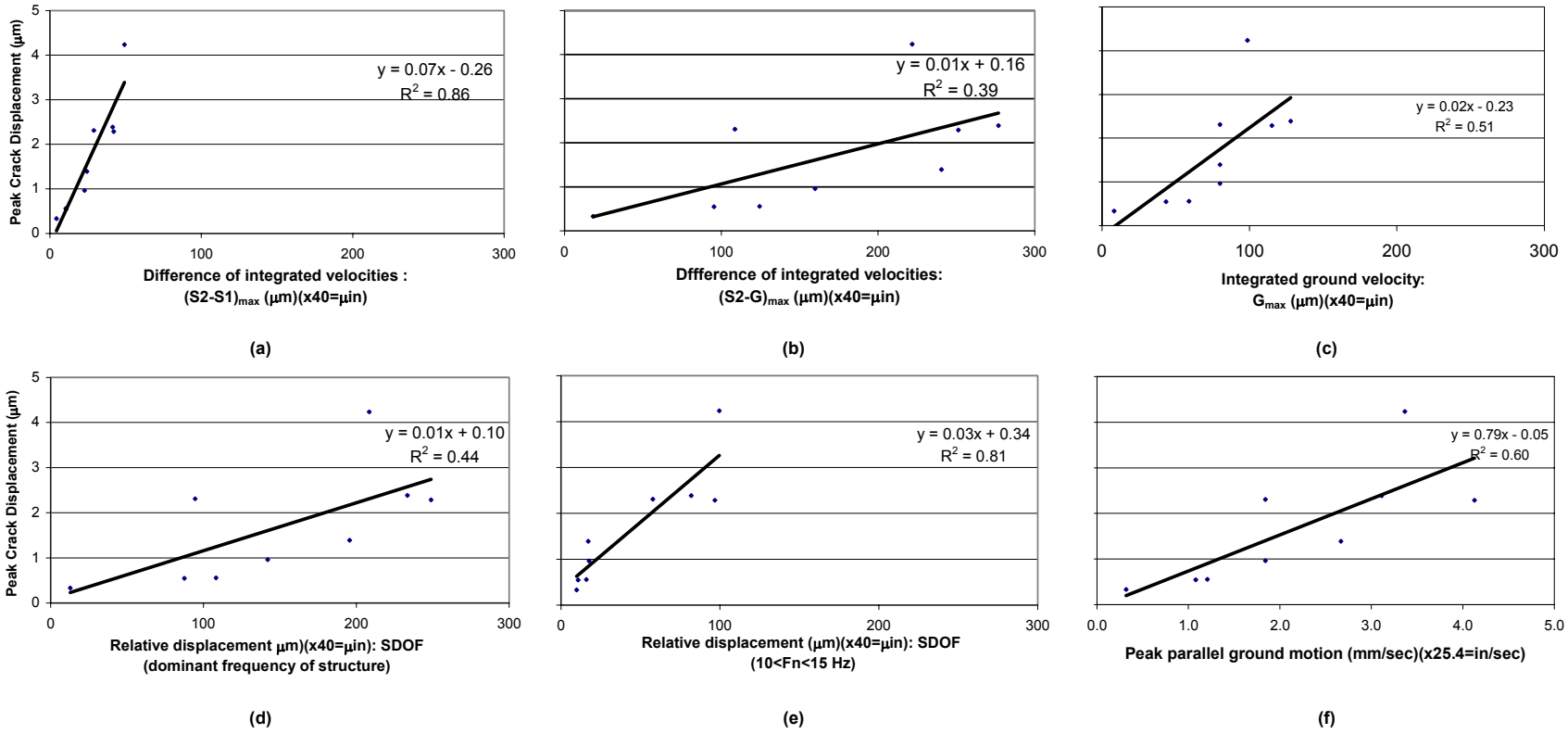

Figure 4.16 Correlations between measured crack displacements and computed displacements and peak radial ground motions

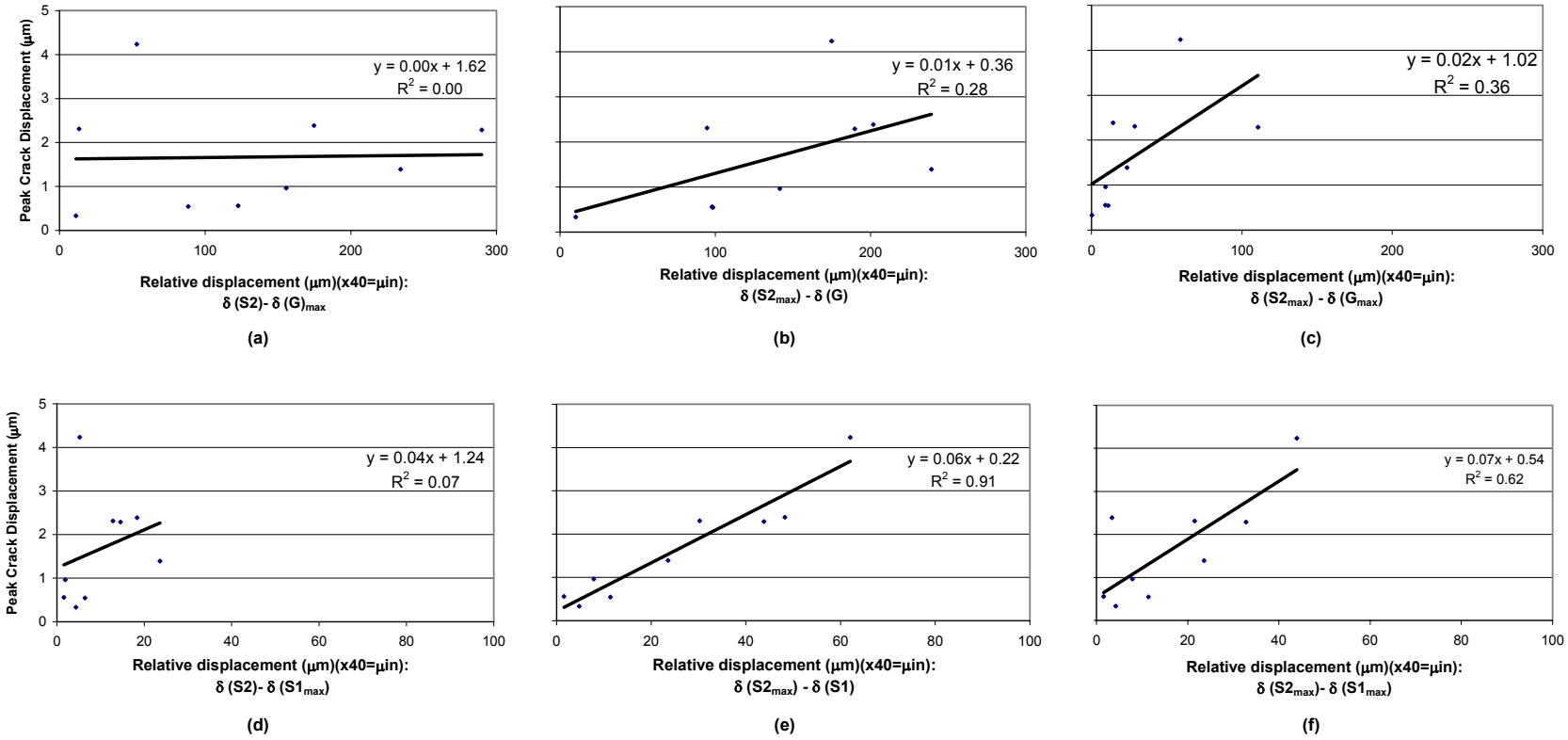

Figure 4.17 Correlations between measured crack displacements and computed relative displacements

CHAPTER 5

CONCRETE BLOCK FOUNDATION – INDIANA 1

The Indiana (1) structure, shown in Figure 5.1, is a one-story residential bungalow with a basement, located approximately 1500 ft (457 m) east of a surface coalmine in Francisco, Indiana. Data collected on-site from 18 to 21 August 2001 are summarize in Table 5.10. Four blasts with maximum charge weights/delay between 150 and 584 lbs (68 and 265 kg) produced ground motions of 0.04 and 0.23 ips (1.0 and 5.8 mm/sec), maximum structure responses of 0.06 and 0.29 ips (1.5 and 7.4 mm/sec), and maximum wall responses of 0.19 and 0.51 ips (4.8 and 13.0 mm/sec). Weather data varied cyclically each day with outside temperatures ranging between 59 and 89 °F (15 and 31.7 °C) and outside humidity ranging between 41 and 99%.

Figure 5.1 Indiana house 1

Table 5.1 Summary of structural and crack response for bungalow in Indiana

Time of Blast	Distance	Charge Weight/ Delay	Scaled Distance	Peak Particle Velocity (ips)			Structure response in S1 cluster (ips)		Structure response in S2 cluster (ips)		Midwall responses (ips)		Air Blast	Measured Crack Displacement on masonry block (μin)
	(ft)	(lb)	($ft/lb^{1/2}$)	Vertical	Radial	Transverse	Radial	Transverse	Radial	Transverse	Radial	Transverse	(dB)	
8/18/01 17:33	1439	451	67.8	0.16	0.18	0.23	0.13	0.26	0.21	0.23	0.51	0.47	117	11
8/19/01 13:27	1906	584	78.9	0.09	0.13	0.18	0.14	0.21	0.29	0.15	0.44	0.29	112	7
8/20/01 12:30	3540	451	166.7	0.04	0.05	0.07	0.04	0.08	0.06	0.08	0.19	0.22	116	4
8/20/01 16:05	1035	150	84.5	0.12	0.21	0.20	0.13	0.23	0.20	0.17	0.49	0.47	118	10

Structure Description

As shown by plan and elevation drawings in Figures 5.2 and 5.3, the structure is approximately 22 feet wide by 40 feet long (6.7 x 12.2 m). It is a one-story structure, eight feet (2.4 m) in height, with a basement approximately eight feet in height. The exterior of the structure is covered with aluminum siding; the interior walls, approximately six inches (152 mm) thick, are paneled and covered with wallpaper. The basement walls are constructed of standard-sized concrete masonry blocks.

Location of instrumentation

Locations of all instruments are shown in Figures 5.2 and 5.3. The velocity transducers were installed on and outside of the southeast corner of the structure, closest to the mining activity. The Kaman crack displacement sensor was located on the north side of the structure, on the exposed concrete block foundation, as shown in Figure 5.4. Further details on placement and description are given in Chapter 2.

The foundation of the structure extends above the ground surface on the western end of the structure. The sensor was attached to the foundation for a number of reasons. The interior walls were all paneled and wallpapered without any cracks to instrument. The exterior walls were covered with aluminum siding. Crack response on concrete blocks had not been measured in this study. The monitored crack was chosen because it cut across a unit and appeared to be the most recent and active compared to others observed on the foundation units. The approximate width of the crack is 500 μm (19,800 μin). As shown in Figure 5.4, it is located approximately 2 feet (0.6m) above the porch deck (3 to 4 ft, or 0.9 to 1.2 m, from the ground surface), to the right of the porch screen door. A close-up of the crack can be seen in the inset of Figure 5.4.

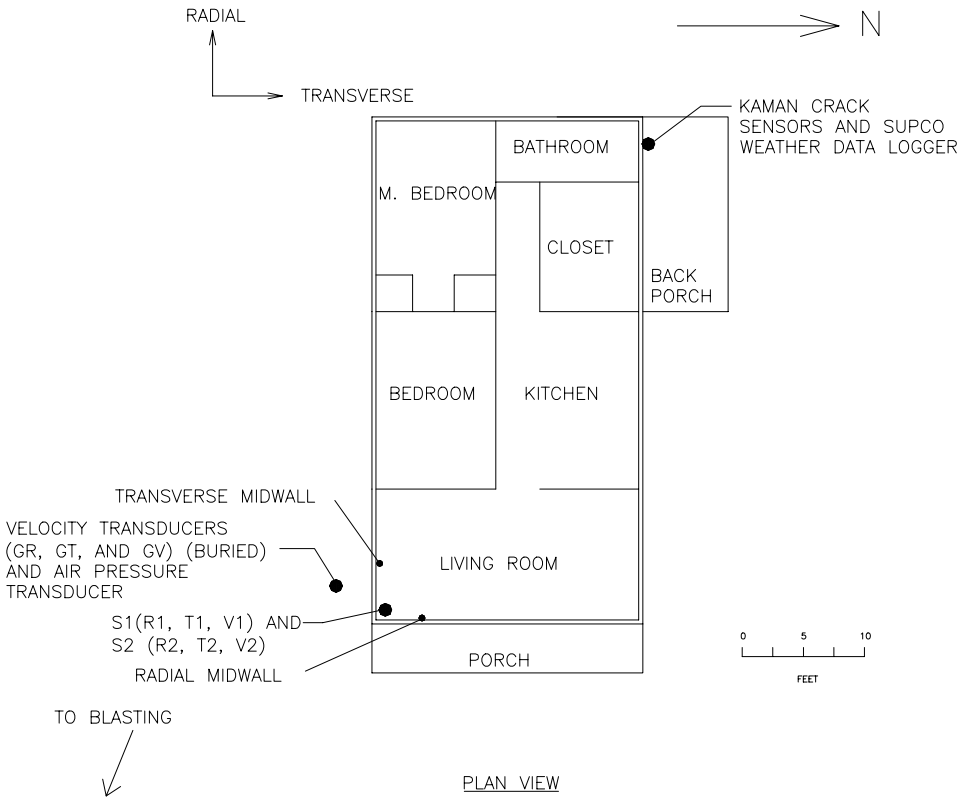

Figure 5.2 Plan view of Indiana house 1

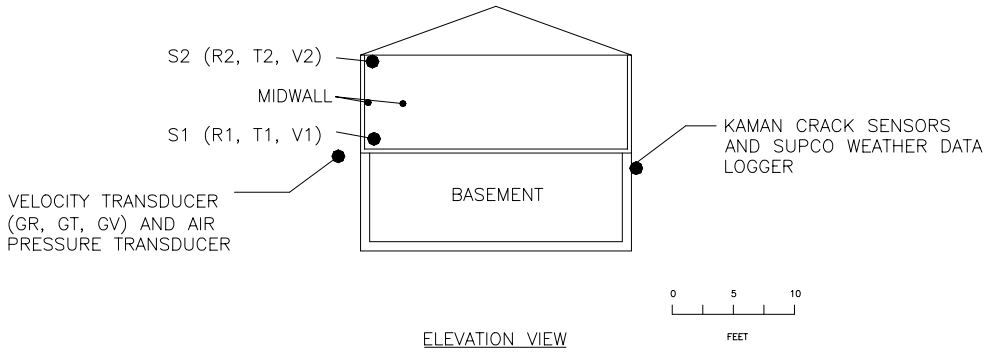

Figure 5.3 Elevation view of Indiana house 1

In addition to the Kaman crack displacement sensor, a Kaman null sensor was also employed on a non-cracked section nearby the crack on the same concrete block unit. The null sensor allowed an in-situ comparison of the instrument response and crack response. This second, "null" sensor can be seen, to the right of the crack sensor, in the magnified inset in Figure 5.4. As described in the introduction, the null response is that of only the material and the sensor itself.

A Supco temperature and humidity datalogger, the same used in all of the OSM studies, was placed to the right of the Kaman sensors and can be seen in Figure 5.4.

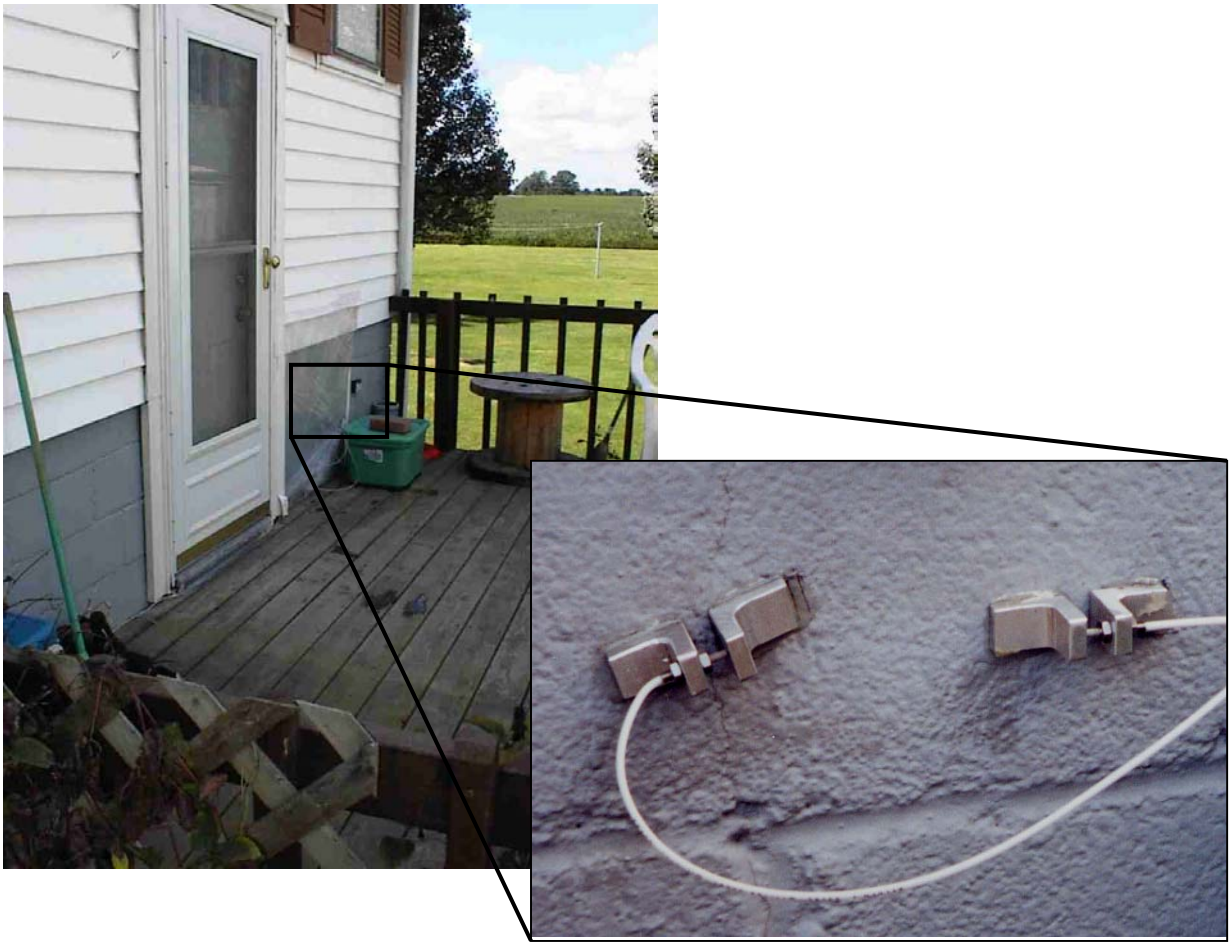

Figure 5.4 Kaman crack displacement sensors and Supco weather logger

For each blast, time histories were collected from the eleven velocity transducers inside and outside of the house for a total of thirteen (13) seconds. Time correlated (within 1/1000 second) time histories of dynamic crack displacements were also collected from the Kaman sensors for twelve (12) seconds.

Structure and crack responses to household events were not observed. The crack was located in the opposite corner of the house from the velocity transducers. Thereby eliminating the possibility of comparing the two different responses to localized household activities.

Transient Responses

Figure 5.5 shows velocity time histories of excitation ground motions and structure responses, compared to the crack response, associated with the blast on 18 August 2001 at 17:34; as shown, this blast produced a peak crack displacement of 0.29 μm (11.5 μin) and a peak radial ground motion of 0.18 ips (4.6 mm/sec). This blast event produced a typical crack response, representative of those measured during the monitoring period.

In Figure 5.6, the time histories of all three components of ground motion, along with the air blast response are compared to the crack response. In addition the lower corner, S1, response of the structure, both radial and transverse, are also shown. Lower response is compared in this case, because the crack is in the foundation rather than the superstructure. All significant structure response, as well as air blast response, occurred within the first seven seconds.

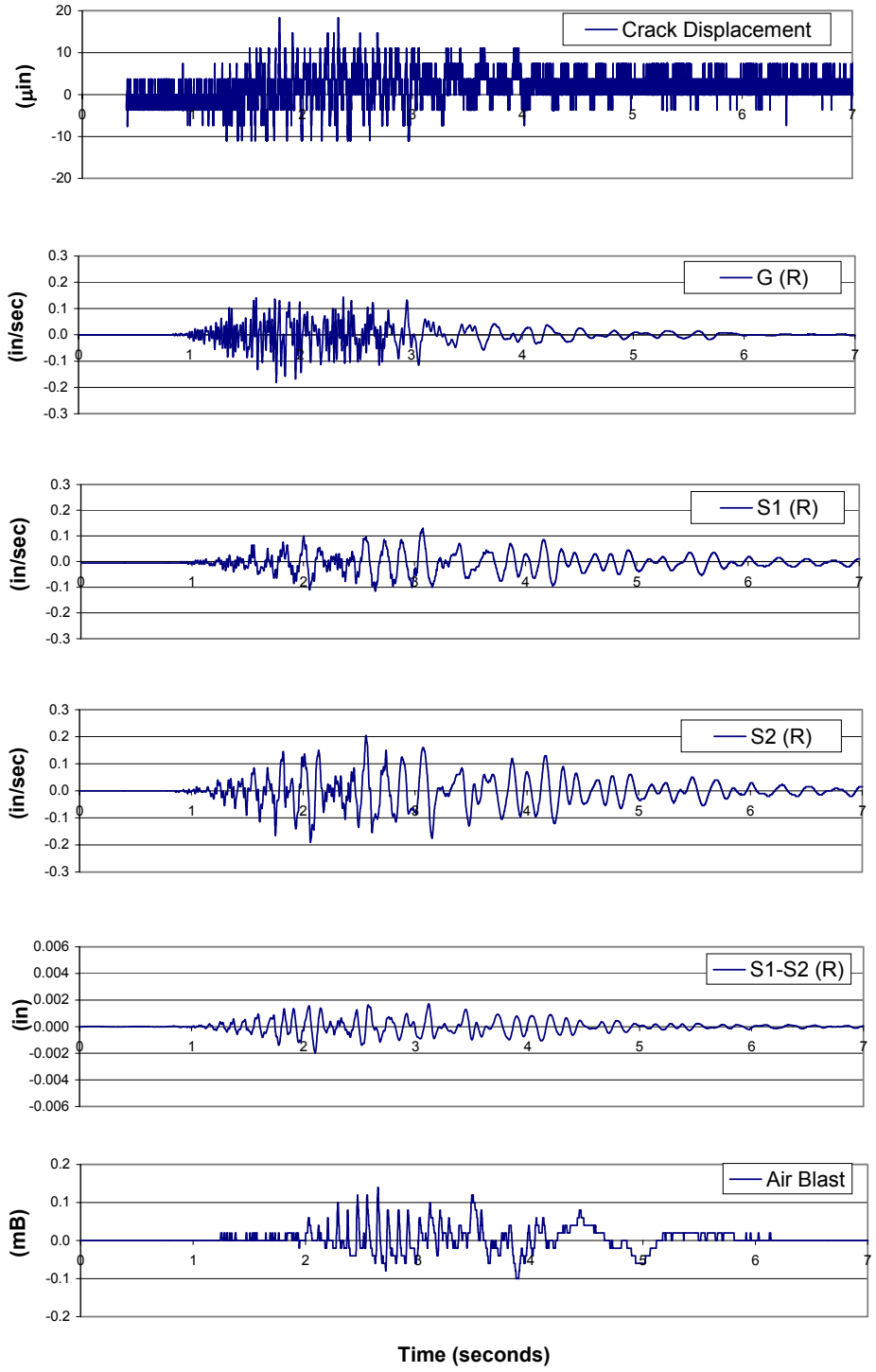

Figure 5.5 Time history of crack displacement on 18 August at 17:34 compared to ground excitation, S1 and S2 response, calculated relative displacement of structure (R1-R2), and air blast

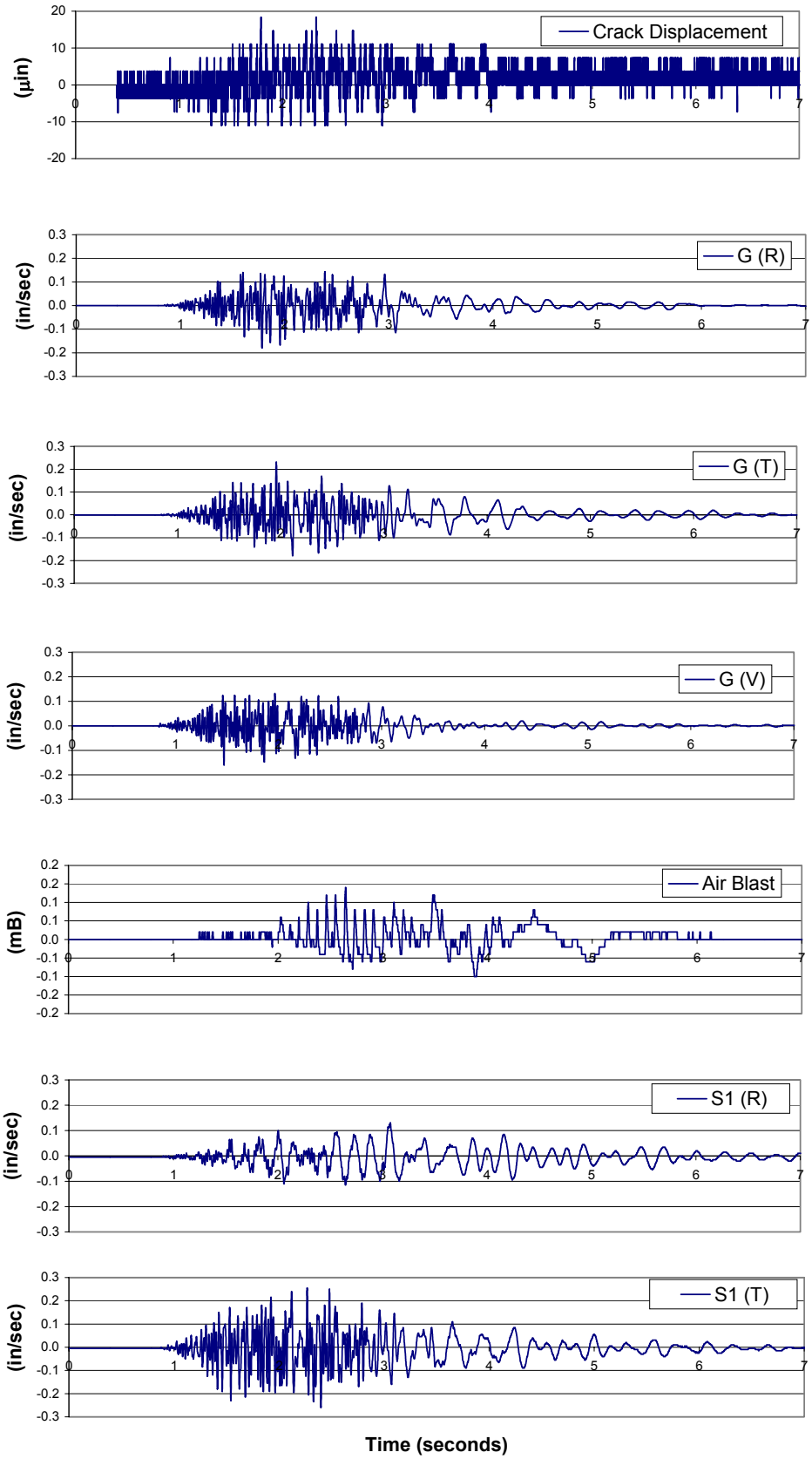

Figure 5.6 Time history of crack displacement compared to ground excitation in the radial, transverse, and vertical directions, air blast response, and S1 radial and transverse structure response (18 August)

The dominant frequency of the structure was estimated using both the zero-crossing method and FFT method. Details on these methods can be found in Chapter 3. The dominant frequency of the structure was computed as 6 Hz using the zero-crossing method, and 9 Hz using the FFT method. The dominant frequency of the structure was taken to be 9 Hz, because that value resulted in stronger correlations with the measured crack displacement, and it was within the typical response range of one-story residential structures. Plots of the computed FFT ratios can be found in Appendix A.

The response spectrum of the radial ground motion, from the blast on 18 August 2001 at 17:33 is displayed as Figure 5.7. The estimated relative displacement from this ground motion relative to the computed dominant frequency of the structure, was 5800 μin (148 μm), as shown by the intersection of the vertical 9 Hertz line with the response spectrum.

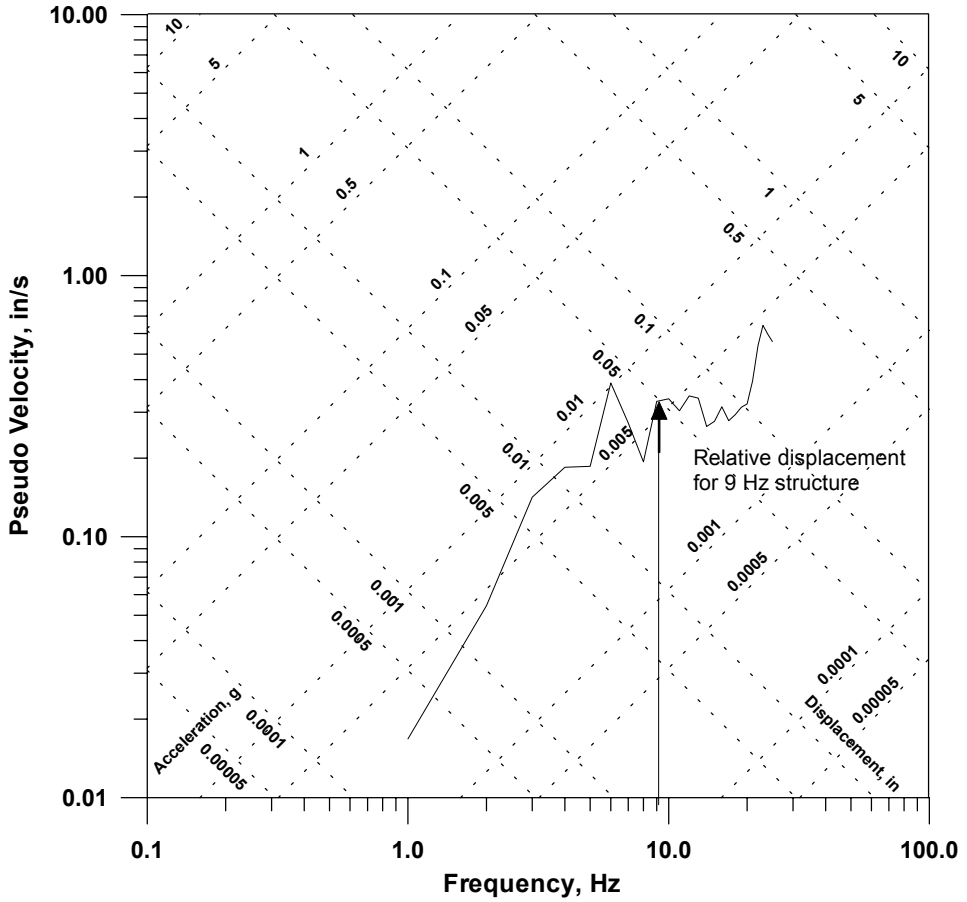

Figure 5.7 Single Degree of Freedom response spectrum of radial motion produced by blast on 8/18/01 at 17:34, showing the estimated relative displacement of a 9 Hz structure

Crack Response to Environmental Effects

Figure 5.8 compares the long-term action of weather indicators (temperature and humidity) with the long-term crack response. 24-hour averages of temperature, crack displacement, and humidity were computed as they were in Chapter 3. Data were only collected during a three-day period, therefore, significant long-term trends were not exhibited. The 24-hour averages of the temperature and the corrected crack displacement remain relatively constant, but the 24-hour averages of humidity show a slight decrease during the monitoring period. The higher average humidity values at the start of the monitoring period is most likely a result of the 0.44 in (11.2 mm) of rain that fell on 18 August 2001 (NOAA); this was the only significant precipitation during the monitoring period.

Table 5.2 lists all average and maximum values for frontal, daily, and weather effects for temperature, corrected crack displacement, and humidity. Corrected crack displacements, as opposed to displacement measured from the crack sensor exclusively, were included in the table even though values were the same or nearly the same. Values of corrected crack response to typical and maximum ground motions associated with coal mine blasts are also included in this table, in order to compare the difference in magnitude between weather-induced and blast-induced crack response.

Table 5.2 Computed crack displacements due to long-term weather phenomena

	Temperature Change (F)	Corrected Crack Displacement (μin)	Corrected Crack Displacement (μm)	Humidity Change (%)
Frontal Effect				
Average deviation of 24 hr average from overall average	2	79	2	5
Max deviation of 24 hr average from overall average	3	118	3	5
Daily effect				
Average of deviations from 24 hr average trend	7	276	7	15
Max deviations from 24 hr average trend	12	354	9	26
Weather Effect				
Average deviations from overall average	7	315	8	13
Max deviations from overall average	11	472	12	31
Vibration Effect				
Typical Ground motion (PPV=0.10 ips)	-	8	0.2	-
Max ground motion (PPV=0.23 ips)	-	12	0.3	-

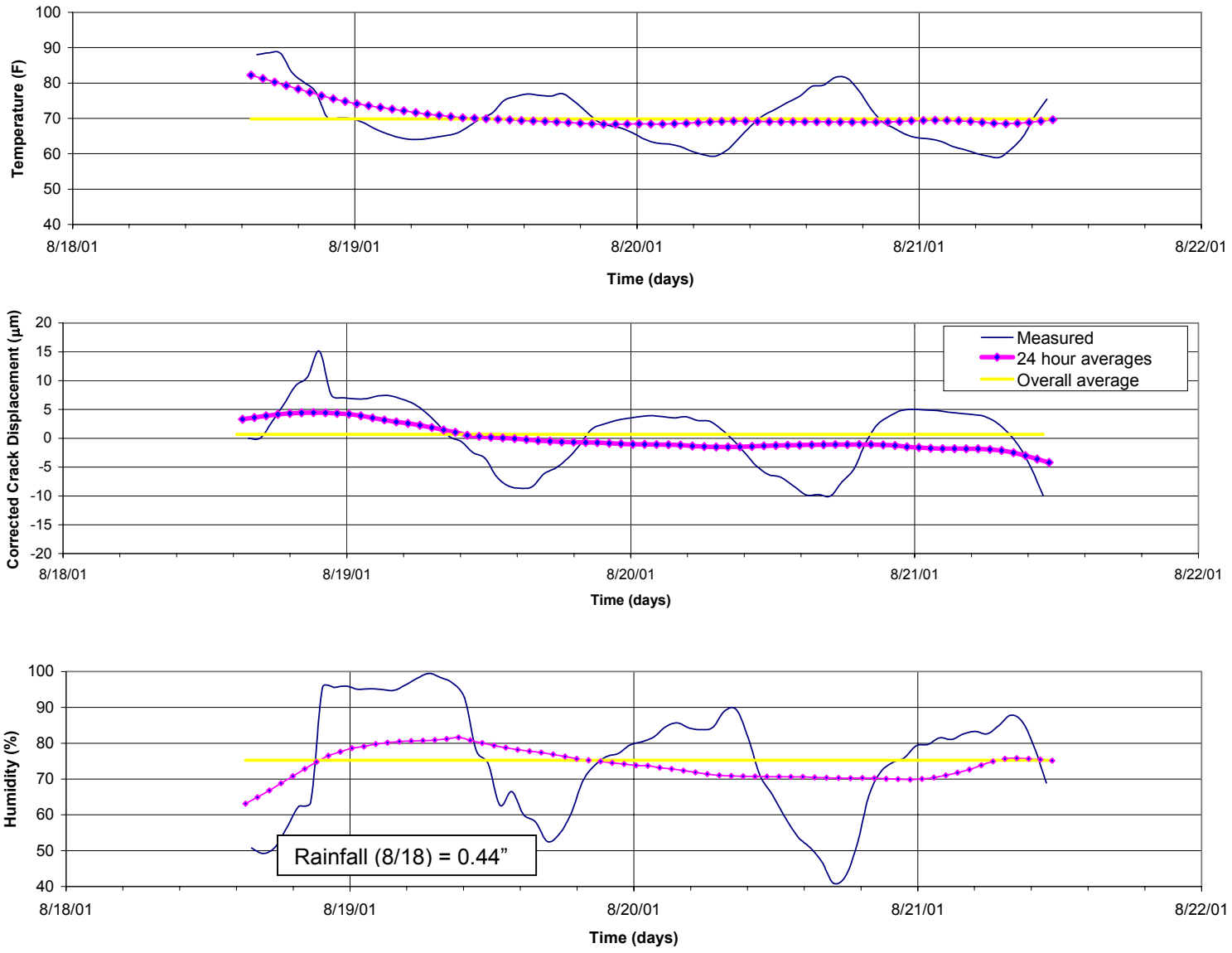

Figure 5.8 Long-term crack displacement and weather versus time

In Figure 5.9, the crack displacements due to different weather phenomena over the entire monitoring period are compared to those due to the blasts. The responses due to the blasts are so minuscule, they cannot be identified by eye on the plot; these blasts are enclosed within the circles on the figure. In comparison, the largest blast vibration of 0.23 ips (5.8 mm/sec) induced a maximum crack displacement of 0.29 μm (11.5 μin), which was less than 1/30 of the maximum weather response of 12 μm (490 μin).

In Figure 5.10, the crack displacements of the null and crack sensors as well as the corrected crack displacements are shown. The purpose of the null sensor is to provide information regarding temperature effects and drift of the sensor itself. It is attached to the uncracked material to incorporate the uncracked material response as well. As can be seen, little to no displacements were recorded by the null sensor. Nonetheless, these displacements were subtracted from the crack sensor displacements and used as the appropriate displacements for this study.

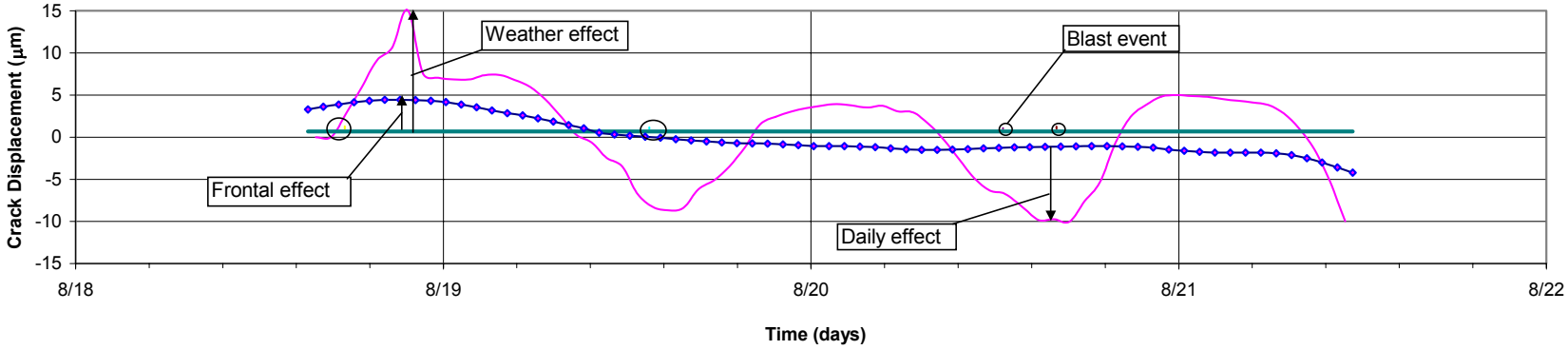

Figure 5.9 Typical crack displacements due to long-term phenomena and maximum zero to peak dynamic blast events

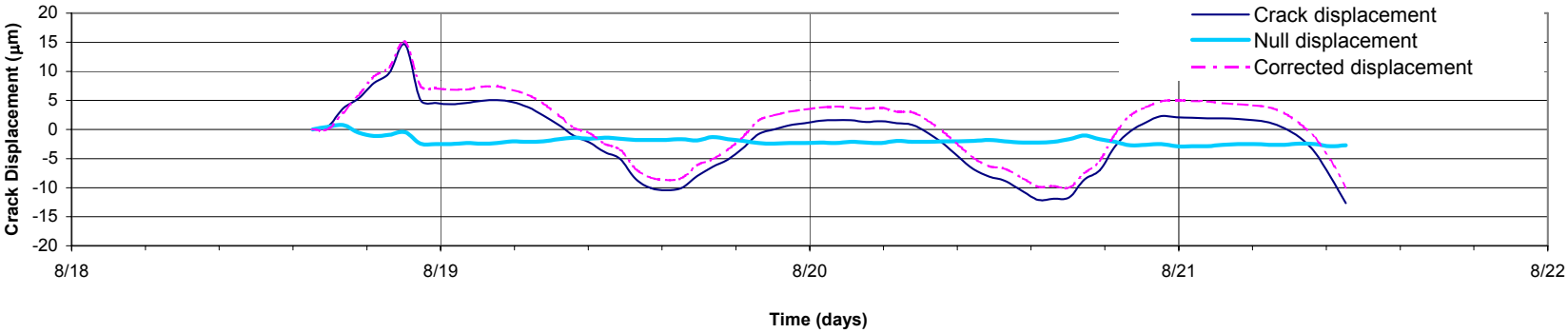

Figure 5.10 Long-term displacements of both crack and null sensors and the resulting corrected crack displacement

Comparisons of computed displacements with measured crack displacement

The maximum measured crack displacement produced by each shot is compared in Table 5.3 to various computed wall displacements based on structure responses, and peak ground motion measured in the direction parallel to the cracked wall. All responses analyzed were those in the radial direction. All comparisons are presented graphically in Figures 5.11 and 5.12. Details of the methods used to compute displacements are presented in Chapter 3.

There were no significant correlations between predicted relative displacements and measured crack displacements. The largest correlation was found from the relationship between measured crack displacement and peak radial ground motion (regression coefficient of R^2=0.90), shown in Figure 5.11 (f). The regression values resulting from the relationships between measured displacements and SDOF relative displacements were computed as R^2 =0.62 and R^2=0.67. These relationships are shown in Figure 5.11 (e) and (f), respectively. The lowest regression coefficients were produced by the relationships with approximated relative displacements. The highest coefficient among all six approximated relative displacements was R^2=0.56, for the non-time correlated between S2 and G ($S2_{max}$-G_{max}), as shown in Figure 5.12 (c).

Given the location of the crack, little correlation would be expected with the same measures found with other structures. The methods of computed displacement all incorporate the assumption that the crack is located in the superstructure. This crack was located in the foundation, and response would be expected to correlate with ground strain. As described by others (Dowding 1996), ground strain is proportional to the peak particle velocity. As was mentioned above, the highest correlation was found between the measured crack displacement and the ground motion, which further supports these expectations.

Table 5.3 Summary of computed and measured displacements

Date of Shot	Relative displacement, δ, of structure by method (μin)						Peak ground motion in the radial direction (μin/sec)	Measured crack displacement (μin)
	Integration of Velocities			δ from SDOF method	Approximation with $\delta = V/2\pi f$			
	$(S2-S1)_{max}$	$(S2-G)_{max}$	G_{max}	From response spectra for f_n of 9 Hz Average of $10 < f_n < 15$ -	Estimated from V and f at G_{max} $S2_{max}$ G_{max} and $S2_{max}$	Estimated from V and f at $S1_{max}$ $S2_{max}$ $S1_{max}$ and $S2_{max}$		
8/18/01 17:33	1970	5470	2690	5836 4075	2218 4369 2269	1078 2435 1449	0.24	11
8/19/01 13:29	2980	7190	3780	6810 3803	3328 5722 2187	1663 3078 2463	0.19	7
8/20/01 12:30	750	1570	1020	851 1149	647 1003 346	388 726 1229	0.32	3
8/20/01 16:05	2470	4430	2400	7811 6389	79 1928 1530	499 2659 1179	0.20	10

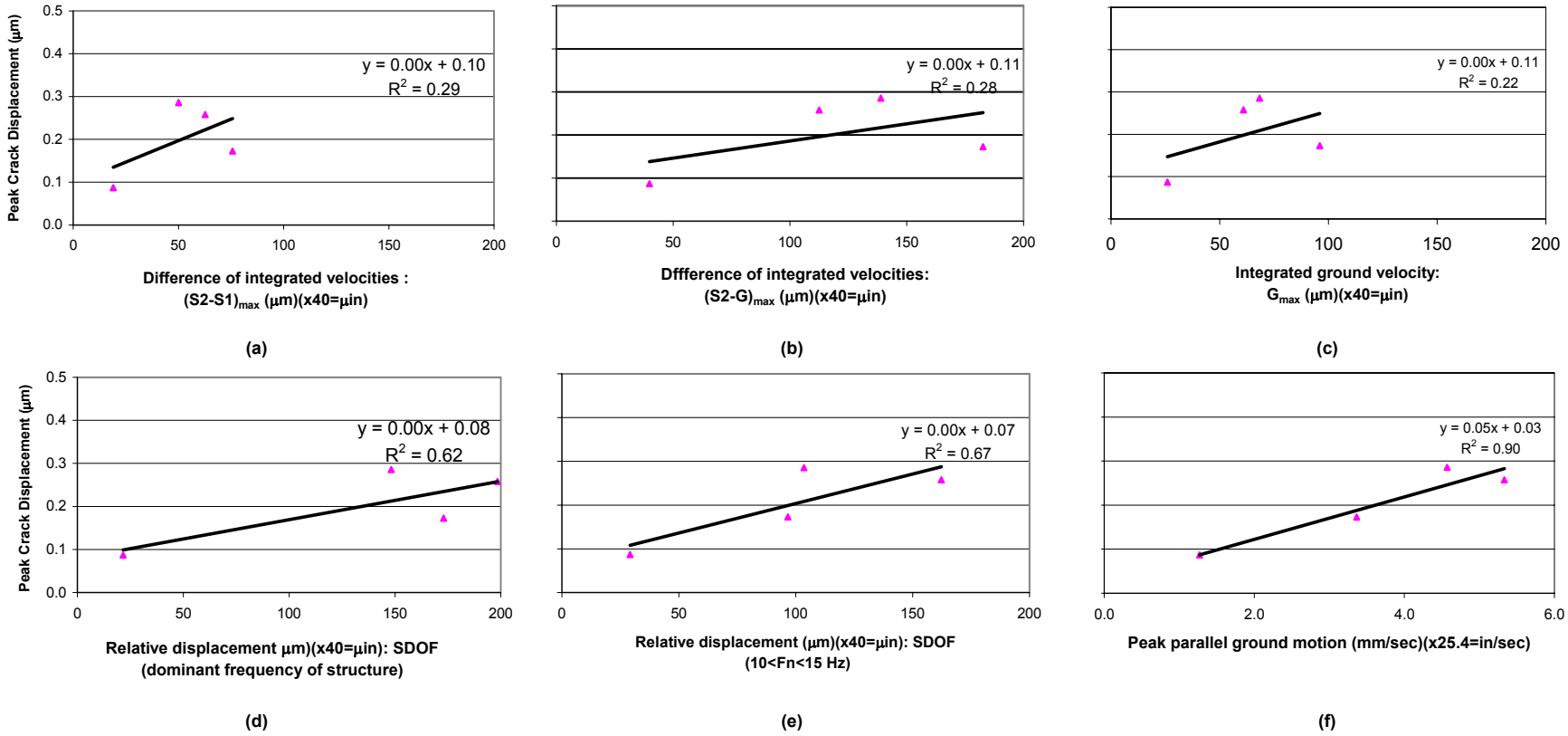

Figure 5.11 Correlations between measured crack displacement and computed displacement and radial ground motion

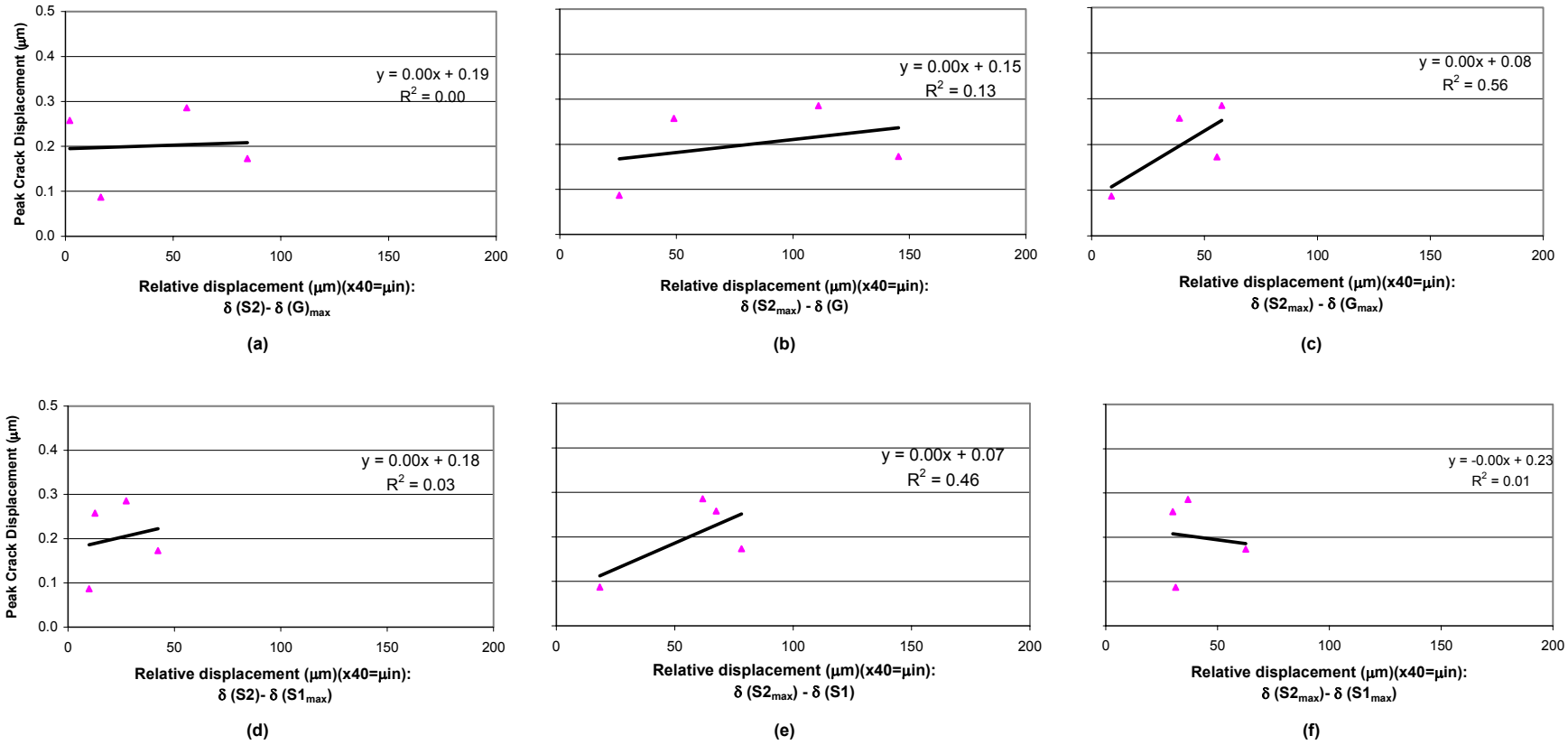

Figure 5.12 Correlations between measured crack displacement and computed relative wall displacements

CHAPTER 6

DISTRESSED FRAME HOUSE – INDIANA 2

The Indiana (2) structure, shown in Figure 6.1, is a one and a half story wood frame house located approximately 3000 ft (914 m) from surface coal mining in Francisco, Indiana. Data collected on site from 22 to 24 August 2001 are summarized in Table 6.1. Four blasts with maximum charge weights/delay between 301 and 1051 lbs (137 and 478 kg) produced ground motions of 0.06 to 0.30 ips (1.5 to 7.6 mm/sec), maximum structure responses of 0.05 to 0.25 ips (1.3 to 6.4 mm/sec), and maximum wall responses of 0.06 to 0.84 ips (1.5 to 21.3 mm/sec). In addition, a number of household activities were simulated in order to obtain comparative structure and crack responses. Weather data varied cyclically each day with inside temperatures ranging between 72 and 89 °F (22.2 to 31.7 °C) and indoor humidity ranging between 54 to 91%.

Figure 6.1 Indiana (2) structure

Table 6.1 Summary of structural and crack response for distressed frame house in Indiana

Time of Blast	Distance	Charge Weight/ Delay	Scaled Distance	Peak Particle Velocity (ips)			Structure response in S1 cluster (ips)		Structure response in S2 cluster (ips)		Midwall response on kitchen wall (ips)		Air Blast	Measured Crack Displacement above kitchen sink (μin)
	(ft)	(lb)	($ft/lb^{1/2}$)	Vertical	Radial	Transverse	Radial	Transverse	Radial	Transverse	Radial - Top	Bottom	(dB)	
8/22/01 17:30	2081	1051	64.2	0.23	0.30	0.28	0.14	0.18	0.24	0.25	0.23	0.84*	126	537
8/23/01 13:00	3730	301	215.0	0.04	0.07	0.06	0.04	0.05	0.05	0.07	0.06	0.05	110	131
8/23/01 17:40	4163	447	196.9	0.05	0.07	0.06	0.05	0.05	0.05	0.07	0.06	0.06	106	101
8/24/01 12:10	3358	301	193.7	0.05	0.06	0.05	0.05	0.06	0.05	0.06	0.06	0.07	114	90

*For the first shot this midwall measured the transverse direction on the west living room wall

Structure Description

As shown by plan and elevation drawings in Figures 6.2 and 6.3, the structure is approximately 28 feet wide and 38 feet long (8.5 x 11.6 m). It is a one and a half story, wood-framed residential structure, 9 feet to 20 feet (2.7 to 6.1 m) high, with a 7-foot (2.1-meter) high basement. The wood-stud, clapboard covered, exterior walls are covered with aluminum siding. They are approximately 6 inches (152 mm) in thickness. The first story interior walls are comprised of plaster and lath and are approximately 4 inches (102 mm) thick. The upper story was left unfinished and did not have any walls, which left all of the structural components exposed. The basement walls were constructed with concrete block masonry units, as shown in Figure 6.4. Two by eights were placed 16 inch (406 mm) center-to-center as floor joists, with cross ties connecting them, to support the structure.

Location of Instrumentation

Locations of all instruments are also shown in Figures 6.2 and 6.3. Eleven velocity transducers were installed on and outside of the southwest corner of the structure, closest to the mining activity. The crack displacement sensor was located in the kitchen above the window looking out at the blasting, as shown in Figure 6.5. Further details on placement and description of the instrumentation are given in Chapter 2.

This crack whose width was estimated from photographs to be approximately 1200 μm (47,400 μin) in width, was chosen for instrumentation because it was on the wall facing the mine and was obviously active. The crack spanned the entire distance (approximately 18 in or 457 mm) from the window frame to the ceiling and was uniformly open for this entire distance. The sensor was placed 5 in (127 mm) above the window frame. Cracking continued on the same wall, underneath the kitchen sink to the floorboard. The wall opposite the instrumented, on the other side of the kitchen, also had similar cracking, spanning from the ceiling to the floorboard, in the same plane of space. Cracking in this location was also apparent on the basement walls. The basement floor slab appeared to have been poured in sections, where the division of the slab lined up with the large crack.

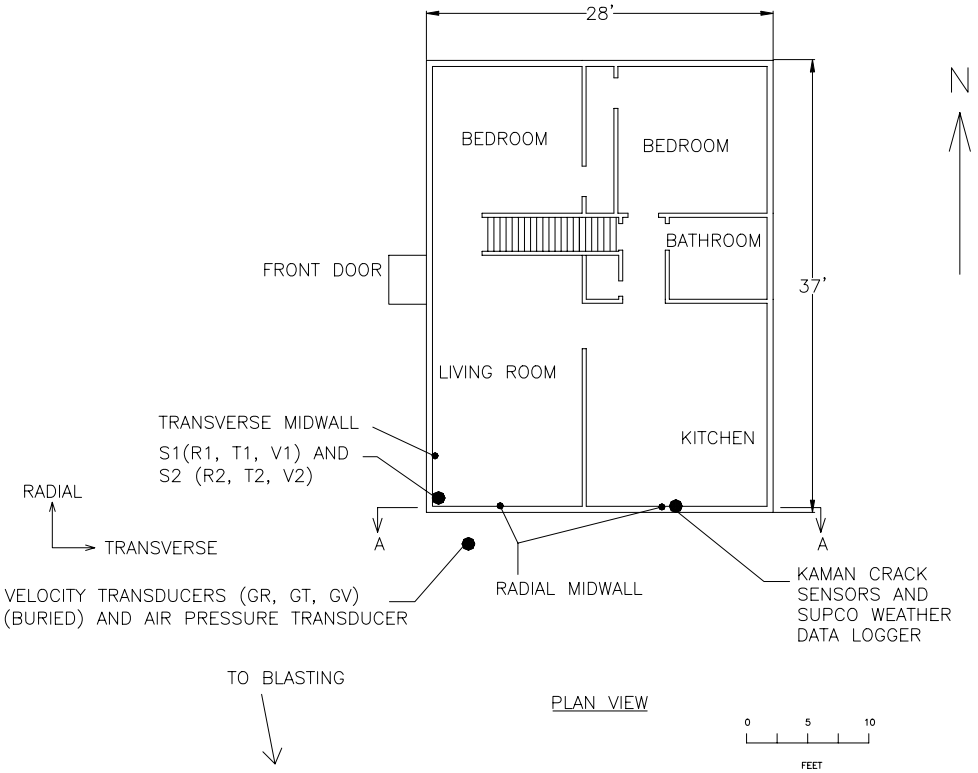

Figure 6.2 Plan view of Indiana house 2

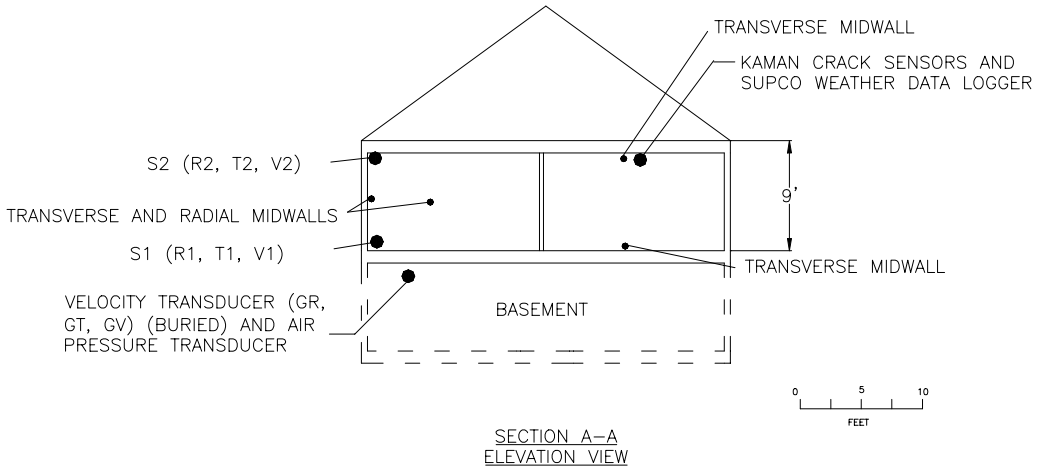

Figure 6.3 Elevation of Indiana house 2

Figure 6.4 Basement walls of Indiana house 2

Figure 6.5 Crack displacement sensors and Supco datalogger

As shown in Figure 6.5, a Kaman "null" sensor was installed nearby an uncracked wall material. The purpose of the null sensor is explained in Chapter 2. The Supco temperature and humidity datalogger was placed adjacent to the displacements sensors, to the right. In addition, two velocity transducers were installed adjacent to the Kaman sensors as well; one measuring the vertical, one measuring the radial. A third radial transducer was attached near the floor in line with the other two transducers.

For each blast, time histories were collected from eleven velocity transducers inside and outside of the structure for a total of twelve seconds. After the first shot, the two midwall transducers were moved into the kitchen, one adjacent to the crack sensor, above the window, and the other right above the floorboard, in line with the other midwall transducer. Time correlated (within 1/1000 second) time histories of dynamic crack displacement were also collected from the Kaman sensor for a total of ten seconds.

Transient Responses

Figure 6.6 shows velocity and displacement time histories of excitation ground motions and structure response, as well as crack response, associated with the blast on 22 August 2001 at 17:30. As shown, this blast produced a peak crack displacement of 13.6 μm (537 μin) and a peak transverse ground motion (parallel to the wall) of 0.25 ips (6.4 mm/sec). Unlike the three previous structures, the crack monitored was not located on a radial wall but rather on a transverse wall, therefore all time histories are those in the transverse direction. This blast produced the largest crack response during the monitoring period, as well, as the largest crack response observed in all four OSM structures. However, it is important to note that this crack was also the largest crack of the four instrumented.

In Figure 6.7, the time histories of all three components of ground motions, along with the air blast response are compared to the crack response (for the same blast). In addition, the upper corner, S2, responses of the structure, both radial and transverse, are also shown.

Figure 6.8 shows velocity and displacement time histories of excitation ground motions and structure response, as well as the crack response, associated with the blast on 23 August 2001 at 13:00; this blast produced a peak crack displacement of 3.3 μm (130 μin) and a peak

transverse ground motion of 0.06 ips (1.5 mm/sec). This crack displacement was more representative of an average crack response. All significant response, including that from the air blast, occurred within the first seven seconds.

In Figure 6.9, the time histories of all three components of ground motions, along with the air blast response are compared to the crack response. In addition, the upper corner, S2, responses of the structure, both radial and transverse, are also shown.

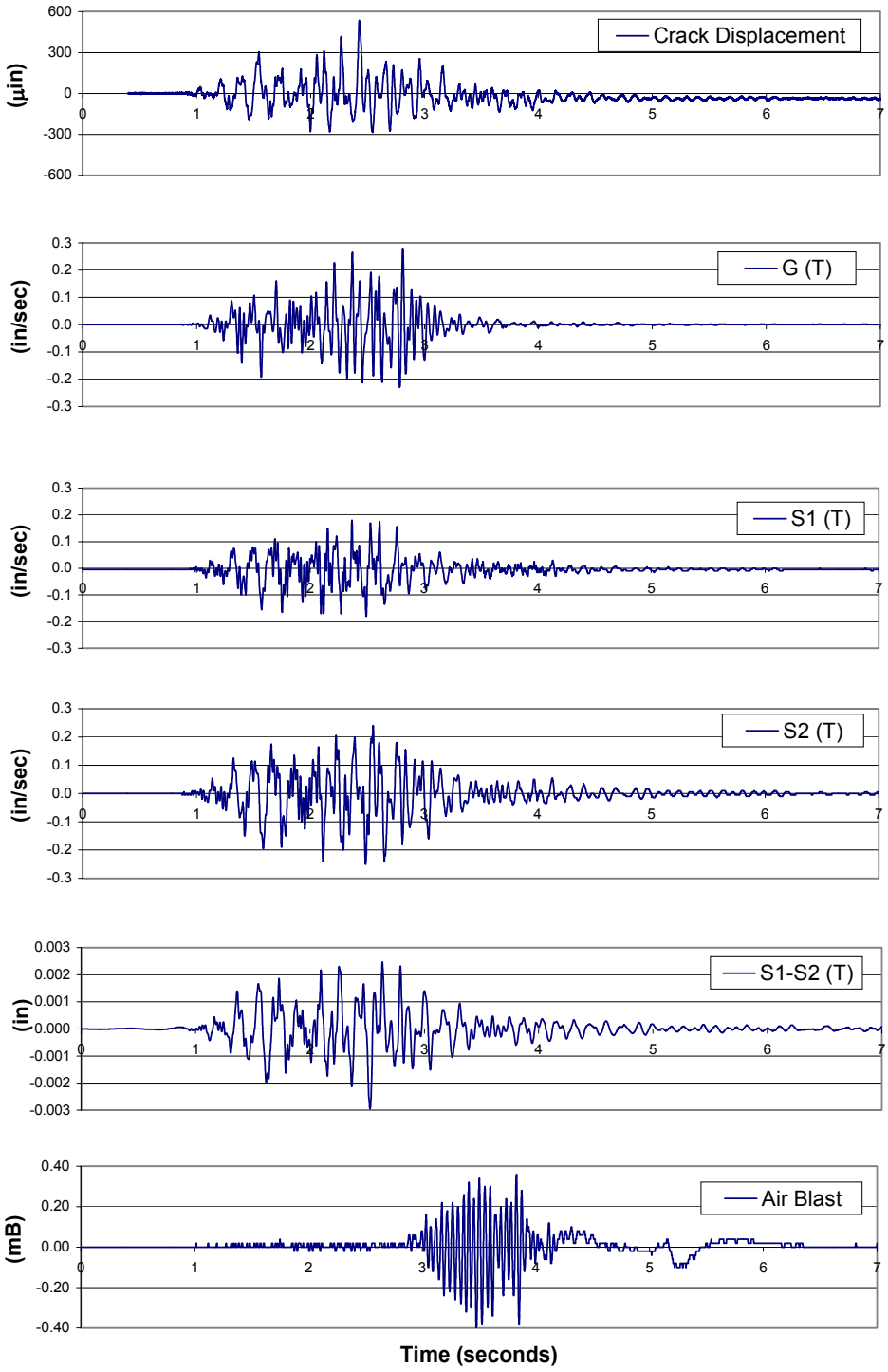

Figure 6.6 Time history of crack displacement on 22 August 2001 at 17:30 compared to ground excitation, S1 and S2 response, calculated relative displacement of structure (R1-R2), and air blast

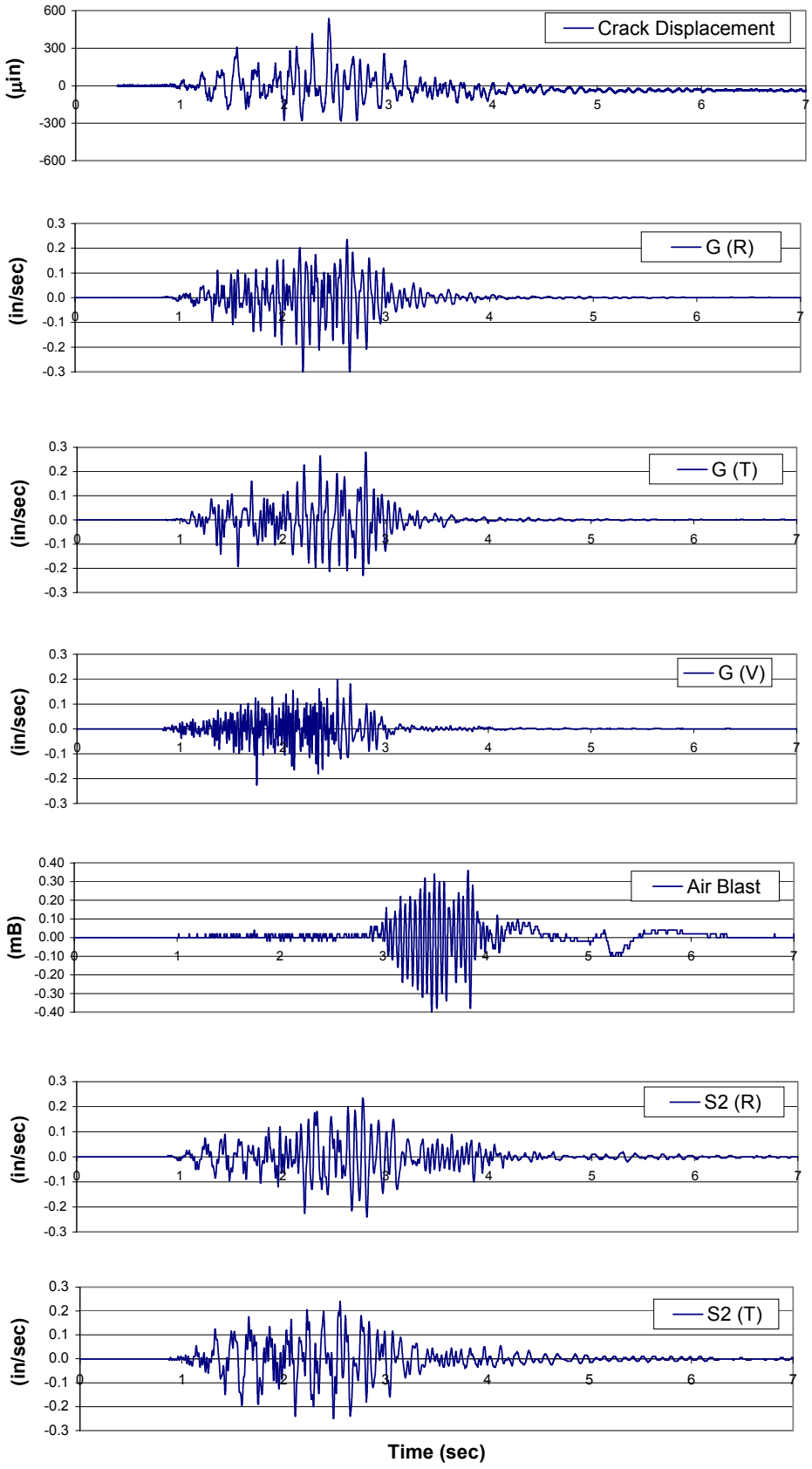

Figure 6.7 Time history of crack displacement on 22 August 2001 at 17:30 compared to ground excitation in the radial, transverse, and vertical directions, air blast response, and S2 radial and transverse structure response

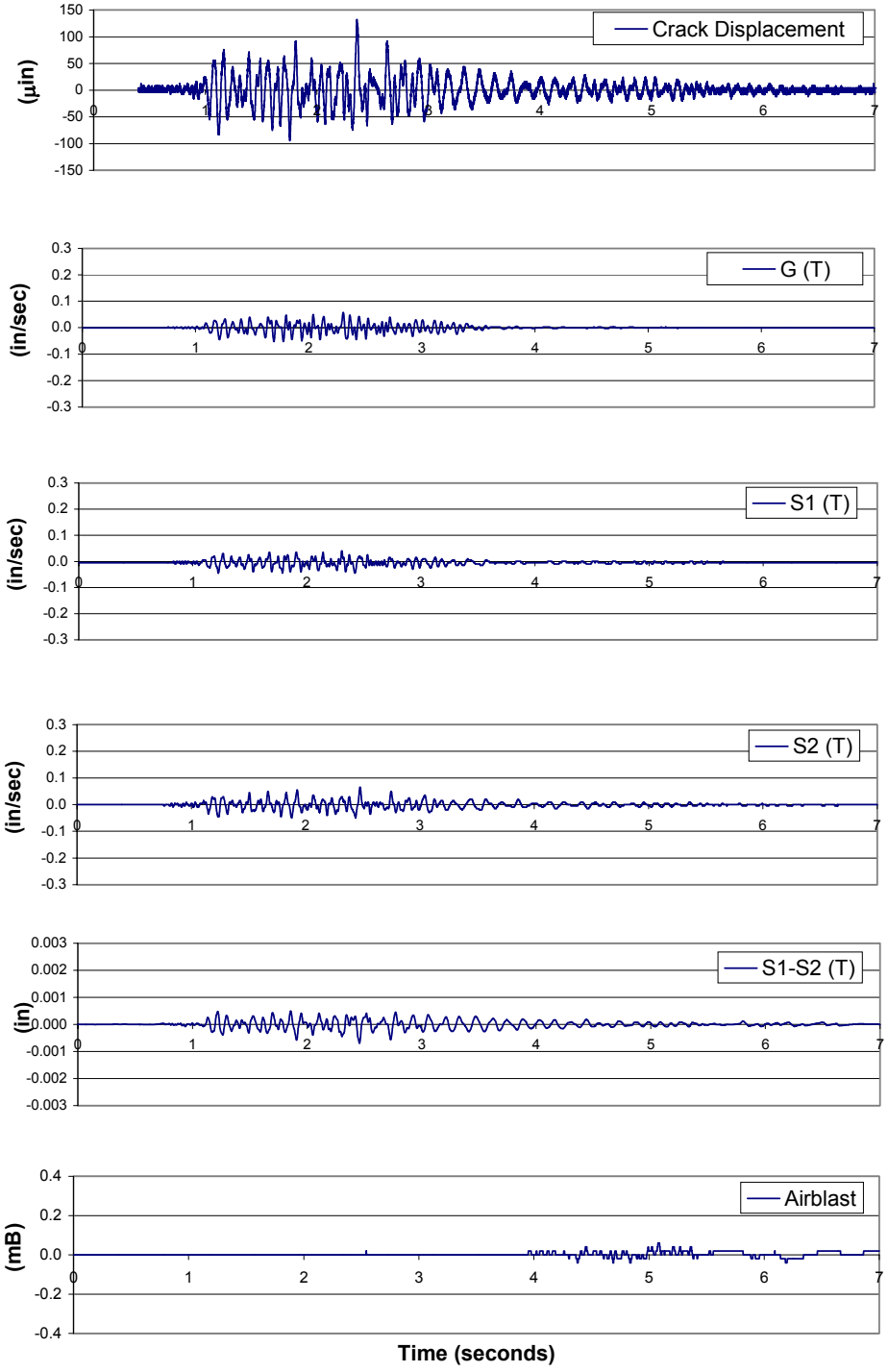

Figure 6.8 Time history of crack displacement on 23 August 2001 at 13:00 compared to ground excitation, S1 and S2 response, calculated relative displacement of structure (R1-R2), and air blast

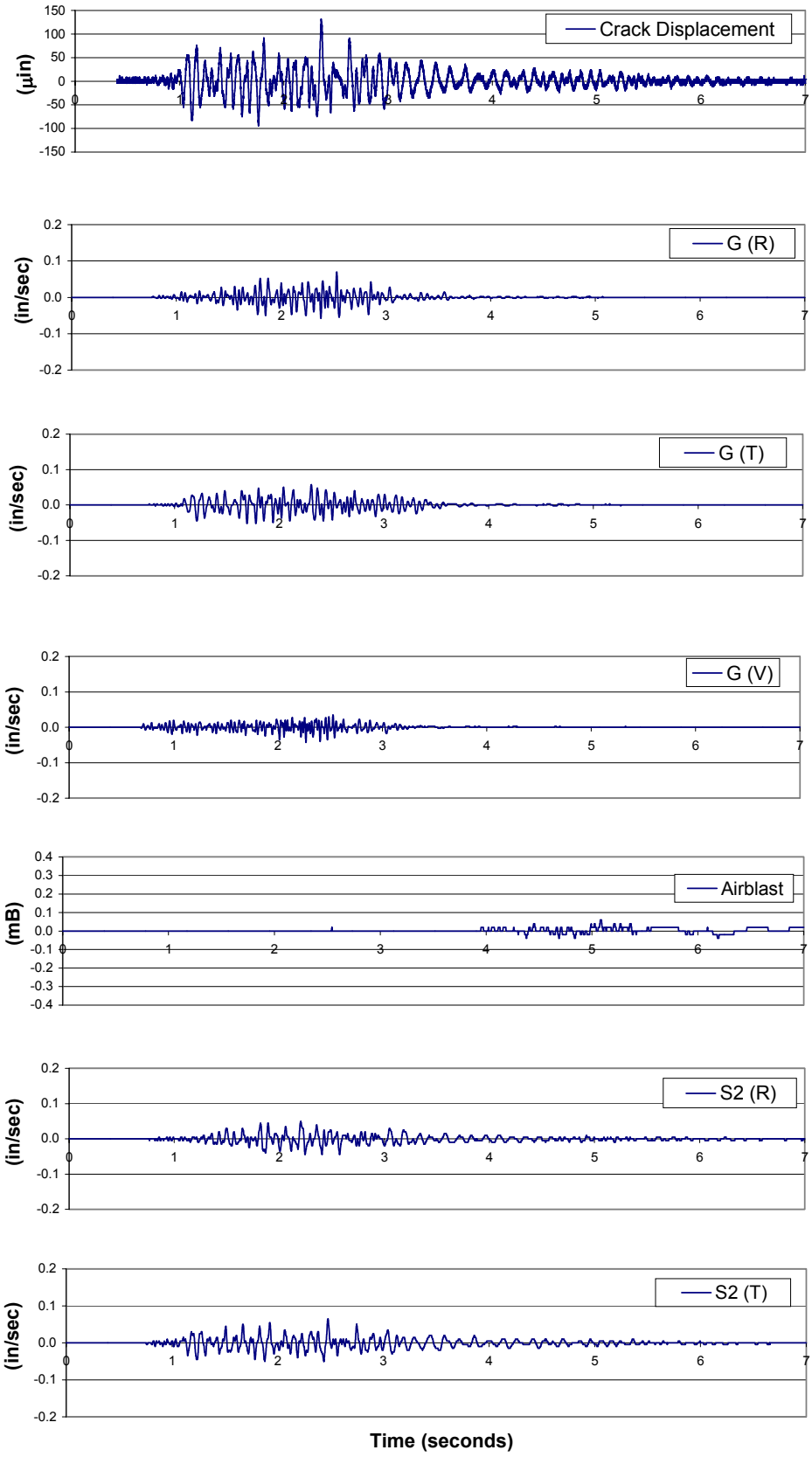

Figure 6.9 Time history of crack displacement on 23 August 2001 at 13:00 compared to ground excitation in the radial, transverse, and vertical directions, air blast response, and S2 radial and transverse response

The dominant frequency of the structure was estimated using both the zero-crossing method and FFT method. Both methods resulted in the same dominant frequency for the structure, 8 Hz.

The response spectra of the transverse ground motion, from the 22 August 2001 blast at 17:30 and the 23 August 2001 blast at 13:00 are displayed as Figure 6.10. The estimated displacements of the structure with a dominant frequency of 8 Hz were 5900 μin (150 μm) and 2400 μin (61 μm), respectively, as shown by the intersection of the vertical 8 Hz line with each response spectrum.

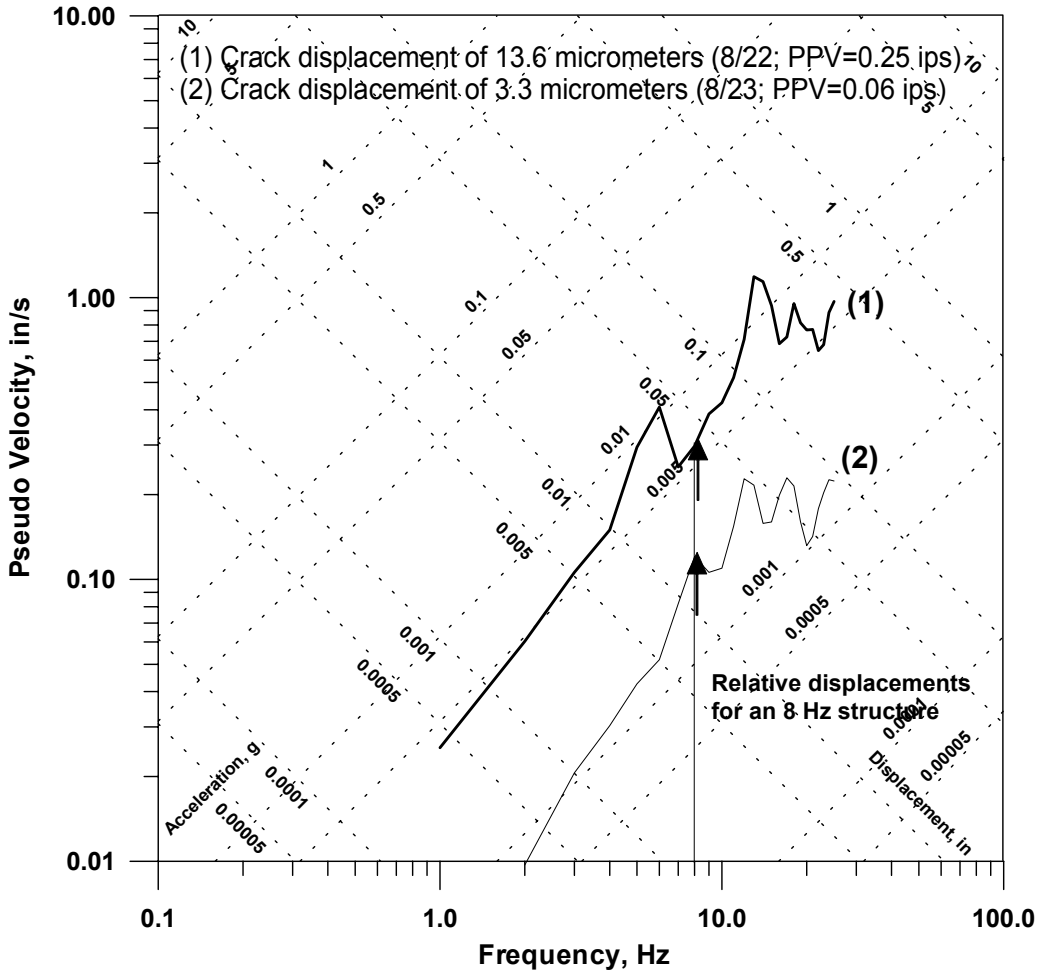

Figure 6.10 Single Degree of Freedom response spectra of transverse motions produced by blasts on 22 August 2001 at 17:30 and 23 August 2001 at 13:00, showing estimated relative displacement of a 8 Hz structure

Crack Response to Household and Blast Events

Table 6.2 presents the measured crack displacements corresponding to all significant dynamic events during the monitoring period. Household events, such as, hammering the wall, shutting windows, slamming doors, jumping, and moving furniture, were performed in order to measure the responses of the crack and compare them to responses from the blasts. Blast-induced displacements are included for comparison. Approximate distances between the location of the activity and the crack are also presented in the table.

Displacements for the household events and the blast-induced events, were very similar. Blast-induced events were typically around 3 μm (119 μin), with the exception of the first blast, which was around four times larger. Houeshold activity closest to the crack produced some of the largest displacements, as expected. The largest household activity displacement recorded was that of 10.8 μm (427 μin). This displacement was produced when a corner of the living room couch was lifted up and dropped to the ground. The remaining household events averaged around 2 μm (51 μin).

Table 6.2 Summary of measured crack displacements associated with dynamic events

Activity	Approximate distance from crack and transverse midwall (feet)	Peak Crack Displacement (μin)	Peak Crack Displacement (μm)	Midwall Transverse response (in/sec)
Hammering next to crack	1	87.2	2.2	N/A
Shutting window below crack	3	161.2	4.1	N/A
Slam kitchen window on East wall	8	78.1	2.0	0.14
Drop couch in living room	14	425.2	10.8	0.04
Jumping at landing of second story stairs	27	56.3	1.4	0.03
Slam basement screen door	14	65.0	1.6	0.02
Shut drawer in kitchen, next to sink	5	43.0	1.1	0.11
Shut upper cupboard door (adjacent to crack)	2	174.0	4.4	0.01
Close upper cupboard door (adjacent to crack)	2	51.9	1.3	0.07
Jump in living room	16	73.0	1.9	0.02
Shot 1 (8/22/01 at 17:30)	2085	535.4	13.6	0.23
Shot 2 (8/23/01 at 13:00)	3735	129.9	3.3	0.06
Shot 3 (8/23/01 at 17:40)	4170	102.4	2.6	0.06
Shot 4 (8/24/01 at 12:10)	3365	90.6	2.3	0.06

Crack Response to Environmental Effects

Figure 6.11 compares the long-term action of weather indicators (temperature and humidity) with the long-term crack response. 24-hour averages of temperature, crack displacement, and humidity were computed as they were in Chapter 3. Since the monitoring period was so short, large weather front changes were not expected. However, the humidity and crack displacement do exhibit an increase over the three days. The 24-hour average humidity increased from 70% to 90% over the course of the measured period. The typical daily temperature change appears to be around 25°F (-3.9 °C) and the daily humidity change appears to be around 25%.

Table 6.3 lists all average and maximum values for frontal, daily, and combined weather effects for temperature, crack displacement, and humidity. Values of crack response to typical and maximum ground motions associated with coal mine blasts are also included in this table, in order to compare the difference in magnitude between weather-induced and blast-induced crack response.

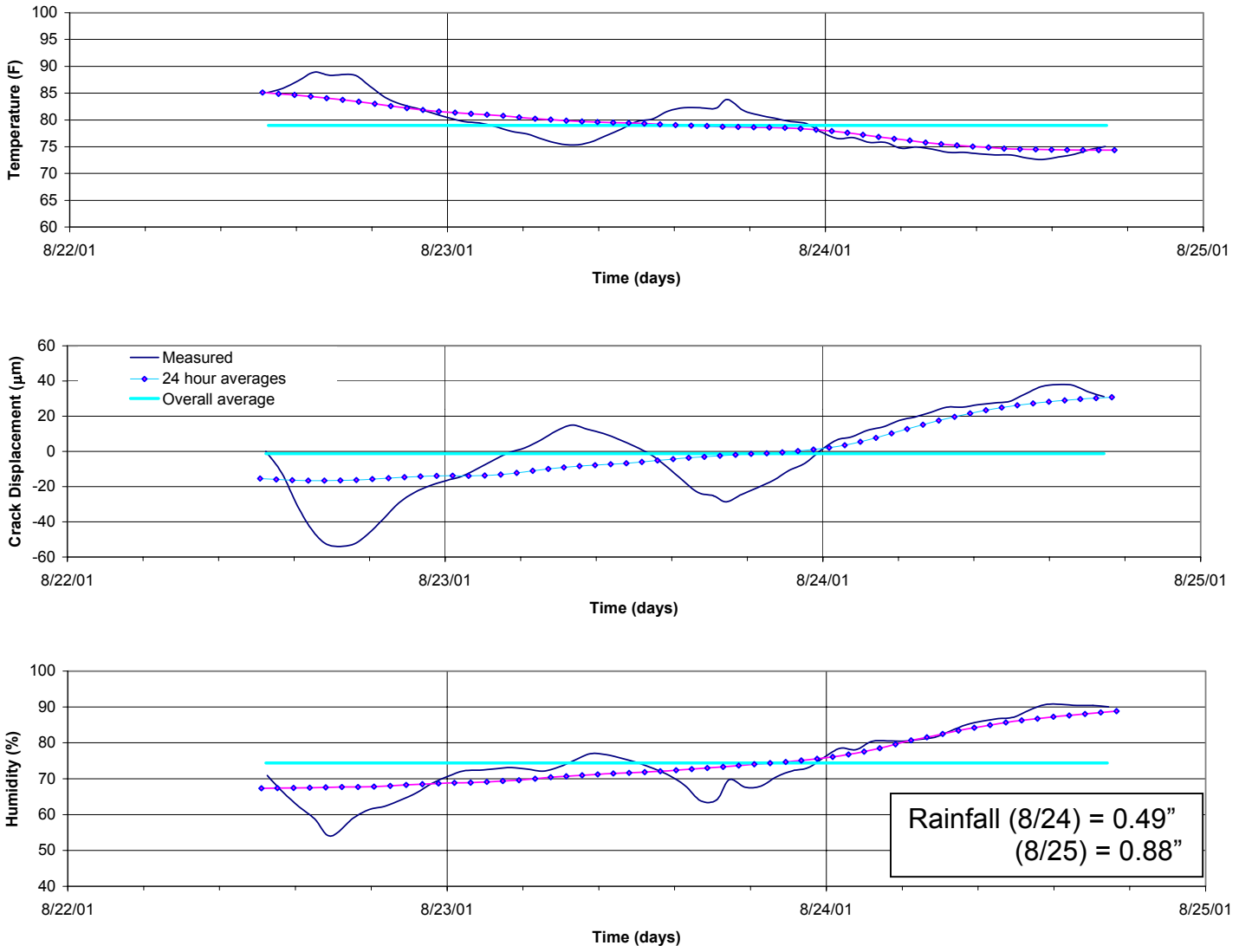

Figure 6.11 Long-term crack displacement and weather versus time

Table 6.3 Computed crack displacements due to long-term weather phenomena

	Temperature Change (DegF)	Corrected Crack Displacement (μin)	Corrected Crack Displacement (μm)	Humidity Change (%)
Frontal Effect				
Average deviation of 24 hr average from overall average	3	591	15	6
Max deviation of 24 hr average from overall average	3	630	16	7
Daily effect				
Average of deviations from 24 hr average trend	3	551	14	4
Max deviations from 24 hr average trend	4	984	25	6
Weather Effect				
Average deviations from overall average	6	1299	33	11
Max deviations from overall average	9	2042	52	18
Vibration Effect				
Typical Ground motion (PPV=0.10 ips)	-	181	4.6	-
Max ground motion (PPV=0.30 ips)	-	535	13.6	-

In Figure 6.12, the crack displacements due to different weather phenomena measured over the three days are compared to that produced by the four blasts. Since blast responses are relatively small, they are encircled. The blast that occurred at 13:00 on 23 August 2001, with ground motion measuring 0.06 ips (1.5 mm/sec) in the transverse direction, produced a crack displacement of 3.3 μm (130 μin). The largest blast that occurred during the three days, on 22 August 2001, with a ground motion measuring 0.25 ips (6.4 mm/sec) in the transverse direction, produced a crack displacement of 13.6 μm (535 μin). The estimated crack displacement of 4.6 micrometers, which corresponds with a typical ground motion of 0.10 ips (2.5 mm/sec), is less than 1/10 of the crack displacement due to the maximum weather effect of 52 μm (2117 μin). This ratio would more than likely be smaller if there had been more time to capture the true weather variation.

Also in Figure 6.12 are the displacements measured by the Kaman crack and null sensor, as well as the corrected crack displacement. Details on the purpose of the null sensor can be found in Chapter 2. All crack displacements used for the long-term analysis of this structure are those of the corrected crack displacements. The null sensor exhibited little to no variation over the three days, however, to be certain, any displacement that did occur was subtracted from the crack reading at the appropriate time. Again the short period of observation limits the conclusions regarding typical behavior, as the first 12 hours of data represent the accommodation of the instrument to the wall.

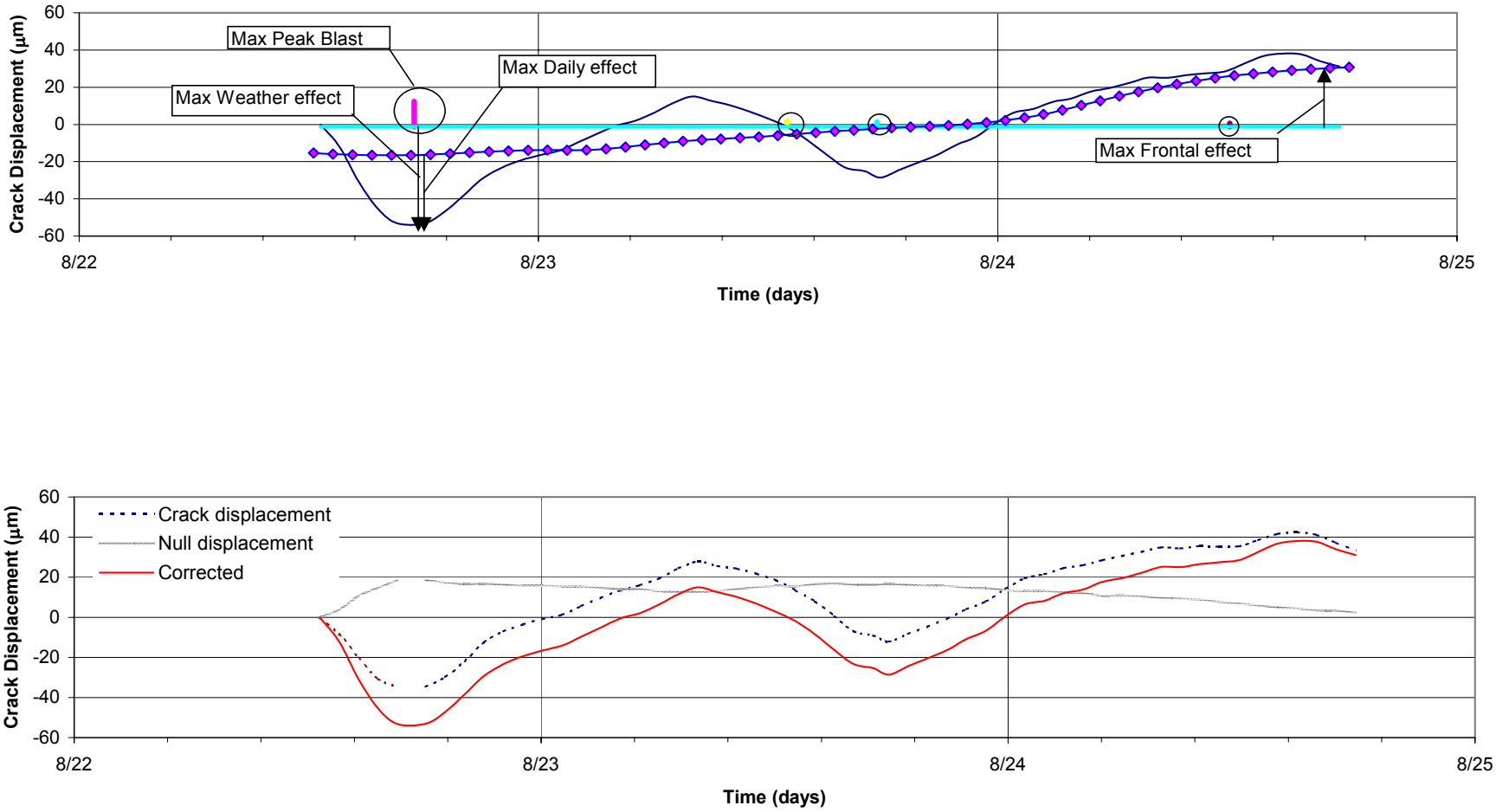

Figure 6.12 Typical crack displacements due to long-term phenomena and maximum zero to peak dynamic blast events

Comparisons of computed displacements with measured crack displacement

The maximum measured crack displacement produced by each shot is compared in Table 6.3 to various computed wall displacements based on structure responses, and peak ground motion measured in the direction parallel to the cracked wall. All responses analyzed were those in the transverse direction. All comparisons are presented graphically in Figures 6.13 and 6.14. Details of the methods used to compute displacements are presented in Chapter 3.

For this structure, all of the relationships yielded almost perfect correlations, with the exception of one; none of the other structures had regression coefficients as high. Perhaps the reason for this, is the large range in blast response. The first blast that was monitored was much larger than the other three and contained a different frequency contour, as shown in the response spectrum. This blast was the closest and had the largest charge/delay out of all four blasts. For the other three blasts, the crack responses were all fairly similar in magnitude.

Table 6.4 Summary of computed and measured displacements

Date of Shot	Relative displacement, δ, of structure (μm)						PPV (in/sec)	Measured crack displacement above kitchen window (μm)
	Integration of Velocities			δ from SDOF	$\delta = V/2\pi f$			
	Upper corner - Lower corner	Upper corner - Ground	Ground	From response spectras	Estimated from V and f at	Estimated from V and f at		
				at f_n of 8 Hz	g_{max}	S1 $_{max}$		
				Avg for 10 <f_n<15	S2 $_{max}$	S2 $_{max}$		
				-	g_{max} and $S2_{max}$	$S1_{max}$ and $S2_{max}$		
8/22/2001 17:30	75	133	97	150 259	104 32 53	43 93 68	0.28	13.6
8/23/2001 13:00	18	25	17	61 56	12 22 1	7 22 6	0.06	3.3
8/23/2001 17:40	13	22	15	37 54	11 25 1	9 12 5	0.06	2.6
8/24/2001 12:10	10	23	14	22 32	7 27 5	9 11 10	0.045	2.3

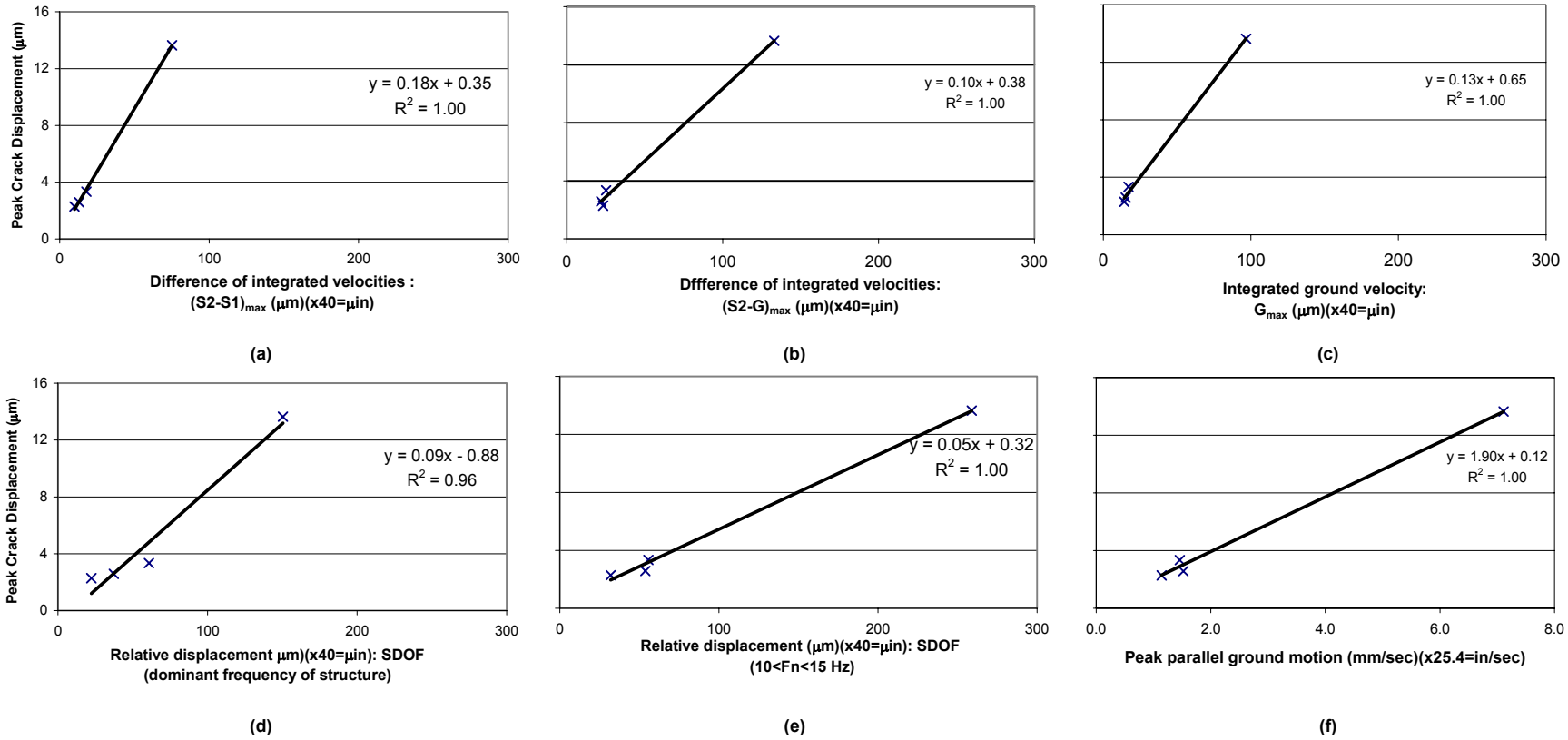

Figure 6.13 Correlations between measured crack displacements and computed displacements and peak transverse ground motions

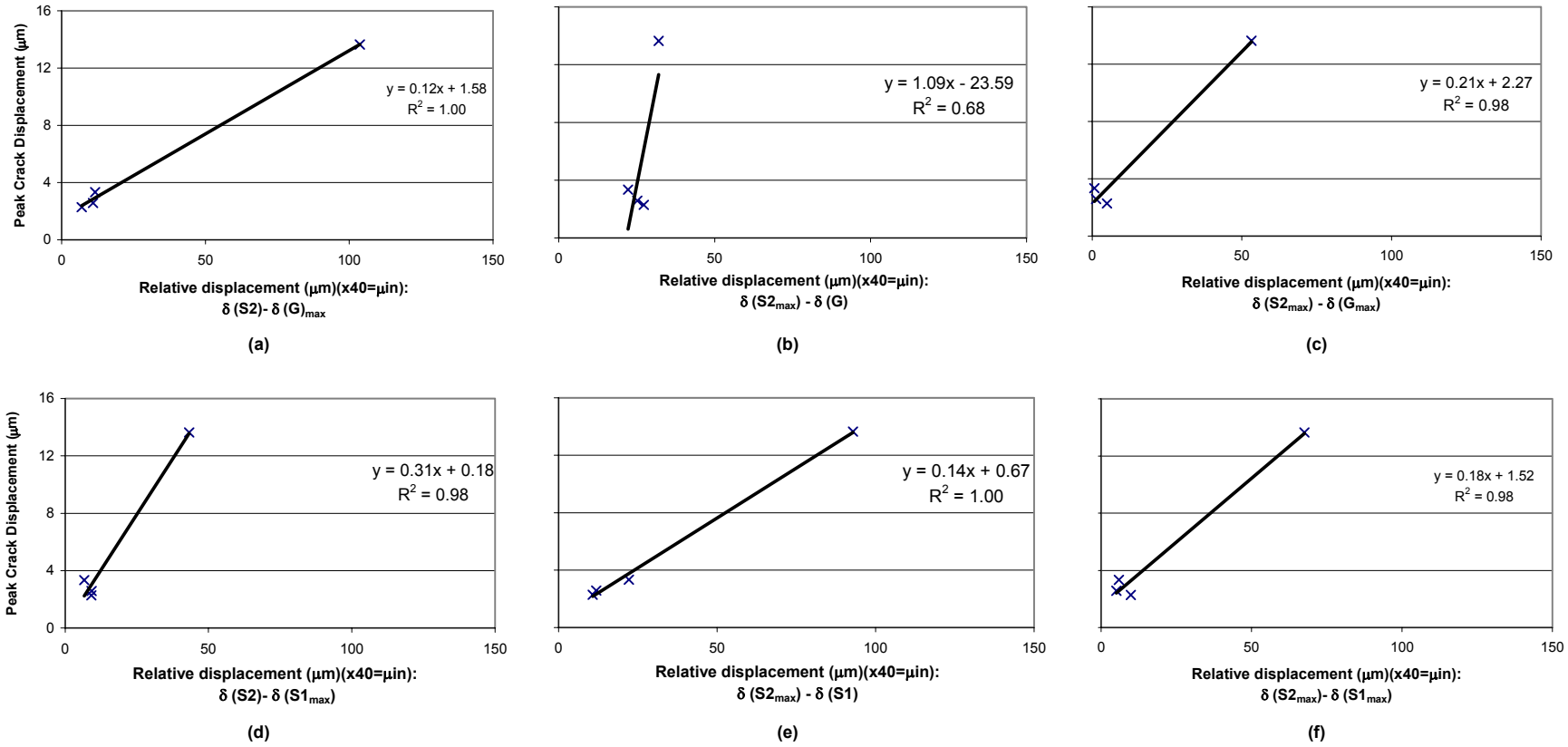

Figure 6.14 Correlations between measured crack displacements and computed relative displacements

CHAPTER 7

CONCRETE BLOCK HOUSE – WISCONSIN

The Wisconsin structure, shown in Figure 6.1, is a stone-faced, concrete block house, adjacent to a limestone quarry. Blasting operations are conducted approximately 1500 to 2000 feet (457 to 609 m) away from the back of the structure. Data has been collected intermittently, on-site since August of 2000. (Louis 2000) Data presented in this chapter were collected from 29 November 2001 to 15 January 2002 to compare the responses of two different crack sensors. As shown in Table 7.1, fifteen blasts produced ground motions of 0.03 to 0.18 ips (0.8 to 4.6 mm/sec), which produced crack displacements of 0.9 to 23.7 μm (35.6 to 936 μin) at three different cracks. In addition, a number of household activities were simulated in order to obtain comparative responses of two different types of displacement sensors. Weather data varied cyclically each day with outdoor temperatures ranging between 23 °F and 68° F (-5 to 20 °C), and outside humidity ranging between 26% and 95%.

This chapter compares the measurements recorded by the two different types of sensors, for both long-term and dynamic effects. In November of 2001, two LVDT sensors were installed in the structure, one adjacent to the Kaman null sensor, and the other adjacent to the Kaman Crack 1 sensor, shown in Figures 7.2, 7.3, and 7.4. This change enabled the comparison of LVDT and Kaman sensor response to the dynamic and long-term behavior of Crack 1. Previous analyses have compared crack response to dynamic and long-term effects. (Louis 2000)

Figure 7.1 Wisconsin concrete block house

Table 7.1 Summary of crack response for concrete block house in Wisconsin

	Ground Motion			Peak air pressure	Crack Displacement			
	R in/sec	T in/sec	V in/sec	(dB)	Crack 1 - LVDT (μin)	Crack 1 - Kaman (μin)	Crack 2 (μin)	Crack 3 (μin)
11/30/01 8:17	0.15	*0.10*	0.11	114	131	106	157	332
11/30/01 10:59	0.08	0.07	0.07	106	81	80	92	176
11/30/01 11:29	0.15	*0.10*	0.09	114	175	150	202	235
12/5/01 9:03	0.06	0.05	0.03	106	119	76	98	338
12/7/01 12:02	*0.09*	*0.10*	0.06	105	112	79	157	115
12/7/01 12:28	0.18	0.13	0.07	107	187	156	171	933
12/17/01 8:36	0.08	0.07	0.07	104	56	57	93	144
12/17/01 10:15	0.08	0.06	0.05	98	106	89	54	195
12/17/01 11:53	0.07	0.07	0.05	100	125	89	65	288
12/18/01 10:01	0.15	*0.10*	0.09	108	131	102	128	408
12/18/01 10:31	0.11	0.08	0.09	105	112	87	90	384
1/4/02 9:33	0.03	0.03	0.04	113	44	36	162	145
1/4/02 13:06	0.12	0.06	0.10	106	87	71	136	514
1/15/02 10:15	0.15	0.06	0.12	108	150	110	132	223
1/15/02 10:45	0.08	0.08	0.10	107	81	76	141	580

Structure Description

As shown in Figure 7.1, the structure is a one-story, concrete masonry block structure with a concrete masonry block basement that opens out to a backyard, one story below the front yard. A garage is located South of the house. As shown, the exterior walls are faced with stone. Figure 7.2 displays the plan and elevation view of the structure.

The first floor joists are supported by a wooden principal beam running lengthwise in the radial direction. The ceiling is supported by transverse wooden joists, which are supported at the center by the lengthwise center wall, which in turn rests on the basement support beam. This center wall was removed in the computer room, which lead to the ceiling crack, Crack 2. The openings between the kitchen and living room, as well as that between the entry way and living room appear to be supported by beams. These beams seem to be unusually connected to the opening walls, which have lead to Cracks 1 and 2.

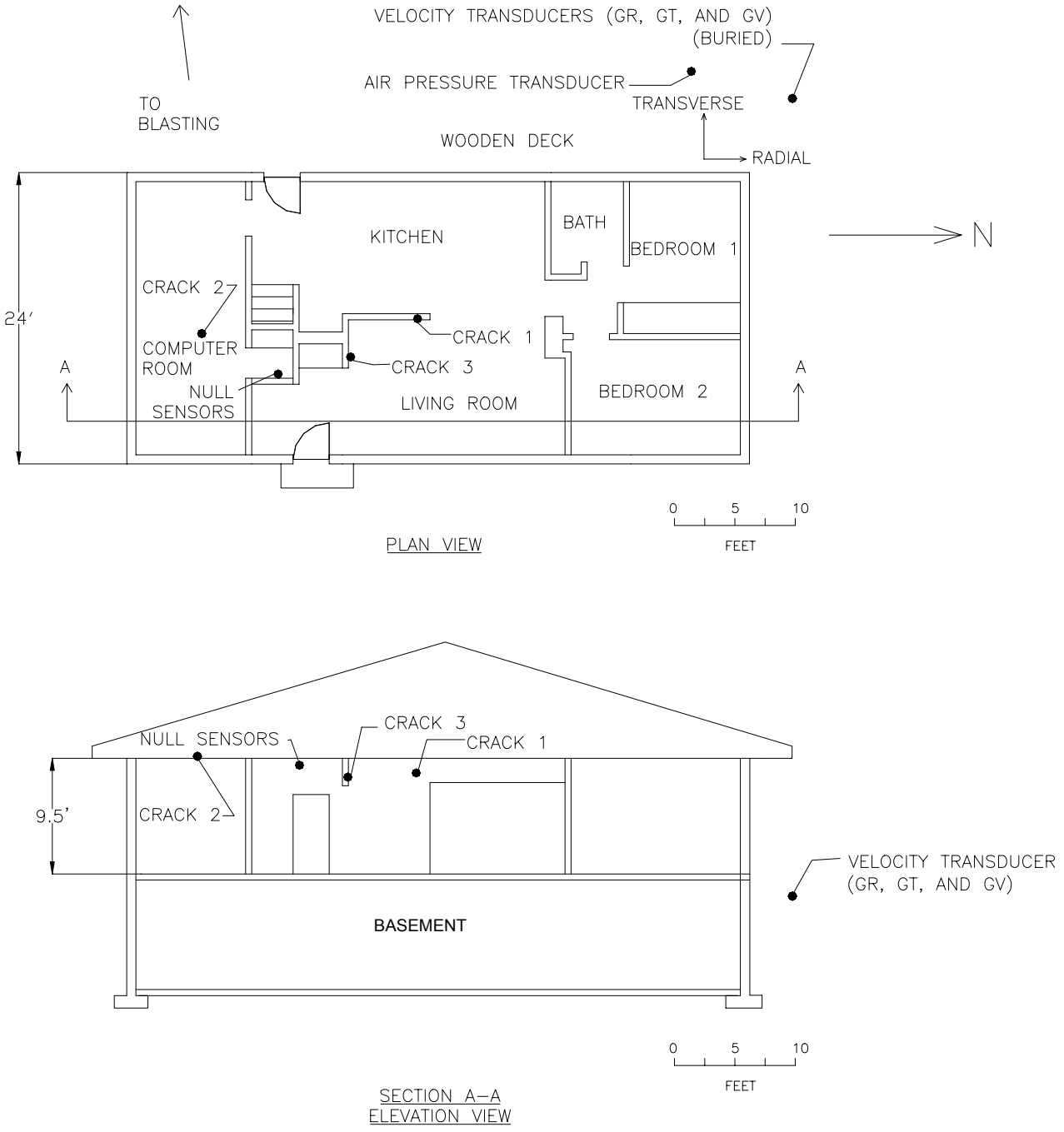

Figure 7.2 Plan view and elevation view of Wisconsin concrete block house

Location of Instrumentation

Locations of all crack displacement sensors are shown in Figure 7.2. Kaman sensors span three different cracks and a Kaman null sensor is mounted on an uncracked wall section. Of the LVDT sensors, one spans Crack 1, adjacent to the Kaman sensor, as shown in Figure 7.3; the other, a null sensor, is located over the uncracked wall section, adjacent to the Kaman null sensor, as shown in Figure 7.4.

Crack 1, shown in Figure 7.3, is located in the living room at the top of the wall separating the kitchen and the living room. It spans a crack that seems to be created by expansion and contraction of the beam supporting ceiling joists above the entrance to the living room from the kitchen. While the crack is approximately 500 μm (19,800 μin) wide, it is constrained in a raised dimple that might be as wide as 5000 μm (198 mm). This raised dimple implies that this crack has been repeatedly repaired, as a result of its high weather response.

The location of the null sensors, as shown in Figure 7.4, is above the doorway separating the main entrance hall and the computer room, on an uncracked wall section. This location was originally chosen for the Kaman null sensor because it was an uncracked portion of wall close to the other Kaman sensors, as well as, at the same approximate height on the wall. As stated in Chapter 1, a null sensor is employed to separate the non-crack response of the sensor from the crack response. Null responses are typically small and negligible. This was verified by the Kaman sensors in the 2000 Louis study, and again in this study, with the LVDT sensors. Figure 7.5 displays the minute displacement measured by the null sensor in comparison to that measured by the crack sensor.

All three outdoor sensors have been replaced or moved since the 2000 Louis study. A new outdoor temperature and humidity sensor (a Vaisala HMD/W50), is now located on the North face of the house on the bottom of the window sill. The current range of the sensor is 23 to 131°F (-4 to 55 °C); therefore, the minimum temperature recorded is 23 °F (-4 °C), even though the temperature has more than likely gone below this value during the monitoring period. In addition, a new three-axis Geosonics geophone, as shown in Figure 7.6, was installed due to the failure of the radial axes, and the air pressure transducer has been replaced with a Larcor

overpressure microphone, as shown in Figure 7.7. Due to improper wiring of the microphone, however, accurate measurement of air pressure has not been recorded.

Figure 7.3 Kaman and LVDT displacement sensors spanning Crack 1

Figure 7.4 Kaman and LVDT null displacement sensors

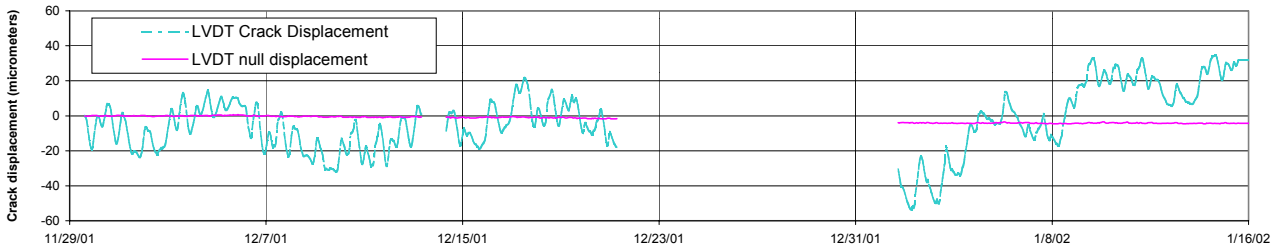

Figure 7.5 Comparison of LVDT crack and null response

Figure 7.6 Geophone

Figure 7.7 Air pressure transducer

The Data Acquisition System (DAS) has remained in the same location since the original installation of this site. Details on the Somat 2100 DAS employed at this site can be found in Louis (2000).

Extent of Monitoring

For each blast, time histories were collected from the three-axis geophone, the air pressure transducer, the three Kaman crack sensors, and the LVDT crack and null sensors for a total of three seconds. Motion of 0.02 ips (0.5 mm/sec) triggered the DAS to record these time histories simultaneously.

Long-term data were also recorded during this time period. Every hour, readings of temperature and humidity (indoor and outdoor), and crack response from the three Kaman crack sensors and the LVDT crack and null sensors were recorded by the DAS.

In addition, crack displacements and ground motions were measured in response to the simulation of household activities, after the installation of the LVDT sensors.

Comparative Responses to Ground Motions

Figure 7.8 shows the time histories of excitation ground motions and crack response associated with the blast on 7 December 2001 at 12:02. As shown, this blast produced peak displacements of 2.0 and 2.9 μm (79 and 115 μin) for Crack 1 from the Kaman and LVDT sensors, respectively. The peak particle velocity of 0.09 ips (2.3 mm/sec) associated with this blast is typical of blasting operations.

Time histories associated with the remaining fourteen blasts can be found in Appendix C.

The natural frequency of the structure was previously estimated using the FFT method in the Louis study (2000). Response spectra for two blasts, one on 30 November 30 2001 at 11:29 and one on 15 January 2002 at 10:15 are displayed as Figure 7.9. The relative displacements of the structure with an estimated dominant frequency of 11 Hz from the two blasts were 1600 μin (40 μm) and 700 μin (18 μm), respectively, as shown by the intersection of the vertical 11 Hz line with each response spectrum.

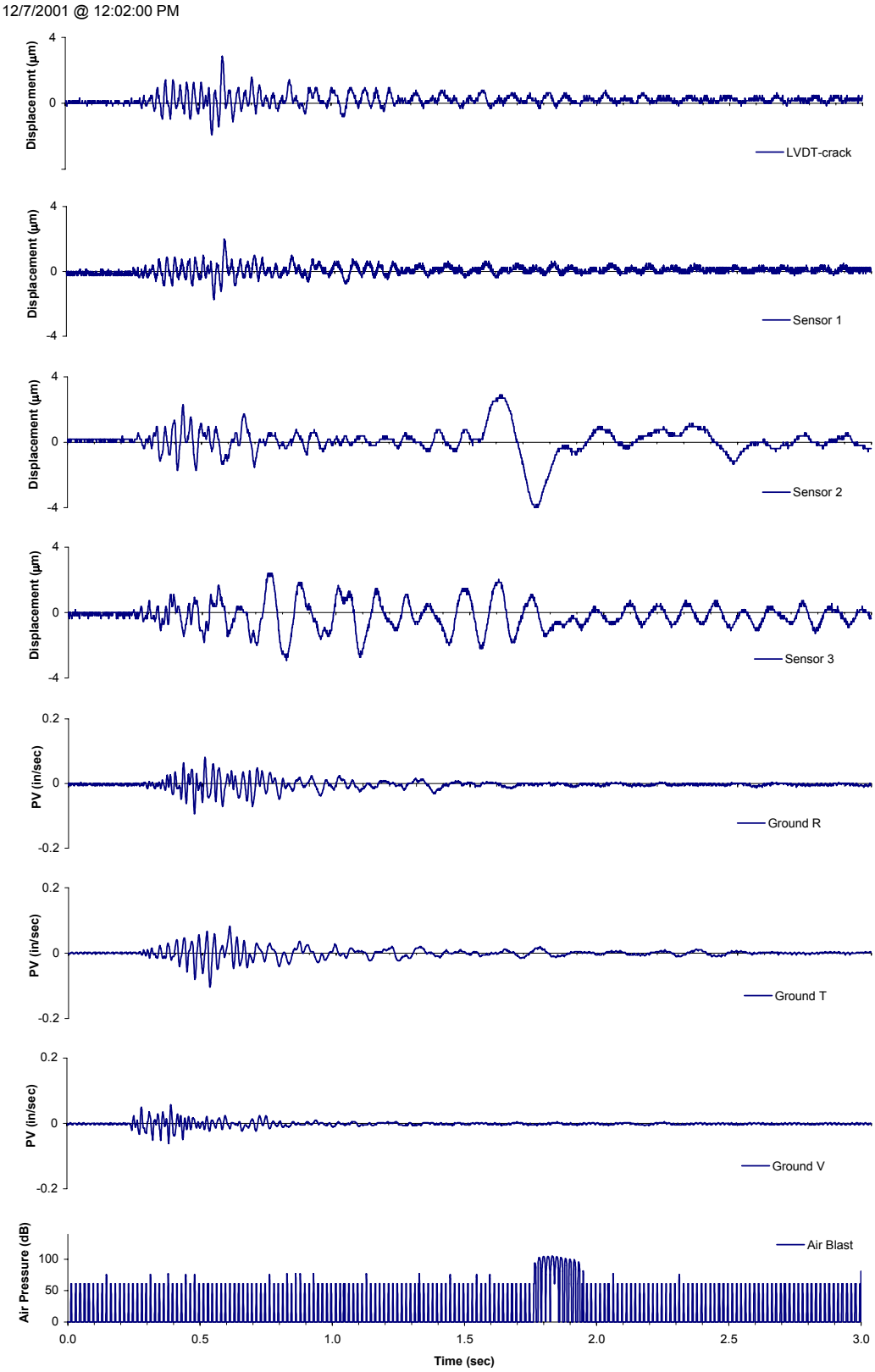

Figure 7.8 Time histories of crack displacements, ground motion, and air blast recorded for blast on 7 December 2001 at 12:02

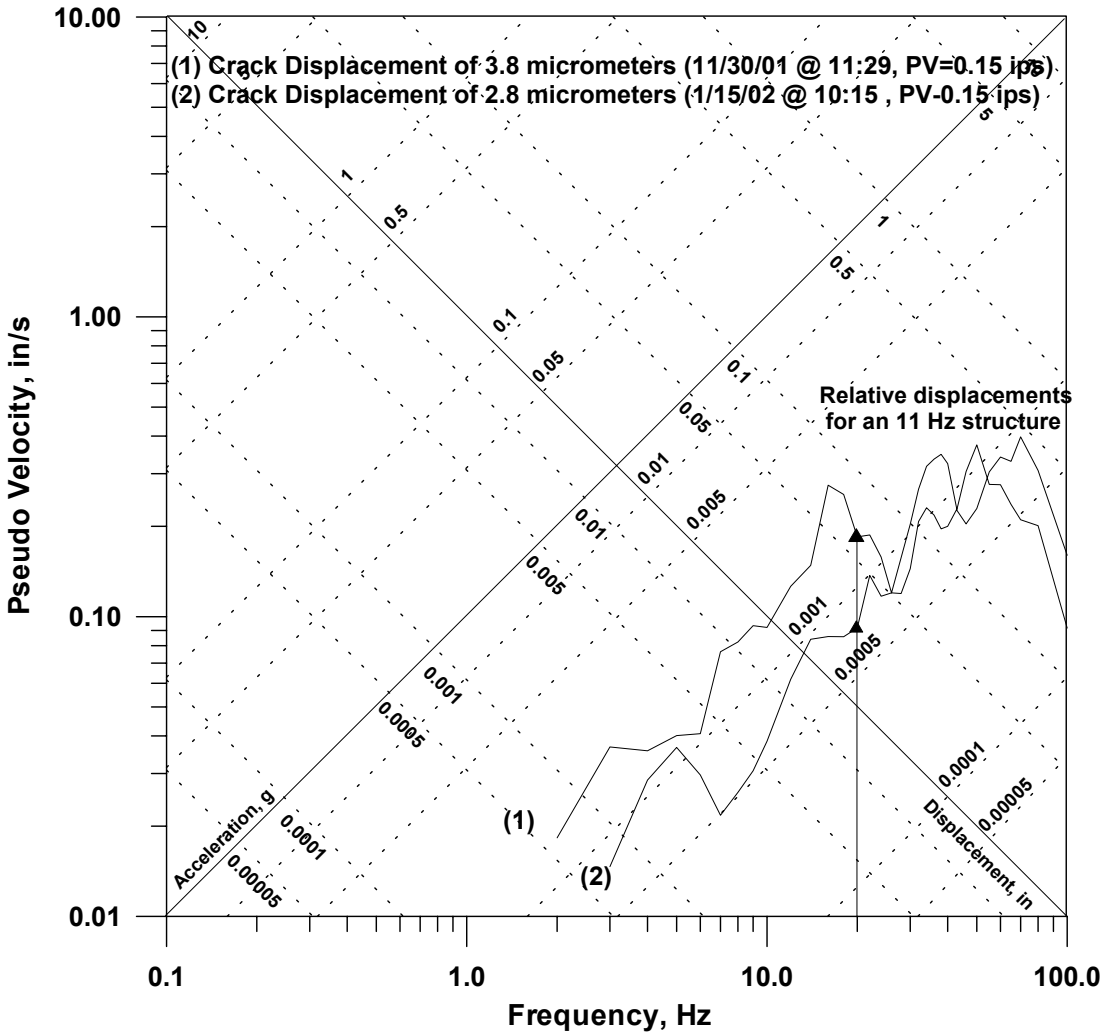

Figure 7.9 Single Degree of Freedom response spectra of radial motions produced by blasts on 11/30/01 and 1/15/02, showing estimated relative displacement of an 11 Hz structure

Peak, in-plane displacements of Crack 1associated with the fifteen blast events measured by the Kaman and LVDT sensors are compared, in Figure 7.10. As displayed and enumerated in Table 7.1, the LVDT measurements were consistently larger than the Kaman sensor for all fifteen blasts; however, the difference between the two sensors was relatively small for any single event. A regression coefficient of 0.91 was found as the relationship between the two sensor types. This high correlation of peak responses, along with the almost duplicate time histories recorded by each crack sensor, shows that little difference exists between the measuring capabilities (and/or restrictions) of each sensor for blast events that excite the entire structure.

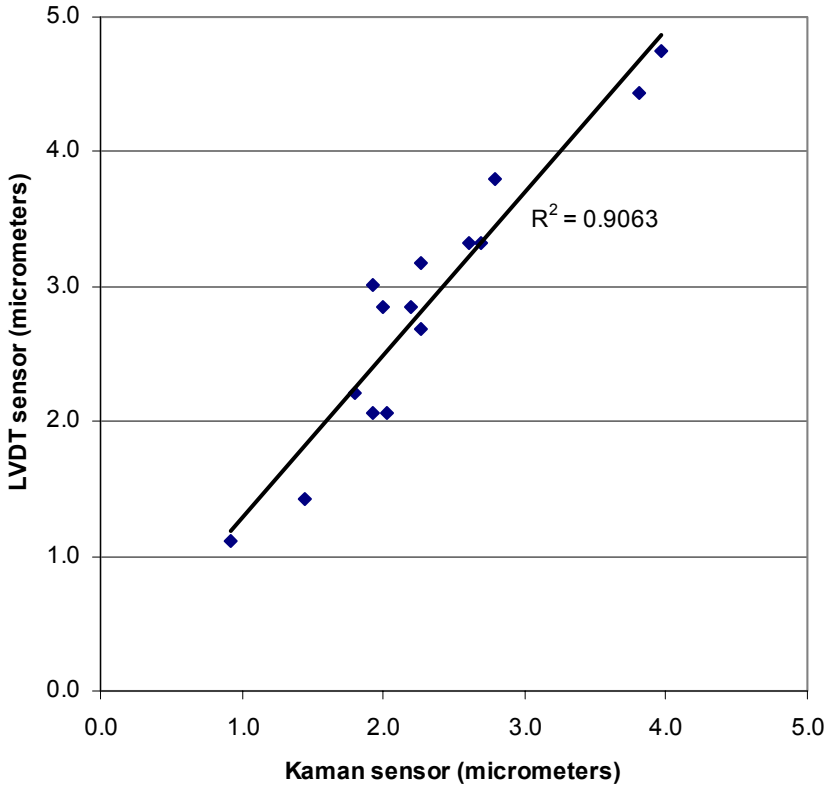

Figure 7.10 Comparison of displacements measured from Crack 1

Crack Response to Environmental Long-term Effects

Long-term displacements measured by the two sensors over the same crack were also compared. Figures 7.11 and 7.12 compares the long-term action of weather indicators (temperature and humidity) with the long-term crack responses of the Kaman SMU-9000 sensor and LVDT DC750 sensor, respectively. 24-hour averages of temperature, crack displacement, and humidity were computed as they were in Chapter 3. Table 7.2 lists the average and maximum displacements for the frontal, daily, and weather effects for temperature, crack displacement (for both the Kaman and LVDT sensors), and humidity. Values of crack response to typical and maximum ground motions associated with coal mine blasts are also included in this table, in order to compare the difference in magnitude between weather-induced and blast-induced crack response.

As seen in the two figures, the long-term response of Crack 1 as measured by the two sensors was remarkably similar. Figure 7.13 displays the long-term response of the two different sensors in the same plot. Over the seven week period of observation, the two sensors display the exact same pattern. Each begins at –5 μm (-198 μin) and ends at –22 μm (-869 μin). The ratio of LVDT to Kaman response was approximately 5 to 4 for both the weather and blast effects.

As with the other cases, displacements associated with weather effects are much larger than those associated with blast events. The maximum weather effect displacement of 47 μm (1850 μin) determined during the monitoring period for the LVDT sensor is more than 25 times the peak displacement of 5 μm (197 μin) associated with a typical ground motion of 0.09 ips (2.3 mm/sec). For the Kaman sensor, the maximum weather effect displacement of 37 μm (1457 μin) was measured as more than 10 times the same dynamic displacement.

Table 7.2 Computed crack displacements due to long-term weather phenomena

	Temperature Change (DegF)	Indoor Crack Displacement (μin)	Indoor Crack Displacement (μm)	Indoor Crack Displacement (μin)	Outdoor Crack Displacement (μm)	Humidity Change (%)
Frontal Effect						
Average deviation of 24 hr average from overall average	12	1696	43	904	23	9
Max deviation of 24 hr average from overall average	31	6111	155	3102	79	27
Daily effect						
Average of deviations from 24 hr average trend	5	1977	50	927	24	11
Max deviations from 24 hr average trend	12	3956	100	2245	57	25
Weather Effect						
Average deviations from overall average	12	2422	62	1214	31	14
Max deviations from overall average	34	8556	217	4226	107	37

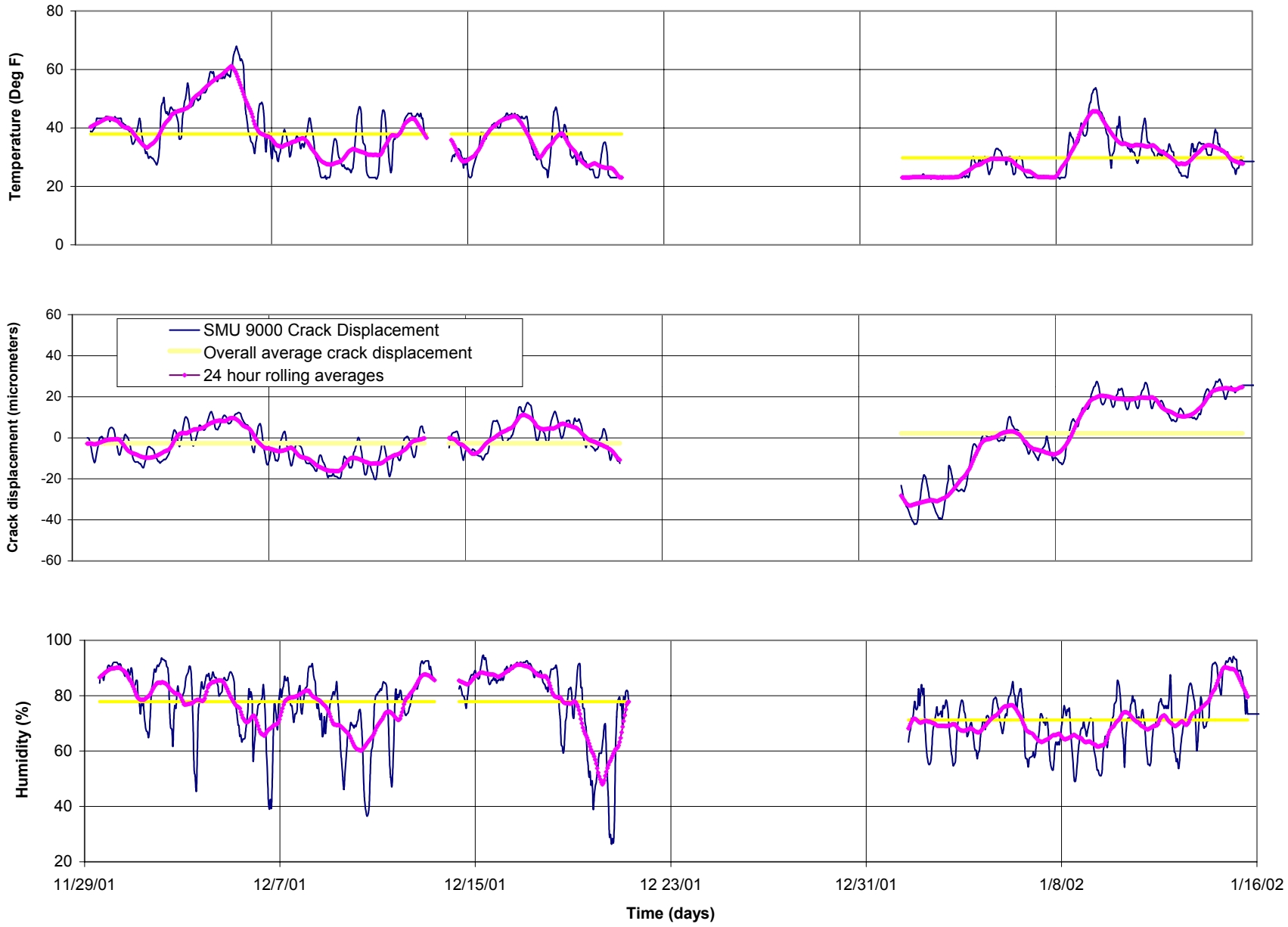

Figure 7.11 Long-term Kaman crack displacement and weather versus time

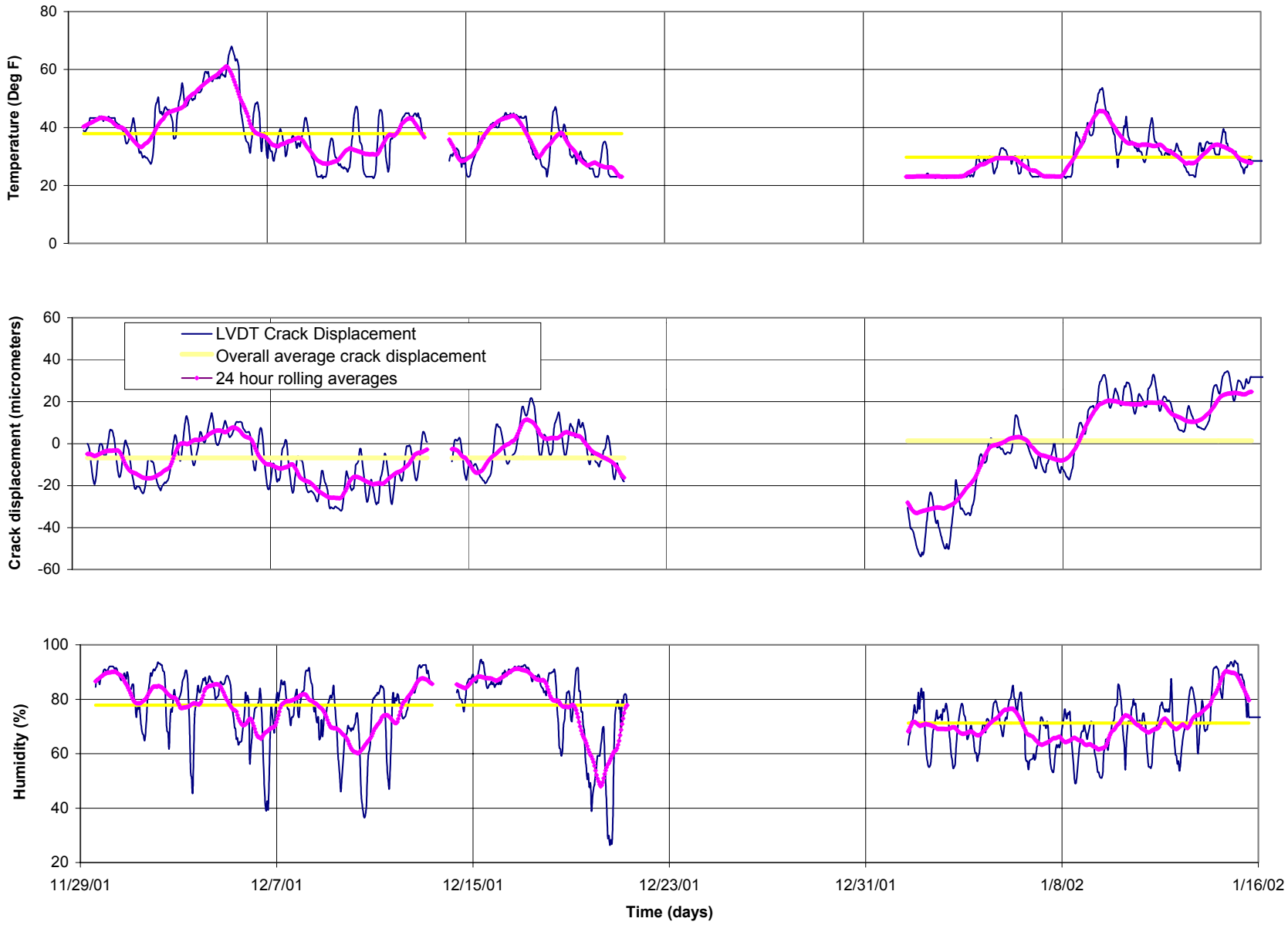

Figure 7.12 Long-term LVDT crack displacement and weather versus time

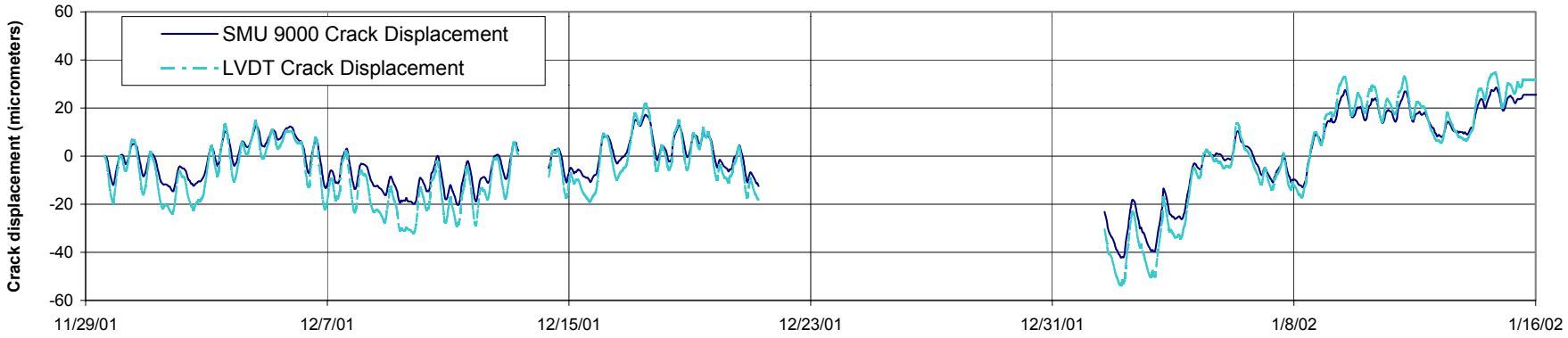

Figure 7.13 Comparison of LVDT long crack displacement with Kaman SMU 9000 sensor

Comparative Response to Occupant Activities

Table 7.3 presents the measured crack displacement resulting from occupant-induced events, which were simulated in order to compare sensor response nearby localized deformation. Time histories of these events are shown in Figure 7.14. A few select displacements measured during blasting events were also tabulated, in order to compare the differences in measurements between both sensors, corresponding to dynamic events of varying intensity. Once again, the magnitudes of displacements measured by the LVDT sensor were larger than those measured by the Kaman sensor. However, the differences between sensor responses were much larger for the localized events that originated closer to the sensors' location.

Table 7.3 Summary of measured crack displacements associated with dynamic events

Activity	Approximate distance from Crack 1 (feet)	Peak Crack 1 Displacement - Kaman (μm)	Peak Crack 1 Displacement - Kaman (μin)	Peak Crack 1 Displacement - LVDT (μm)	Peak Crack 1 Displacement - LVDT (μin)
Pound on wall near crack 1	1	5.5	218	20.7	815
Pound on wall near crack 3	6	0.8	32	1.9	74
Running through house	-	10.3	404	17.6	691
Slam front door	12	1.7	68	3.1	123
Blast of PPV=0.09 ips	2000	2	79	3	118
Blast of PPV=0.18 ips	2000	4	157	5	197

These large differences for nearby localized events may have resulted from a variety of factors. They no doubt provide higher mode responses as indicated by the spiked time history recorded when pounding on the wall near Crack 1, which is shown in Figure 7.14. Time histories of localized events also do not exhibit the same symmetry as do the whole structure responses resulting from ground motions, such as that shown in Figure 7.8.

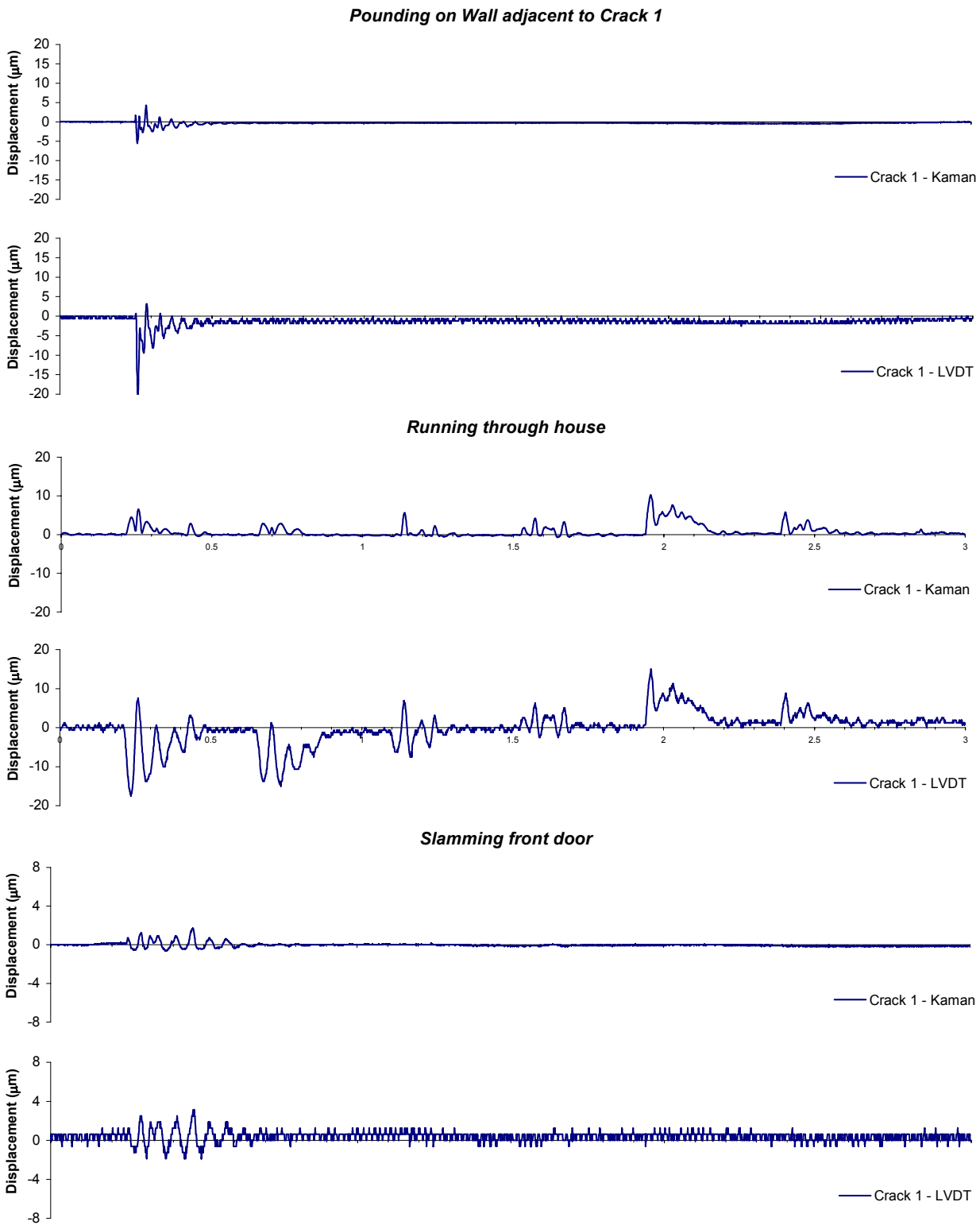

Figure 7.14 Time histories of occupant activities listed in Table 7.3

Comparisons of measured crack displacement with common estimates of structural response

The maximum measured crack displacement produced by each shot is compared in Table 7.4 to various computed values of displacements and peak radial ground motions. These comparisons were made in order to determine the correlation that exists between the measured crack displacement and these various responses, and are graphically presented in Figure 7.15. Fewer correlations were determined for this structure because response velocities were not measured. All responses analyzed were those in the radial direction.

The best correlation found was that between the measured crack displacements and the peak ground motions in the radial direction (regression coefficient of R^2=0.73), as shown in Figure 7.15 (e). The correlations found between the measured displacements and the three types of computed displacement, were relatively the same (regression coefficients between 0.51 and 0.65).

Table 7.4 Summary of computed displacements and measured displacements

	Relative displacement, δ, of structure (μin)				
Date of Shot	Integration of Ground Velocity	δ from response spectras at f_n of 11 Hz	δ from response spectras Avg for 10 <f_n<15	PPV (in/sec)	Measured Kaman crack displacement (μin)
11/30/01 8:17	24	37	32	0.15	**2.7**
11/30/01 10:59	11	22	21	0.08	**2.0**
11/30/01 11:29	25	40	44	0.15	**3.8**
12/5/01 9:03	19	32	30	0.06	**1.9**
12/7/01 12:02	12	20	19	0.09	**2.0**
12/7/01 12:28	46	97	82	0.18	**4.0**
12/17/01 8:36	14	18	17	0.08	**1.5**
12/17/01 10:15	13	41	36	0.08	**2.3**
12/17/01 11:53	13	49	40	0.07	**2.3**
12/18/01 10:01	25	70	56	0.15	**2.6**
12/18/01 10:31	22	35	33	0.11	**2.2**
1/4/02 9:33	5	9	9	0.03	**0.9**
1/4/02 13:06	8	16	14	0.12	**1.8**
1/11/02 10:15	13	18	20	0.15	**2.8**
1/11/02 10:45	14	33	28	0.08	**1.9**

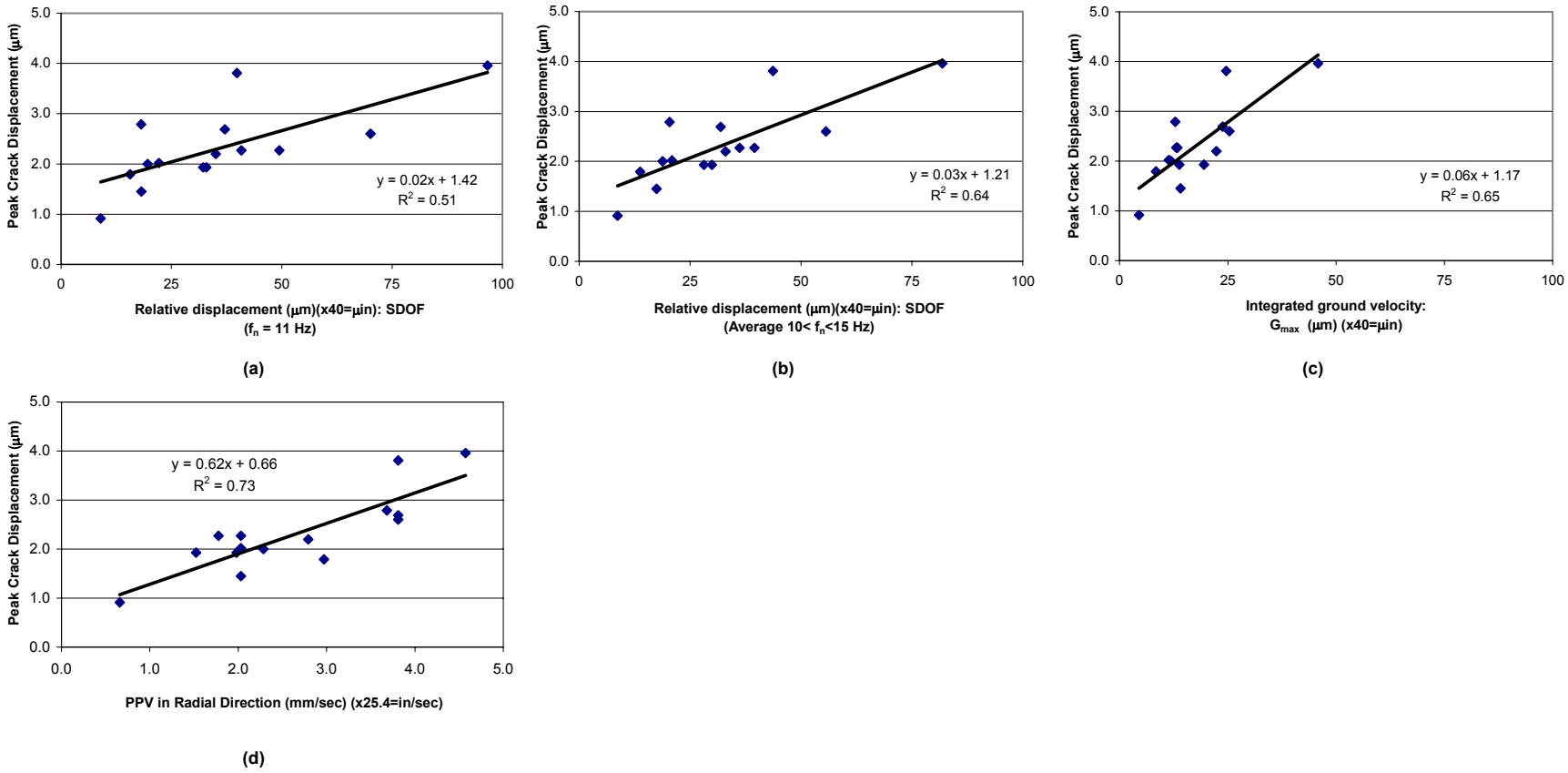

Figure 7.15 Correlations between measured crack displacement and computed displacements and peak radial ground motion

A Kaman and LVDT sensor were affixed over the same crack adjacent to each other to compare the responses to ground motion, weather events, and occupant activities. The ratio of LVDT to Kaman response was consistently 1.25, or 5 to 4, for the maximum ground motion and weather effects. The long-term time histories of responses were remarkably consistent without correction from the null sensors. Both reported similar crack width change over the seven-week interval of observation. Only for the localized occupant activities did the consistency diminish. More research is necessary to identify the reason for the difference in response to the localized events.

The consistency in the ratios of response to transient ground motion and long-term weather effects indicates that each sensor could be employed to compare the effects without prejudice. While the LVDT might report higher dynamic response, it would also report higher response to environmental factors. To determine which sensor measures displacements more accurately, further studies involving the implementation of different sensor types would be necessary. However, for the purpose of the ACM and OSM studies, both sensors prove accurate and adequate to measure crack displacements in this structure and others.

CHAPTER 8

STUCCO AND TILE BLOCK CHAPEL – MINNESOTA

The Minnesota structure, shown in Figure 8.1, is a stucco-faced, tile block structure, located 180 feet (55 m) from anticipated pile driving for road and bridge construction. In June of 2001, autonomous crack monitoring instrumentation was installed to collect data in order to compare effects of ground motions produced by pile driving and weather on interior and exterior cracks. The instrumentation includes the following channels of observation: 3 axes of ground motion, 1 noise (air blast) transducer, 4 channels of crack displacement (static and dynamic), and indoor and outdoor temperature and humidity. The four channels of crack displacements are allocated in pairs. Each pair, indoor and outdoor, consists of a sensor spanning a crack and a companion null sensor spanning a non-cracked portion of the wall adjacent to the crack. The purpose of autonomous crack monitoring is to display via the internet to interested parties the comparison of crack movements produced by dynamic events to those produced by environmental changes or household activities.

Structure Description

The sixty-year old chapel, shown in Figure 8.1, is located on the corner of East Diamond Lake Road and Stevens Avenue in Minneapolis, Minnesota, adjacent to I35W. It is constructed of hollow tile covered with stucco on the outside and a combination of stucco and plaster and lath wall cover on the inside. The structure consists of two main sections, the main chapel space,

which faces East Diamond Lake Road, and the church school rooms at the North end of the structure. The monitored cracks are located in and on the chapel as it is closer to the anticipated construction.

As shown in Figures 8.2 and 8.3, the chapel is 2 ½ stories high with a basement. The height of the structure at the nave is approximately 33 to 44 feet (10.0 to 13.4 m), while the height in the vestibules is approximately 22 feet (6.7 m). The area of the chapel is approximately 80 feet by 40 feet (24.4 x 12.2 m).

Figure 8.1 Stucco and tile block chapel

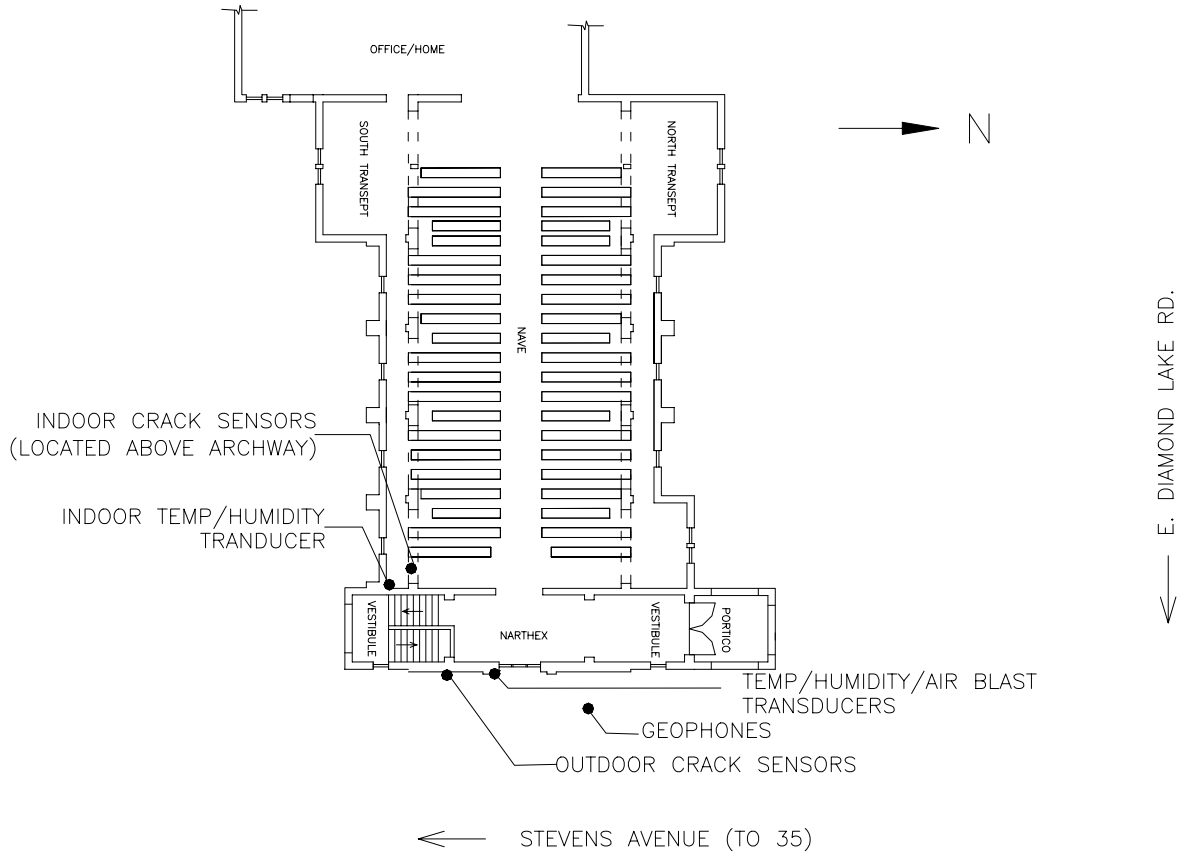

Figure 8.2 Plan view of chapel

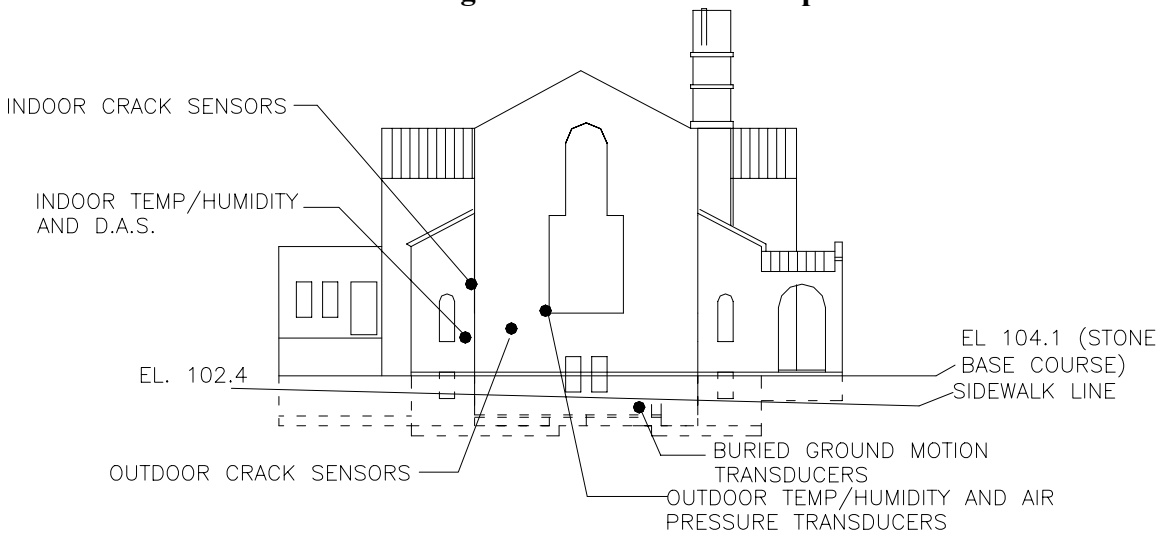

Figure 8.3 Elevation view of chapel

Location of instrumentation

LVDTs (or Linear Variable Differential Transformers) have been employed for this ACM study. The sensors employed, are the DC 750-050 and DC 750-125 LVDTs produced by MacroSensors. The 050's, illustrated in the schematic drawn in Figure 8.4, have a stroke range of ± 1.3 mm or ± 0.05 in (± 3.17 mm or ± 0.12 in for the 125's) and voltage range of ± 10 volts. Each sensor is deployed in the same configuration. The conversion factor for the 050 is 7.87 volts/millimeter (0.31 volts/in) and that for the 125 is 3.15 volts/millimeter (0.12 volts/in).

The LVDT consists of two parts: a moveable magnetic core that is threaded onto a stainless steel screw and attached to the aluminum bracket; and a circular body with an cylindrical inner opening in which the core is able to translate parallel to the cylindrical axis. The core is centered within the body of the sensor, without contact, and moves relative to the body. This relative displacement changes the magnetic field in the core, which in turn changes the output voltage.

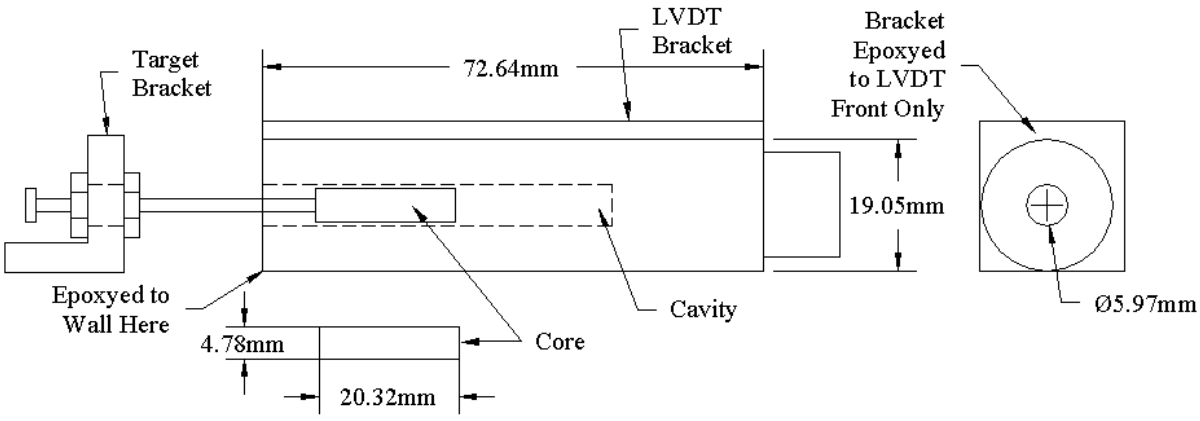

Figure 8.4 Schematic of DC 750 series LVDTs

As noted in Figure 8.2, two of the LVDTs were placed inside of the structure over plaster, while the other two were placed outside of the structure over stucco. Of each of the two pairs, one of the sensors was placed over a crack, while the other was placed nearby, over an un-cracked portion of the wall.

As shown in Figure 8.5, the indoor sensors were placed in the southwest portion of the chapel, at the center of an archway at the East end of the chapel, approximately 12 ft (3.7 m) above the floor. All of the arches along the nave are cracked at the top center. This location was

chosen because it was at the East end of the chapel, closest to the proposed construction, and also because the crack appeared to be active. There were obvious attempts to repair the crack. The crack, which spans vertically from the arch to the ceiling, is approximately 800 μm (31,600 μin) wide.

As shown in Figure 8.6, the outdoor sensors were placed along the East wall of the structure, to the left of the large stained glass window, approximately six feet from the ground surface. The crack spans horizontally, and is approximately 1000 μm (39,500 μin) wide. The crack is stained, which indicates long-term activity. This location east of the interior crack, was chosen because of its proximity to the proposed construction, 100 to 200 ft (30 to 61 m) from the East wall.

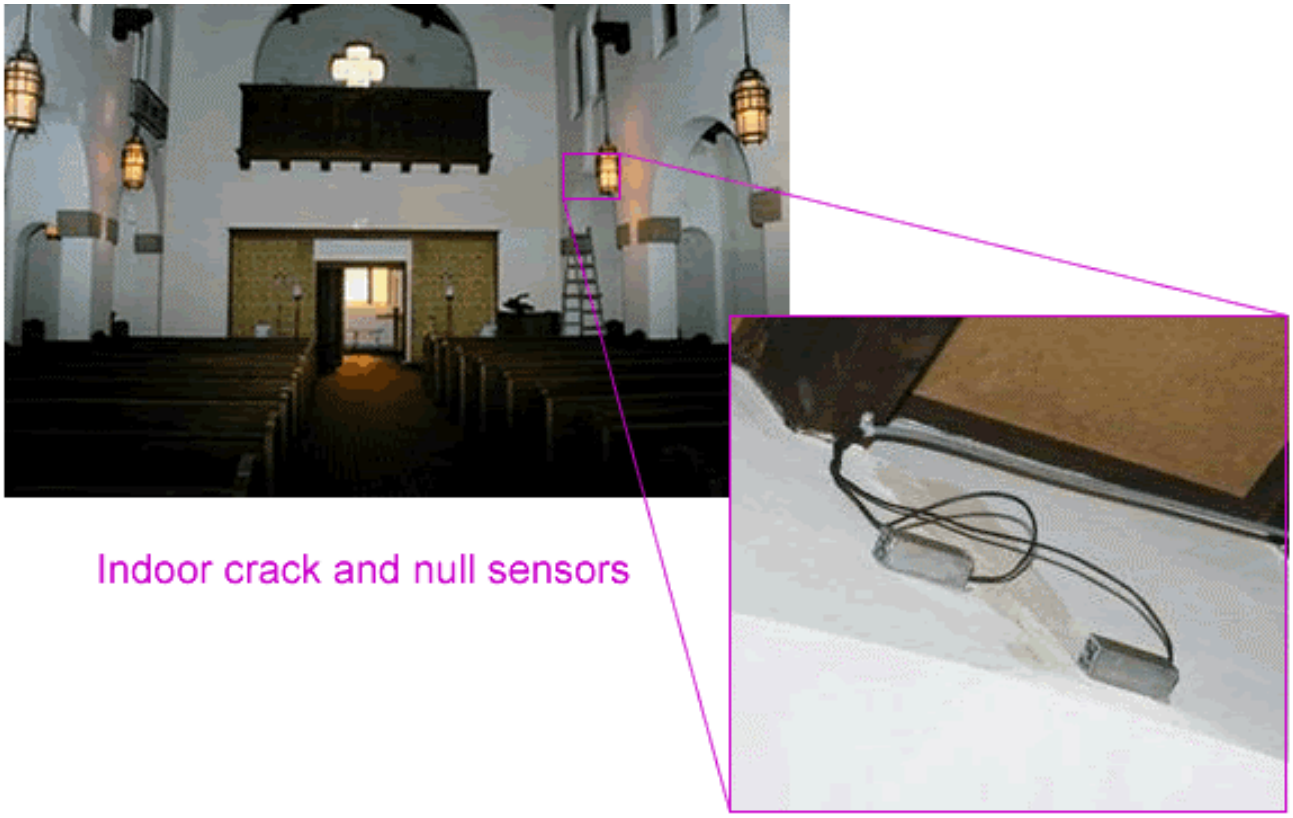

Figure 8.5 Indoor LVDTs in Minnesota chapel

Figure 8.6 Outdoor sensors on Minnesota chapel

In addition to the displacement sensors and ground motion transducers, indoor and outdoor temperature and humidity sensors, and a Larcor overpressure microphone were installed. The locations of these additional sensors are indicated in Figures 8.2 and 8.3. The block of three transducers that measure vertical and two components of horizontal ground motion was buried approximately one foot under the ground surface, approximately seven feet (2.1 m) away from the East wall of the chapel. The orientation of the block is the same as that employed at the OSM structures and in Wisconsin. One Vaisala Temperature and Humidity Measurement instrument was placed in the vicinity of the indoor displacement sensors, directly in the corner, above the heating duct, approximately seven feet (2.1 m) above the floor surface. The other Vaisala was placed outside near the outdoor displacement sensors at the corner of the large stained glass window, which is approximately five feet (1.5 m) above the ground surface. The

overpressure microphone is located adjacent to the outdoor Vaisala instrument, as shown in Figure 8.6. Due to improper wiring of the microphone, however, accurate measurement of air pressure has not been recorded.

The Data Acquisition System (DAS) was placed in the southwest corner of the chapel under the archway on which the indoor transducers was fixed. It was attached to the bottom of a pew seat, oriented parallel to the nave of the chapel as shown in Figure 8.7. The industrial modem and 12V power supply were also attached underneath the pew. All details on instrumentation and configuration of the system can be found in Appendix D.

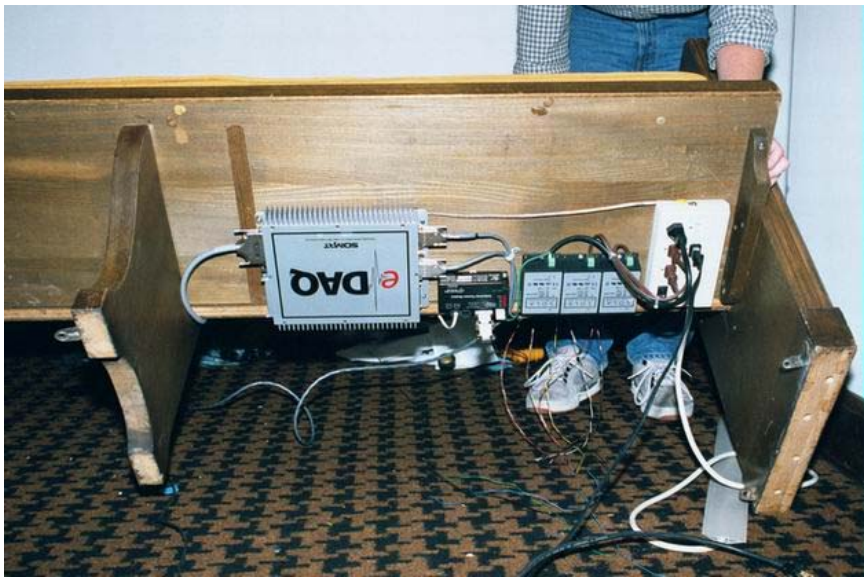

Figure 8.7 Data acquisition system

Extent of Monitoring

The data being collected by the DAS consist primarily of hourly readings from the LVDTs and the weather sensors. Once an hour, nine samples are taken from each channel, at a rate of 1000 samples per second, and averaged to return a single value. In addition, threshold values have been set to trigger the collection of dynamic data when certain levels of ground motion are detected. Currently, this threshold value is set at 0.02 ips (0.5 mm/sec). Therefore, whenever ground motions of 0.02 ips (0.50 mm/sec) are detected, a three second stream of data

are recorded by the DAS. These three-second data streams record the ground motions, crack displacements, and air pressure.

The DAS is also configured to record manual burst data during an ongoing test, at any given time, for any given amount of time. Therefore, if any dynamic events are expected to occur, it would be possible to collect a constant stream of data during a specified time interval.

Crack Response to Environmental Effects

Figures 8.8 and 8.9 compare the long-term action of weather indicators (temperature and humidity) with the long-term crack response of the indoor and outdoor sensors, respectively. Temperature, crack displacement, and humidity are plotted on the same time scale to illustrate interrelationships. Long-term crack displacement, temperature, and humidity were all measured hourly during the monitoring period. The outdoor crack appears to be less active than the indoor crack. During the colder months of December and January, greater cyclic crack displacements can be observed for both outside and inside cracks.

Table 8.1 lists the average and maximum values for the frontal, daily, and combined weather effects for temperature, crack displacement, and humidity. The overall averages for temperature, indoor crack displacement, outdoor crack displacement, and humidity are 60 °F (15.6 °C), 66 μm (2607 μin), -46μm (1817 μin), and 63%, respectively. Further details on the technique of calculating weather displacements can be found in Chapter 3.

Table 8.1 Computed crack displacement due to long-term weather phenomena

	Temperature Change (DegF)	Indoor Crack Displacement (μm)	Outdoor Crack Displacement (μm)	Humidity Change (%)
Frontal Effect				
Average deviation of 24 hr average from overall average	12	43	23	9
Max deviation of 24 hr average from overall average	31	155	79	27
Daily effect				
Average of deviations from 24 hr average trend	5	50	24	11
Max deviations from 24 hr average trend	12	100	57	25
Weather Effect				
Average deviations from overall average	12	62	31	14
Max deviations from overall average	34	217	107	37

Compared to the other structures in previous chapters, the displacements due to weather effects are much larger for this structure. However, it is important to note that the time of observation was much larger than were the times for some of the previous structures. By monitoring the structure response over a greater time period, the structure is affected by more extreme weather fronts, as well as, seasonal changes. The OSM structures in Chapters 3, 5, and 6 were monitored for less than a week; which is too short a time to reliably observe a significant frontal effect. To faithfully compare the magnitude of the displacements, the structures should be monitored for the same length of time during a transition season such as spring or fall.

Figure 8.10 displays a shorter period of time to magnify the changes measured with the crack sensors and to investigate the need for null sensor correction. The top plot defines the maximum displacements from frontal, daily, and weather effects described above. The lower two plots show the crack displacement measured by each crack sensor compared to the displacement corrected by the null sensor. The corrected crack displacement is calculated by subtracting the measurement recorded by the null sensor from its respective crack sensor. These comparisons show that the corrections made with the null sensor are minimal and do not change the variations in long-term response. In this case, they are so minimal as to be unnecessary.

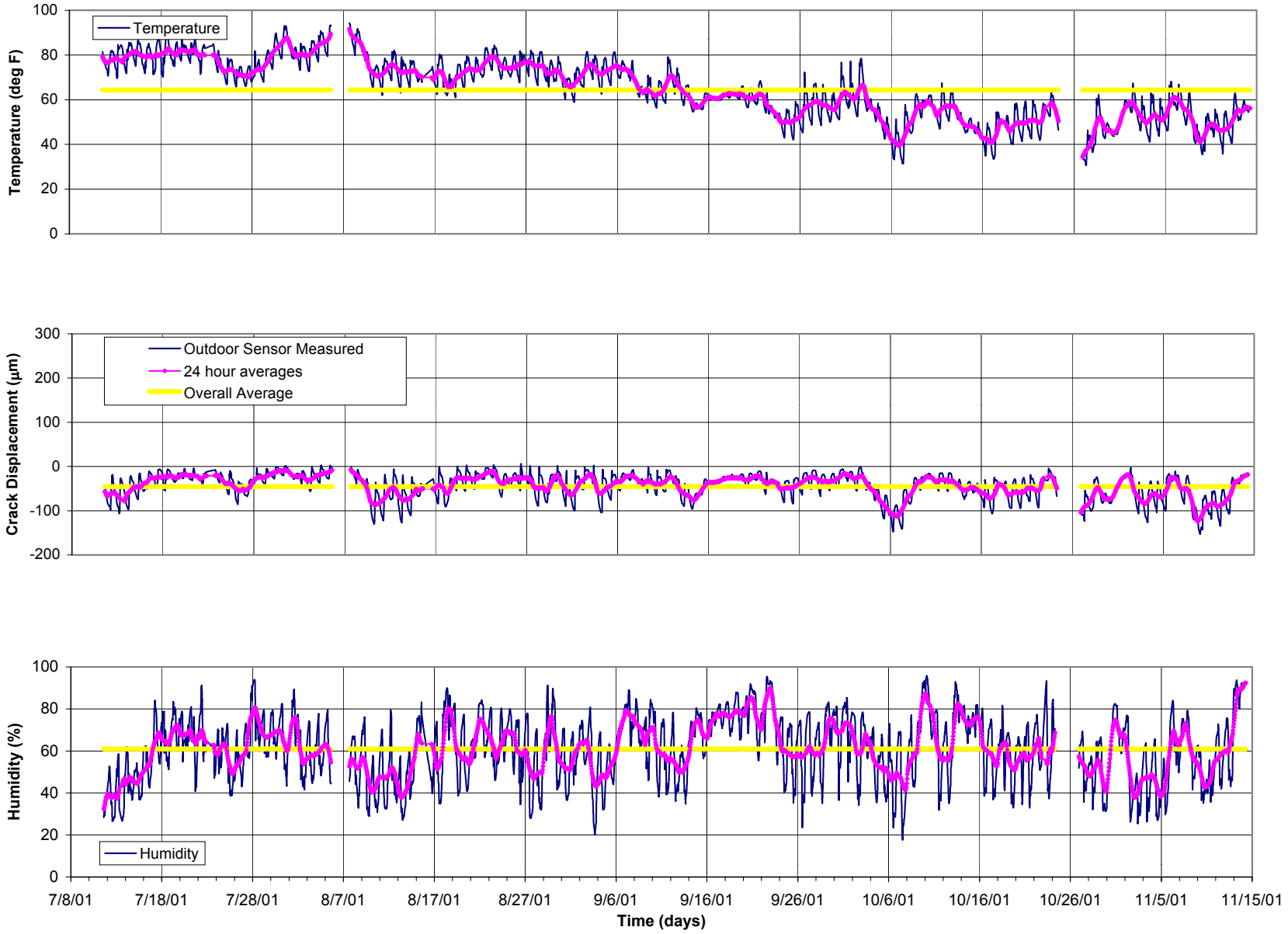

Figure 8.8 Long-term indoor crack displacement and weather versus time

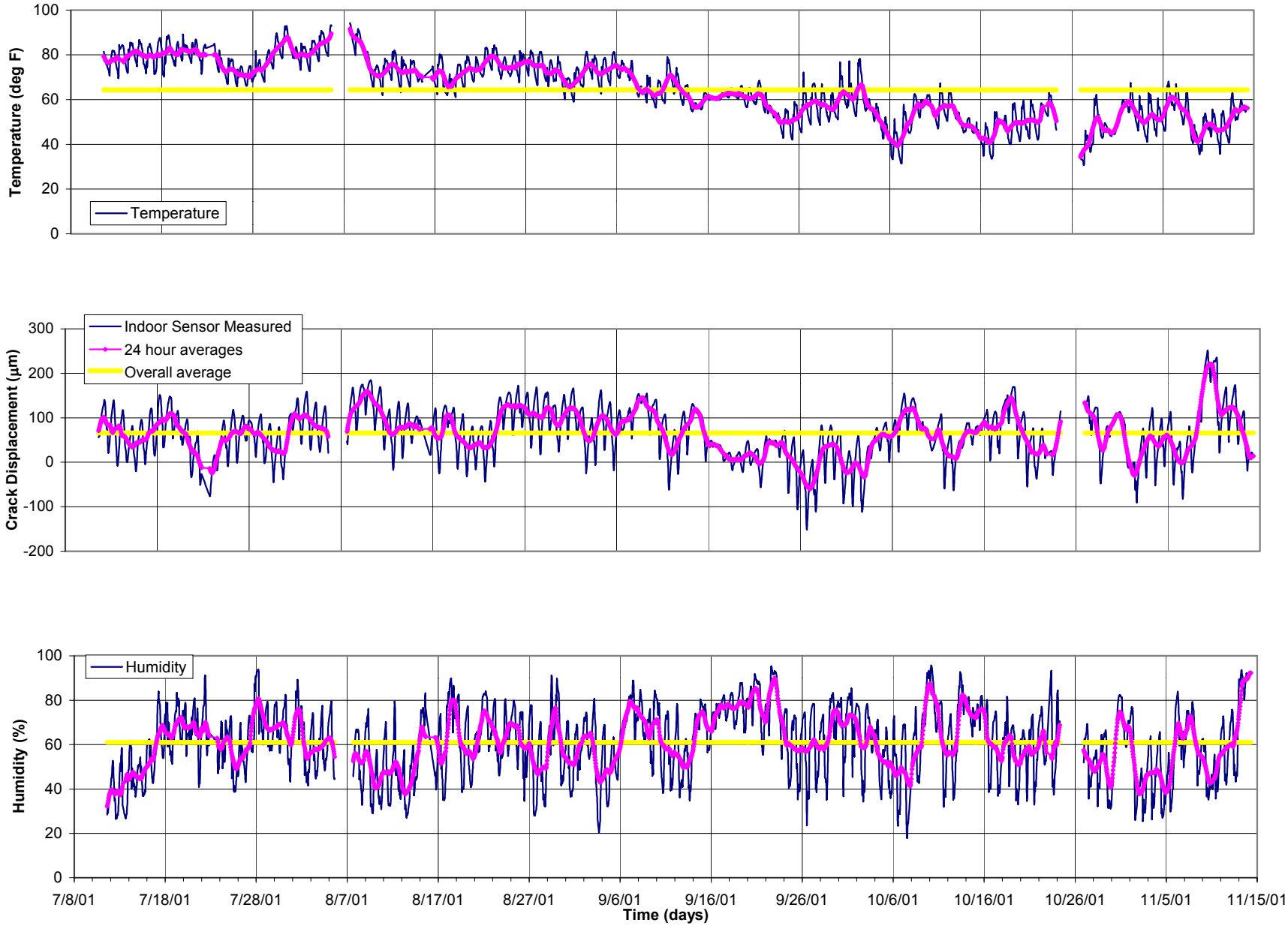

Figure 8.9 Long-term outdoor crack displacement versus time

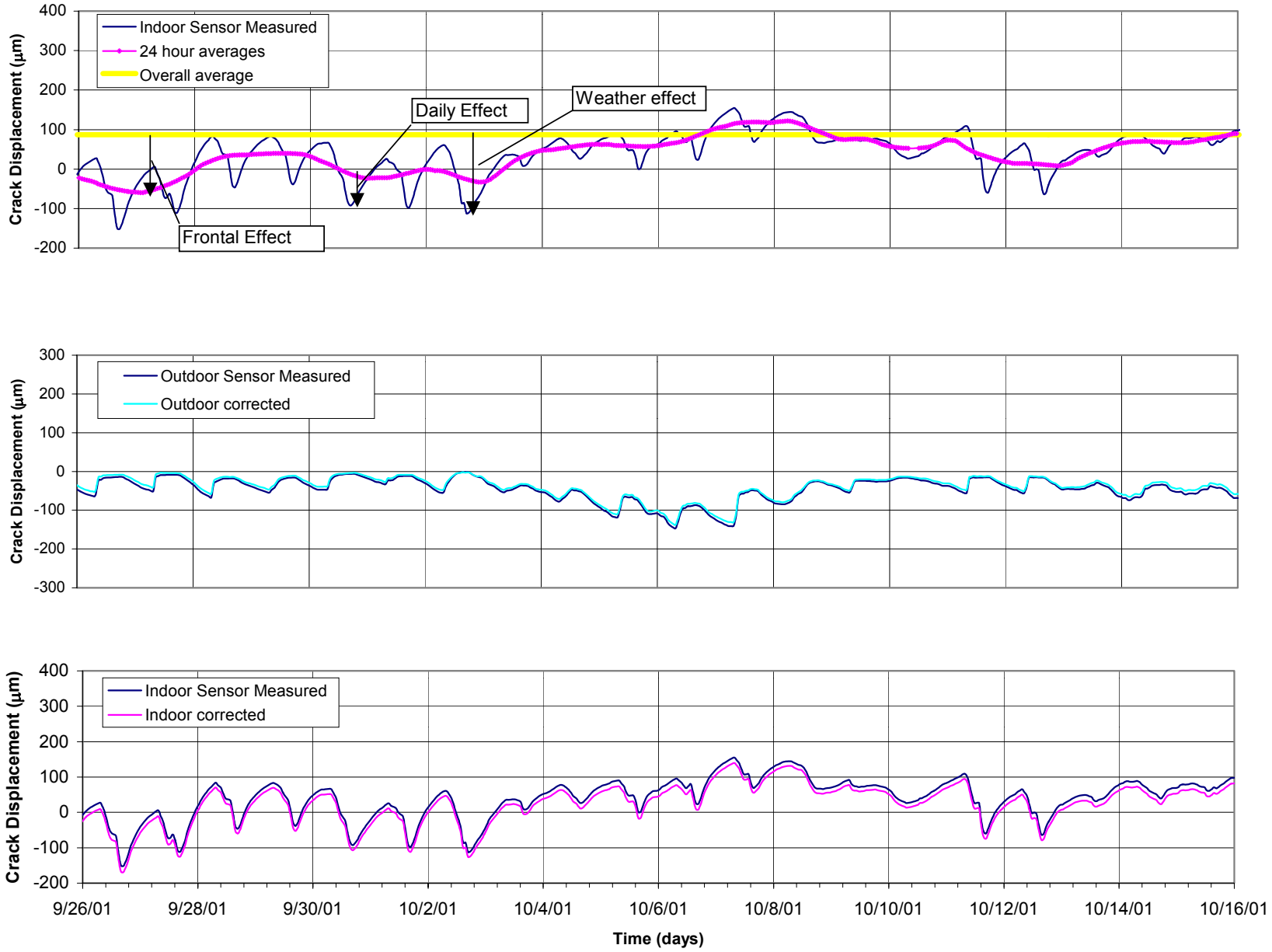

Figure 8.10 Typical crack displacements due to long-term phenomena

CHAPTER 9

SYNTHESIS

This chapter synthesizes the long-term and vibration response of seven structures. Four of the eleven atypical structures instrumented during the Office of Surface Mining 2000-2001 investigation (Aimone-Martin, 2002) were fitted with special instrumentation to monitor crack response. This thesis reports the findings structure by structure in separate chapters, and synthesizes the results by comparing measurements from all four atypical structures as well as that from three other ACM structures. Specially programmed data acquisition devices were employed to detect and compare both long-term, or weather, and transient, or blast effects on the cracks for all seven. Combination of this crack response with the velocity response of the baseline OSM study provides additional insight into the relation between structural, wall, and crack response to vibratory excitation.

The four OSM structures vary widely, and include a double-wide trailer (T), an adobe brick ranch house (A), a concrete block basement wall of a bungalow (B), and a highly distressed wood-framed house (D). The three ACM structures include a stone block house (C), a Victorian wood framed house (V), and a stucco over hollow tile Chapel (S). Observation of the unique, atypical structures extends the database on the response of cracks in relation to both environmental and vibratory effects. Location of the cracks also varies widely, and includes cracks on: 1) interior drywall (T) and (C) and plaster and lath (D) and (V), as well as, 2) exterior concrete block (B), adobe (A), and stucco over hollow tile (S). All structures were one story,

with the exception of the chapel (S) and the Victorian house (V), and all but the adobe house (A) were founded on a basement.

Environmental and Vibratory Effects

Environmental and vibratory responses of cracks for the four atypical houses are compared with those from three other houses in Table 9.1, and the bar chart in Figure 9.1. Response is defined as the micrometer change in crack width. All comparisons in this synthesis are based on data within this thesis, with the exception of one structure, (V). Responses presented in this chapter for the Victorian structure (V) were obtained during the development of the data acquisition device (Siebert, 2000).

The seven homes geographically were widely distributed in central Pennsylvania (T), northern New Mexico (A), southern Indiana (B & D), southern Wisconsin (C), northern Illinois (V), and eastern Minnesota (S). Data were collected during all seasons of the year. In addition to the weather and vibratory crack responses, responses to occupant activities were measured at four of these structures.

Weather effects were monitored over widely variable time periods. Three of the four "atypical" structures were monitored for periods of a week or less. The adobe (A) was observed for nearly a month. The (C), (V), and (S) structures were observed for longer periods, 2 months, 3 months, and 4 months, respectively. The short, week-long periods of observation most likely do not include extreme weather and thus probably under-report weather effects.

Maximum weather effects are at least an order of magnitude greater than the vibratory effects produced by ground motions of 0.1 ips (2.5 mm/sec) for all six of the structures studied. In one case, (T), the maximum weather-induced response is even greater, 40 times greater. As described earlier, the maximum weather effect is defined as the maximum of deviations of the peaks from the overall average crack width change during the study period. The vibratory response is the maximum, zero to peak change in crack width during the vibratory response. Both, the long-term, weather, and transient, vibratory responses are measured by the same sensor and are thus directly comparable.

Table 9.1 Summary of measured displacements due to static and dynamic events

Event	Displacement (micrometers)						
	(T) Trailer Interior Drywall	(A) Ranch Exterior Adobe	(B) Bugalow Exterior Concrete Block	(D) Distressed Frame Interior Plaster/Lath	(C) Block/Stone Interior Drywall[1]	(V) Victorian Frame Interior Plaster/Lath[2]	(S) Chapel Stucco Exterior
Width of crack (micrometers)	700	800	500	1200	500	500	1000
Max Frontal Effect	11	9	3	16	35	100	155
Max Daily effect	16	25	9	25	10	20	100
Max Weather effect	24	25	12	52	44	-	217
Days of observation	5	35	4	3	37	92	126
ΔT (deg F)	13	51	30	17	44	41	63
Max Blast event (ppv in ips)	0.9 (0.32)	4.2 (0.13)	0.3 (0.23)	13.6 (0.30)	7 (0.13)	-	-
Blast event at 0.10 ips	0.3	2	0.2	5	6	-	-
Slamming door (distance to crack in ft)	2.5 (6)	-	-	1.6 (14)	3.5 (7)	10 (5)	-
Jumping (distance to crack in ft)	1.5 (10)	-	-	1.9 (16)	-	-	-
Hammering (distance to crack in ft)	0.2 (11)	-	-	2.2 (1)	-	-	-
Shutting window (distance to crack in ft)	-	-	-	4.1 (3)	-	-	-
Walking on Stairs	-	-	-	-	-	40	-
Foundation Response	-	16	-	-	-	-	-
Seasonal Heating	-	-	-	-	-	300	-

Notes:
(1) Crack #1 (Louis, 2000)
(2) Crack #2 located under stairwell (Seibert, 2000)

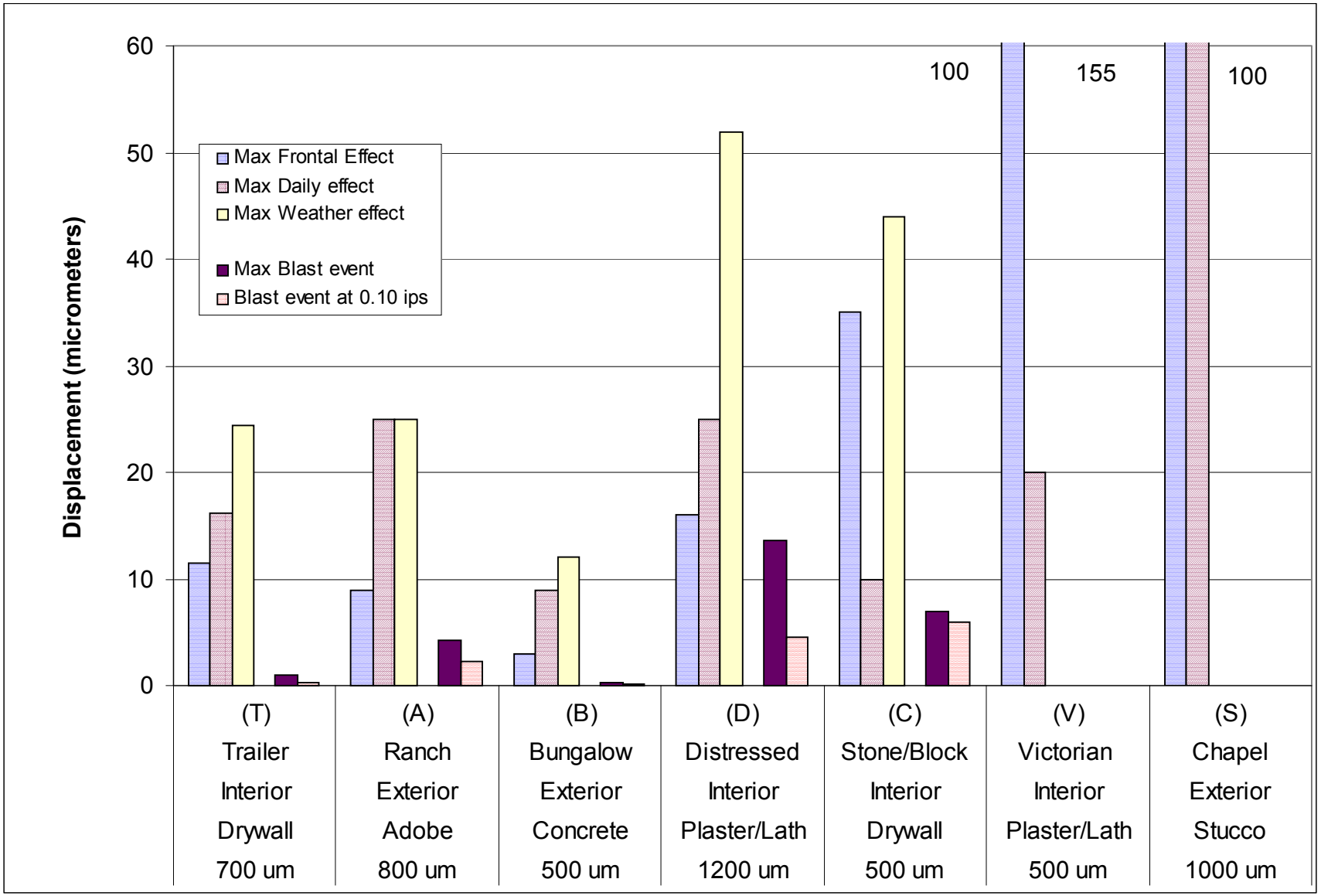

Figure 9.1 Comparison of measured displacements due to static and dynamic events

Crack Response to Environmental Effects and Occupant Activities

There is a weak correlation of crack response with crack width for those cracks in wall covering. The widest crack, 1200 μm (47,400 μin), in the distressed frame, D, displayed the largest weather response as well as the largest response to vibratory excitation. That with the thinnest, 500 μm (19,800 μin), the trailer, T, displayed the least response again to both weather and vibratory excitation. Crack widths were estimated from photographs (by scaling off of known distances) shown in the previous descriptive sections for each structure.

Response to occupant activity can be as large as that produced by vibratory excitation as shown in Table 9.1 and Figure 9.1. Responses presented are a common subset of the widely variable activity tests conducted. Distances to the activity are shown along with the crack responses produced. Those activities closest to the crack produced the greatest response. The greatest response, 40 μm (1580 μin), is produced by walking or running past the crack in a stairway (V), which may contain a construction defect.

Responses to two unique events, a rain storm in New Mexico (A) and seasonal heating in Illinois (V), created large and relatively permanent crack responses. A half-inch rainfall at the adobe home (A) produced a permanent displacement 16 micrometer change that remained for the duration of the observation. This is 8 times greater than the response of the crack to 0.1 ips (2.5 mm/sec) blast-induced ground motions. Over the period of December to March, heating of the wood frame house (V) changed the crack width of a basement crack by 300 μm (11,900 μin). This house is not located near a blast vibration source. However, a comparison can be made through occupant-induced motions. Slamming a door 5 ft (1.5 m) away produced 10 μm. Thus the seasonal heating response is some 30 times greater than that to an adjacent door slam.

Crack Response to Vibratory Ground Motion

Aggregating the crack width response for all homes into a single graph allows comparison of the variability of vibratory response by crack type and/or structure type. The same format has been employed for aggregated data in Figures 9.2 and 9.3, as for each structure individually. The maximum measured crack displacement produced by each shot is compared to

various parameters employed for correlation with calculated, estimated, or approximated relative displacements and/or visual observation of the threshold of cosmetic cracking. The responses analyzed were those motions parallel to the wall containing the crack because the crack displacement was measured in the plane of the crack. Table 9.2 summarizes the regression coefficients determined for these comparisons, which are individually presented in the appropriate chapters. Details of the methods of calculation, estimation, and approximation can be found in Chapter 3. Figure 9.2 contains the correlations with the calculated and estimated displacements, while Figure 9.3 contains the correlations with the approximated displacements.

Table 9.2 Summary of correlations between measured crack displacement and calculated, estimated, and approximated relative wall displacements and PPV parallel to plane of crack

Regression coefficients determined between measured displacement and:	(T) Trailer Interior Drywall	(A) Ranch Exterior Adobe	(B) Bugalow Exterior Concrete Block	(D) Distressed Frame Interior Plaster/Lath	(C) Block/Stone Interior Drywall	(V) Victorian Frame Interior Plaster/Lath	(S) Chapel Stucco Exterior	Average correlation from OSM structures (T-D)	Average correlation from all structures
Calclated displacement: Integrated top-Integrated bottom	0.95	0.87	0.29	0.99	-	-	-	0.78	0.78
Calculation displacement: Integrated top - Integrated ground	0.75	0.39	0.28	0.99	-	-	-	0.60	0.60
Estimated displacement: Integrated ground velocity	0.62	0.51	0.22	0.99	0.65	-	-	0.59	0.63
Estimated displacement: SDOF (f_n of structure)	0.87	0.44	0.62	0.96	0.51	-	-	0.72	0.63
Estimated displacement: SDOF ($10<f_n<15$ Hz)	0.91	0.84	0.67	0.99	0.64	-	-	0.85	0.69
PPV parallel to wall of crack	0.58	0.6	0.9	0.99	0.73	-	-	0.77	0.73
Approximated displacement: $(PV2\pi f)_{top}$-$(PV_{max}2\pi f)_{ground}$	0.35	0	0	0.99	-	-	-	0.34	0.34
Approximated displacement: $(PV_{max}2\pi f)_{top}$-$(PV2\pi f)_{ground}$	0.88	0.28	0.13	0.68	-	-	-	0.49	0.49
Approximated displacement: $(PV_{max}2\pi f)_{top}$-$(PV_{max}2\pi f)_{ground}$	0.19	0.36	0.56	0.98	-	-	-	0.52	0.52
Approximated displacement: $(PV2\pi f)_{top}$-$(PV_{max}2\pi f)_{bottom}$	0.35	0.07	0.03	0.98	-	-	-	0.36	0.36
Approximated displacement: $(PV_{max}2\pi f)_{top}$-$(PV2\pi f)_{bottom}$	0.83	0.91	0.46	0.99	-	-	-	0.80	0.80
Approximated displacement: $(PV_{max}2\pi f)_{top}$-$(PV_{max}2\pi f)_{bottom}$	0.16	0.03	0.01	0.98	-	-	-	0.30	0.30

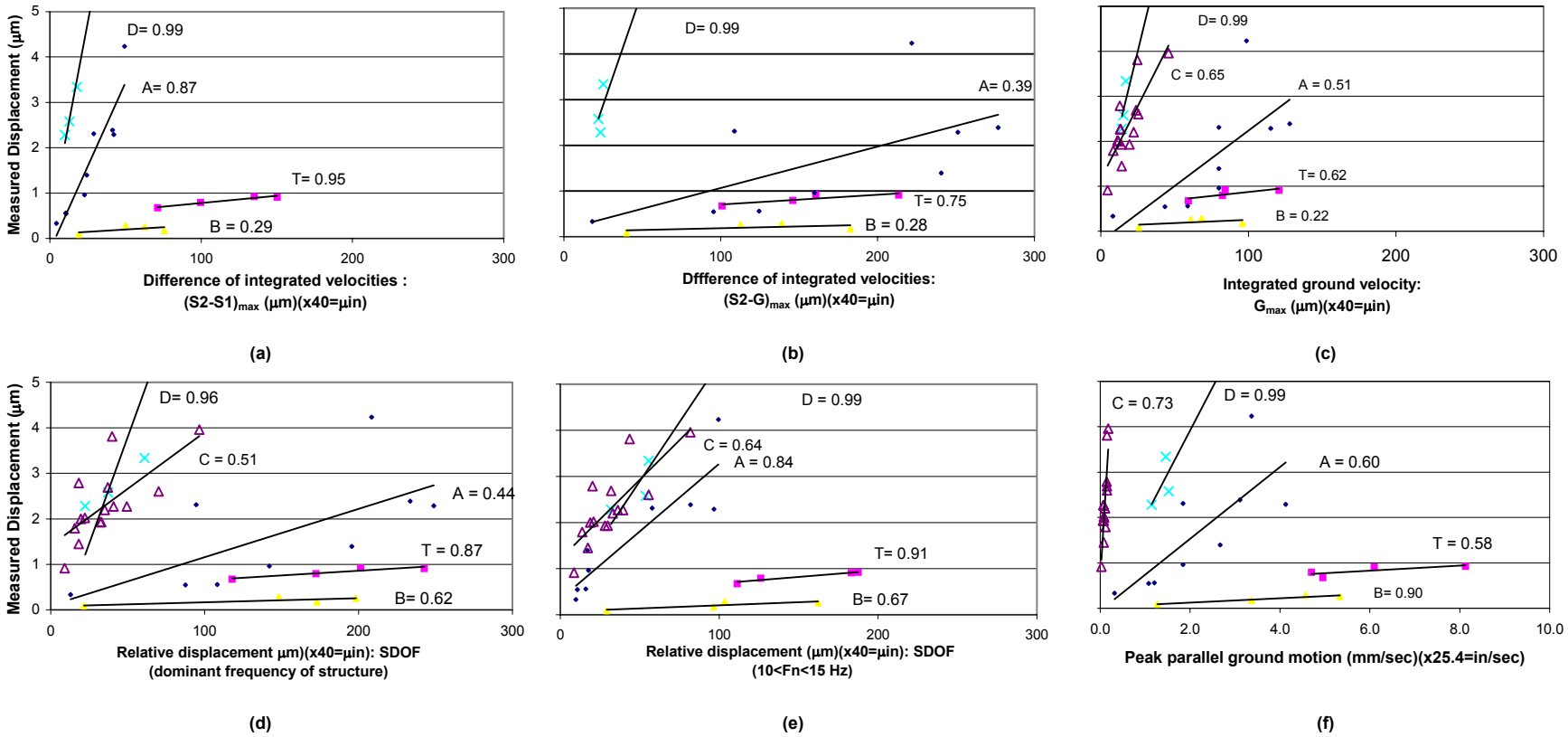

Legend:
T : Double wide trailer
A : Adobe ranch house
B : Concrete block foundation (bungalow)
D : Distressed frame house
C : Concrete block house

Figure 9.2 Comparison of correlations between measured crack displacement and predicted displacements and peak parallel ground motions

First consider the crack location. The crack in the bungalow (B) was located at the top of the concrete block basement wall, only 3 ft (0.9 m) from the ground surface. It has the least response even though it sustained peak particle velocities as high as 0.2 ips (5.1 mm/sec) as shown in Figure 9.2 (f). The low response is expected, as the basement wall moves with the ground and thus is not free to selectively amplify motions as is the superstructure. Such measured displacements of this crack would not be expected to correlate with other measures, which presume free response of the structure. Crack displacement in this basement wall best correlates to peak particle velocity because it is most directly related to ground strains. It has the worst correlation with calculated displacement (between the top and bottom corners of the structure), as these responses are for the above ground, freely responding portion of the structure.

Next consider crack response. The most active of the three cracks in wall covering of the superstructure was also the widest, (D). As can be seen in the crack photographs, this crack was different from the others. It was significantly wider and more uniform in width. The correlations for D are uniformly the highest; however, these high correlations may result from the large range of measured crack width changes as seen in the detailed presentation of D data. The graphs in Figures 9.2 and 9.3 have been truncated at 5 μm (198 μin) for measured crack displacement, to illustrate the comparative trend of all the data. Therefore, the point that represents the crack response (at house D) of 14 μm (553 μin), at a peak particle velocity of 0.28 ips (7.1 mm/sec), is not visible in these figures.

Cracks that are most active when perturbed by ground motion are also seen to be the most active when perturbed by changes in the weather. The most active crack is defined as that which has the steepest slope in Figures 9.2 and 9.3. Cracks in structures C and D would be the most active, and that in B would be the least. Comparison of the slope with the maximum weather effects in Table 9.1 shows that D is twice as responsive to weather changes as T and A. There are too few data points to draw a numerical correlation between these three structures, as the one-week observation period for weather effects was too short to ensure that extreme events were captured. Further insight can be gained when comparing structures A and C, which were monitored for the same length of time. Structure C exhibits the steeper slope in three of its correlations, as well as the higher response to weather effects. This higher response further supports the link between large vibratory response and large weather response. As for the

remaining structure, while the crack in structure B was the least active, its location on a basement wall so close to the ground renders it particularly insensitive to daily changes in weather.

Consider the three cracks that were located above ground, where superstructure response was possible (T, A, and D). Measured crack displacement correlated best with the difference in displacements calculated from motions measured at the top and bottom of the structure, parallel to the plane of the crack. This correlation is shown in Figure 9.2 (a). High correlation is expected, as this difference is the relative displacement of the wall, which is proportional to the gross, in-plane, shear strain in the wall. As such the calculated difference in displacement also could be considered as a direct measurement of the gross wall strain.

The second best correlation with the measured crack displacement is obtained from the pseudo velocity response spectrum (PVRS), for the frequencies between 10 and 15 Hz. The PVRS is a derivative of calculated relative displacement that accounts for the structural response frequency, as well as, the full excitation time history (Dowding, 1996). These correlations are almost identical to that between the two direct measures of wall strain. The single point for a range of frequencies was obtained by averaging the relative displacement responses for each frequency between 10 and 15 Hz. This frequency range corresponds to that of the walls. Correlations are lower with PVRS displacements for the natural frequency of each superstructure, but are still higher than those for other estimates in Figure 9.2, with the exception of structure C.

Typical structural response monitoring is commonly undertaken with motions measured in the ground and upper structure, non-time correlated, and with separate vibration monitors. It is instructive to gauge the effectiveness of various estimates of displacements made with these types of data. Estimates of wall strain can be made from sinusoidal approximations of displacement, which are peak velocities divided by two times Pi times the associated frequency ($PV/2\pi f$), as explained earlier. Displacements approximated from the velocity time histories at various locations can be subtracted to obtain various measures of relative displacement. Approximated relative displacements have been produced from the following pairs of velocity time histories: 1) ground and top corner motions at the time of peak ground motion, 2) ground and top corner motions at the time of peak top corner motion, 3) peak ground and peak top corner motions, regardless of the time at which each occurs. Figures 9.3 (a) to (c) show the

correlations of measured crack displacements with these approximated relative displacements. None of the three possibilities with the top response and the ground response display high correlations as uniformly as the calculated and estimated values in Figure 9.2 identified above.

Another alternative is to measure top and bottom response and ignore ground motion. Approximated relative displacements were also analyzed, where velocity in the bottom corner was used in place of ground motion. These approximations are shown in Figures 9.3 (d) to (f). The highest correlation is found in Figure 9.3 (e). Here, the approximation is computed at the time of maximum top corner response. This approximation of relative displacement differs only from the direct calculation (Figure 9.3 (a)) by the manner in which displacement is obtained.

Structural response velocity measurements were made with small single axis transducers glued to the walls at the corners of the structures. When mounted on cantilevered brackets, large multi-axial devices from commercial vibration monitors may not yield the same quality in data. Even though the standard configuration of velocity transducers is a triaxial block, it is recommended to employ single, uniaxial transducers to simplify mounting difficulties.

These differences in response described above are small compared to the large impact of weather related response demonstrated in Figure 9.1. Changes in crack width produced by ground motions between 0.10 and 0.30 ips (2.5 and 7.6 mm/sec) were less than 5 μm (198 μin), except in one instance; whereas, the maximum weather responses during one week (or smaller) periods of observations were 10 to 50 μm (395 to 1975 μin). The crack in structure D that showed the exceptionally large vibratory response (14 μm or 553 μin), also showed the largest weather response (52 μm or 2054 μin).

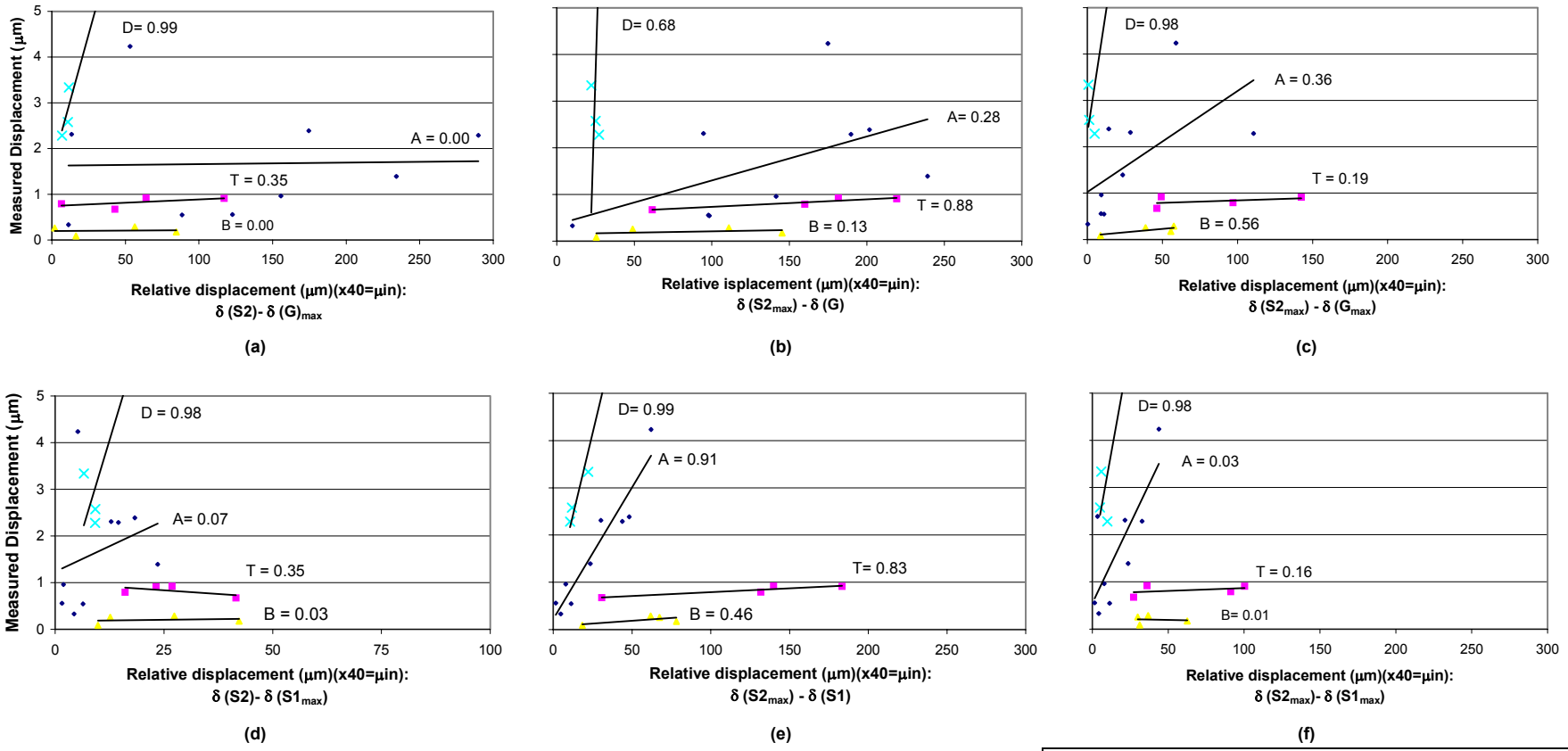

Figure 9.3 Comparison of correlations between crack displacement and calculated relative displacements

REFERENCES

Aimone-Martin, C. and Martell, M-A. (2002). "Response of Non-Traditional Structures to Coal Mine Blasting", New Mexico Institute of Mining and Technology, Socorro, NM.

Dowding, C. H. (1996). Construction Vibrations, Prentice Hall, Upper Saddle River, New Jersey, Chapter 13, "Comparison of Environmental and Vibration-Induced Crack Movement".

Huang, F. et al. (1994). "NUVIB Vibration Analysis Program User's Manual, Version 1.01." Northwestern University, Evanston, IL.

Kosnik, D. (2000). "Java Applet" Internal Report, Infrastructure Technology Institute, Northwestern University, Evanston, IL.

Kosnik, D. et. al, (2000). " Autonomous Crack Monitoring," Internal Report for Infrastructure Technology Institute, Northwestern University, Evanston, IL.Macrosensor (1999). 815 Hylton Road, Unit #8 Pennsauken, NJ. "http://www.macrosensors.com/ghsa.htm".

Louis, M. (2000). Autonomous Crack Comparometer Phase II ,M.S. Thesis, Northwestern University, Evanston, IL.

Nomis Seismographs Data Anaylsis,Version 6.0.0, Nomis Seismographs, Birmingham, AL.

Siebert, D. (2000). Autonomous Crack Comparometer, M.S. Thesis, Northwestern University, Evanston, IL.

Somat Ease version 3.0 (1999). Somat Corporation, Champaign, Il.

Somat TCE eDAQ version3.5.1 (2001). Somat Corporation, Champaign, IL.

Somat TCS for Windows, version 2.0 (1999). Somat Corporation, Champaign, IL.

White Seismographs Data Analysis, Version 5.0.4 (1998), White Industrial Seismology, Inc., Joplin, MO.

APPENDIX A
FOURIER FREQUENCY SPECTRA

Pennsylvania Trailer - 5/22/01 10:38

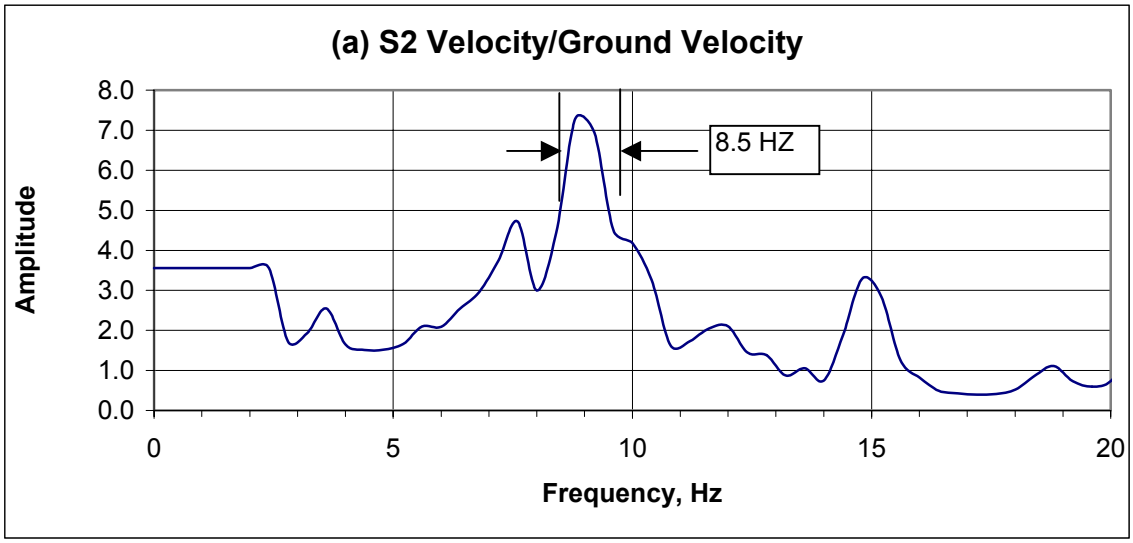

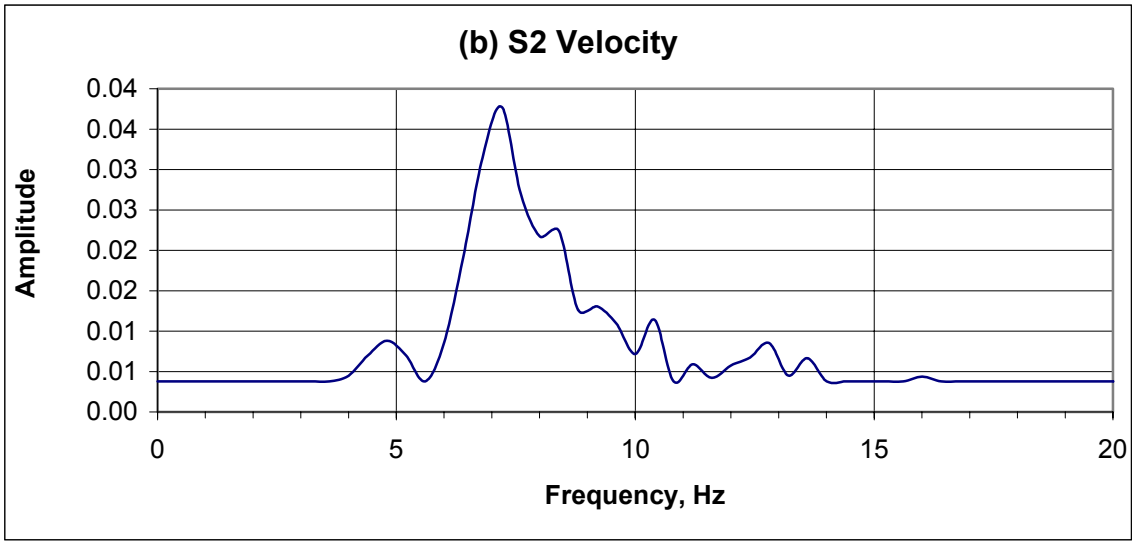

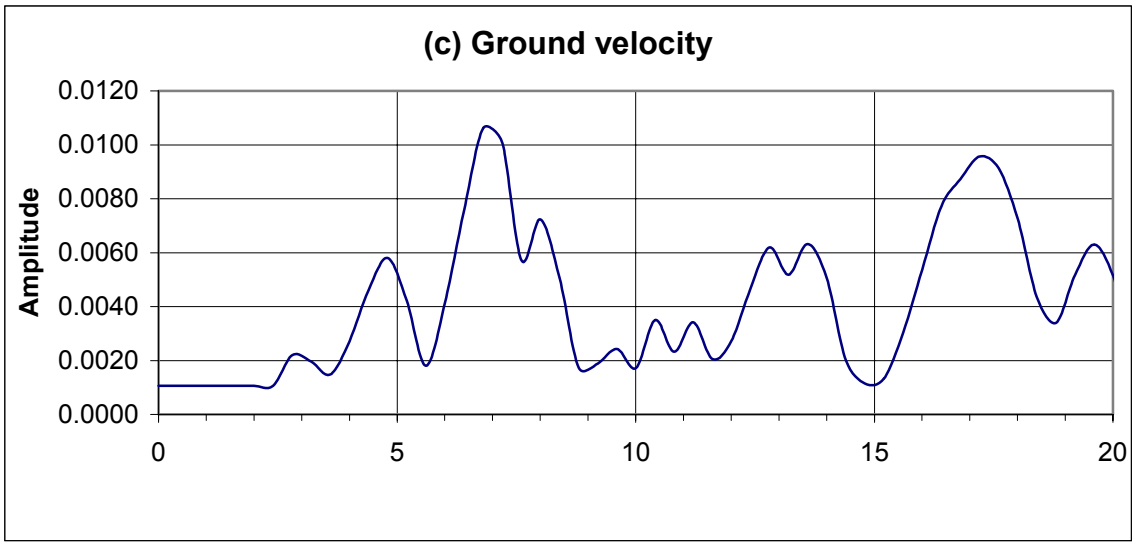

Pennsylvania Trailer - 5/22/01 12:16

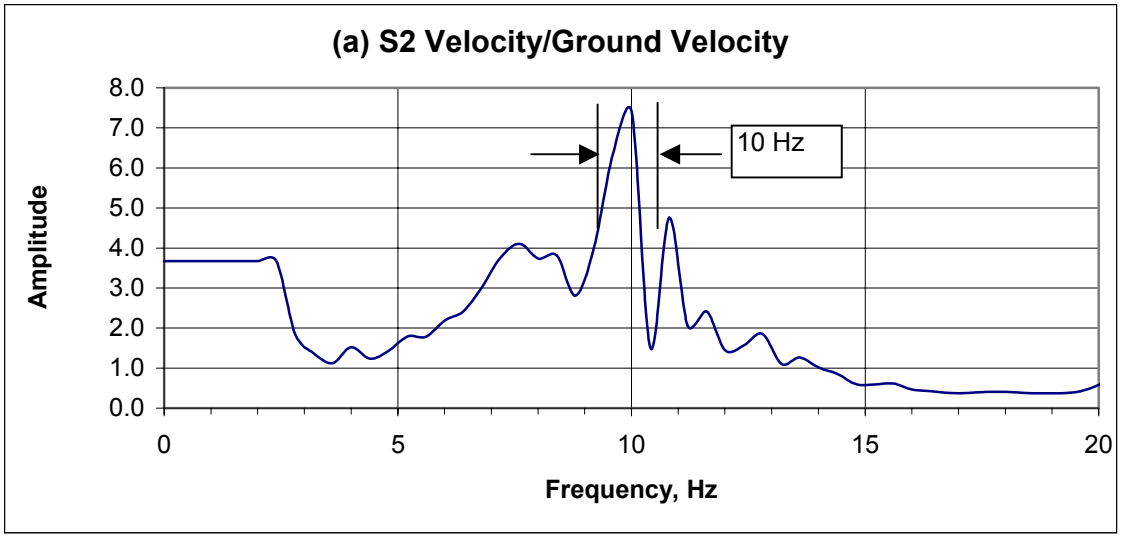

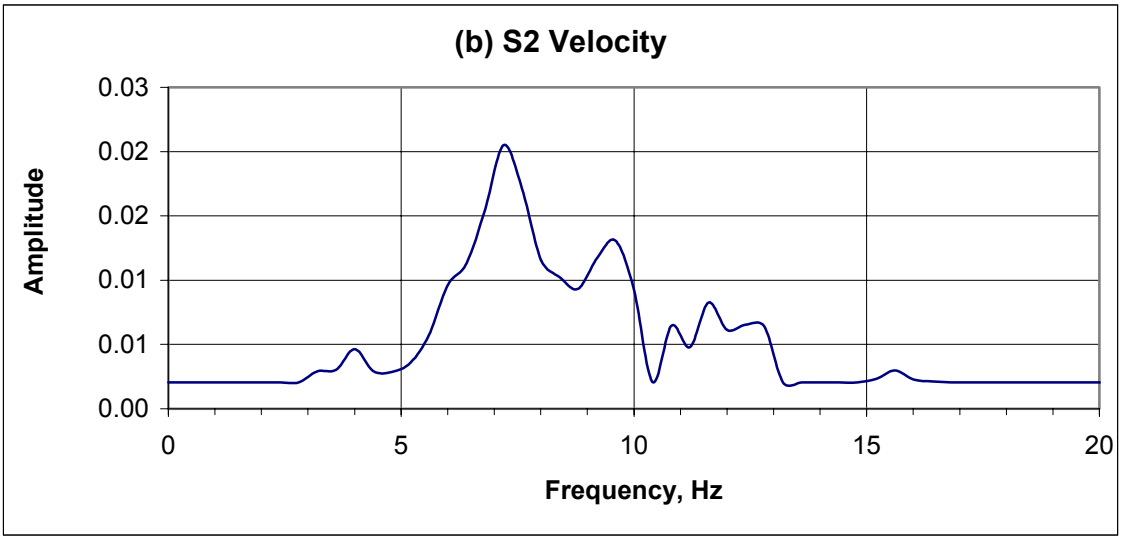

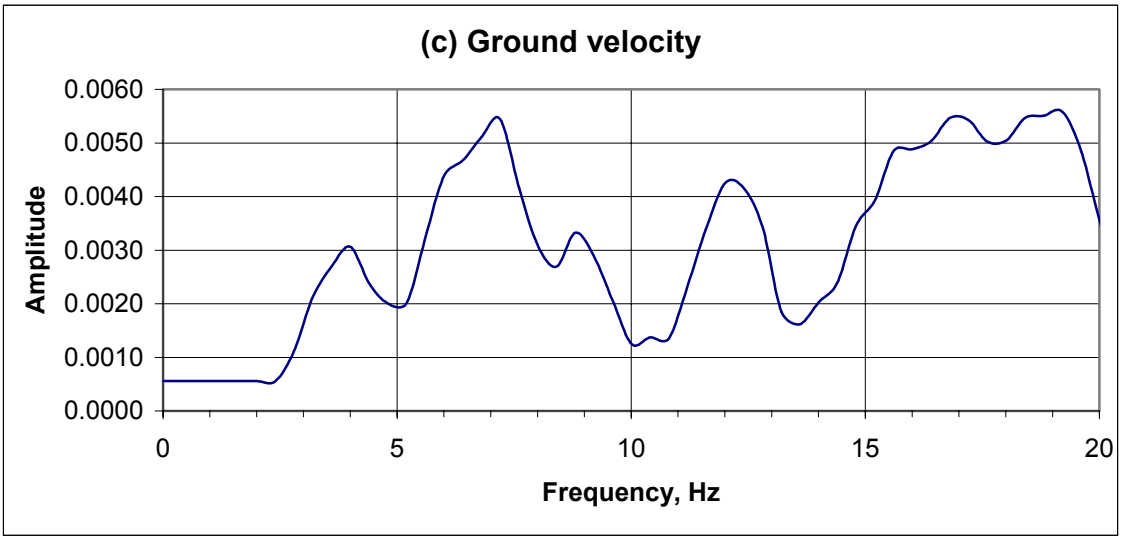

Pennsylvania Trailer - 5/23/01 14:19

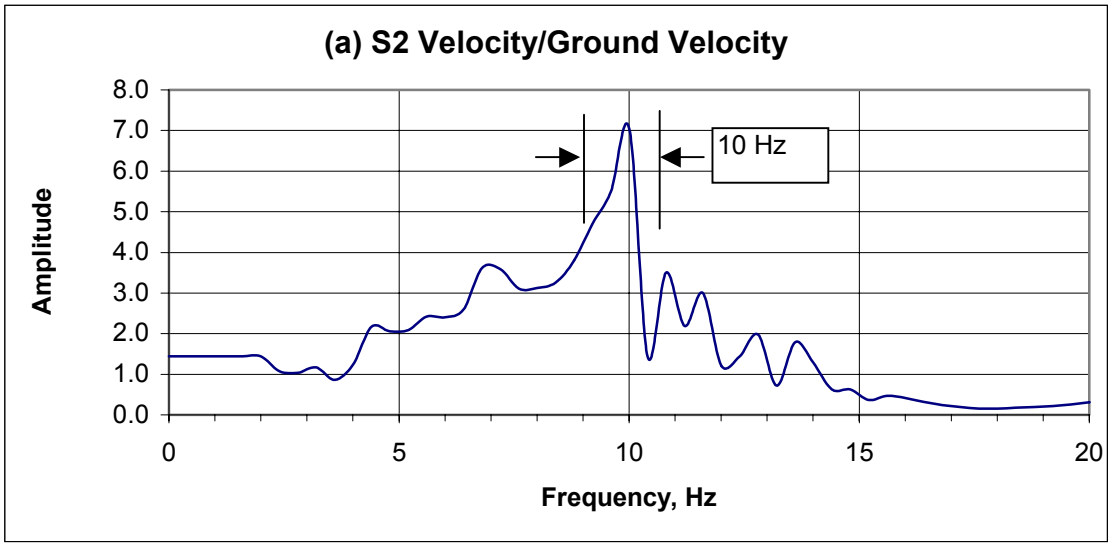

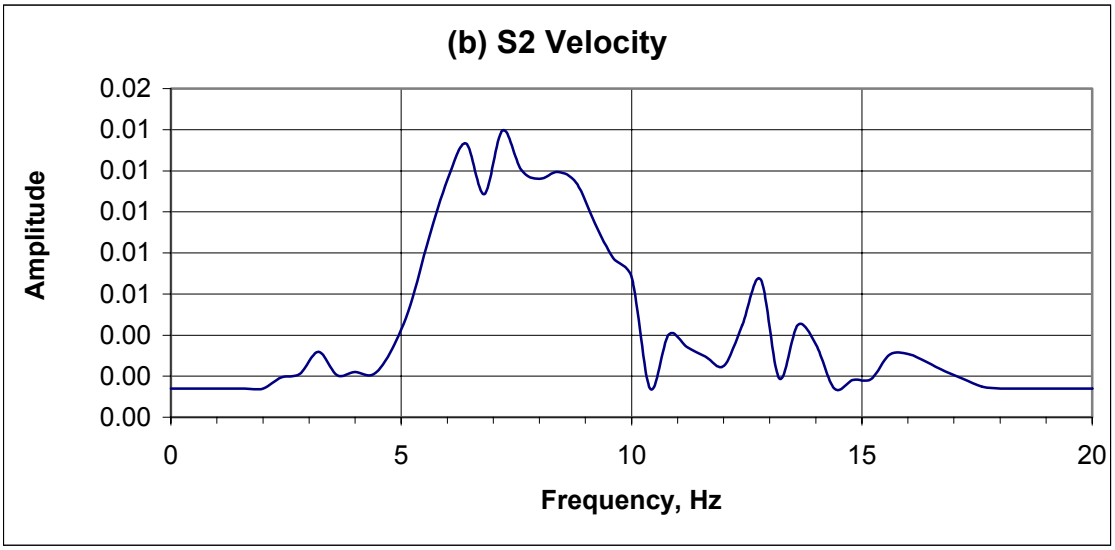

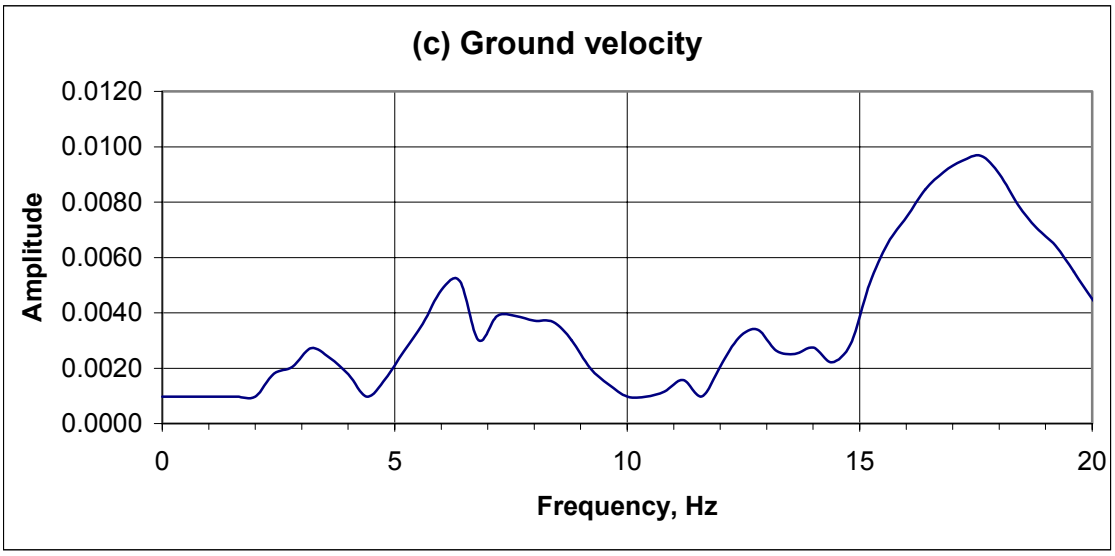

Pennsylvania Trailer - 5/24/01 10:51

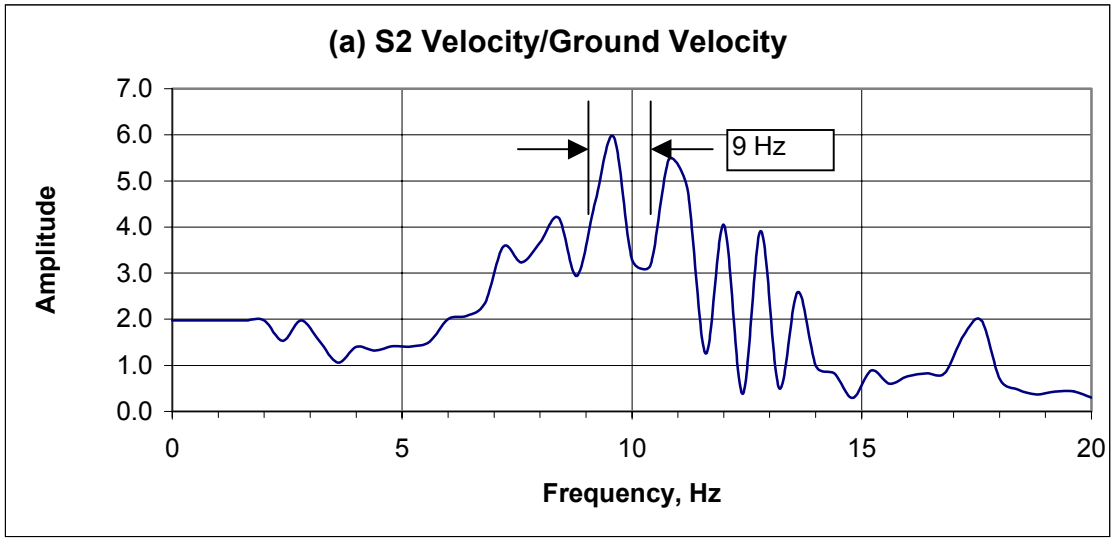

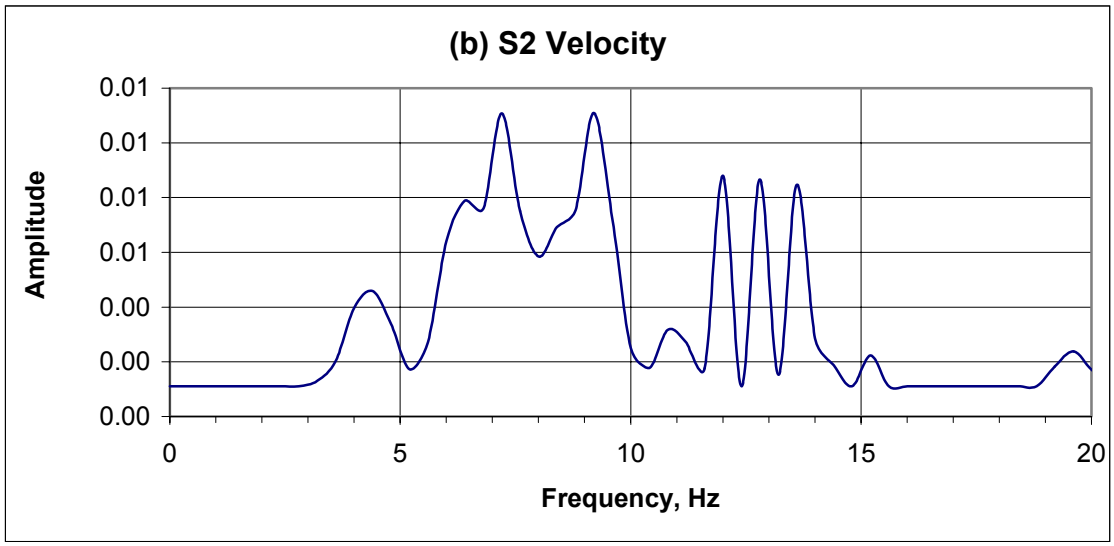

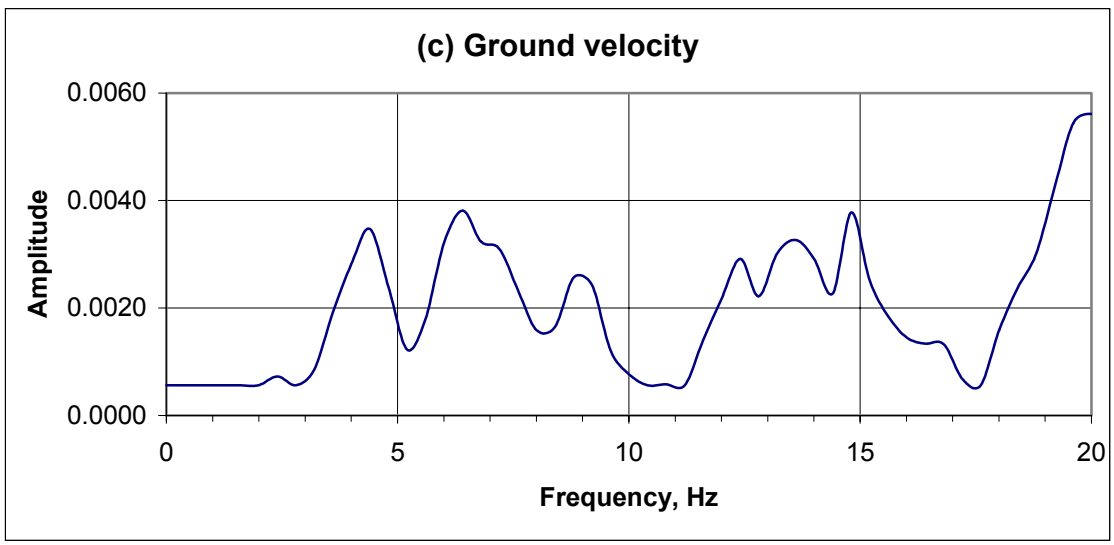

New Mexico Adobe Structure - 6/22/2001 2:20:00 PM

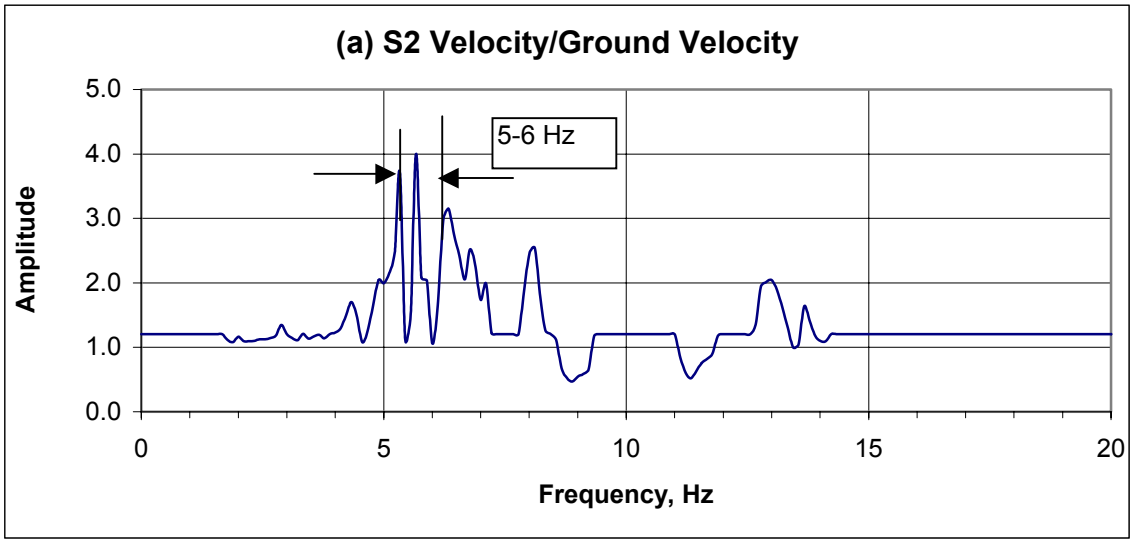

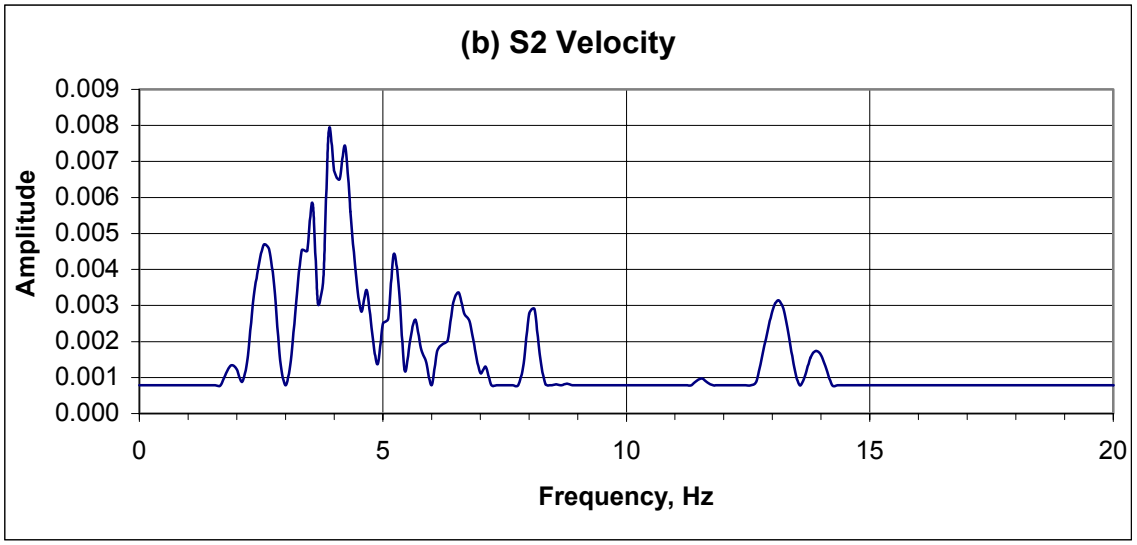

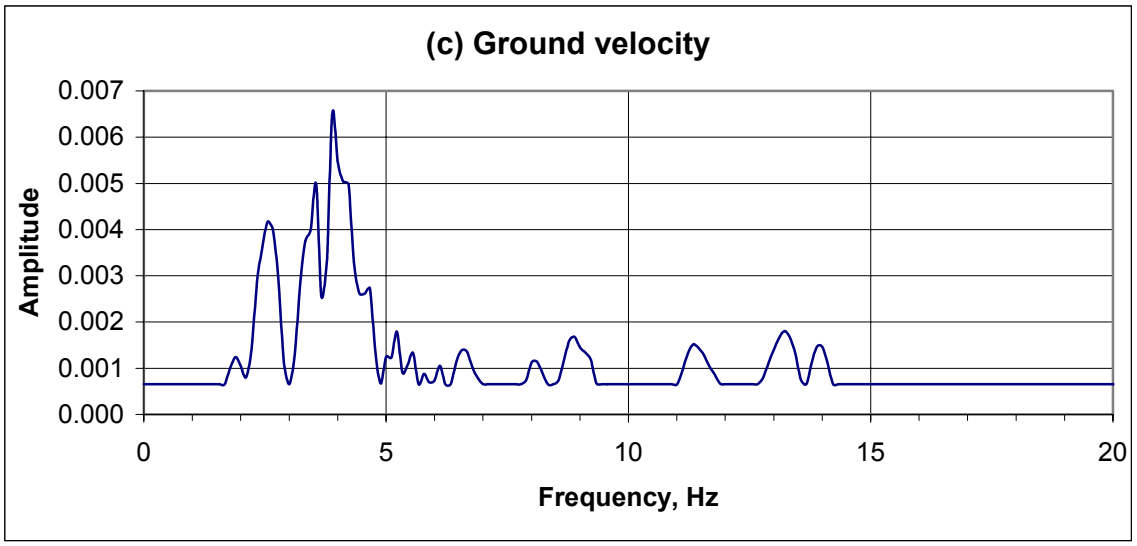

New Mexico Adobe Structure - 6/22/2001 2:20:00 PM

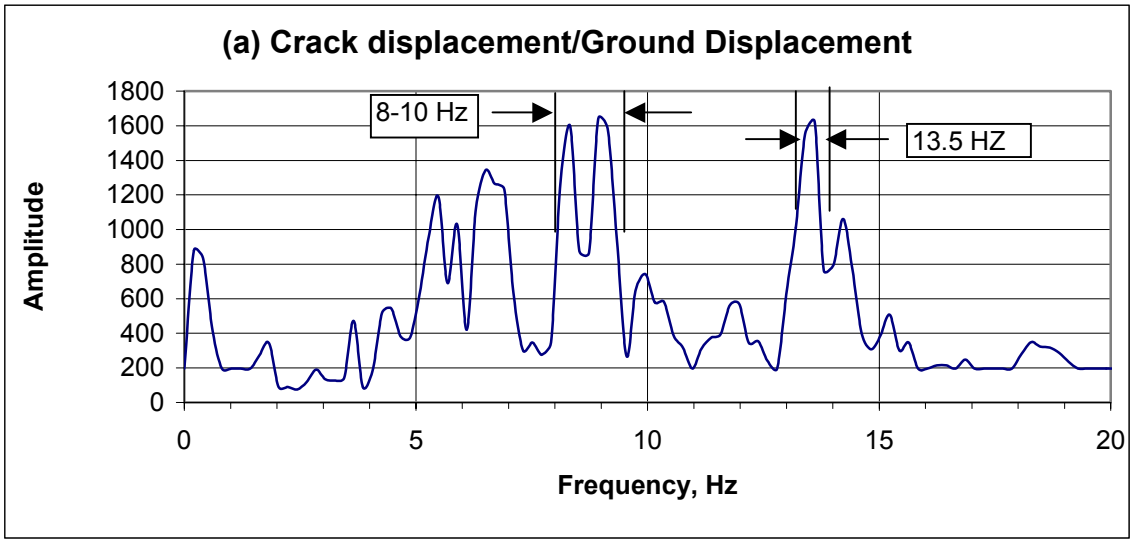

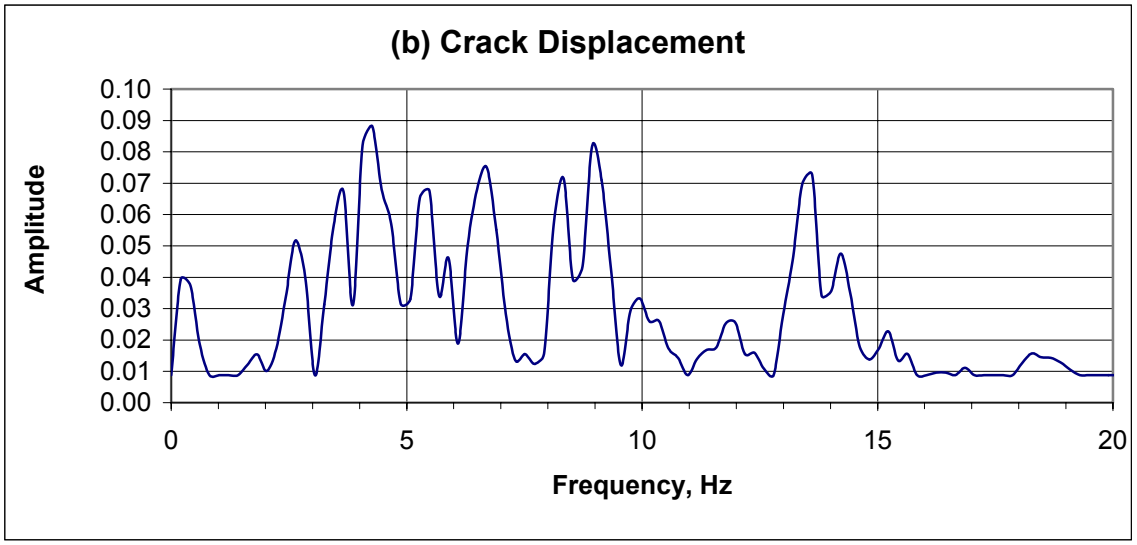

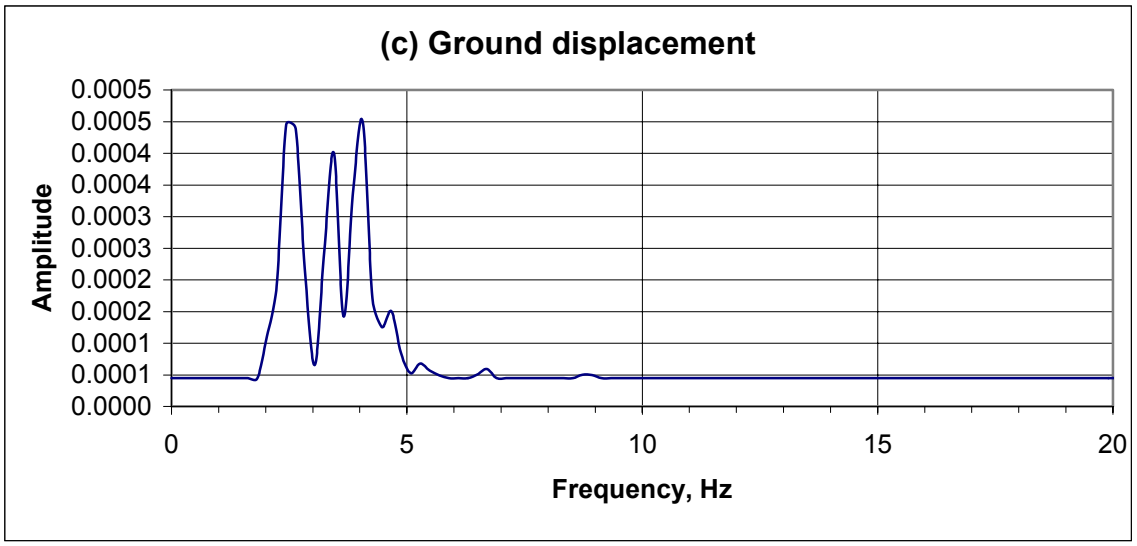

New Mexico Adobe Structure - 7/5/2001 3:03:00 PM

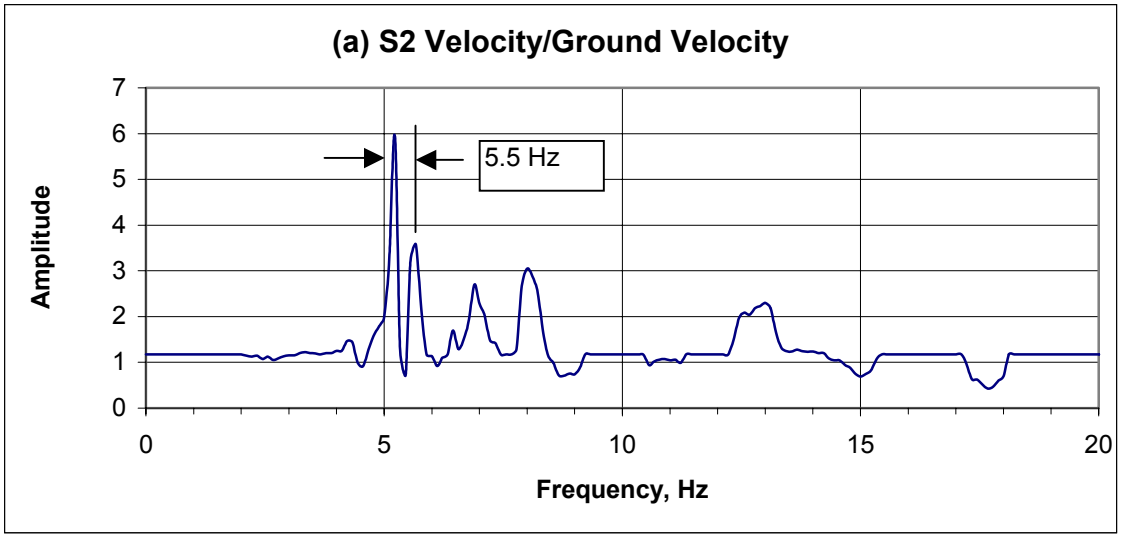

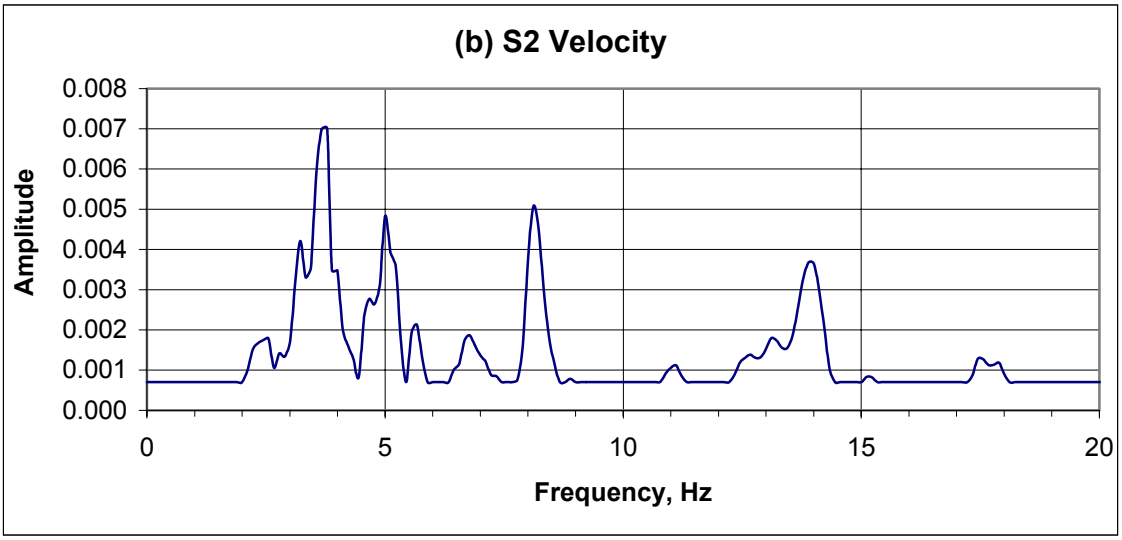

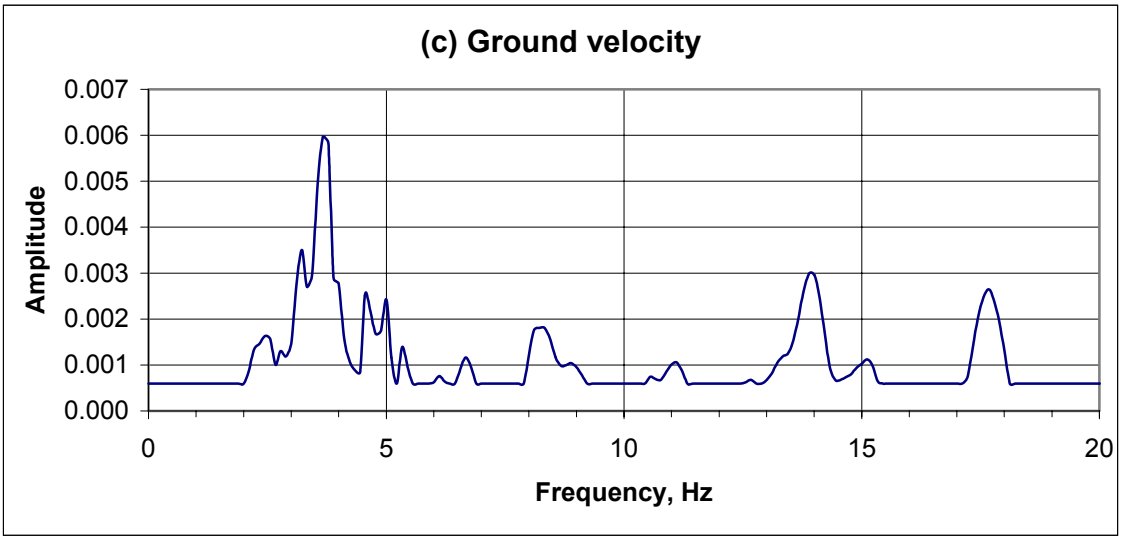

New Mexico Adobe Structure - 7/5/2001 3:03:00 PM

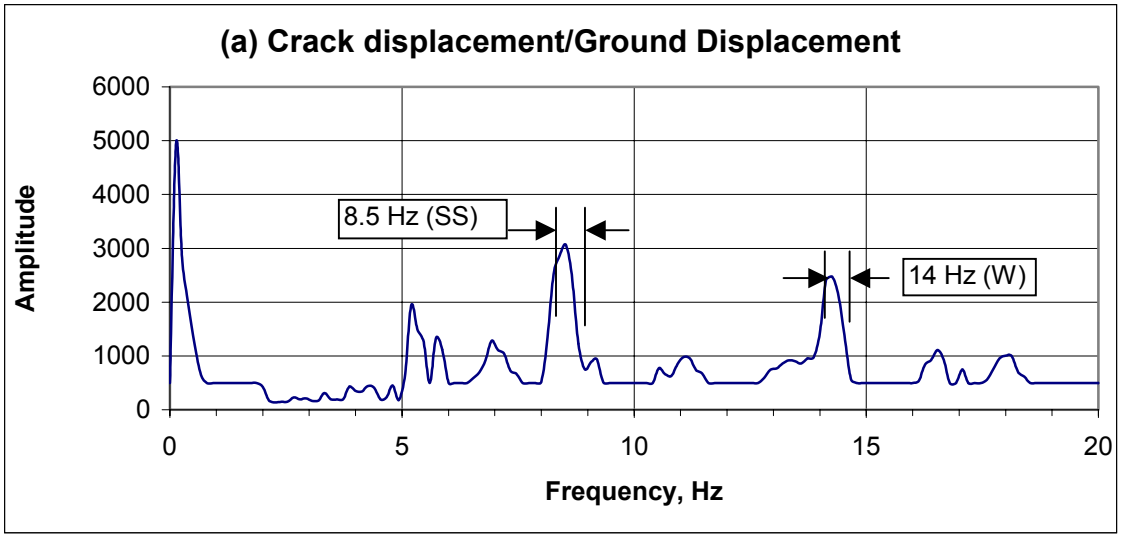

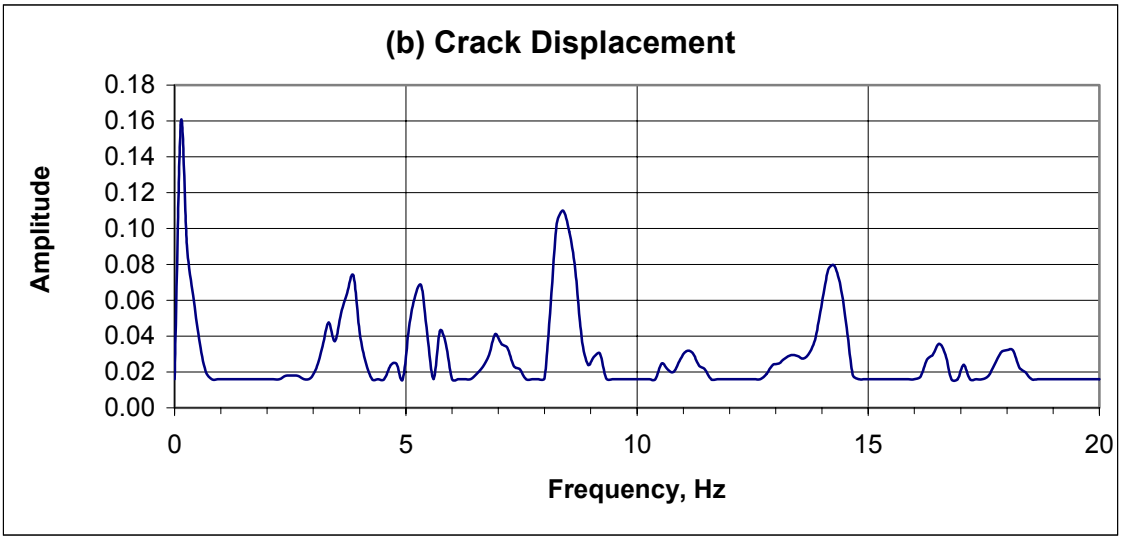

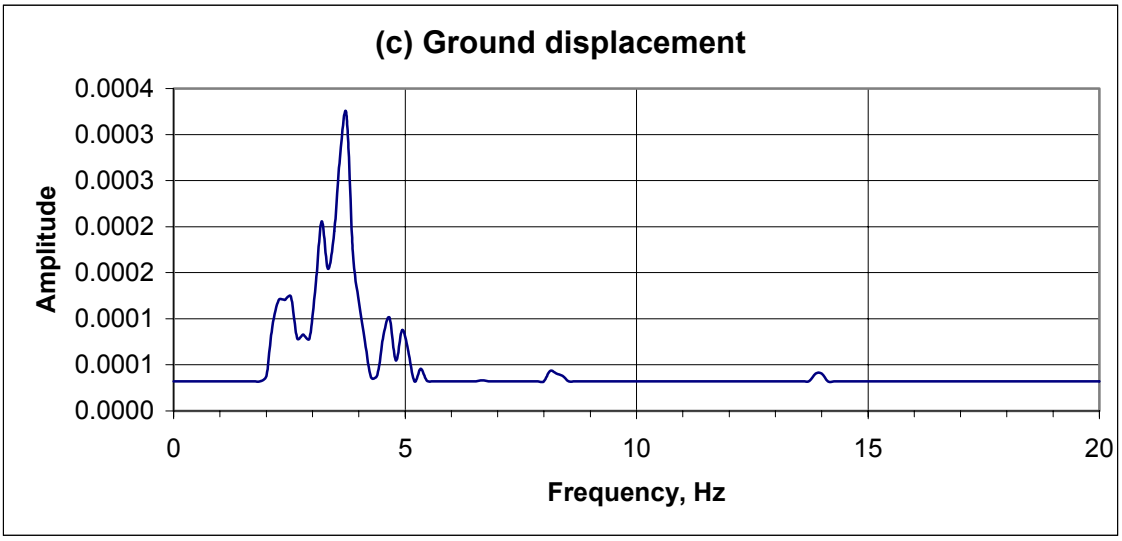

New Mexico Adobe Structure - 7/17/2001 12:51:00 PM

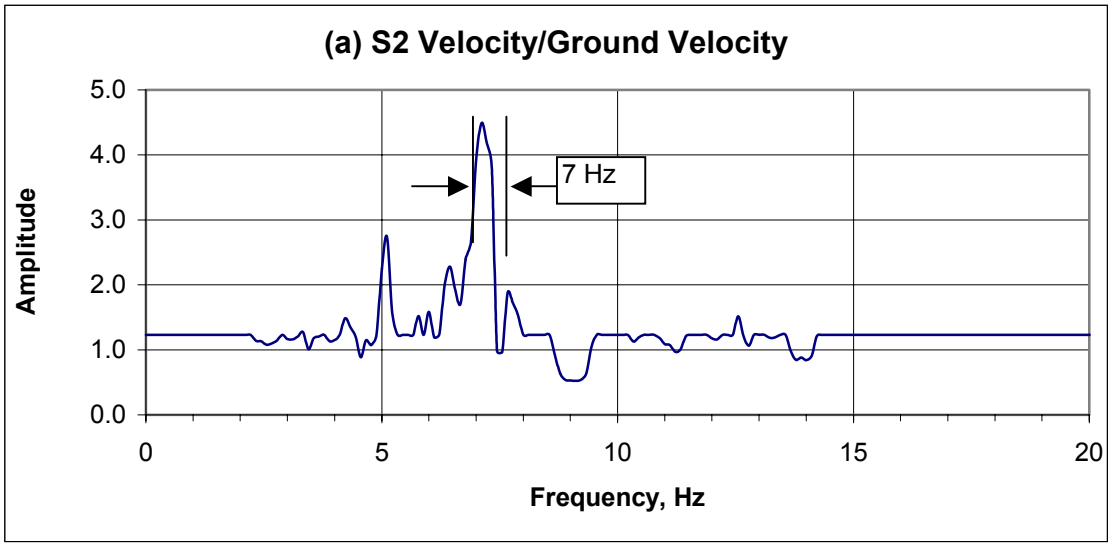

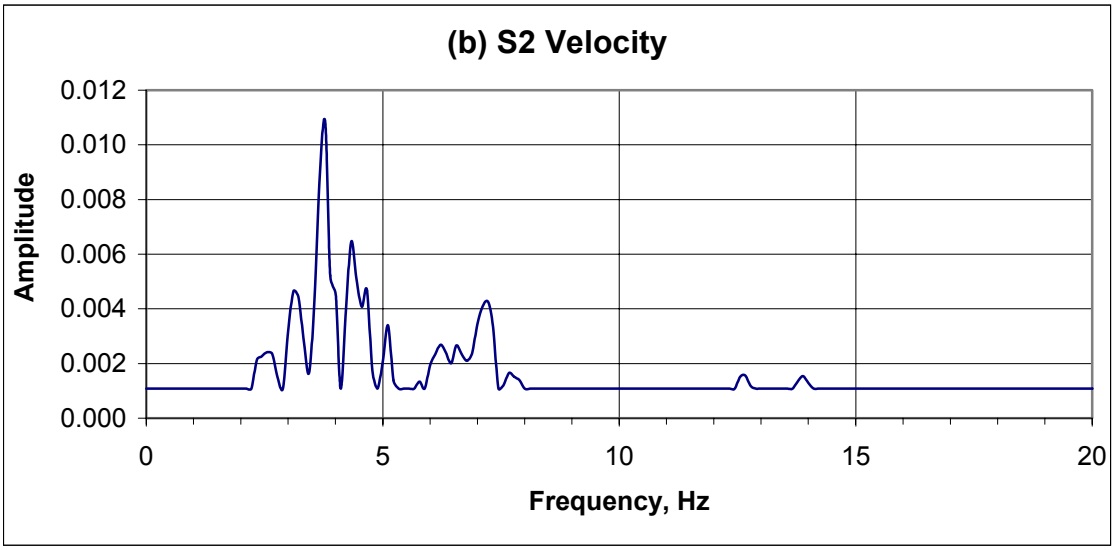

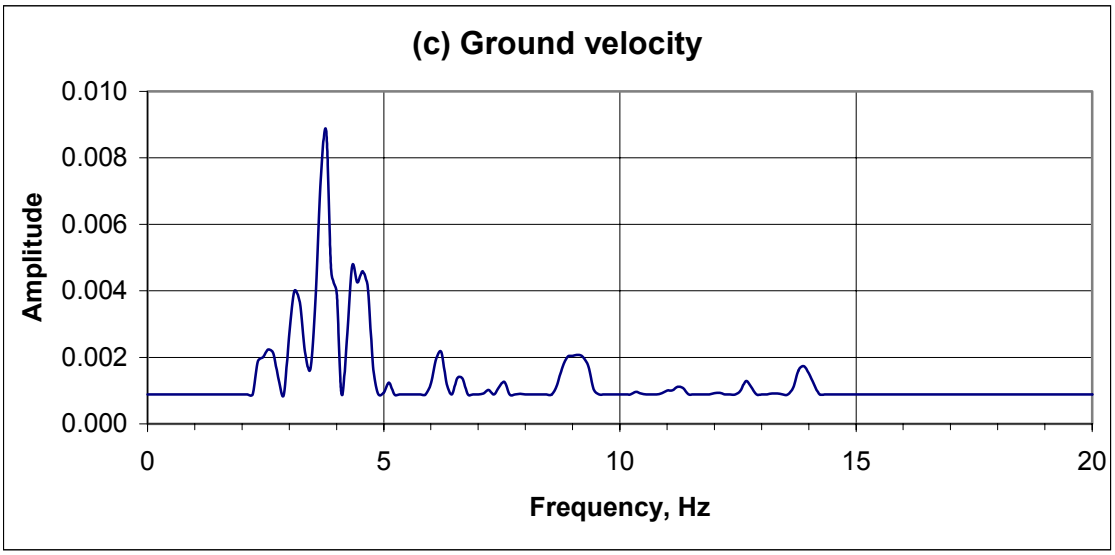

New Mexico Adobe Structure - 7/17/2001 12:51:00 PM

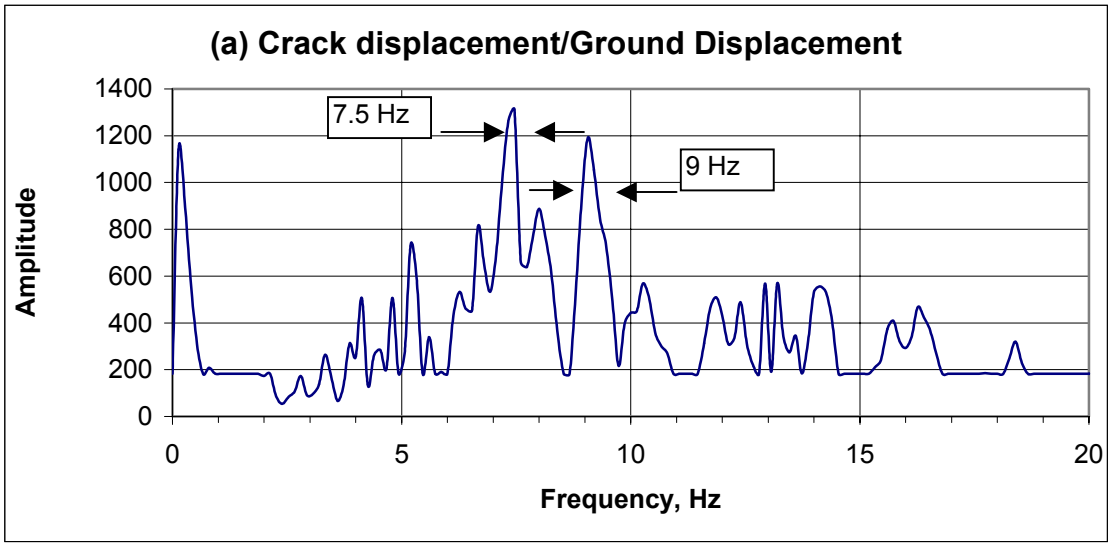

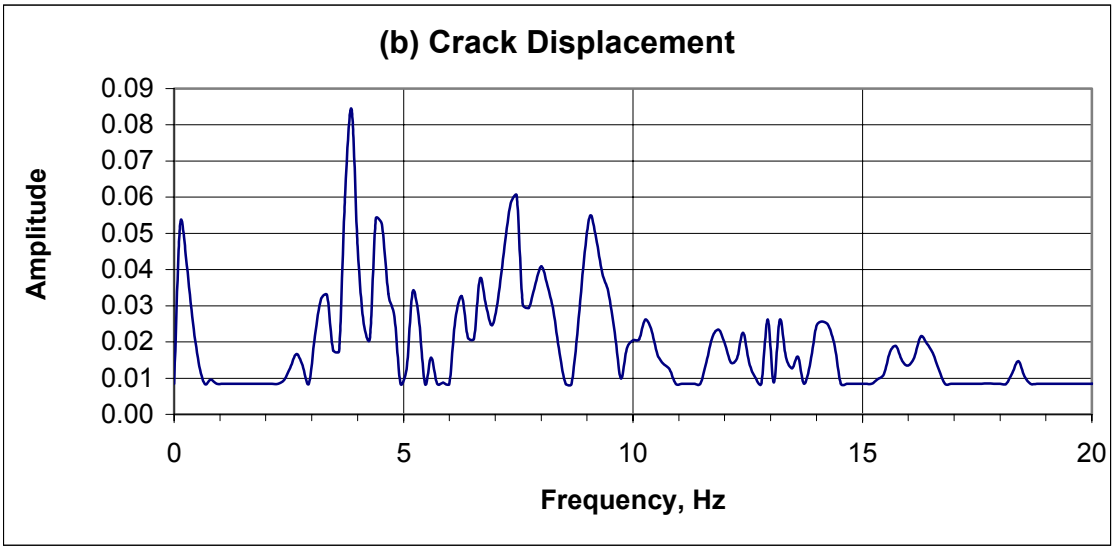

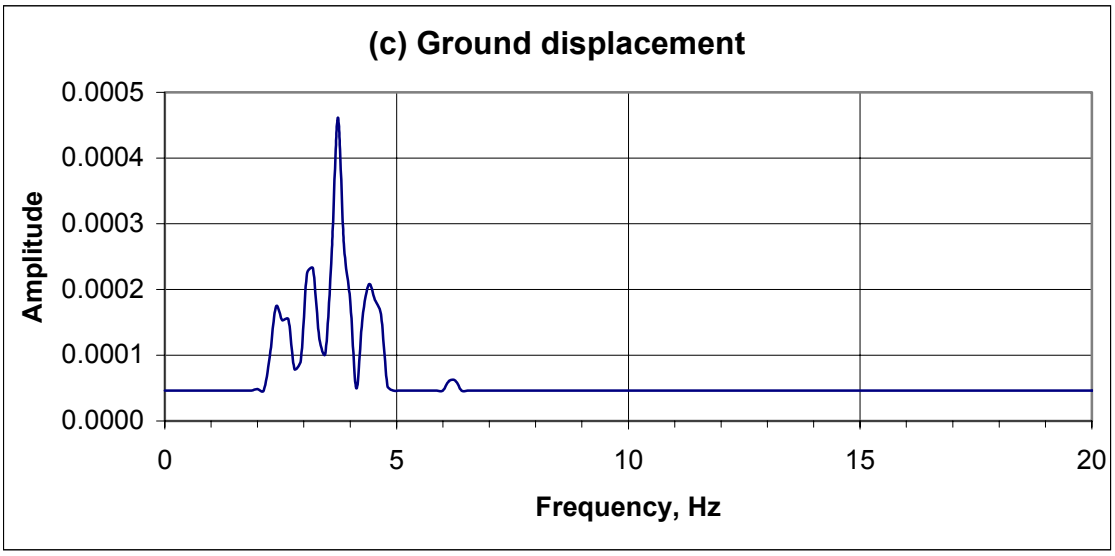

New Mexico Adobe Structure - 7/23/2001 11:22:00 AM

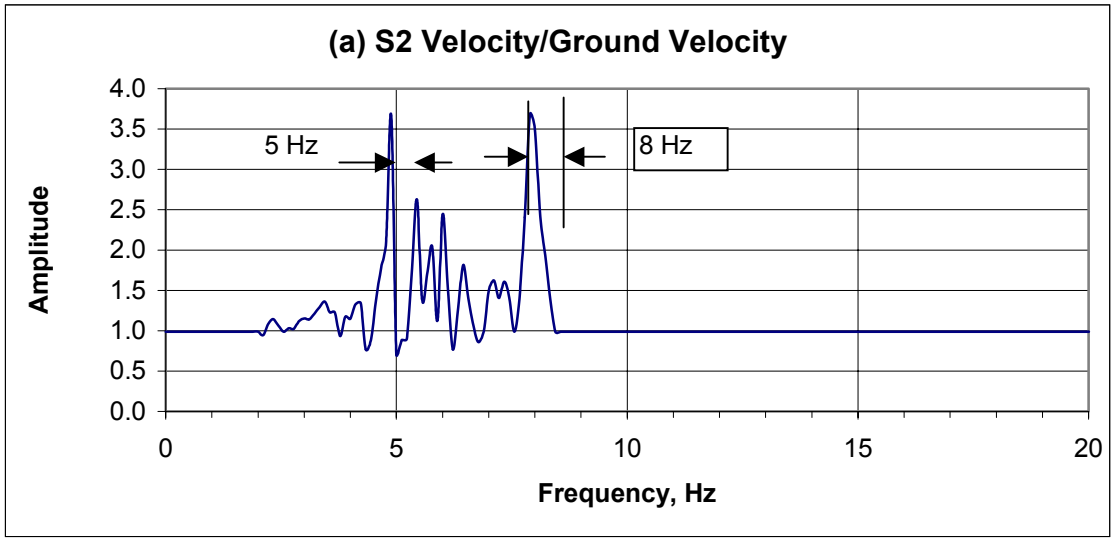

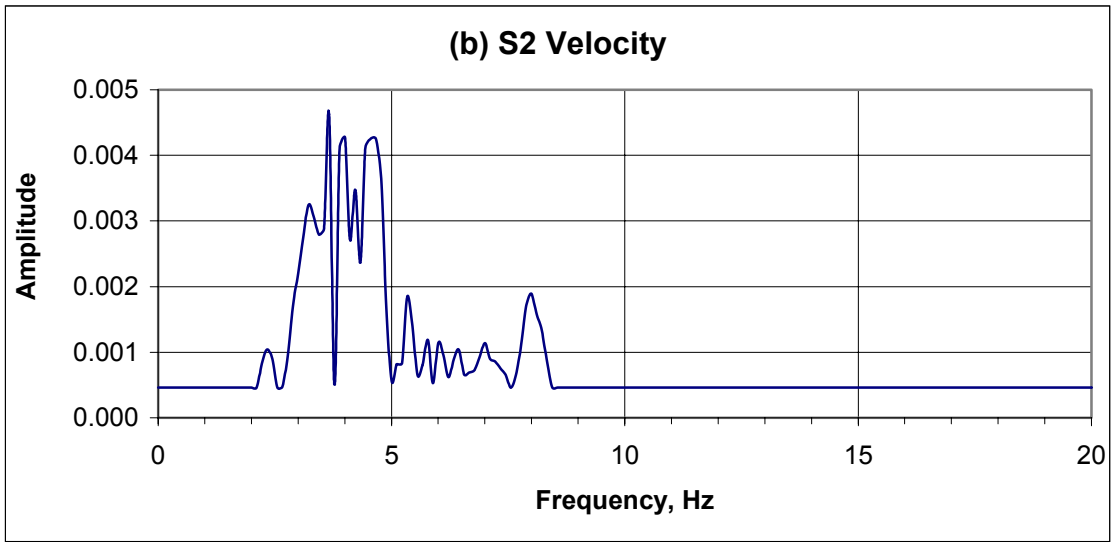

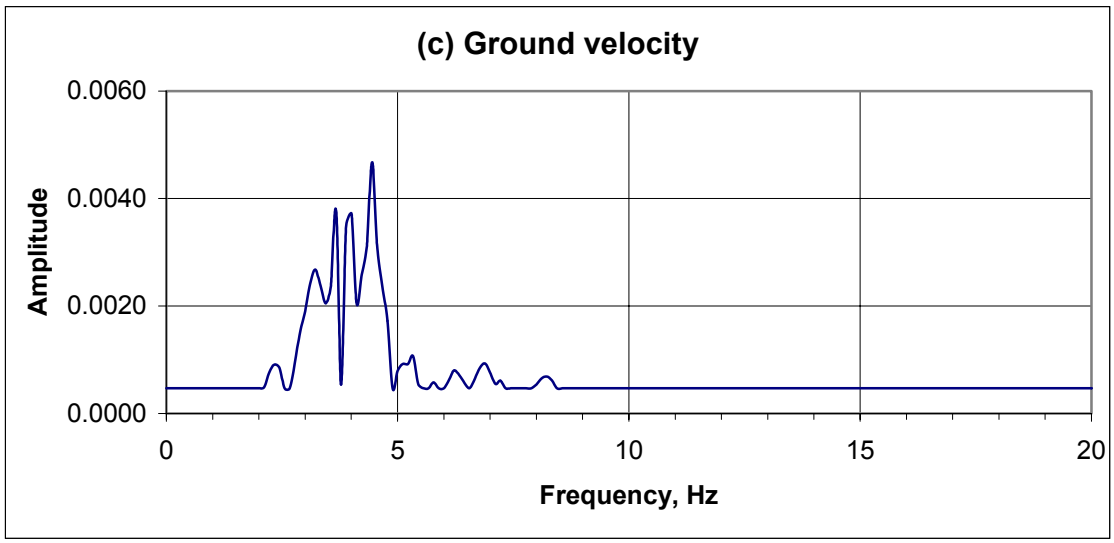

New Mexico Adobe Structure - 7/23/2001 11:22:00 AM

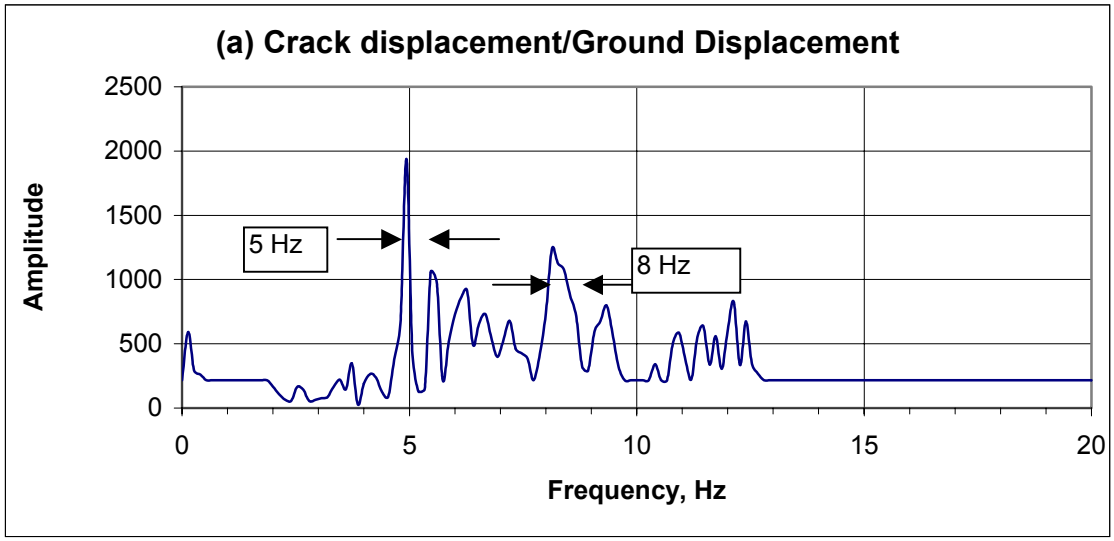

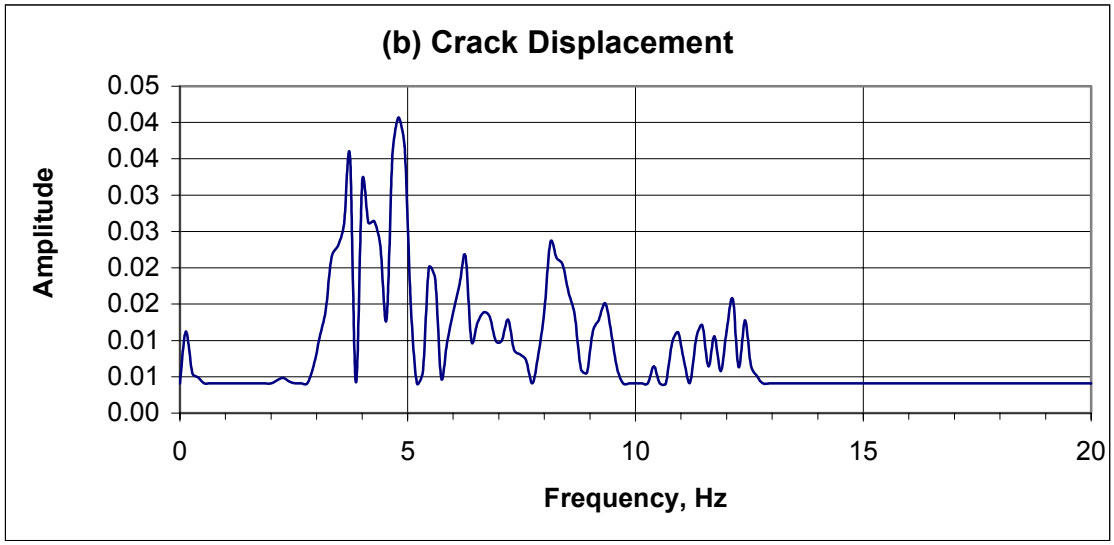

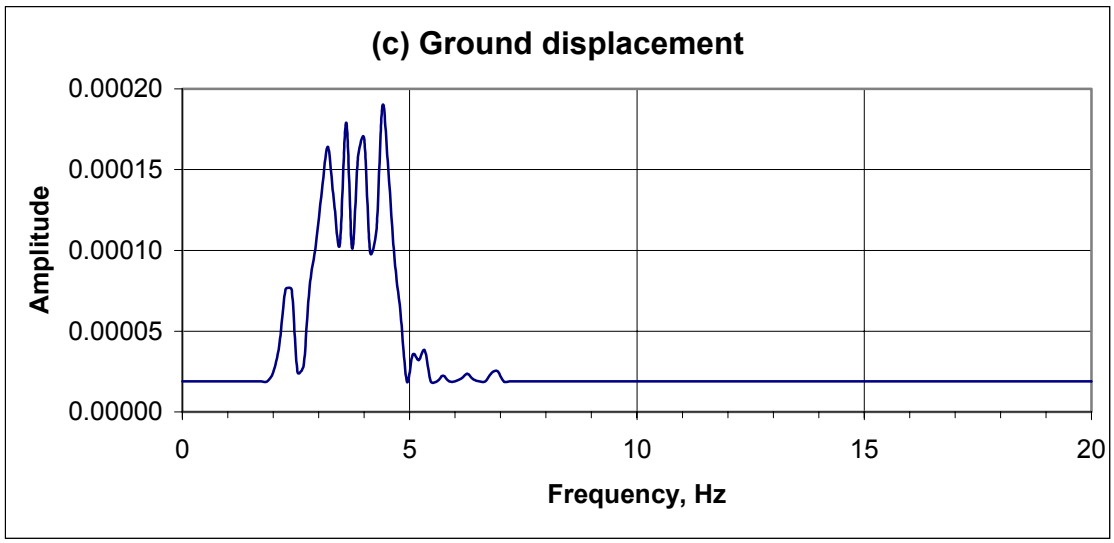

New Mexico Adobe Structure - 7/26/2001 11:04:00 AM

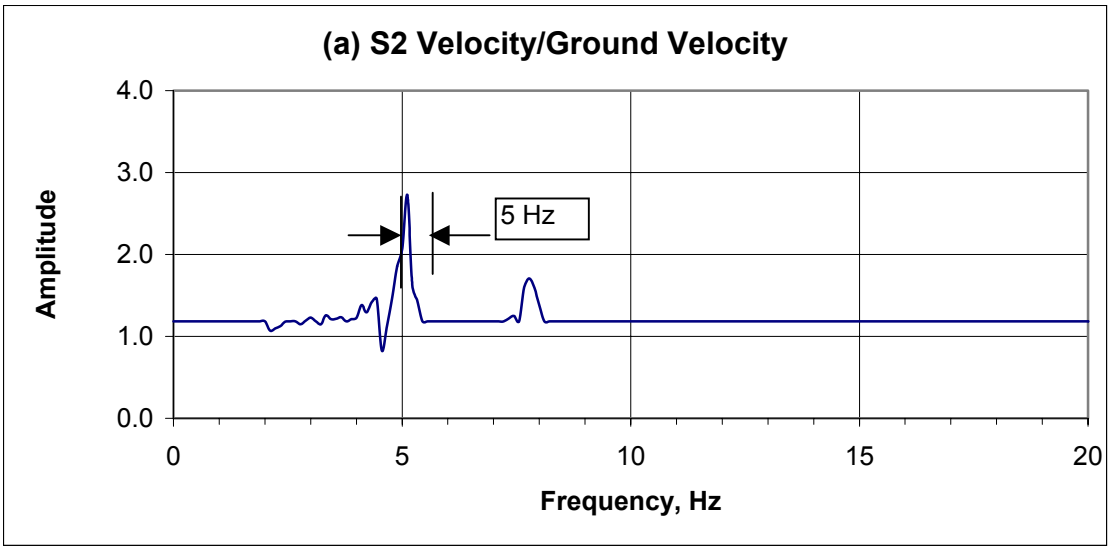

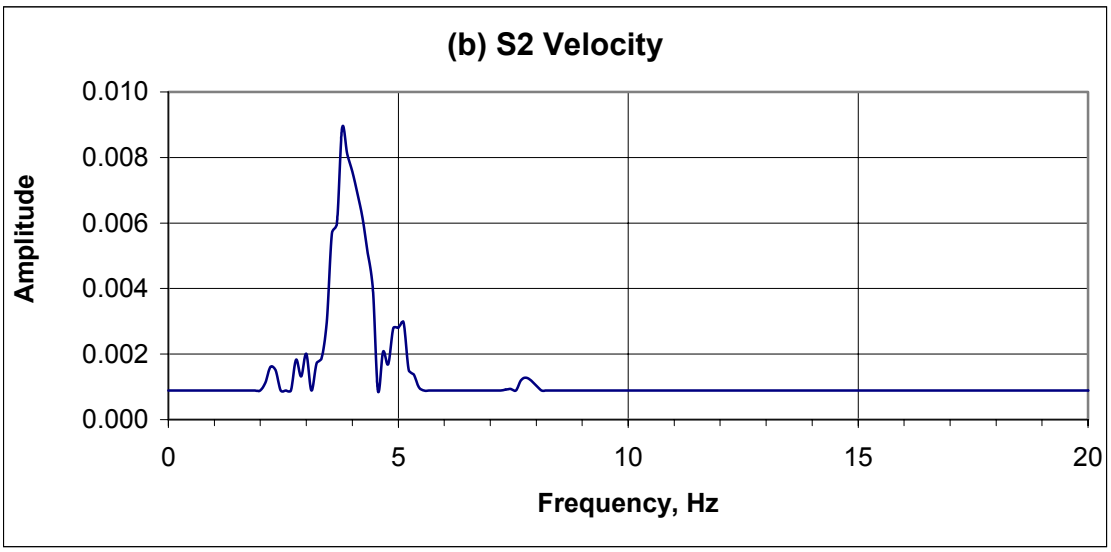

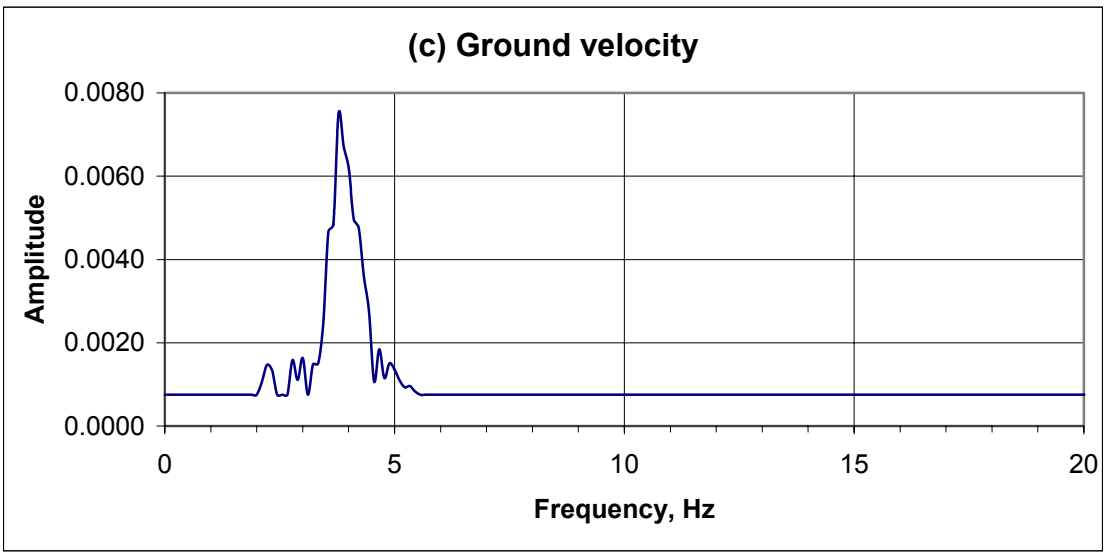

New Mexico Adobe Structure - 7/26/2001 11:04:00 AM

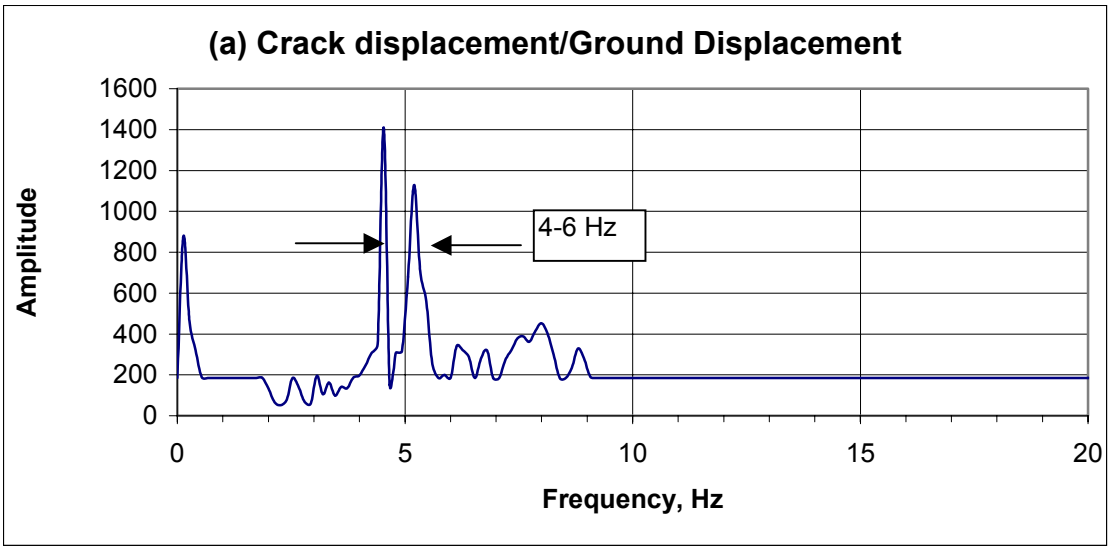

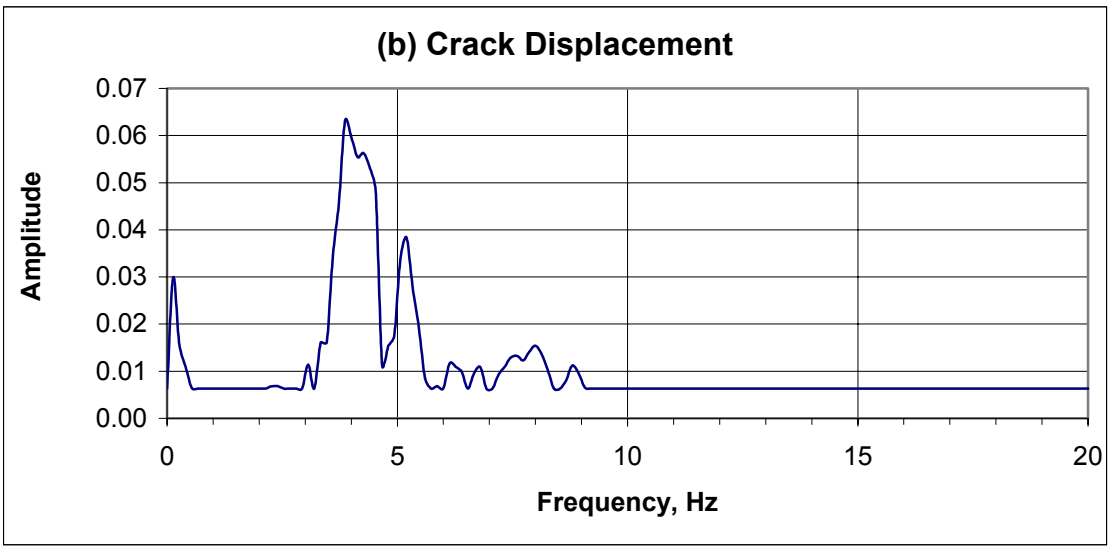

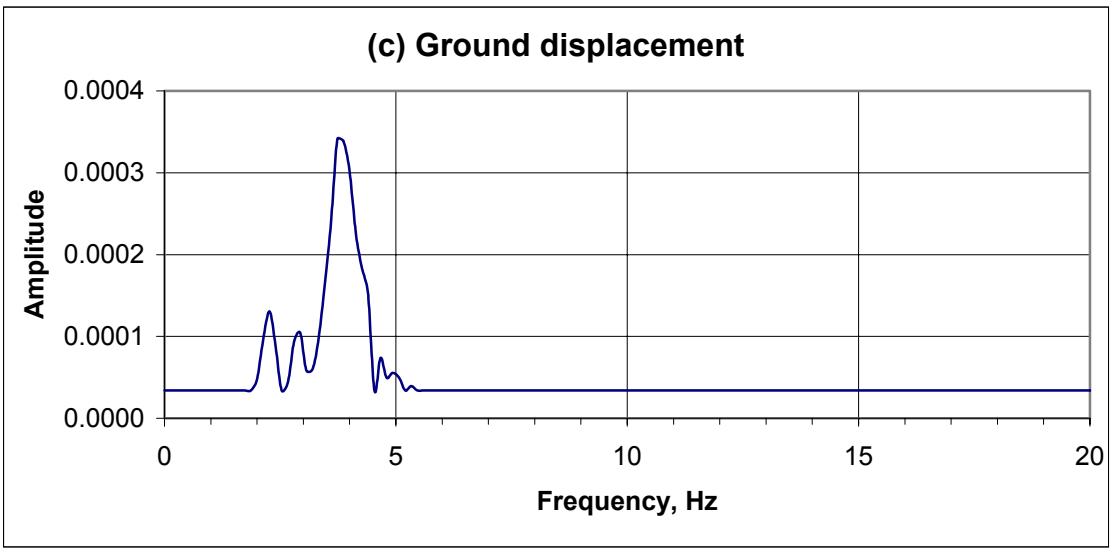

New Mexico Adobe Structure - 7/26/2001 2:55:00 PM

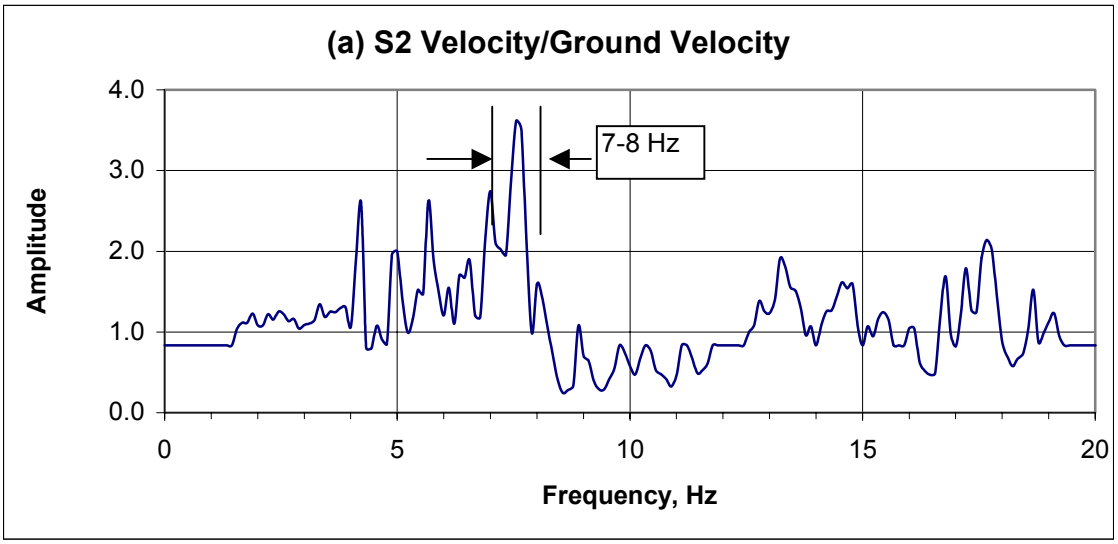

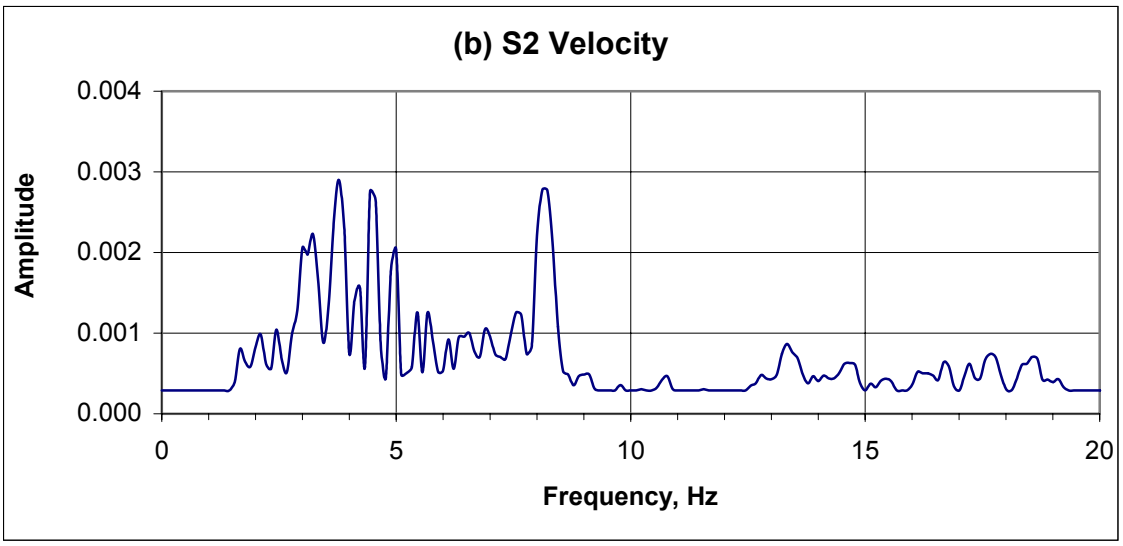

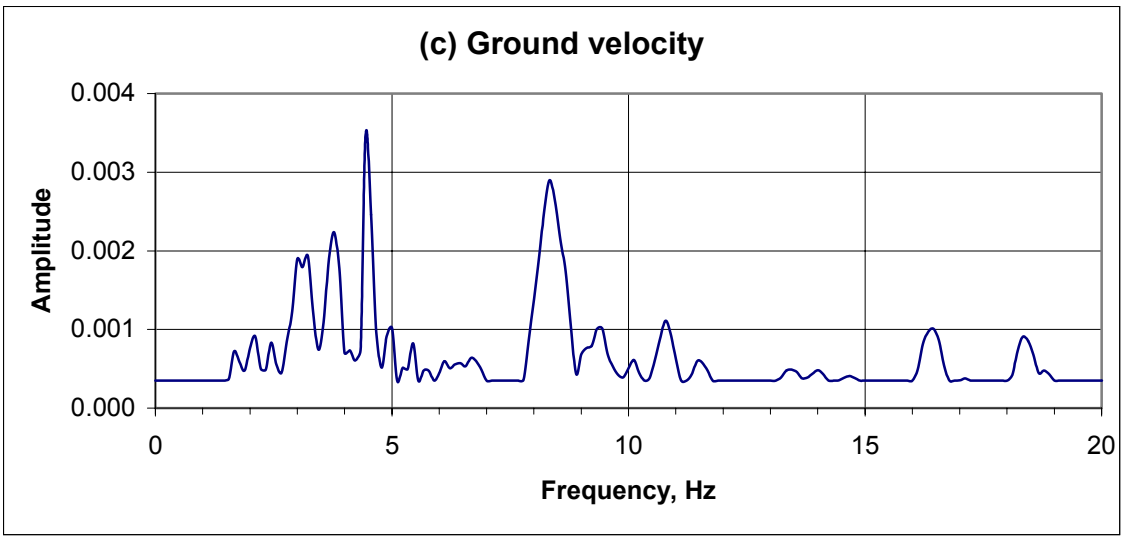

New Mexico Adobe Structure - 7/26/2001 2:55:00 PM

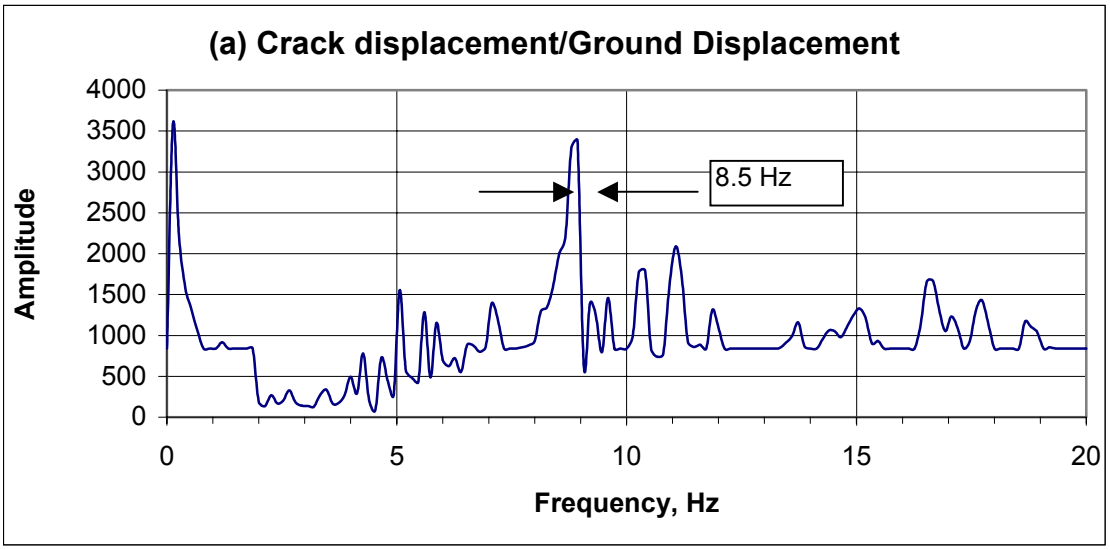

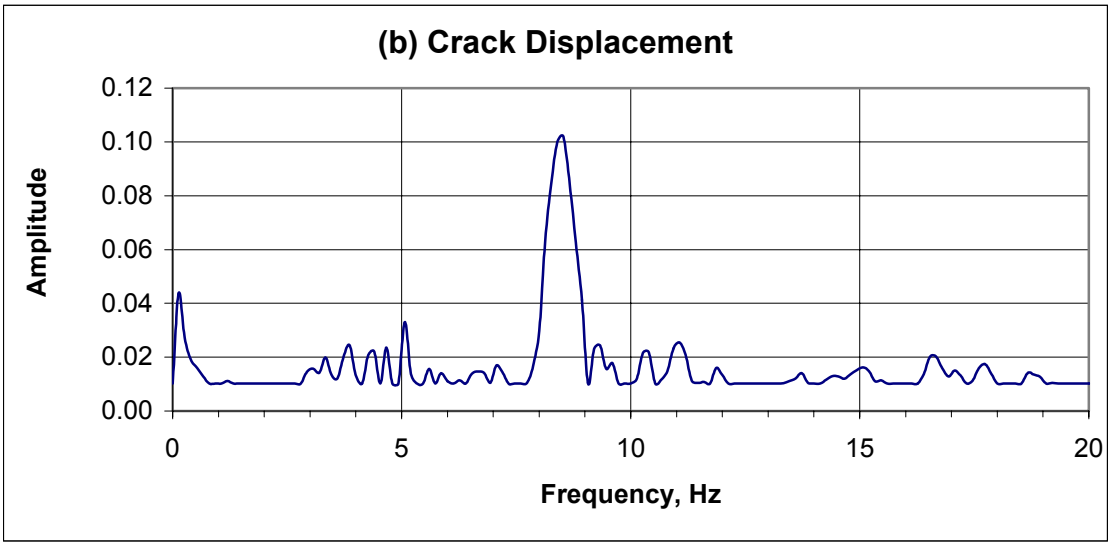

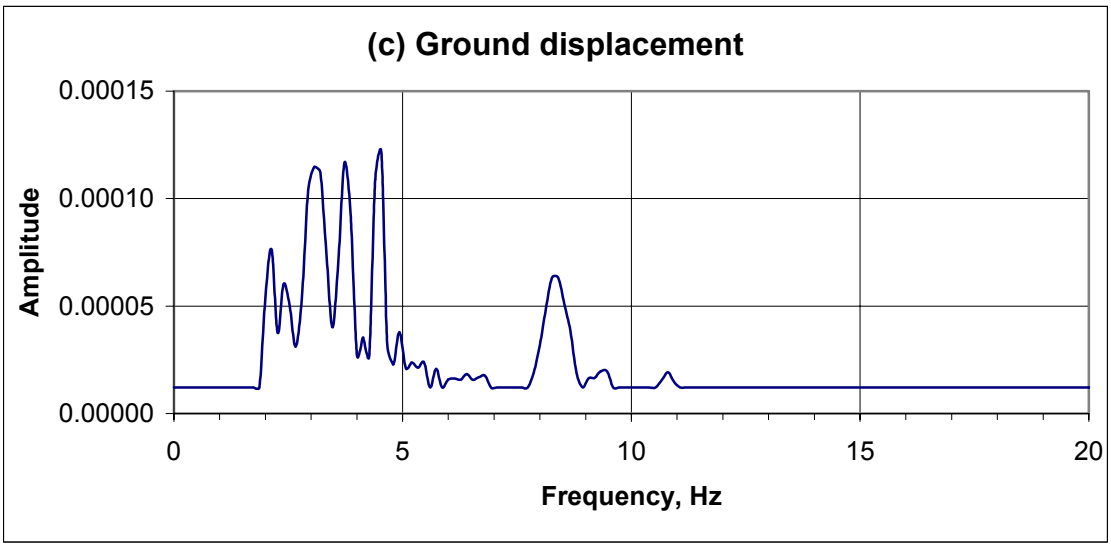

Indiana Bunaglow - 8/18/01 17:33

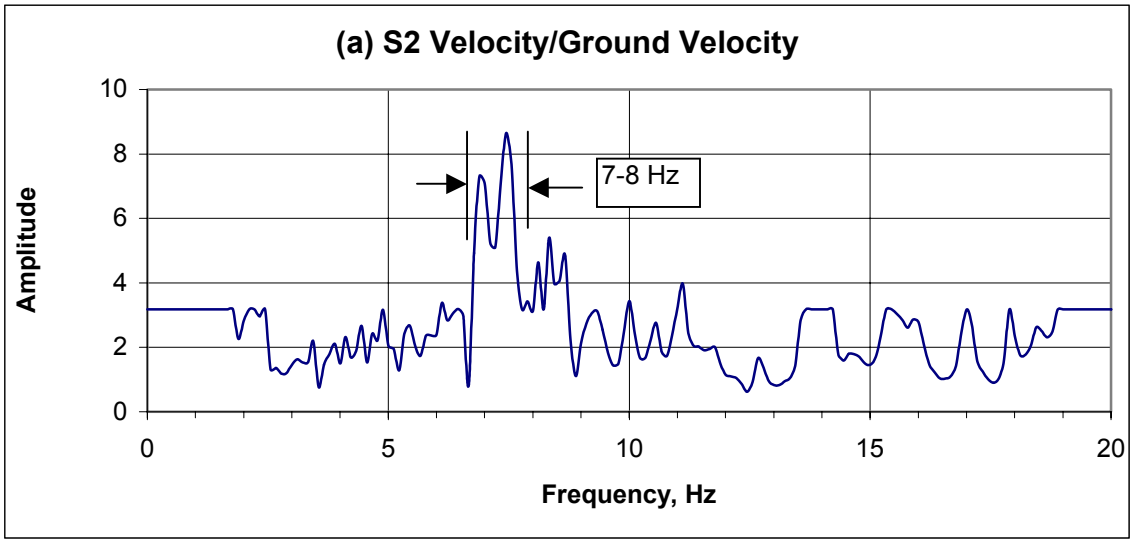

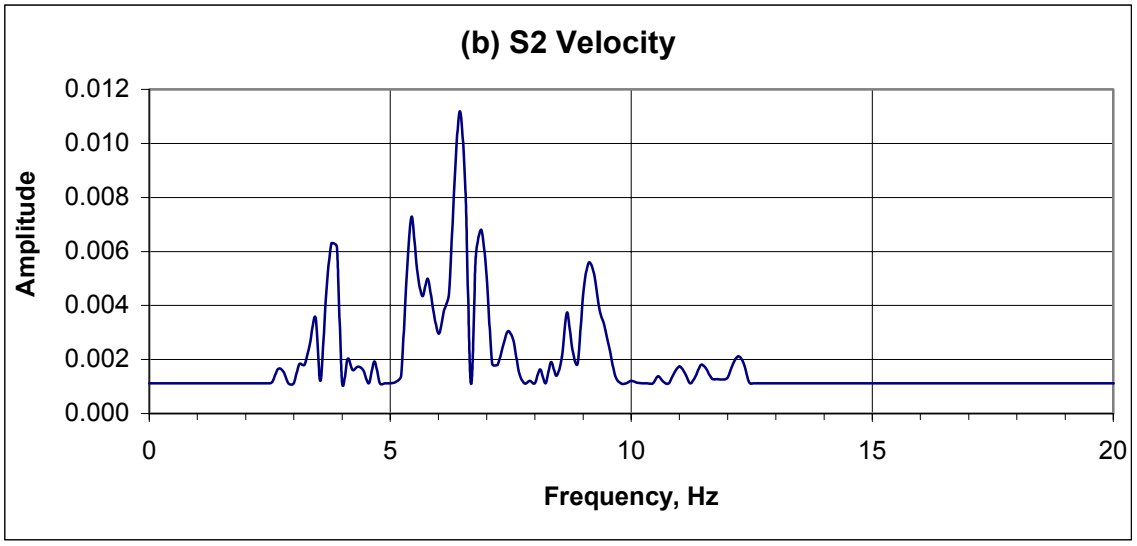

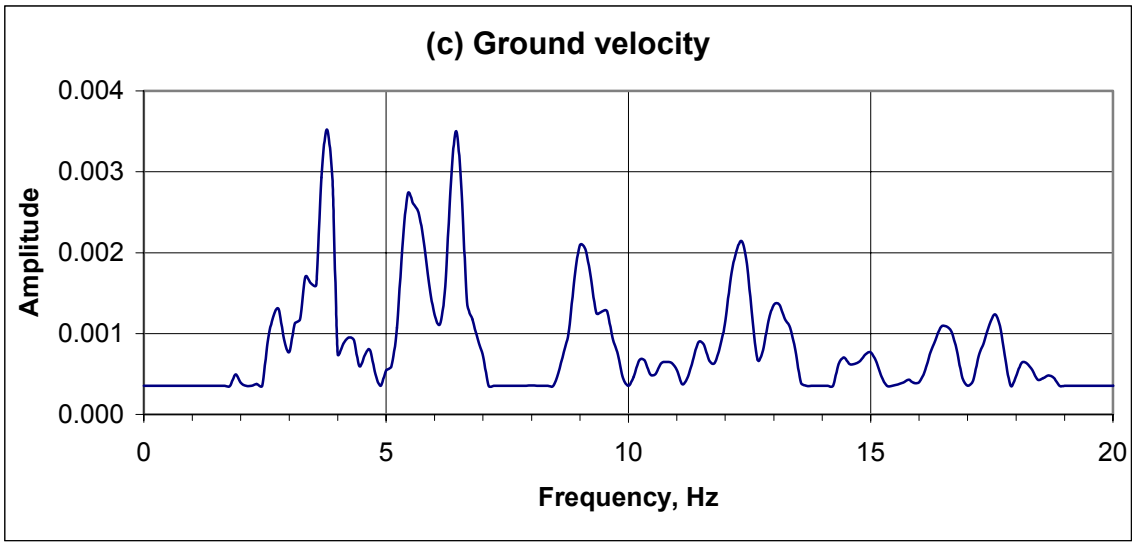

Indiana Bunaglow - 8/19/01 13:27

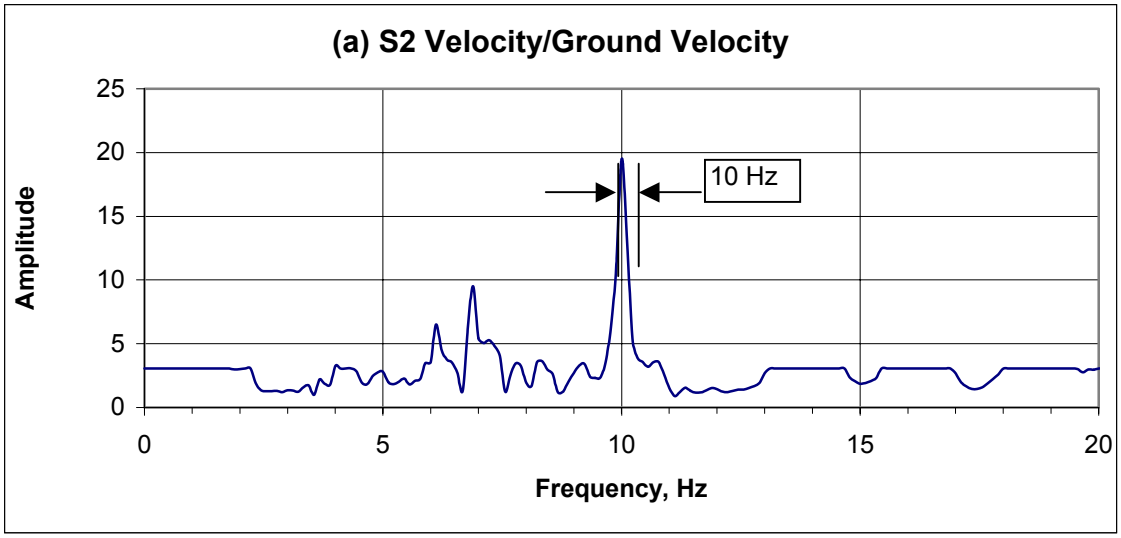

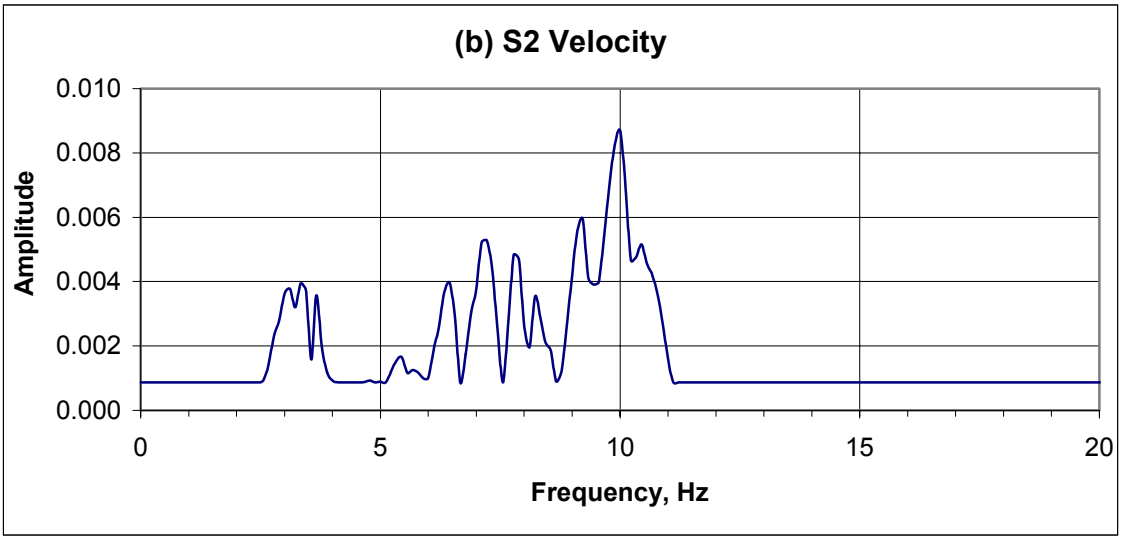

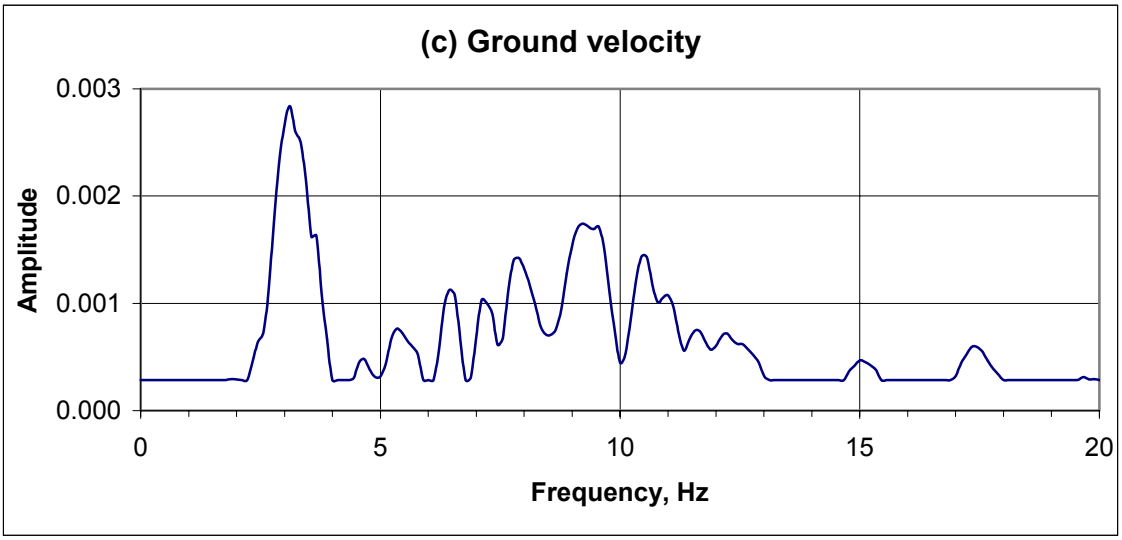

Indiana Bunaglow - 8/20/01 12:30

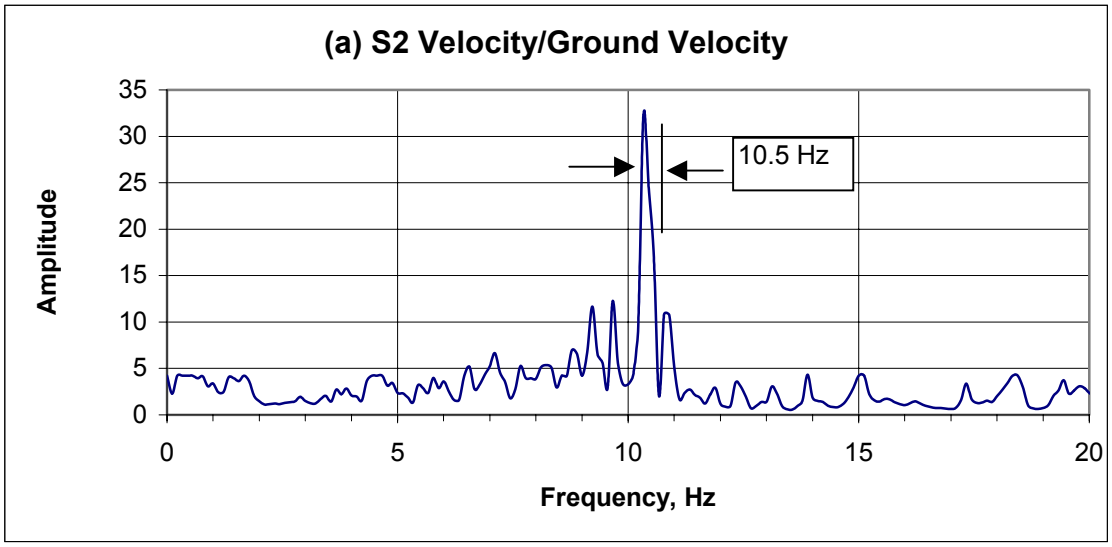

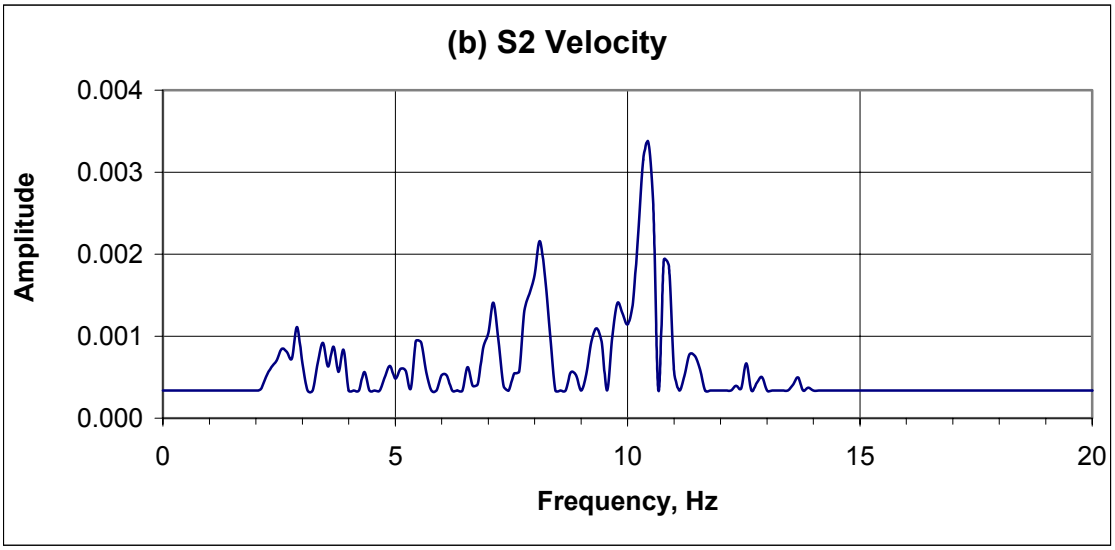

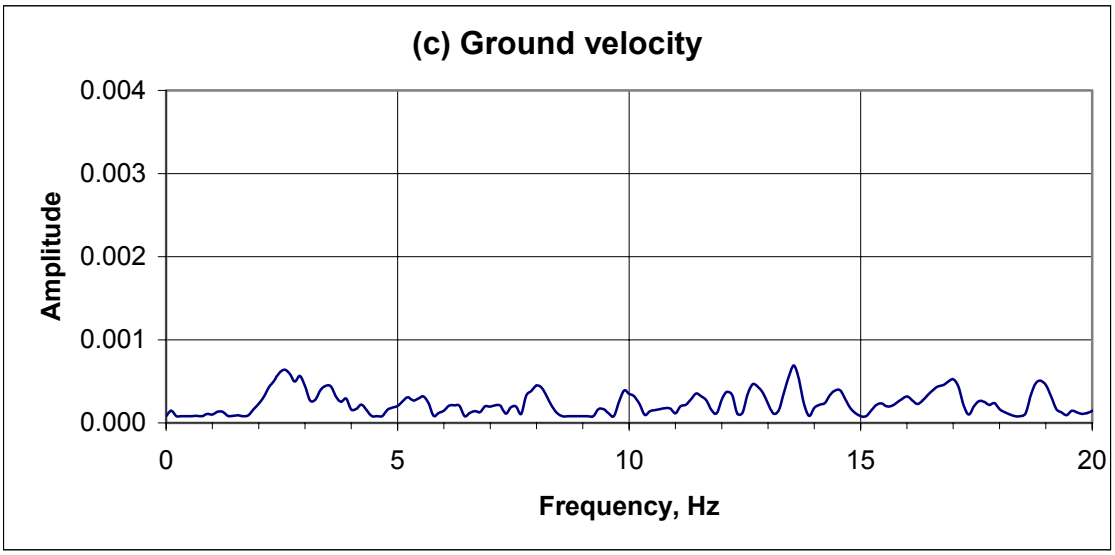

Indiana Bunaglow - 8/20/01 16:05

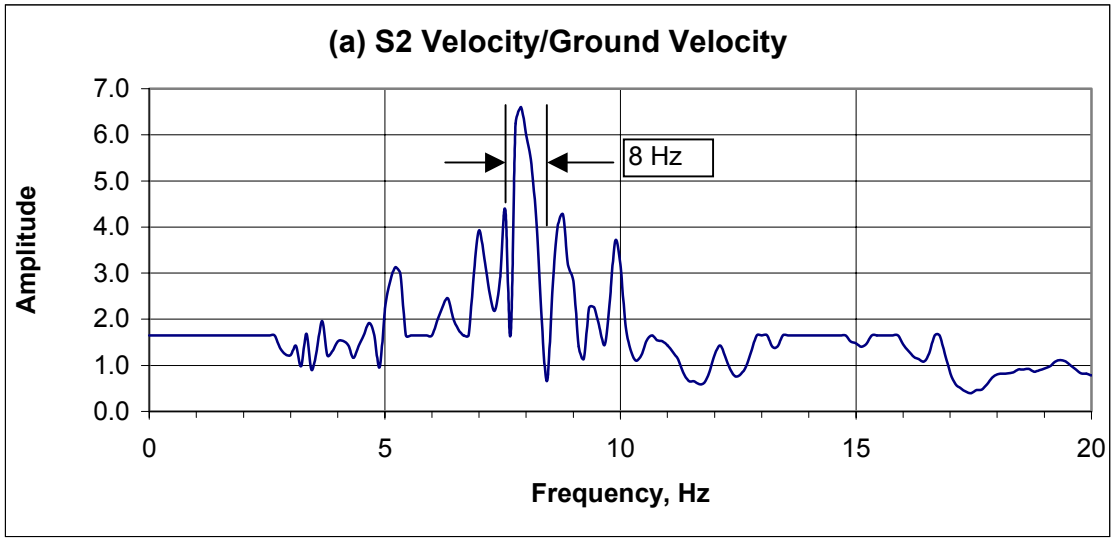

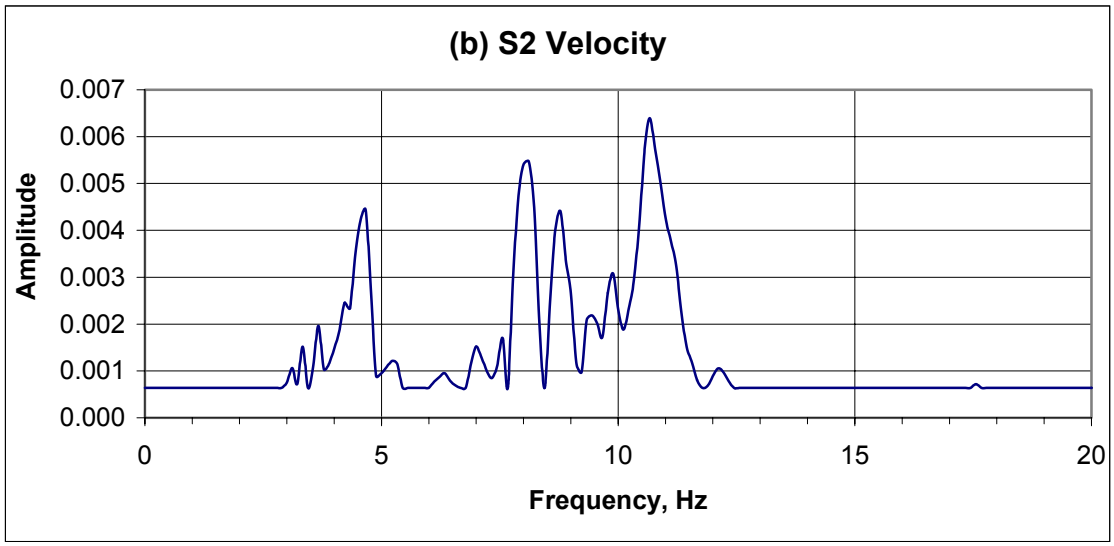

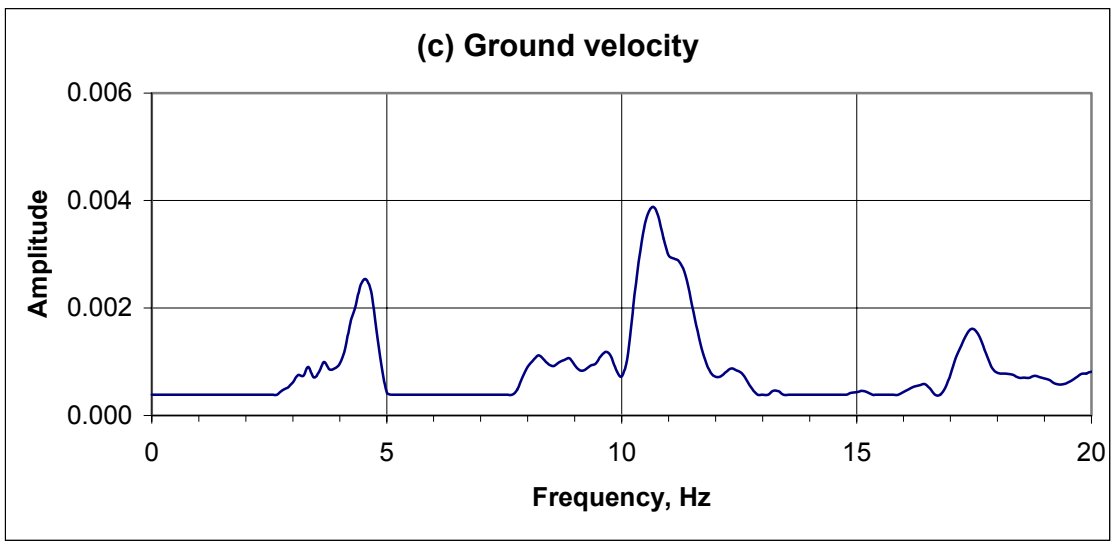

Distressed House - 8/22/01 17:30

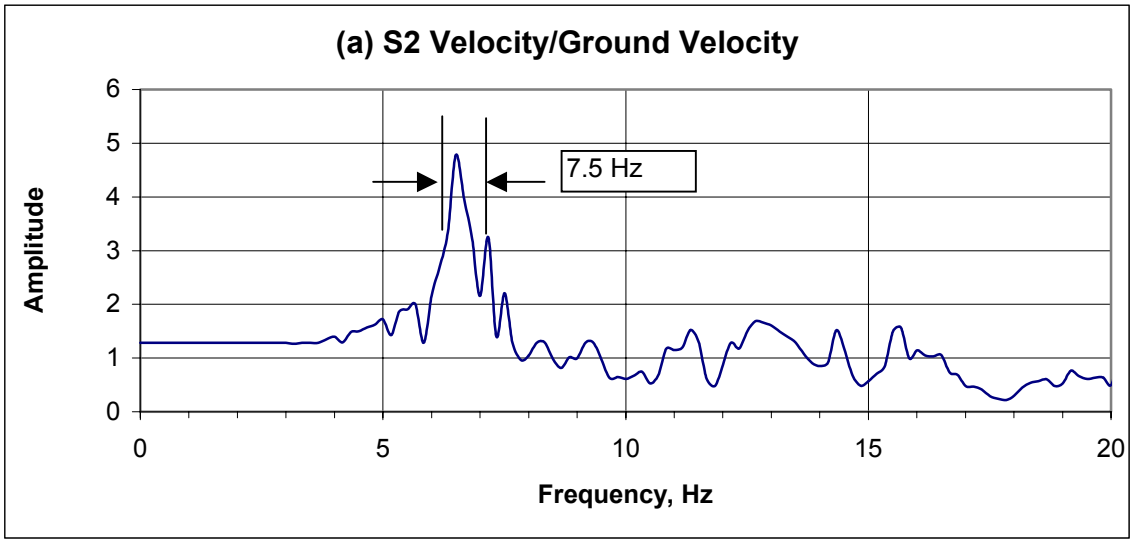

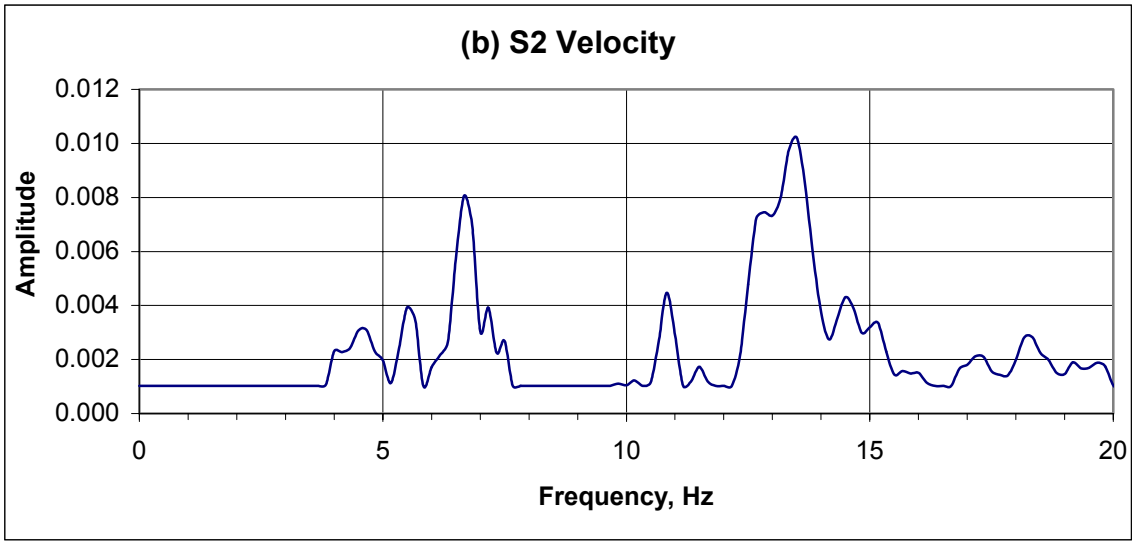

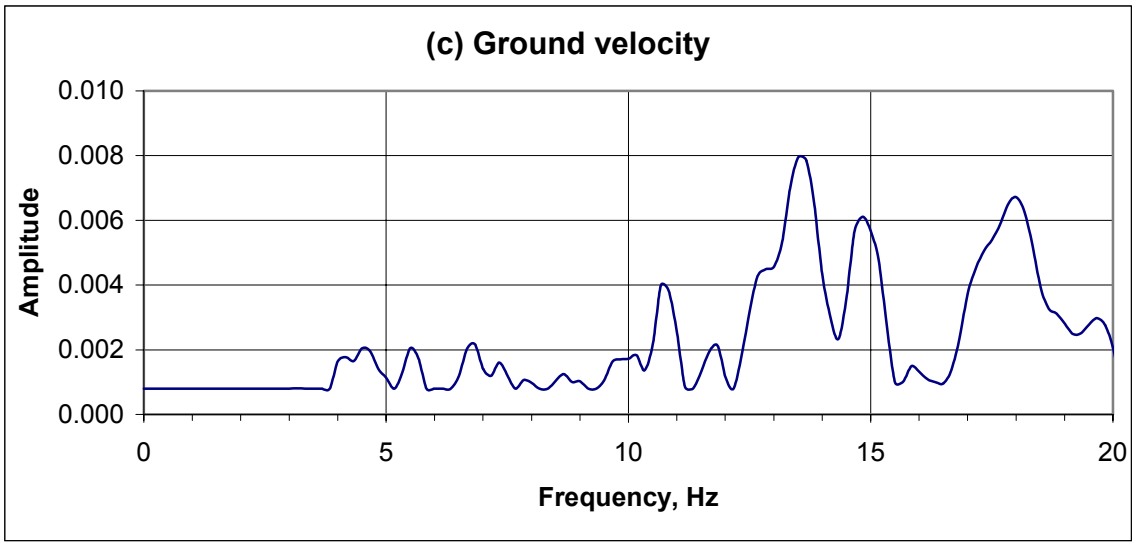

Distressed House - 8/23/01 13:00

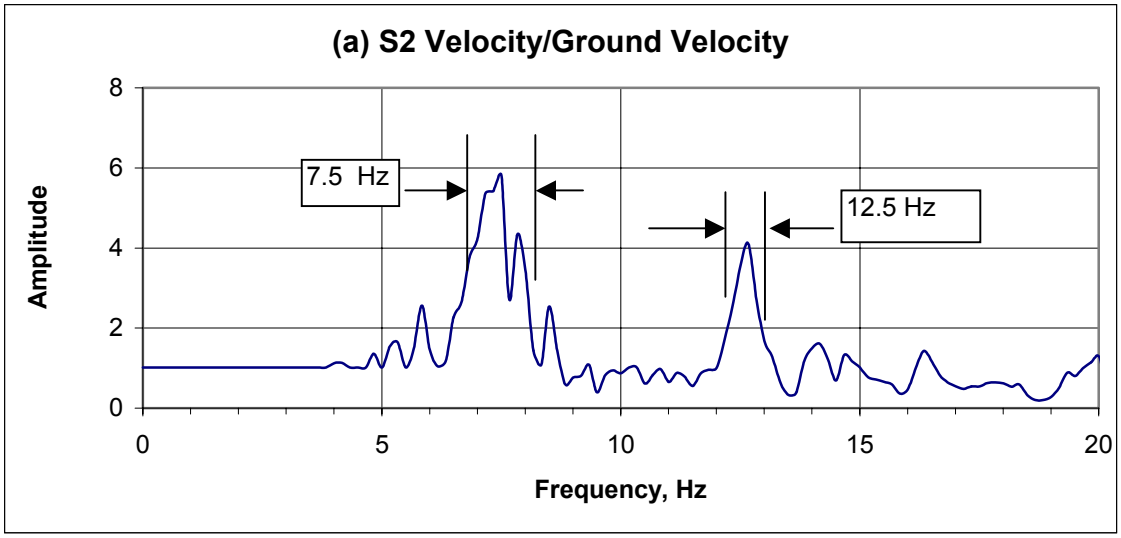

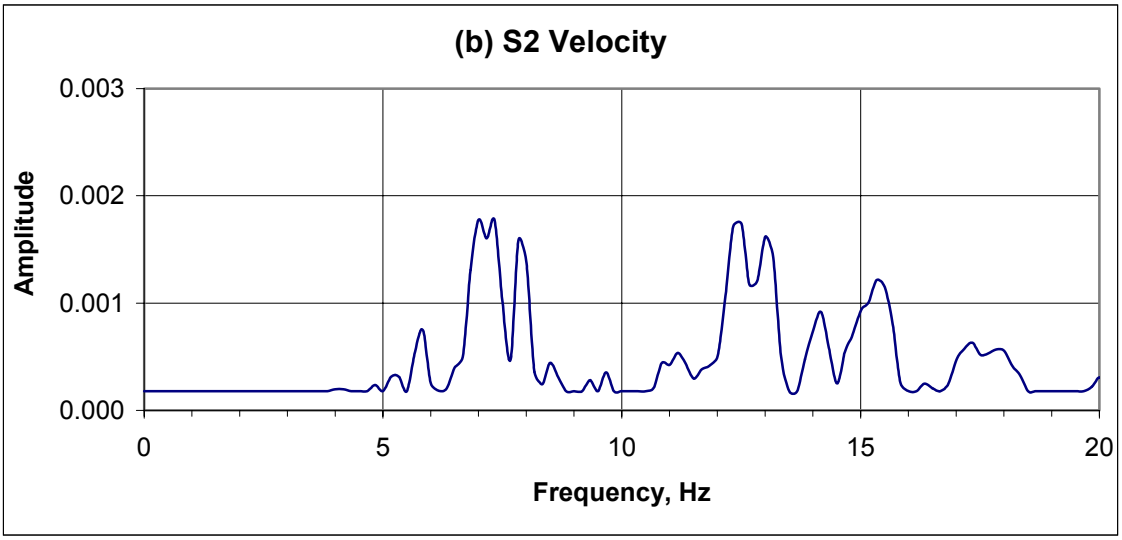

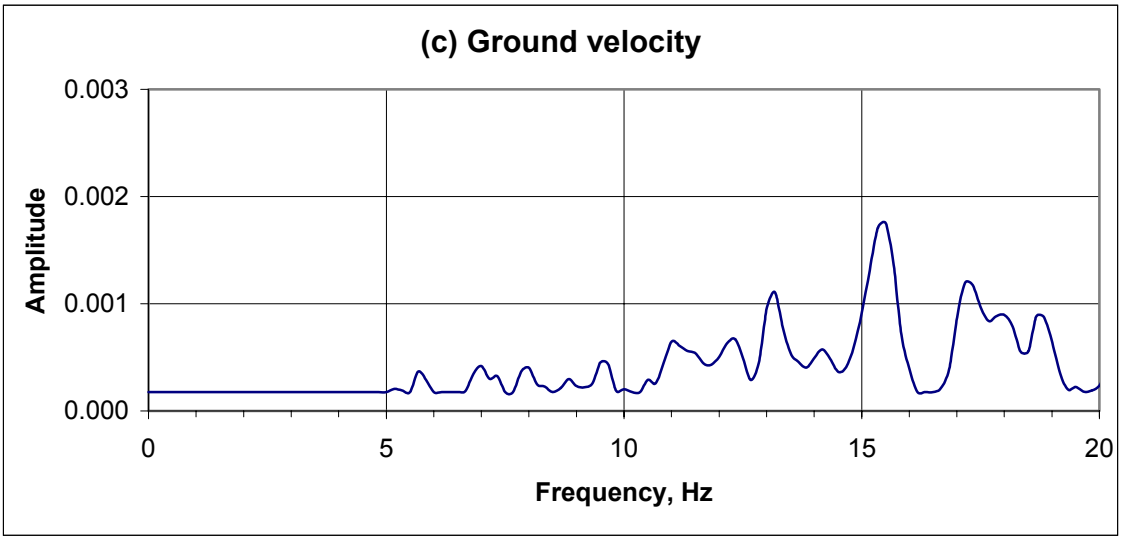

Distressed House - 8/23/01 17:40

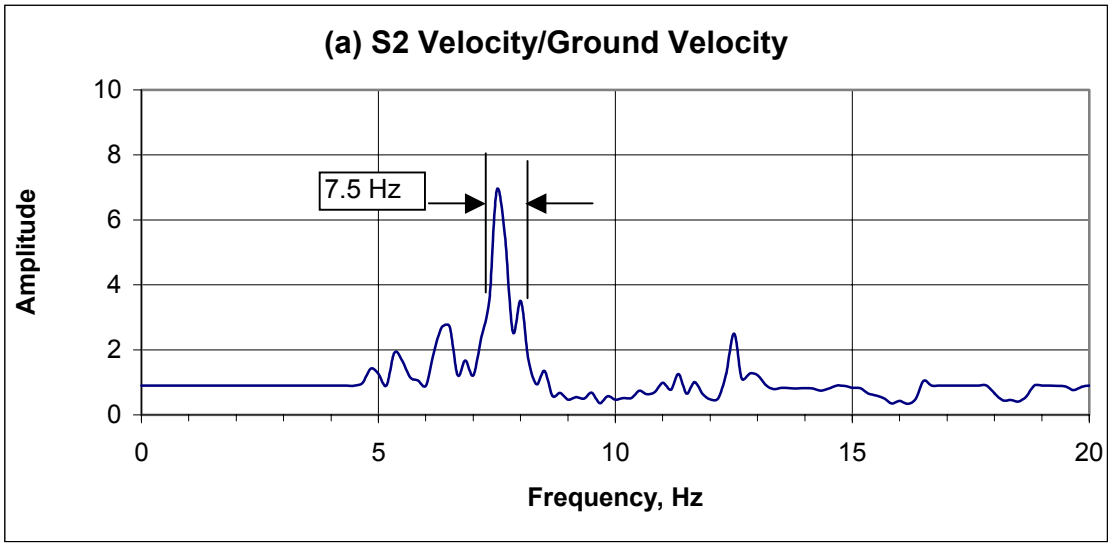

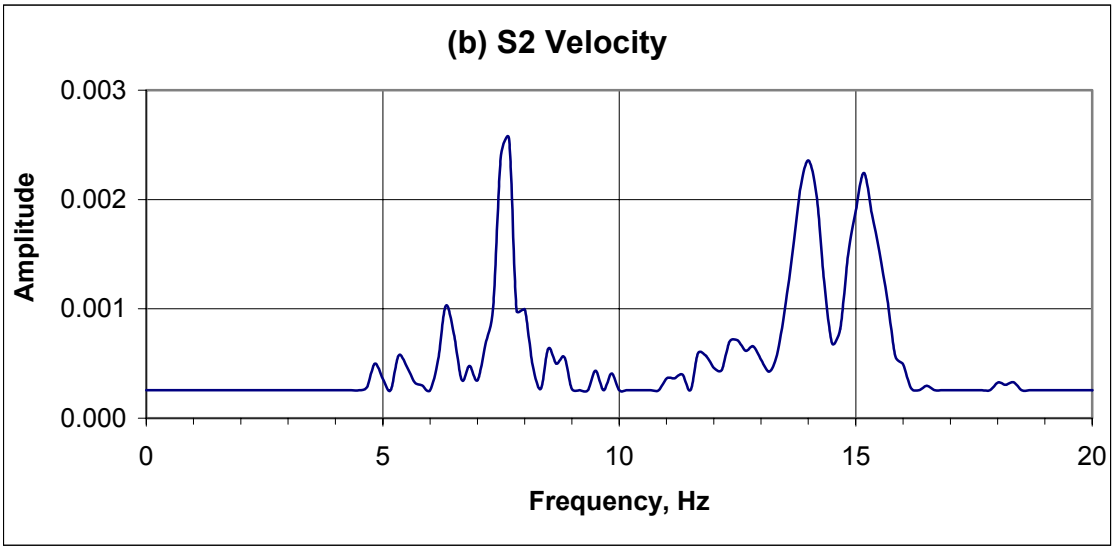

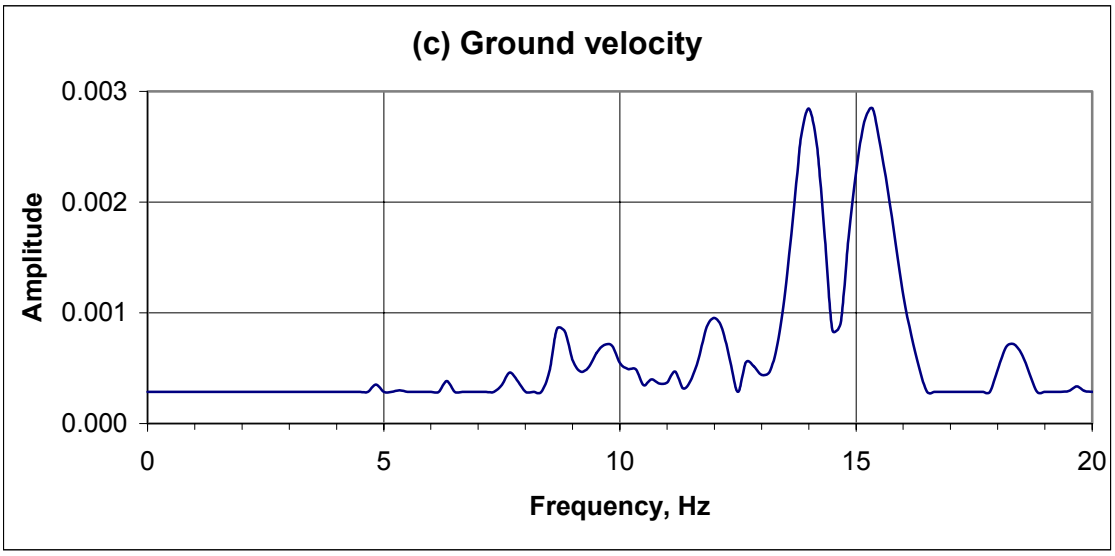

Distressed House - 8/24/01 12:10

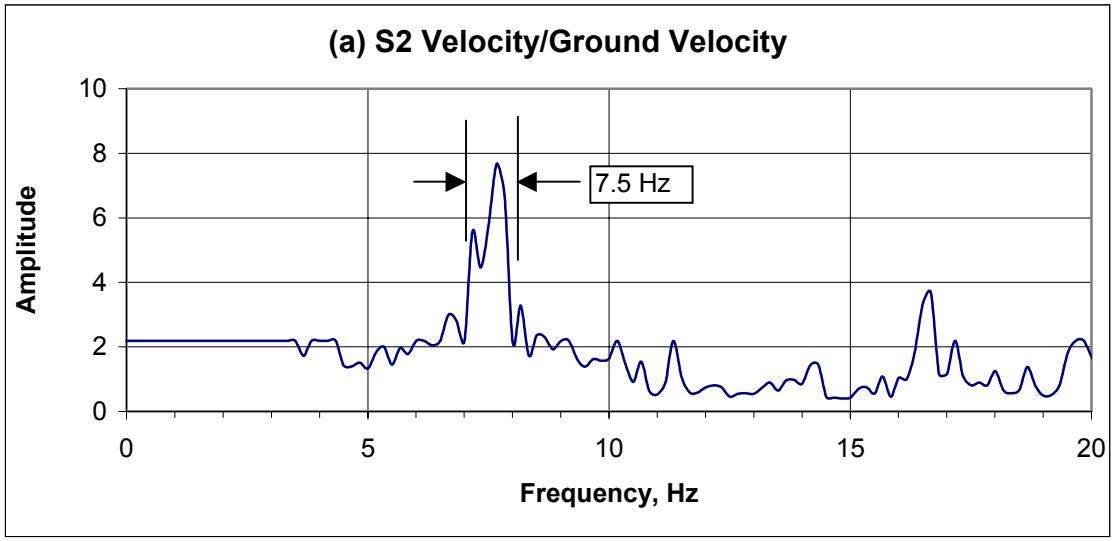

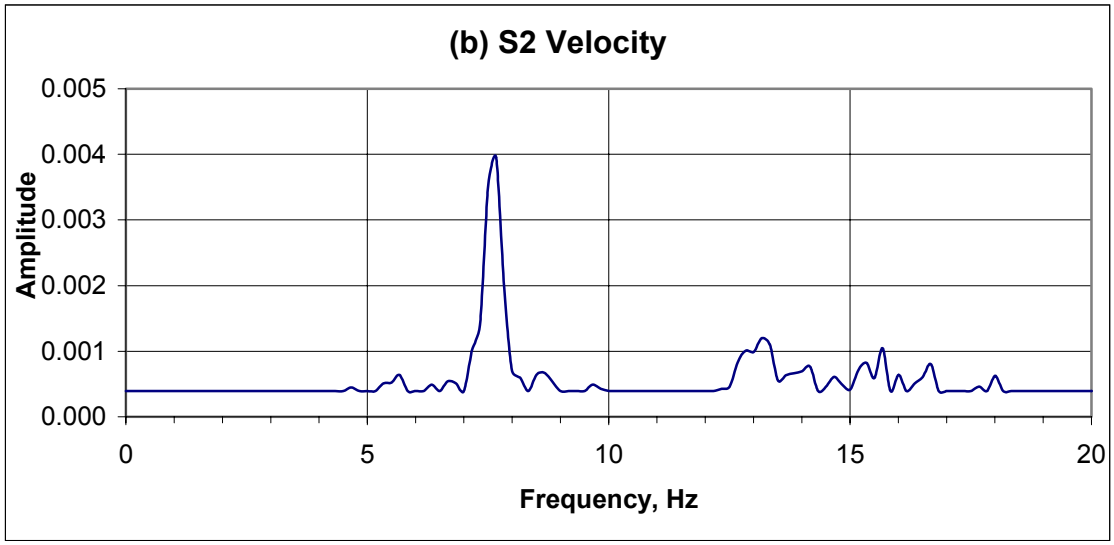

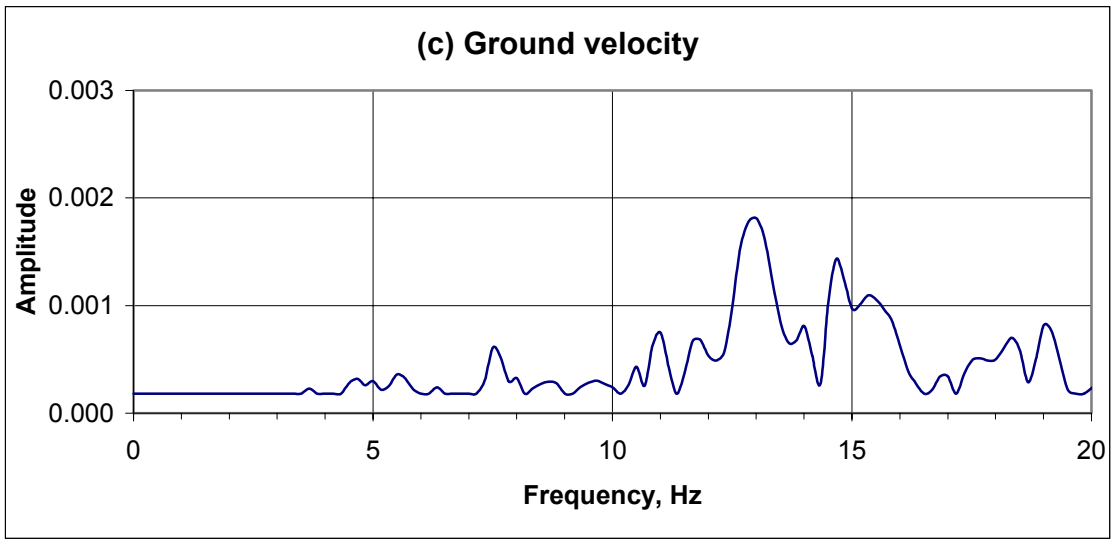

APPENDIX B
SINGLE DEGREE OF FREEDOM MODEL & RESPONSE SPECTRUM

B1. STRUCTURAL ANALOGY

The cracking potential of ground borne vibrations can be discussed most accurately in terms of the response of structures to the passing of the vibration wave form. One of the critical response factors is the amount of differential movement that occurs between structural members or between different points on the same structural member because it causes strains which, in turn, cause cracking.

To compute the differential displacements that may occur in an actual structure or structural component, it is necessary to simplify a structure so that computations are practical. The simplest model that accounts for the dynamic interaction of the three simplified characteristics is the single degree of freedom (SDF) system shown in Figure B-1. The concentrated mass is analogous to the masses of the main components

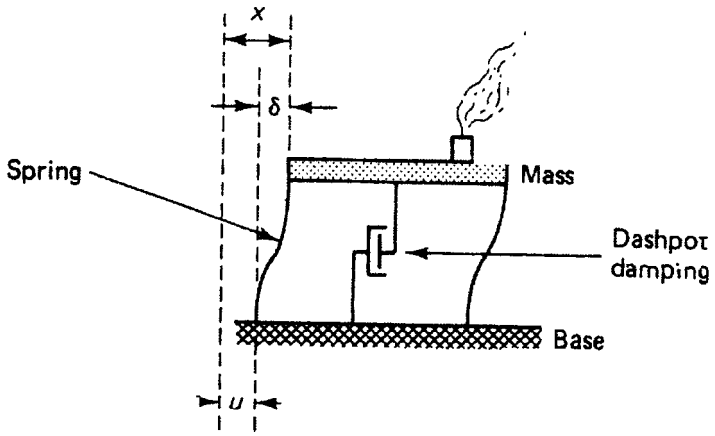

Figure B-1. Single degree of freedom model showing structural and model analogy.

(floors); the spring represents the stiffness of the main components (walls), and the dashpot, through viscous resistance, models the dissipation of energy (connections). The differential movement, δ, is the difference between the absolute displacement of the mass, x, and the absolute displacement of the ground, u. Even multiple degree of freedom systems such as multiple storied structures may be idealized as a single-degree-of-freedom system if one is interested in the dominant or fundamental mode of response. Greater detail on the response of multiple degree of freedom systems can be found in tests on structural dynamics and earthquake engineering

B2. MATHEMATICS OF THE SDF MODEL

The equation of motion for the SDF system in Figure B-1, when subjected to ground

$$m\ddot{x} + c_1\dot{\delta} + k\delta = 0 \qquad \text{(B-1)}$$

excitation, is
where x is the absolute acceleration of the mass, m; c_1 the damping coefficient; the velocity of the mass relative to the ground; k the linear spring constant; and δ the

relative displacement between the ground and the mass. Using the relationship for the relative displacement ($\delta = x - u$, shown in Figure I-1), Equation B-1 becomes

$$m\ddot{\delta} + c_1\dot{\delta} + k\delta = -m\ddot{u} \qquad \text{(B-2)}$$

The circular natural frequency of the undamped spring-mass system, p, is equal to $\sqrt{k/m}$. The fraction of critical damping, β, is equal to $\frac{c_1}{2\sqrt{mk}}$. If the mass is displaced from its equilibrium position, it will not oscillate when released but will simply return to its equilibrium position when c_1 is equal to $2\sqrt{mk}$. Under this condition the system is said to be critically damped. The circular natural frequency of the damped system, p_d, is equal to $p\sqrt{1-\beta^2}$. Equation B-2 can be recast as

$$\ddot{\delta} + 2\beta p\dot{\delta} + p^2\delta = \ddot{u} \qquad \text{(B-3)}$$

in terms of percentage critical damping, β, and circular natural frequency, p. The ground-acceleration time history, which is to be integrated from time zero to time t, is represented by u *(t)*.

Thus if a structure's undamped natural frequency, p, and its fraction of critical damping, β, are known, it is not necessary to define particular values of m, k, and c_1 in order to model the structure accurately. Furthermore, dynamic properties, p and β, can be more accurately measured from a free vibration time history of the building response than calculated from estimates of m, k, and c_1. These measured parameters automatically account for the factors that are difficult to quantify, such as the degree of fixity of the columns (which affects k) and the damping coefficient, c_1.

The preceding discussion dealt with the response of a particular structure to a particular ground motion. However, to distinguish different types of ground motions and their differing cracking potentials, it is necessary to compare the effect of the wave on a wide variety of structures. The response spectrum, which can be calculated from solutions to Equation B-3, provides a mechanism for this comparison.

Solution to Equation B-3 for relative displacements at any time may be expressed in

$$\delta(t) = -\frac{1}{p\sqrt{1-\beta^2}}\int_0^t (\tau)\, e^{\beta p(t-\tau)} \sin[p_d(t-\tau)]\, d\tau \qquad \text{(B-4)}$$

terms of the Duhamel integral of the absolute ground acceleration time history as where δ and are zero at t_0 (Veletsos and Newmark, 1964).

Equation B-4 yields the relative displacement response of an SDF system from a ground-acceleration time history. If a velocity time history is used as the input time history, the relationship between u and δ can be found by integrating Equation B-4 by parts and combining terms (Veletsos and Newmark, 1964). The resulting equation can be expressed as

$$\delta(t) = -\int_0^t \ddot{u}(\tau)\, e^{\beta p(t-\tau)} \left[\cos[p_d(t-\tau)] - \frac{\beta}{\sqrt{1-\beta^2}} \sin[p_d(t-\tau)] \right] d\tau \qquad \text{(B-5)}$$

when δ and as well as *displacement, velocity, and acceleration* are zero at t_0.

B3. CONSTRUCTION OF THE RESPONSE SPECTRUM

When a particle velocity time history such as that of the radial ground motions shown in Figure B-2b is processed by computer with Equation B-5, a relative displacement, "δ", time history is calculated. In the calculated relative displacement time history there will be a maximum, δ_{max}.

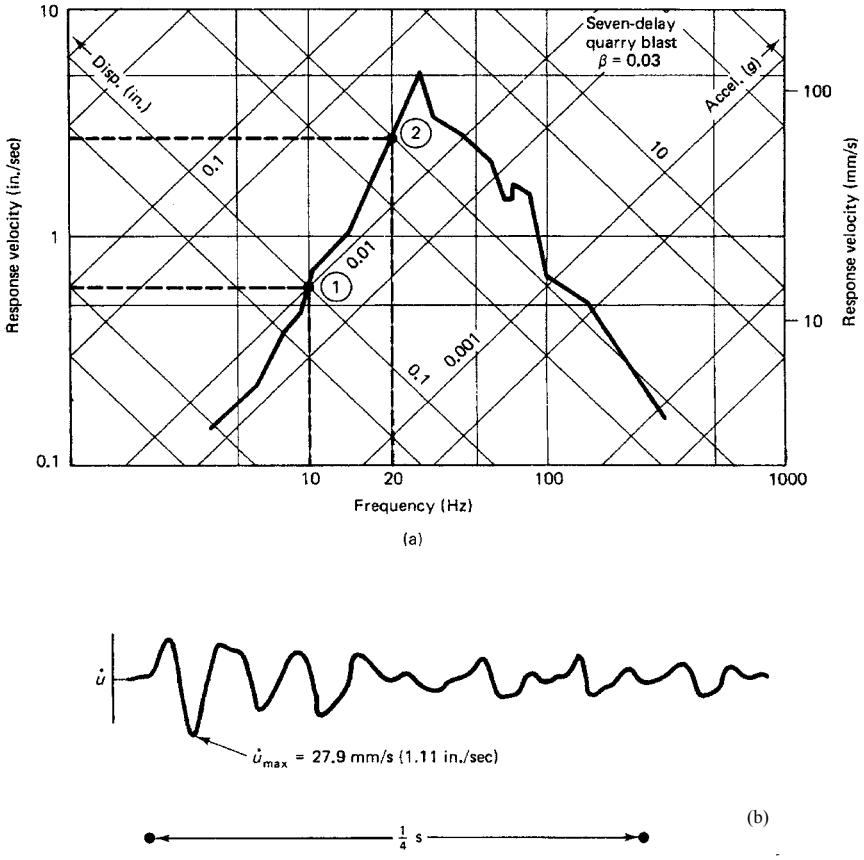

Figure B2. Response spectrum (a) calculated from excitation ground motions (b) showing responses of systems with natural (fundamental) frequencies of 10 and 20 Hz

If that maximum relative displacement is multiplied by p, the structure's circular natural frequency (or $2\pi\ f_s = 2\pi\ (1/T)$),

$$PV = 2\pi\ f_s * \delta_{max} = p * \delta_{max}$$

is called the pseudo velocity (PV). This pseudo velocity is a close approximation of the relative velocity, , if the pulse associated with δ_{max} is approximately sinusoidal

The pseudo velocity response spectrum of a single ground motion, such as that of the seven pulse motion in Figure B2a, is generated from the δ_{max} values of a number of different SDF systems when excited by that motion. Consider two different components of the same structure, a l0-Hz superstructure and the 20-Hz floor. If the ground motions, u *(t)*, of the seven pulse motion are processed twice by Equation B-5 with β, damping, held constant at 3%, and f_s = 10 and 20 Hz, two δ_{max} values will result.

The first computation is made with the l0-Hz system, which has a circular natural frequency of

$$p = 2\pi(10)$$

and results in

$$\delta_{max} = 0.25 \text{ mm } (0.01 \text{ in.})$$

This δ_{max} is then converted to PV as

$$PV_{10} = p\,\delta_{max} = 2\pi\ (10)(0.25) = 15.7 \text{ mm/s } (0.62 \text{ in./sec})$$

and is plotted as point 1 in Figure B-2a. The same computation is then repeated for the 20-Hz system.

$$p = 2\pi(20)$$

$$\delta_{max} = 0.5 \text{ mm } \quad (0.02 \text{ in.})$$

$$PV_{20} = 2\pi\ (20)(0.5) = 63.5 \text{ mm/s } \quad (2.5 \text{ in./sec})$$

and PV_{20} is plotted as point 2 in Figure B2a. If the ground motions are processed a number of times for a variety of f_s's with β constant, the resulting pseudo velocities will form the solid line in Figure B2a.

The response spectrum in Figure B2b is plotted on four-axis tripartite paper. These four axes take advantage of the sinusoidal approximation involved in calculating a pseudo velocity. The axis of the maximum relative displacement, δ, is inclined upward to the left and is the pseudo velocity (PV) divided by $2\pi\phi_\sigma$. The pseudo acceleration (PA) axis is inclined upward to the right and is PV times $2\pi\phi_\sigma$. PA and PV are called pseudo acceleration and pseudo velocity because they are sinusoidal approximations. However, these simplifications closely approximate the absolute acceleration of the mass and the relative velocity for systems with small β values (Veletsos and Newmark, 1964).

APPENDIX C
TIME HISTORIES RECORDED AT WISCONSIN STRUCTURE

November 30, 2001 @ 08:17

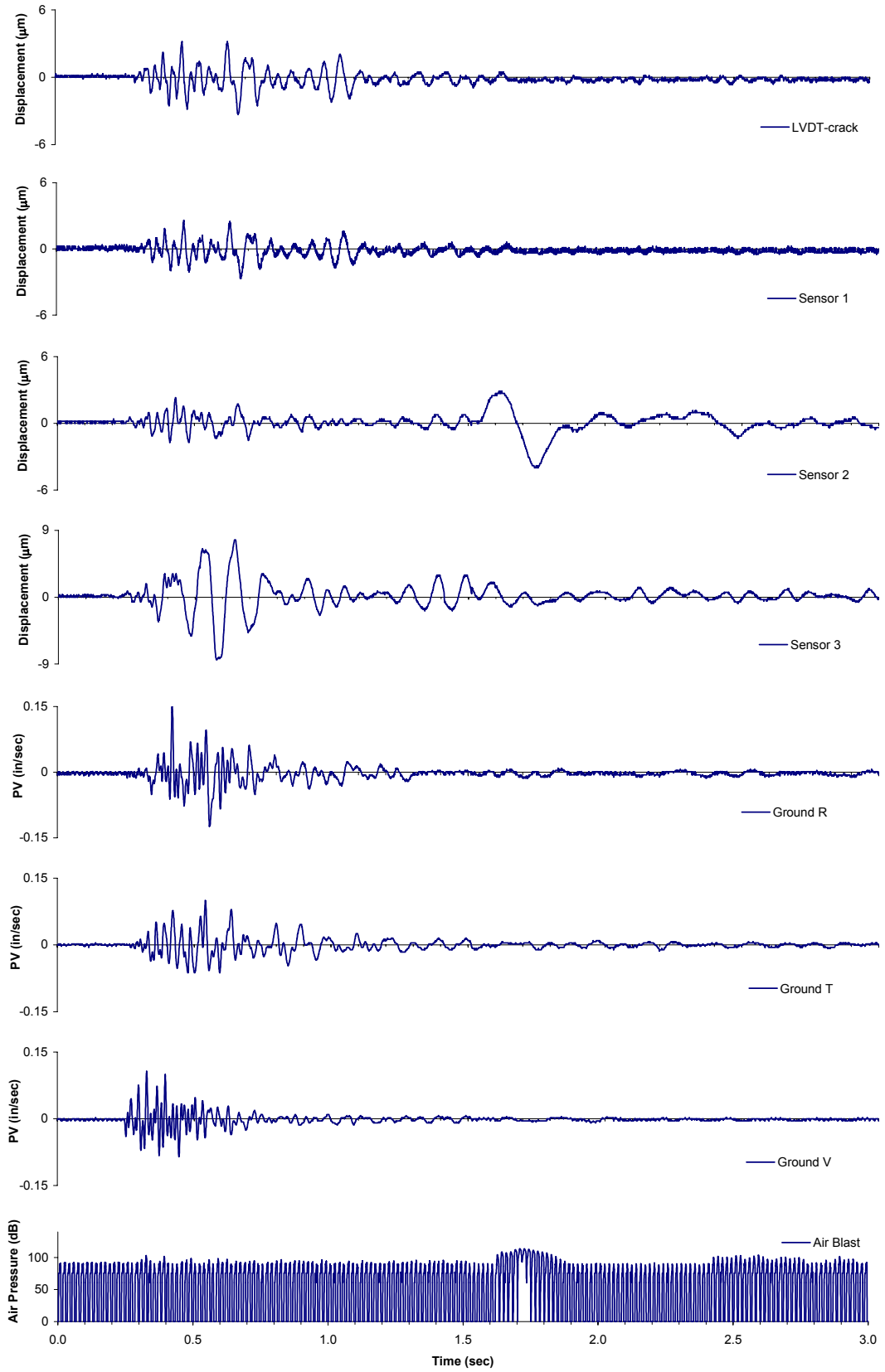

11/30/2001 @ 10:59:00 AM

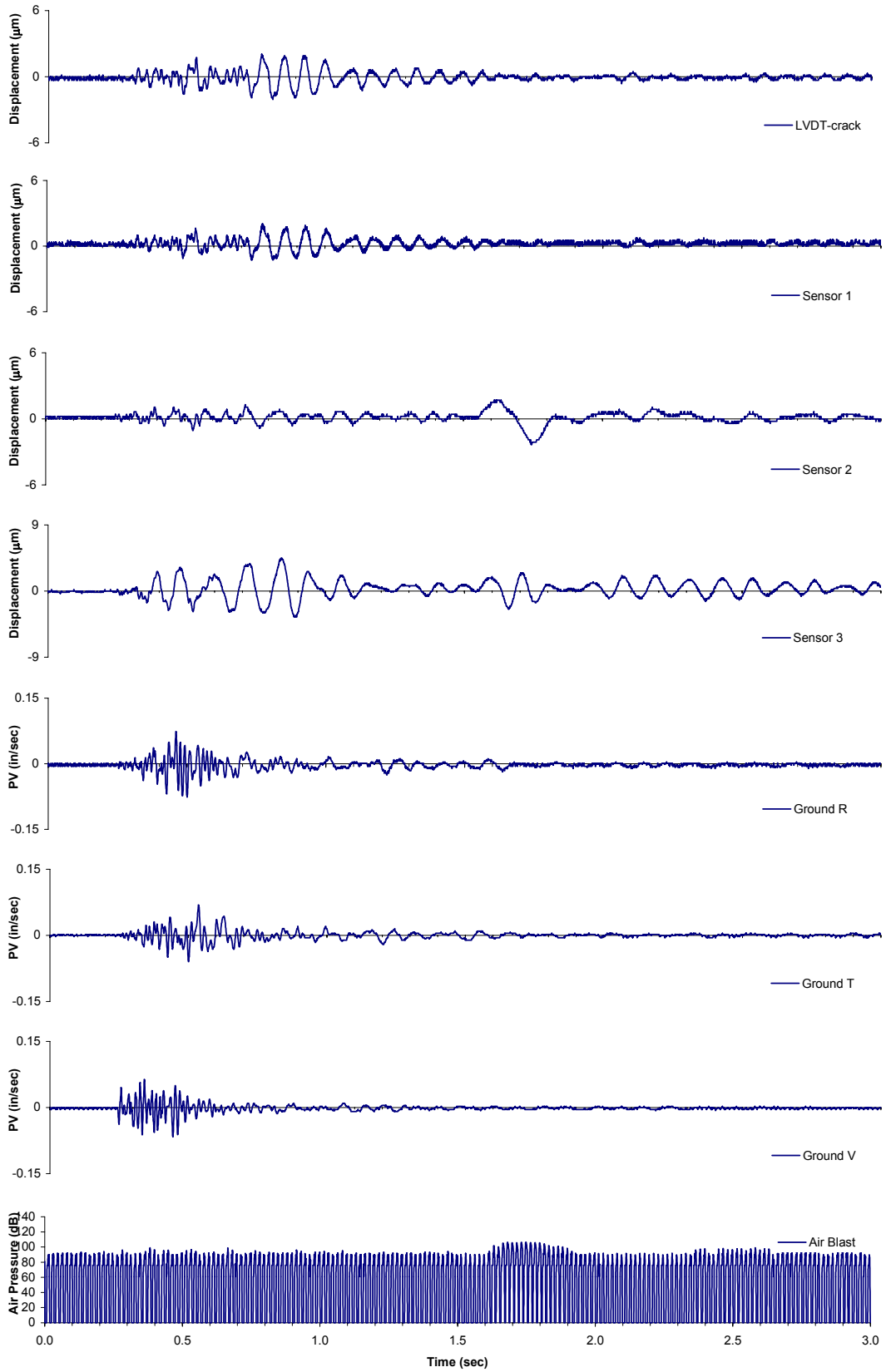

11/30/2001 @ 11:29:00 AM

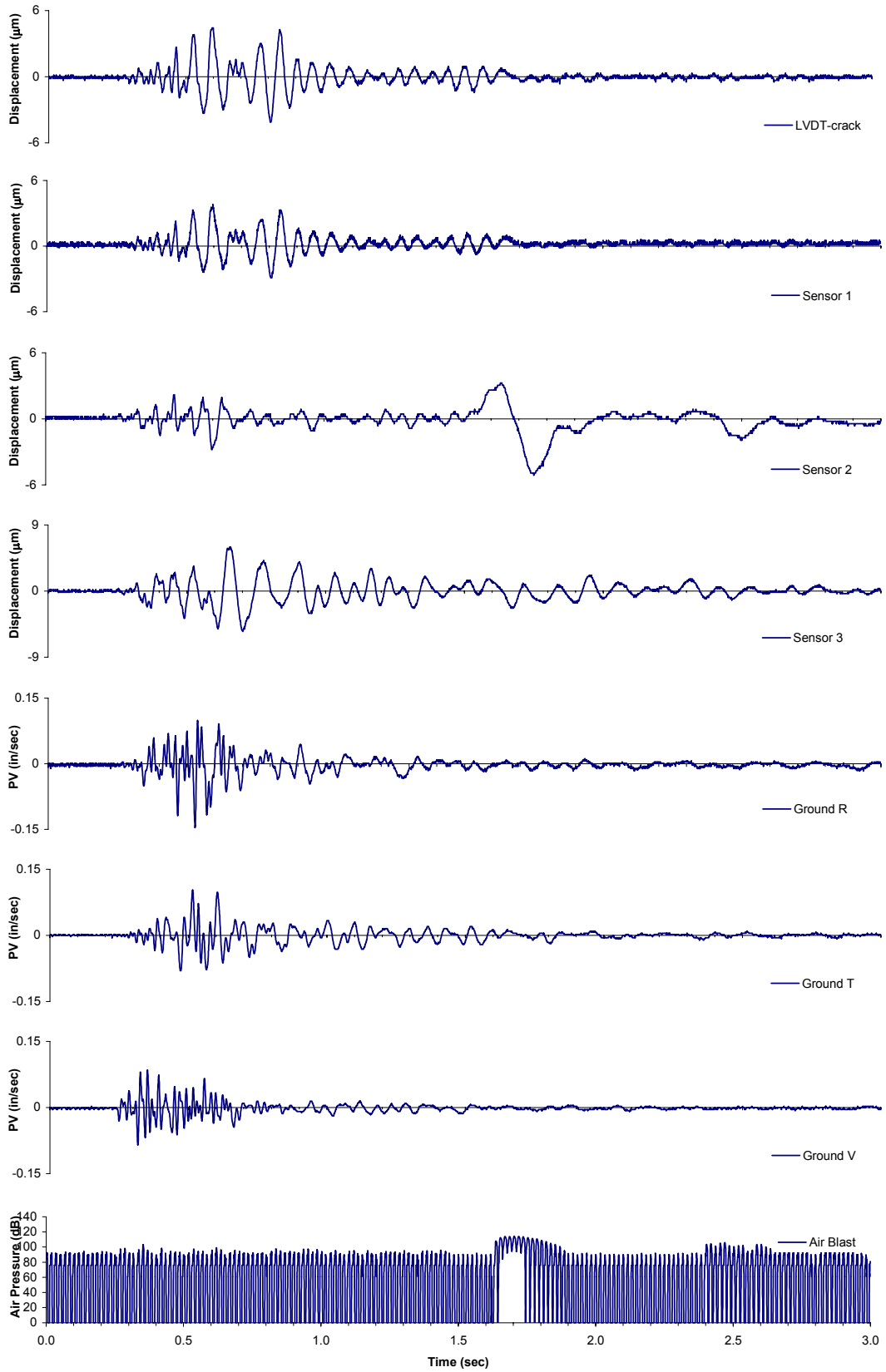

12/5/2001 @ 9:03:00 AM

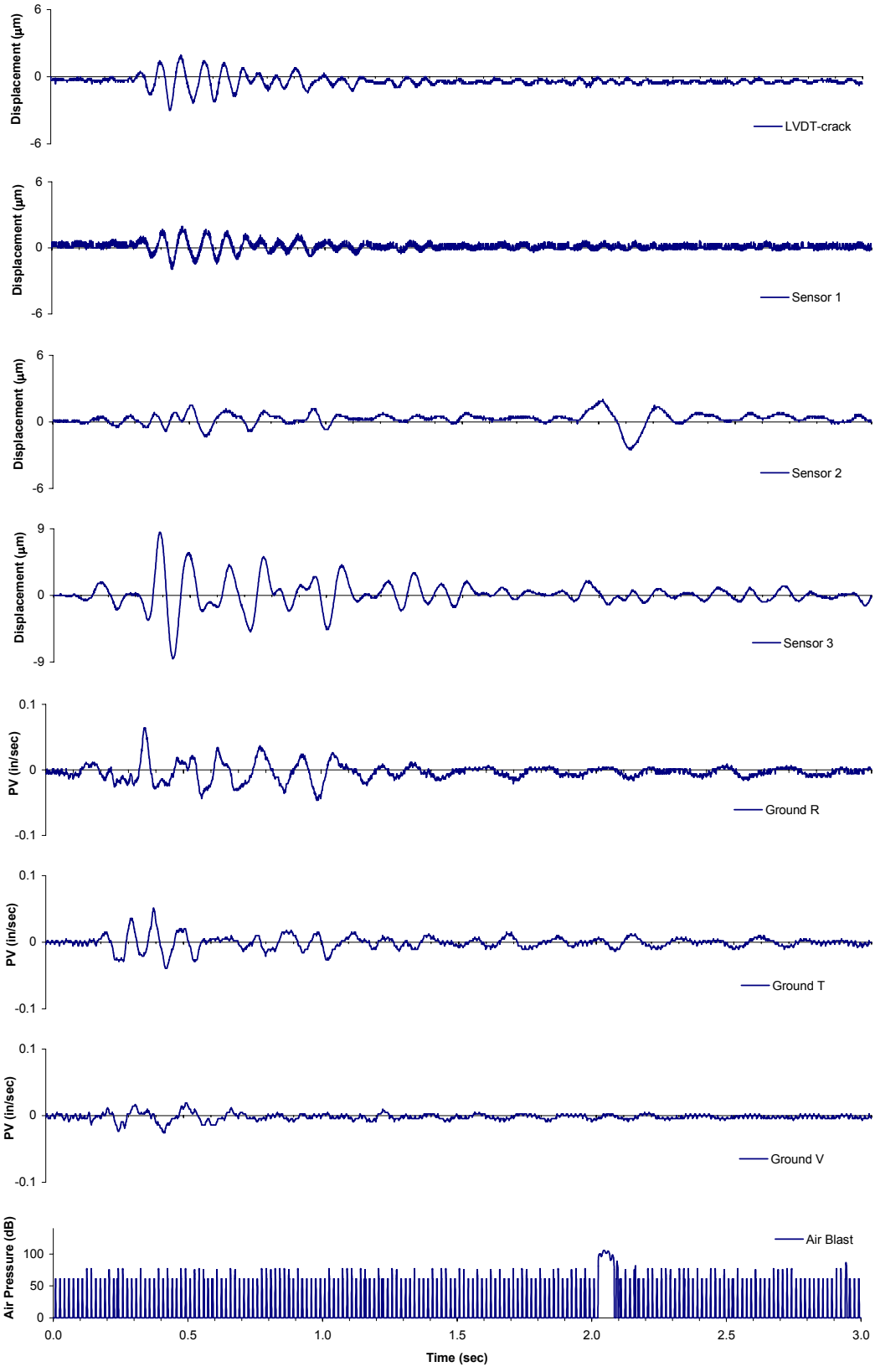

12/7/2001 @ 12:02:00 PM

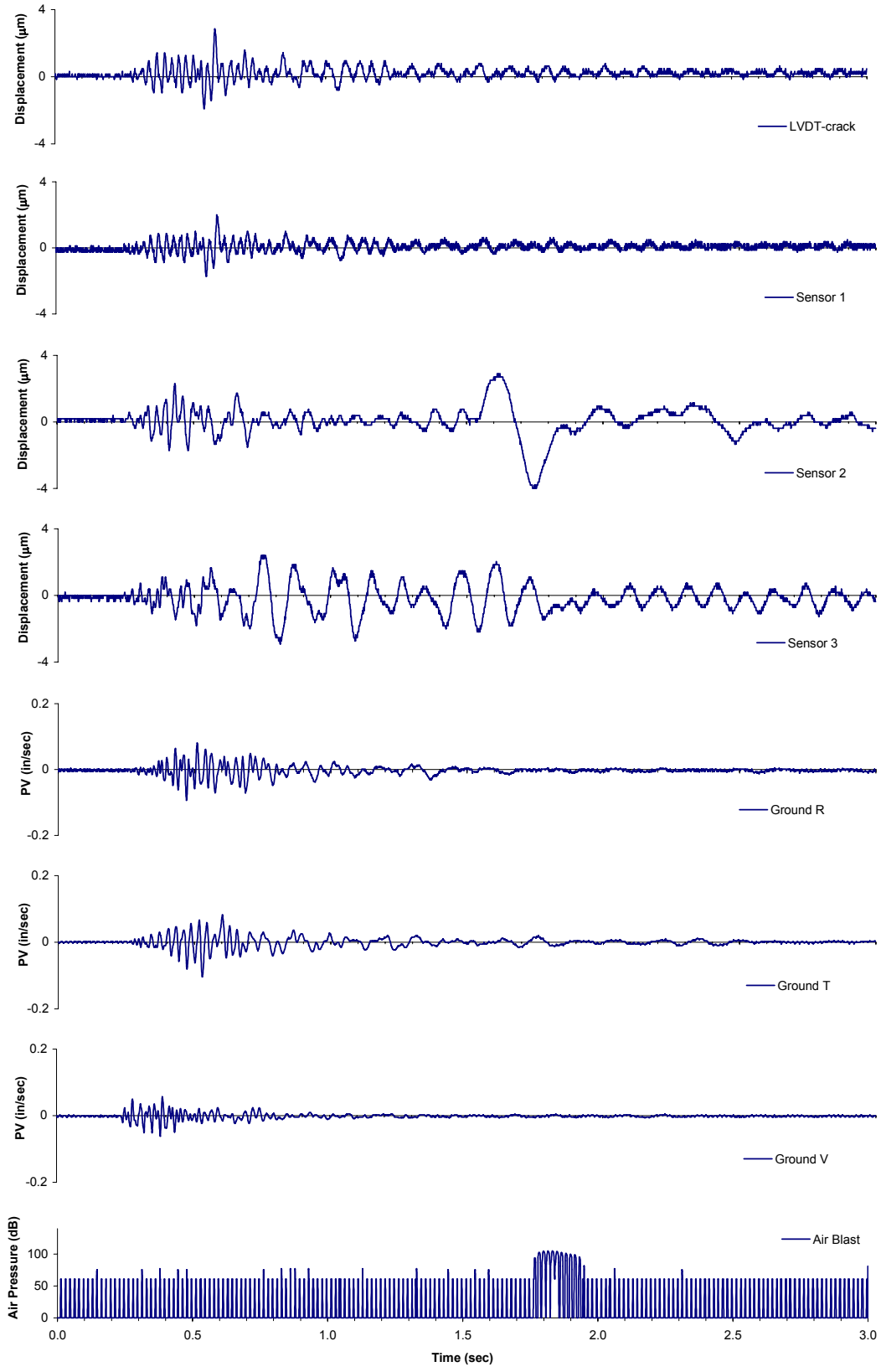

12/7/2001 @ 12:28:00 PM

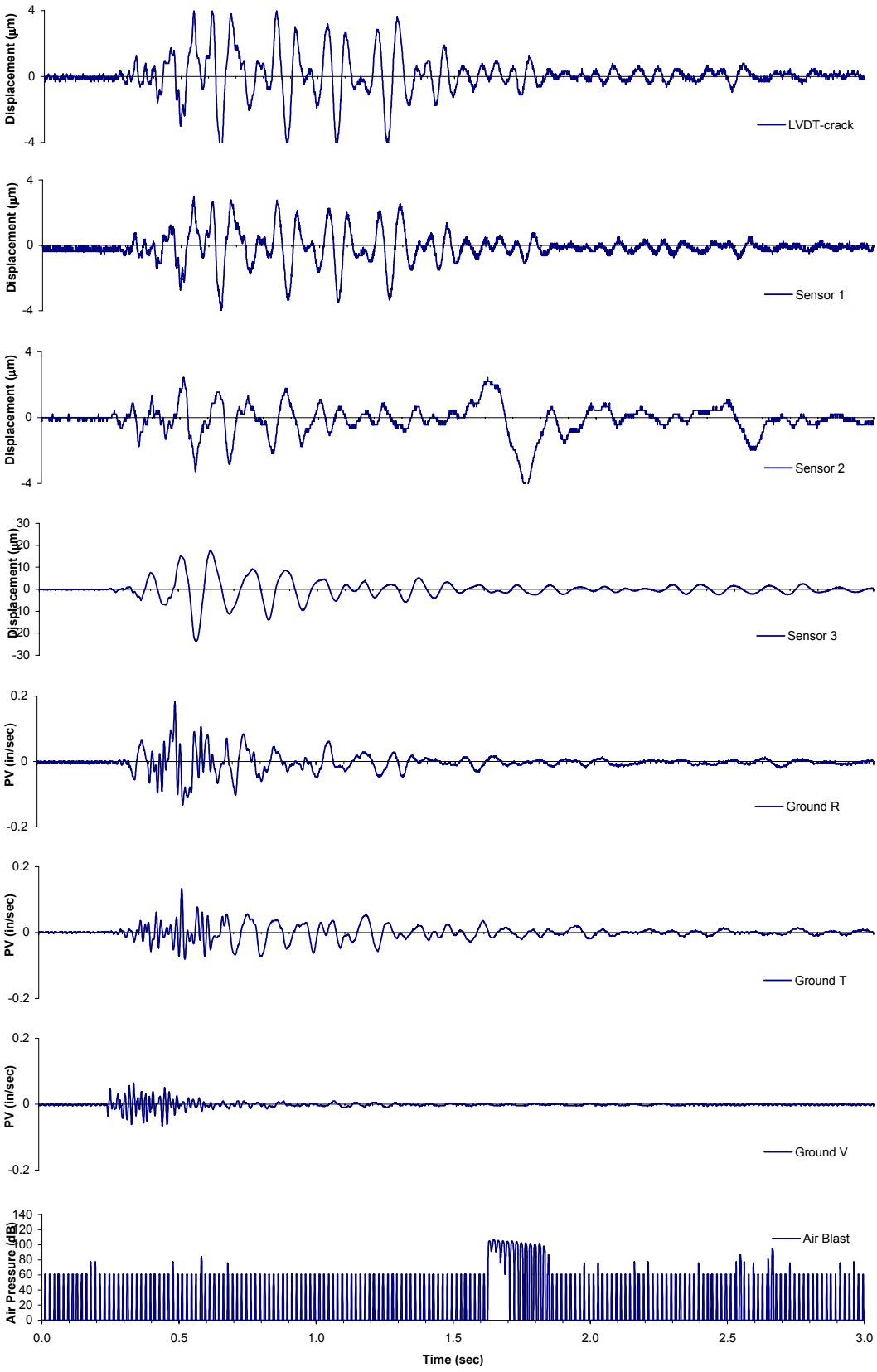

12/17/2001 @ 8:33:00 AM

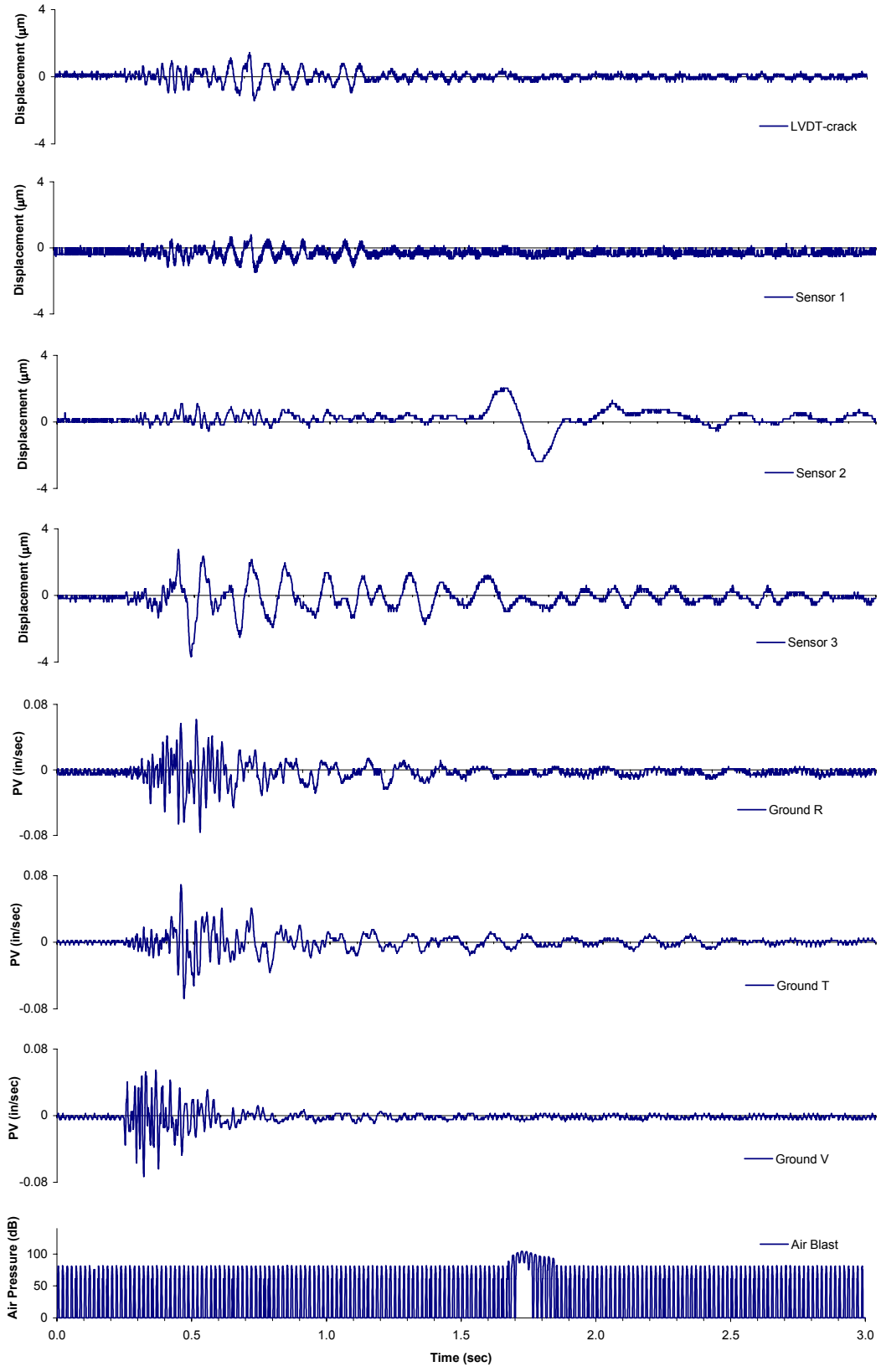

12/17/2001 @ 10:12:00 AM

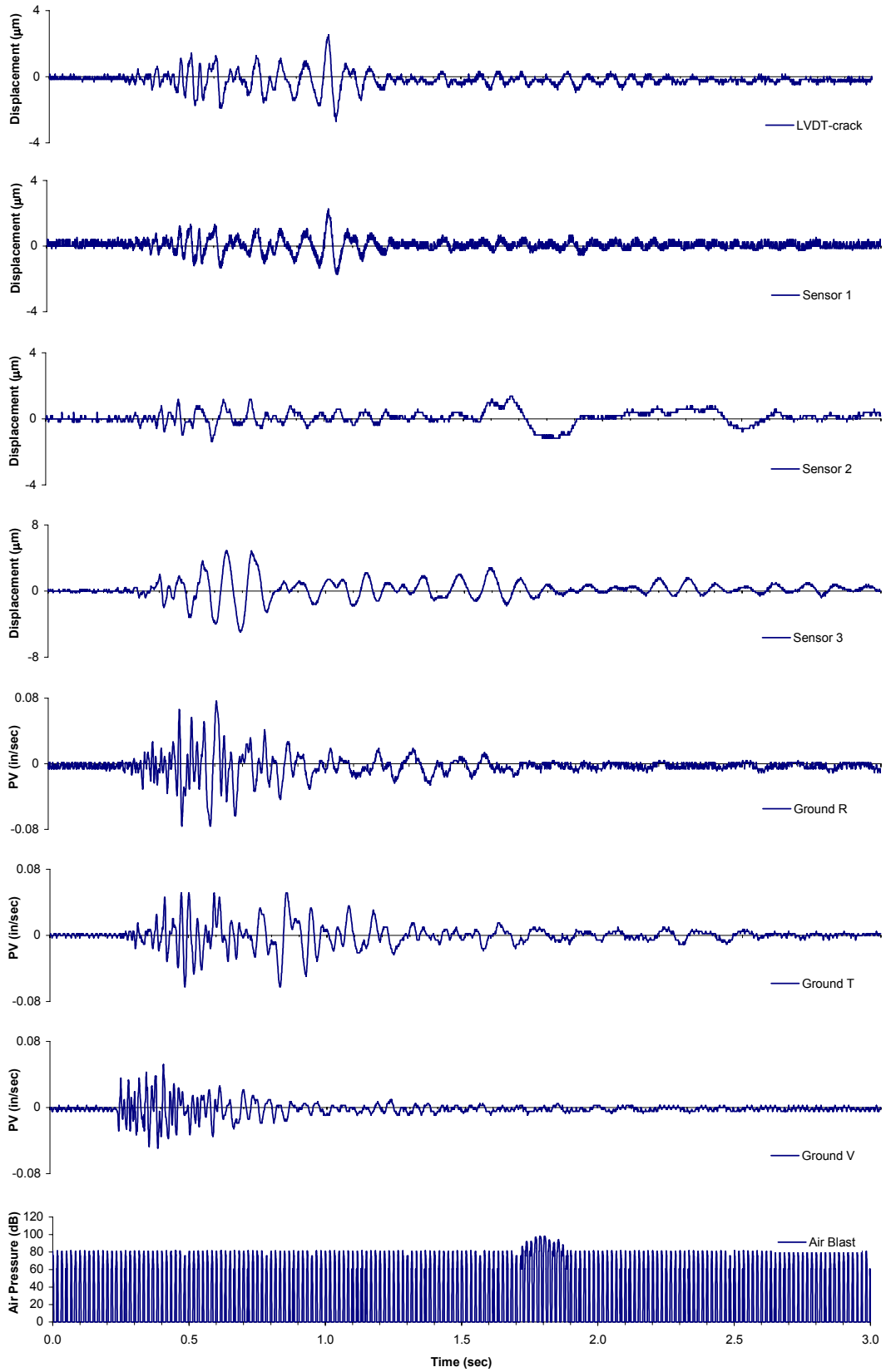

12/17/2001 @ 11:41:00 AM

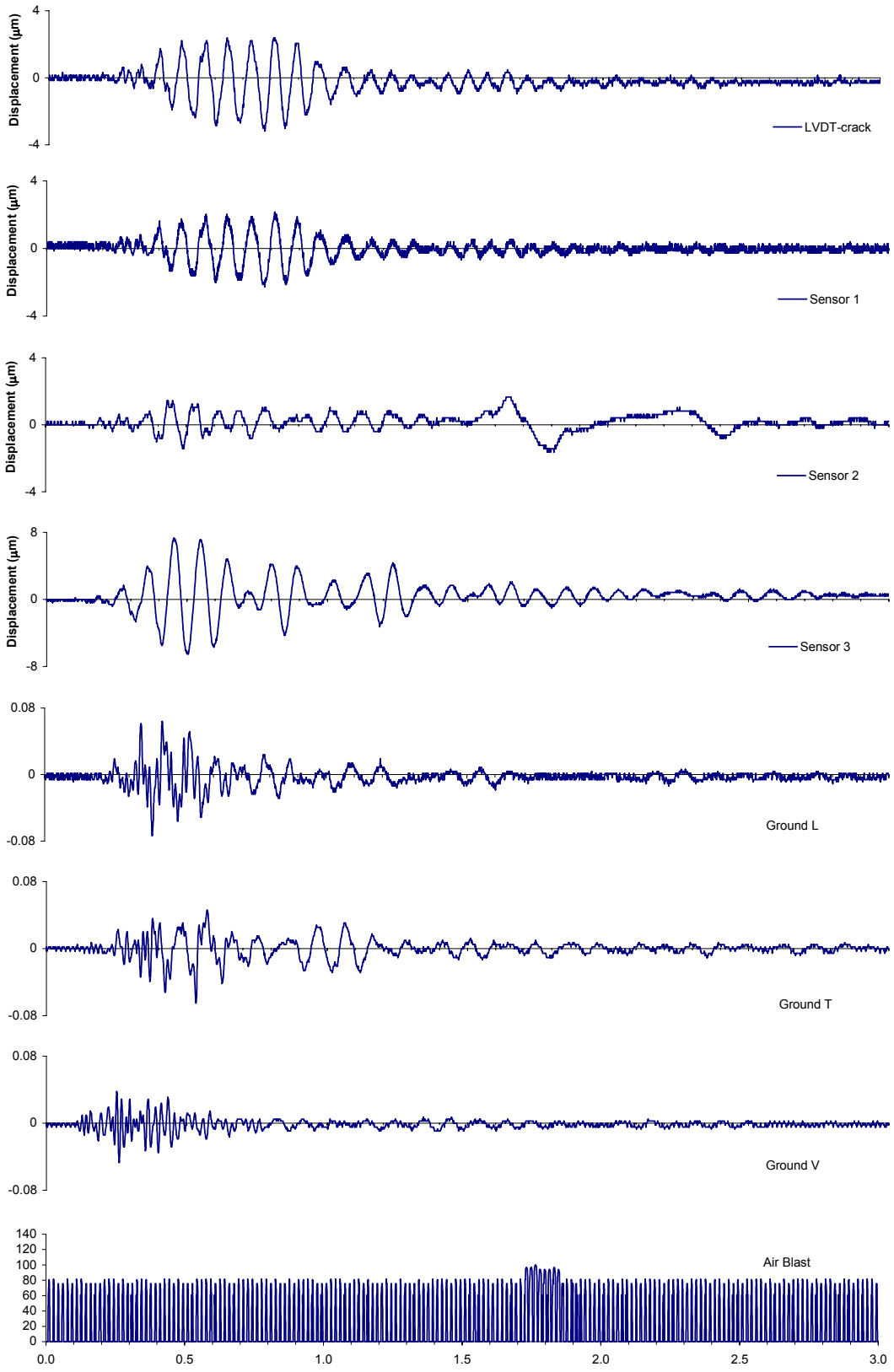

12/19/2001 @ 10:01:00 AM

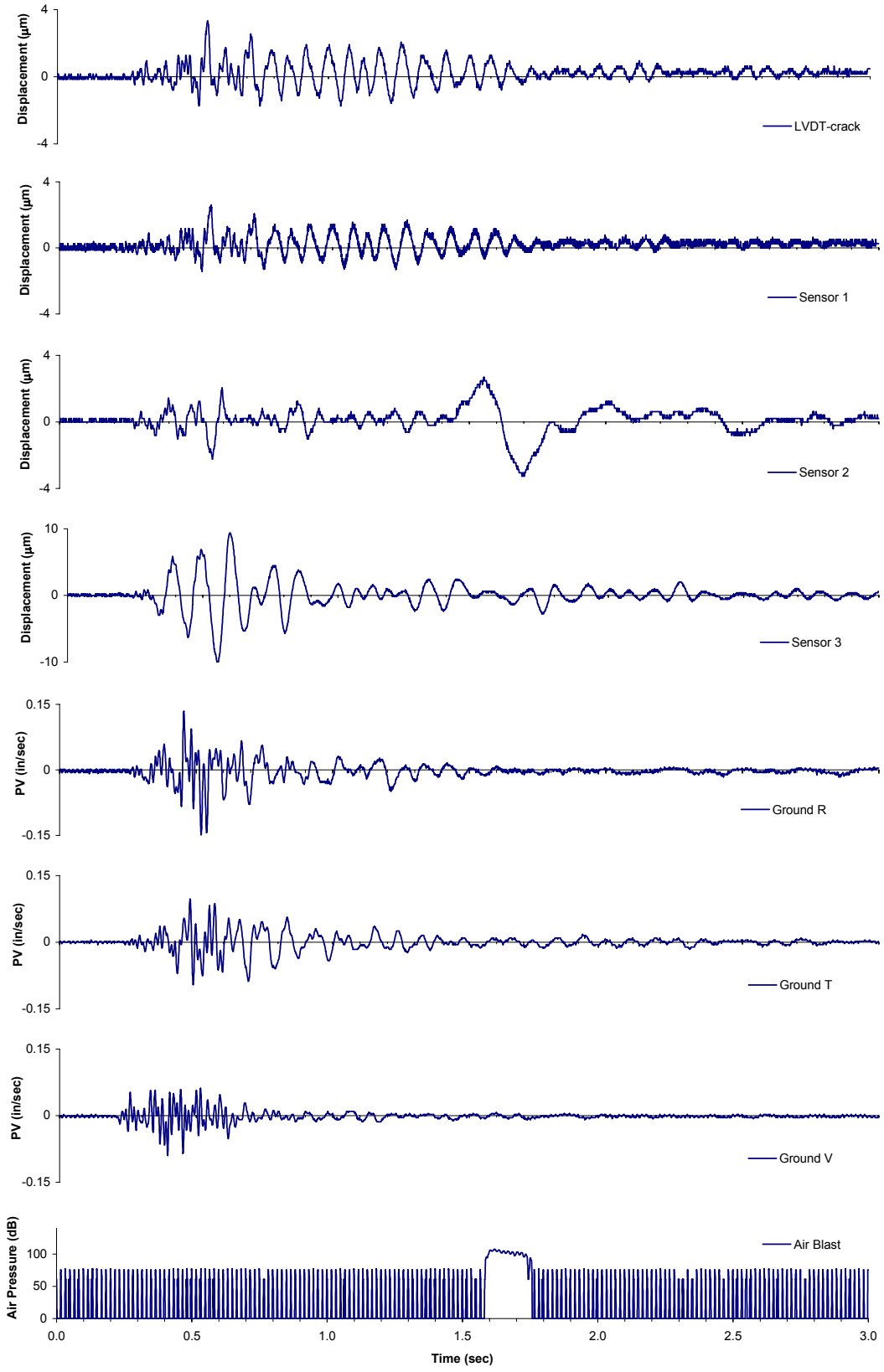

12/19/2001 @ 10:31:00 AM

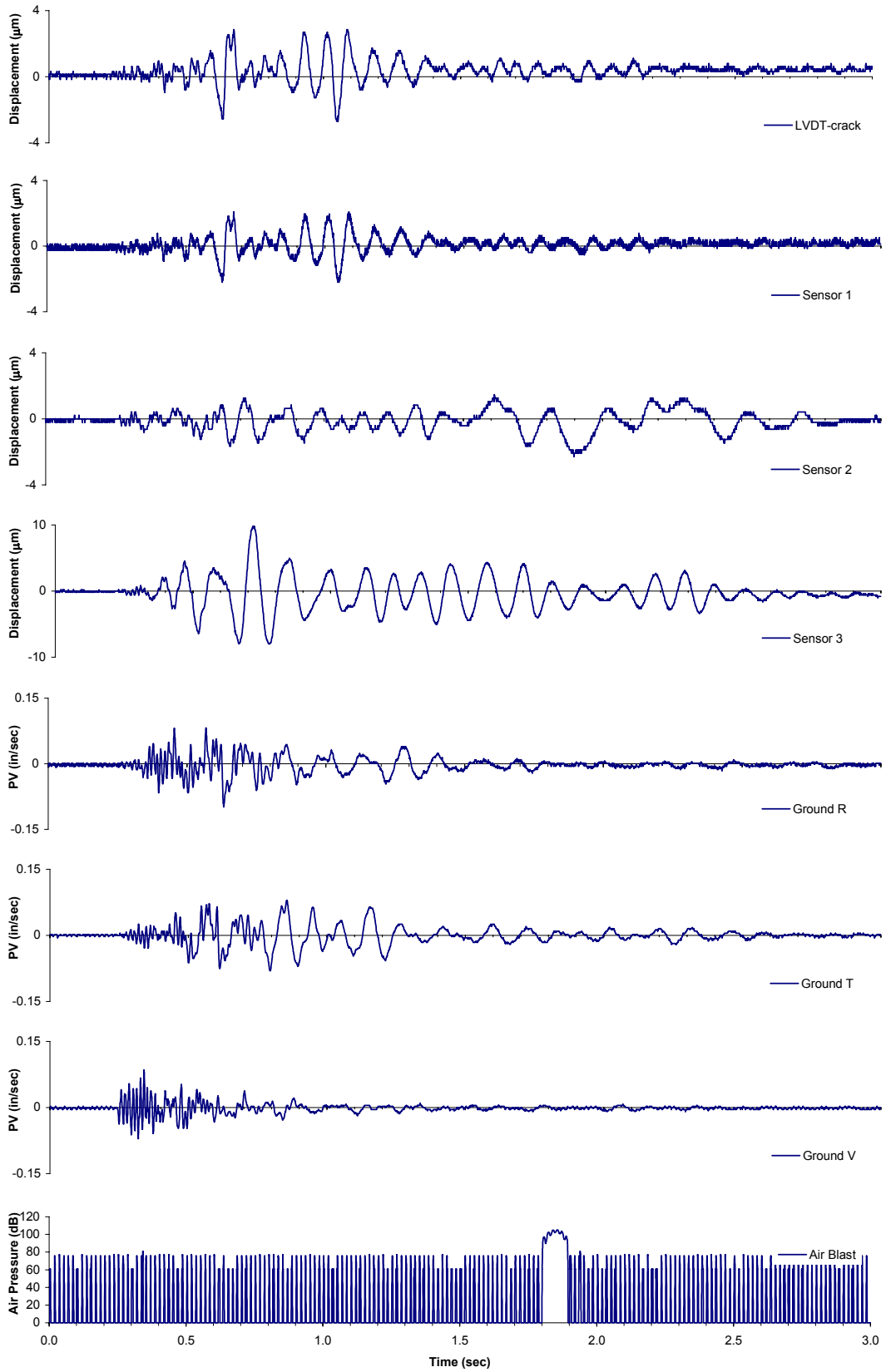

1/4/2002 @ 9:33 AM

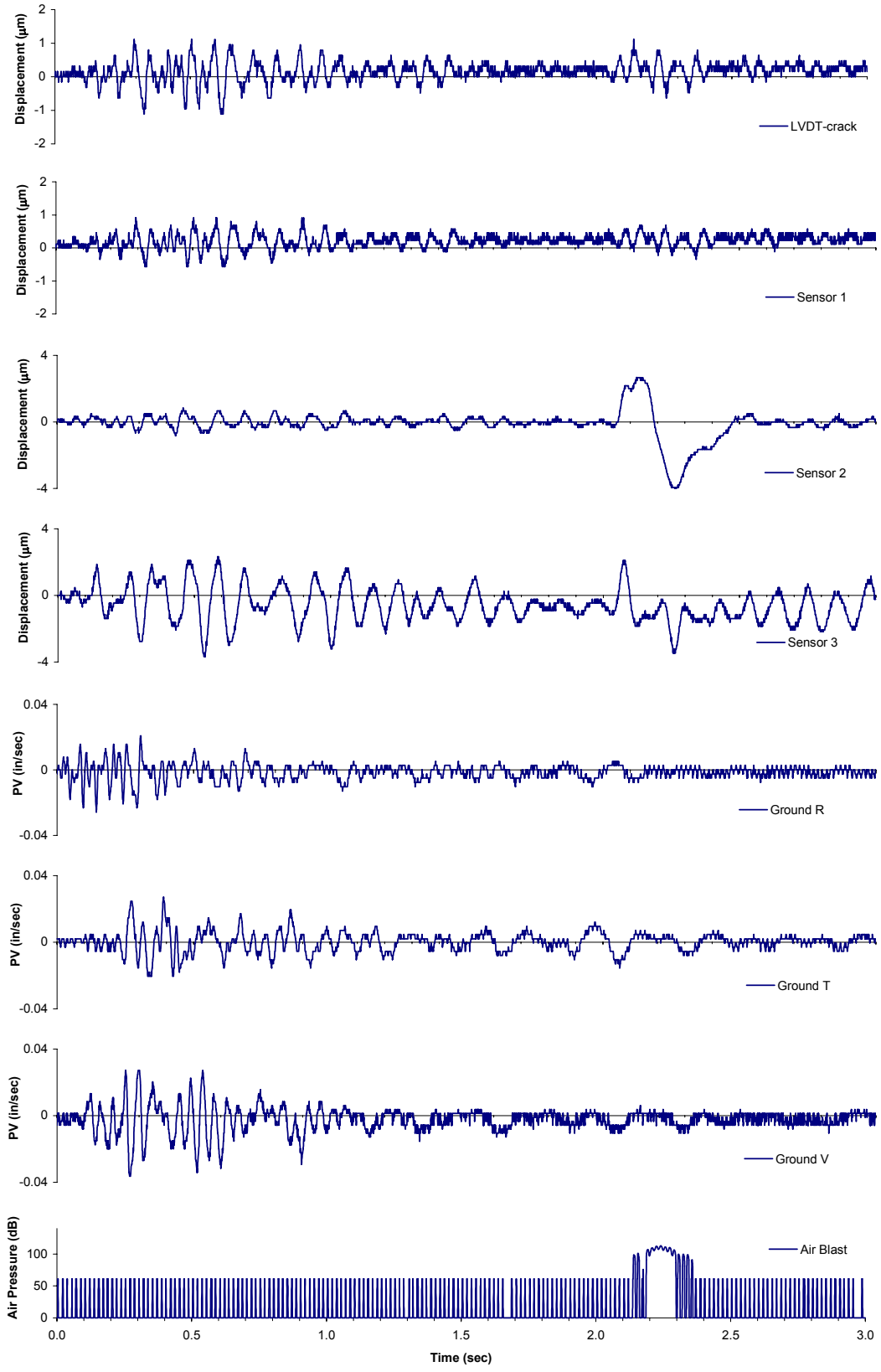

1/4/2002 @ 13:06

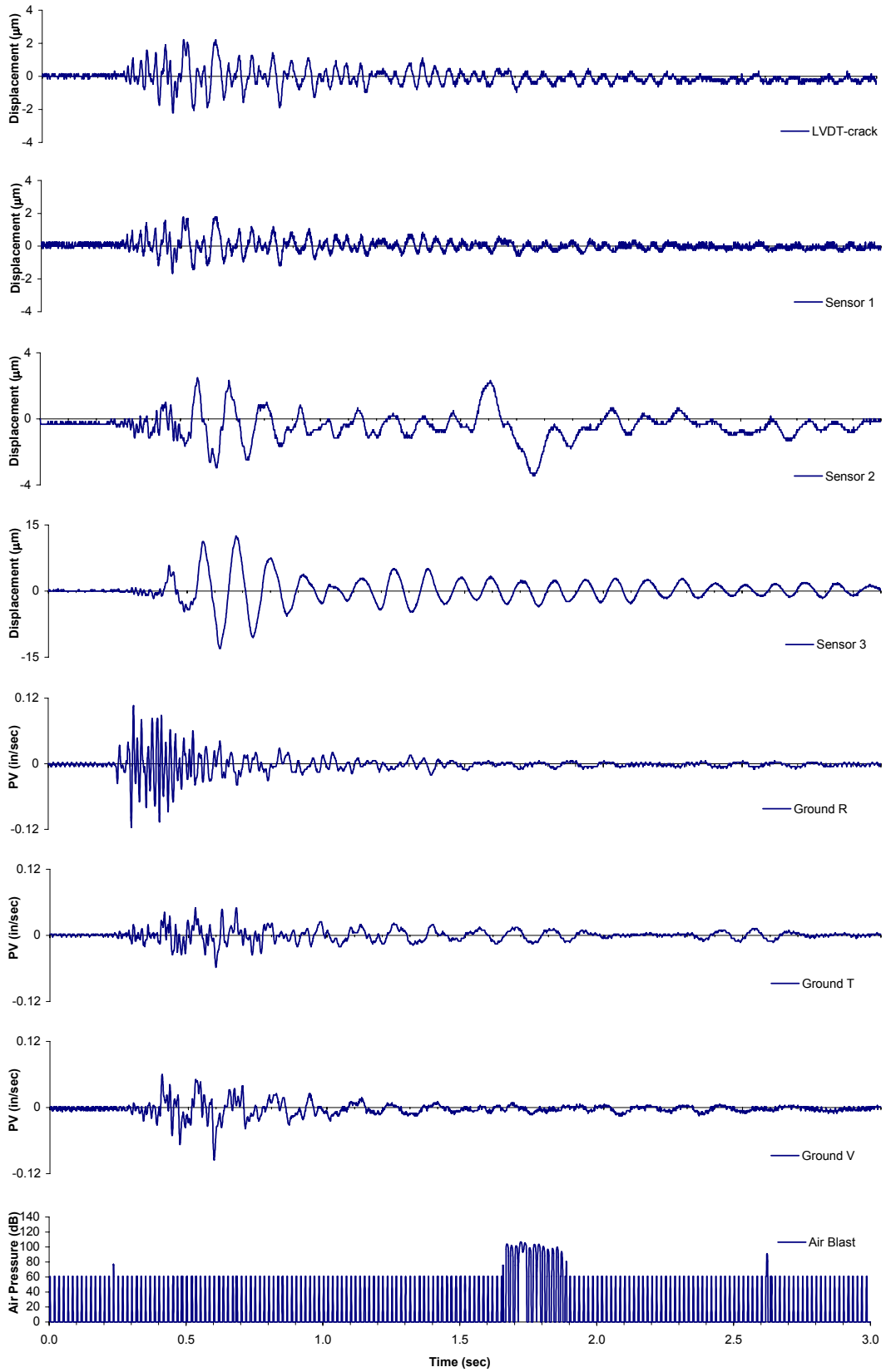
Displacement (µm)
4
2
0
-2
-4
LVDT-crack
Displacement (µm)
4
2
0
-2
-4
Sensor 1
Displacement (µm)
4
0
-4
Sensor 2
Displacement (µm)
15
0
-15
Sensor 3
PV (in/sec)
0.12
0
-0.12
Ground R
PV (in/sec)
0.12
0
-0.12
Ground T
PV (in/sec)
0.12
0
-0.12
Ground V
Air Pressure (dB)
140
120
100
80
60
40
20
0
Air Blast
0.0
0.5
1.0
1.5
2.0
2.5
3.0
Time (sec)

1/11/2002 @ 10:15 AM

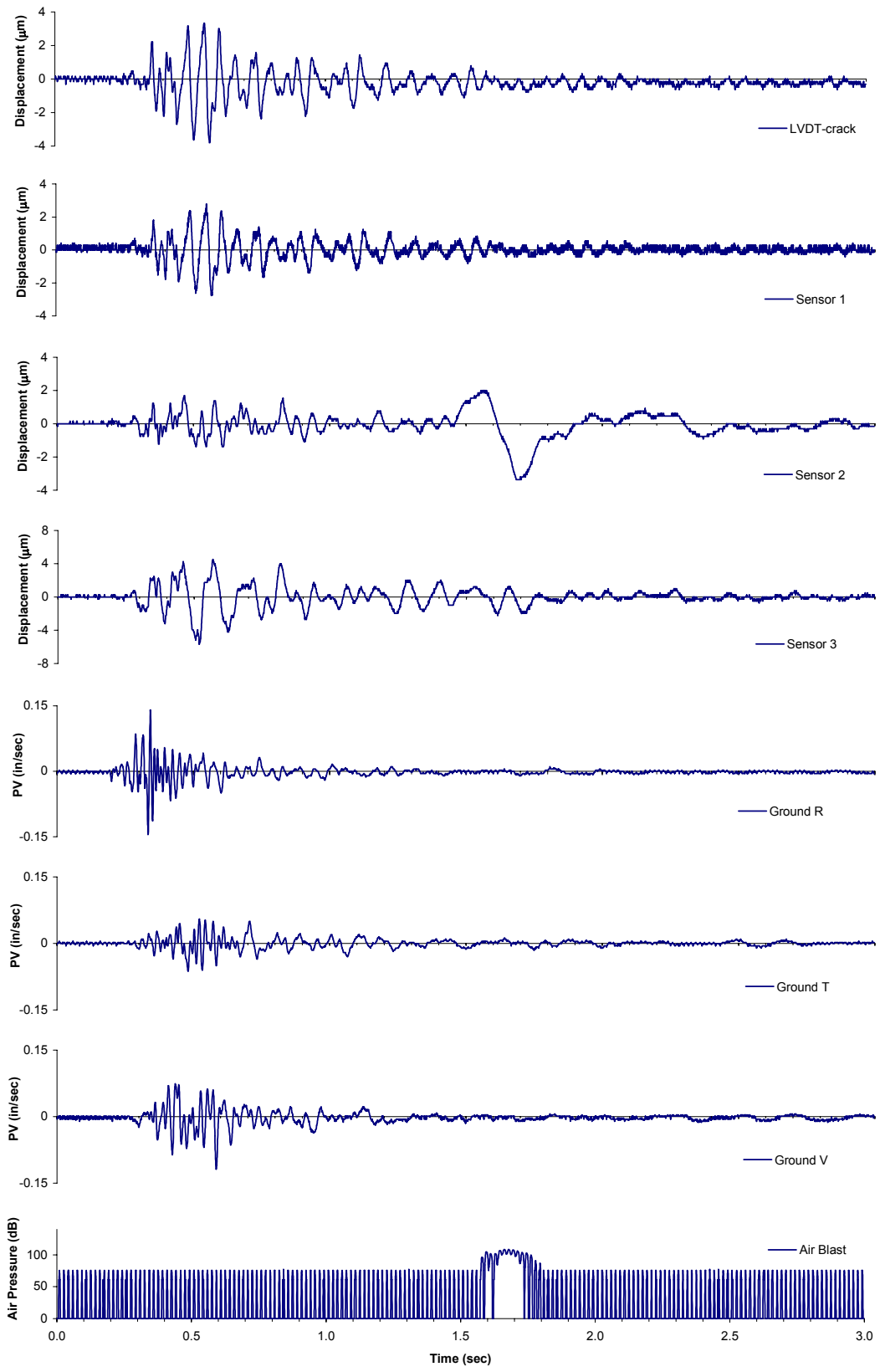

1/11/2002 @ 10:45

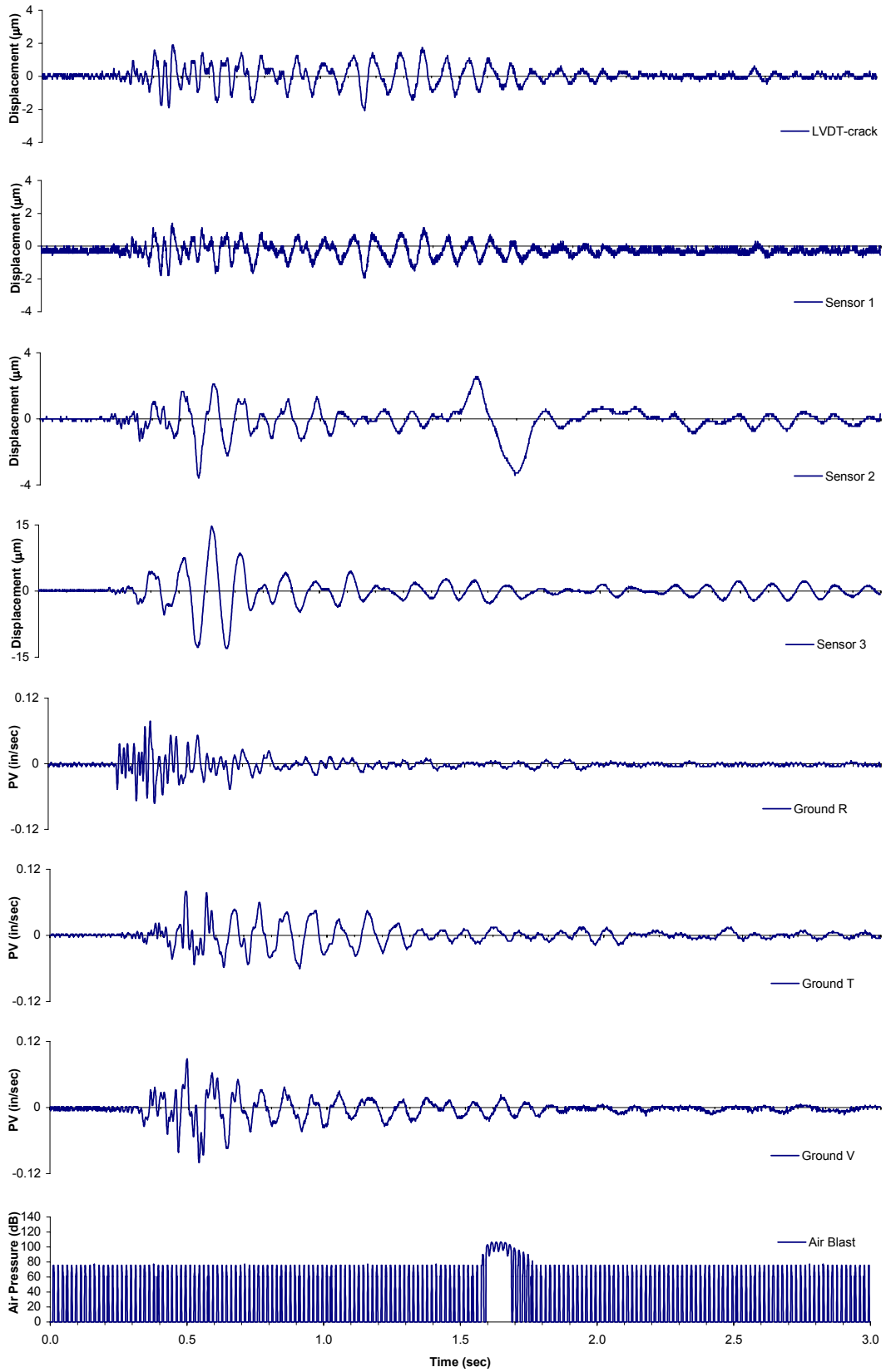

APPENDIX D

INSTALLATION AND CONFIGURATION OF MINNESOTA INSTRUMENTATION

D1. INSTALLATION OF SYSTEM

Installation Process

Installation was conducted from 3 to 5 June 2001. Members of the installation team included: Dan Hogan and Dan Marron, of the Infrastructure Technology Institute, and Laureen McKenna, Civil Engineering graduate student.

The following equipment were installed:

- Somat eDAQ Data Acquisition System
- Blackbox MD3450 Industrial Modem
- 12 Volt Power Supply
- Macrosensors DC750 Series LVDTs (4 – 2 Indoor, 2 outdoor)
- Geosonics Triaxial 4.5 Hz Geophone (3 components of motion)
- Vaisala HMD/W50 Temperature and Humidity Measurement Instruments (indoor and outdoor)
- Larcor Pressure transducer, Model 1289-02
- Belden Multi-conductor cable
- Junction box

For this project, a Somat eDAQ Data Acquisition System (DAS) polls all sensors and transducers, and stores and transmits the data when called. All sensors were wired to the DAS with multi-conductor cables. Wiring of the outdoor sensors required running a multi-conductor cable through the heating duct, located in the southwest corner of the chapel, down into the basement, along the basement ceiling, out the window, and into a junction box. The outdoor sensors were then connected together in the junction box. The metal junction box currently rests in the window well near the outdoor sensors. A schematic of the wiring in the junction box is shown as Figure D1.

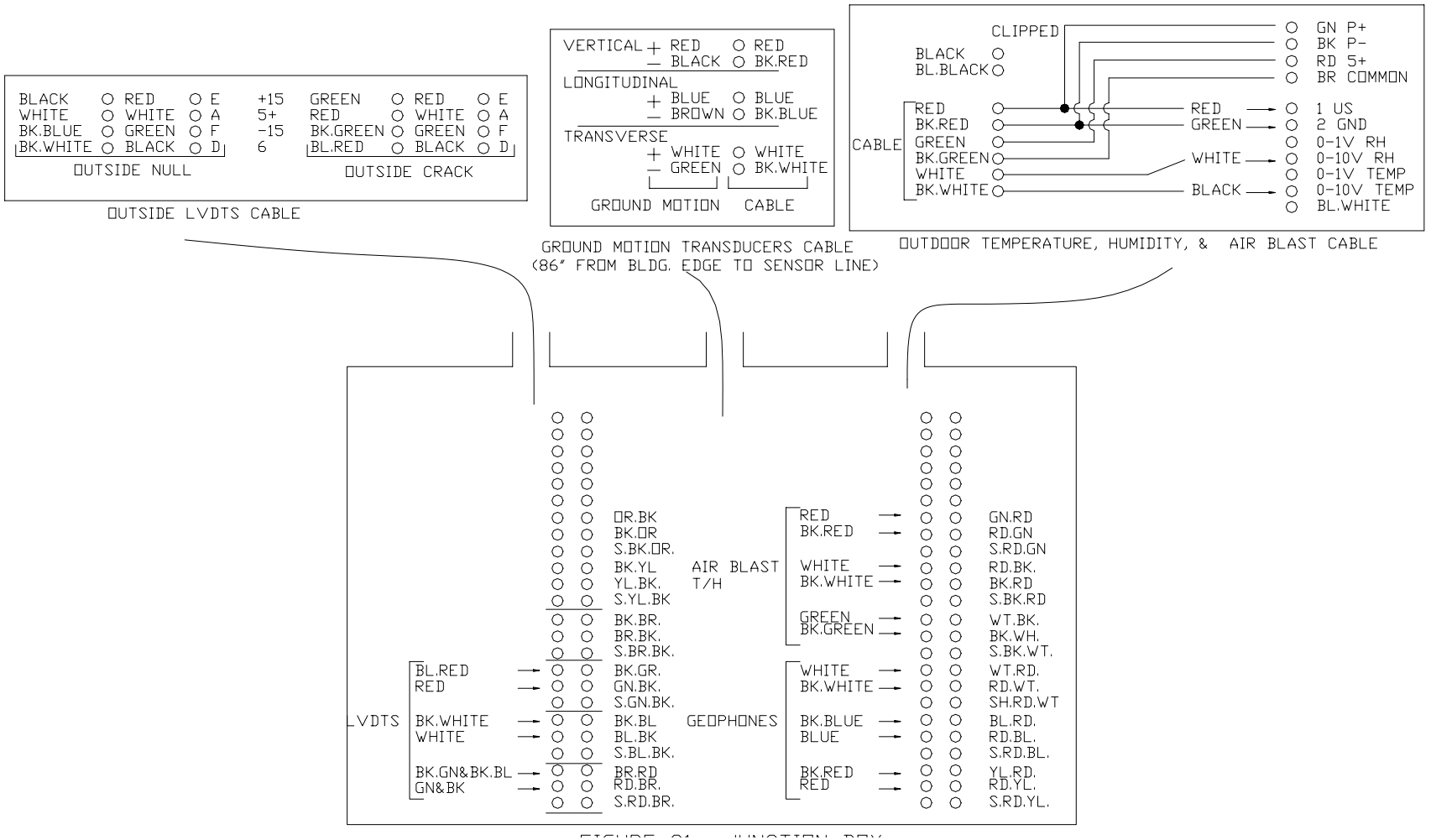

Figure D1. Junction box

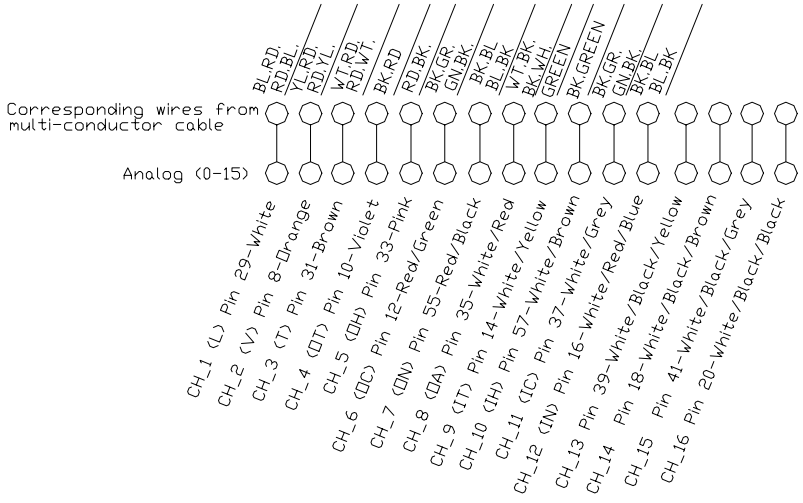

Figure D2. Junction strip connecting eDAQ to sensors

System Capacity

Settings of the system components are listed in Table D1. The transducers record ground motion in three directions (Longitudinal, Vertical, and Transverse) with the output in volts. The Vaisala's measure temperature in degrees and relative humidity in percent. The LVDTs record displacements in voltage. Since the sensors spanning over the cracked portion of the walls span the width of the crack, the displacements are those of the changes in the crack's width. These sensors are referred to as the Outdoor Crack and Indoor Crack. The sensors spanning over the un-cracked portion of the two walls, which are referred to as the Outdoor Null and Indoor Null, record displacement, if any, from expansion or contraction of the sensor or wall material. The Null sensors are included in this system as an accuracy check and typically do not exhibit any significant displacement. The air pressure sensor measures air pressure in volts. However, the wiring of the sensor is incorrect and does not return accurate measurements. Rewiring of the sensor will take place at some later date.

As long as power is supplied to the DAS, it is constantly recording voltage output from the ground motion, crack displacement, temperature, humidity, and air pressure sensors. However, what the DAS stores in its memory depends on how the system is configured for each channel. The latest version of the configuration file can be found in Section D3, WinTCS Configuration File.

Table D1. System Settings

	Channel	**Range of sensor**	**Initial values from installation**
1	Longitudinal	± 1 volt	0.003 volts
2	Vertical	± 1 volt	0.003 volts
3	Transverse	± 1 volt	0.003 volts
4	Outside Temperature	23 to 131° F (-5 to 55° C)	22.9° C
5	Outside Humidity	0 to 100% RH	50%
6	Outside Crack	± 10 volts	0.68 volts
7	Outside Null	± 10 volts	-1.74
8	Outside Air Pressure	± 10 volts	7.5
9	Inside Temperature	23 to 131° F (-5 to 55° C)	19.9° C
10	Inside Humidity	0 to 100% RH	60%
11	Inside Crack	± 10 volts	-1.09
12	Inside Null	± 10 volts	-0.005

D2. AUTOMATION PROCESS

Data Retrieval

In order to retrieve data from the DAS, a modem has been installed to establish a remote connection between the DAS and a PC at the Infrastructure Institute at Northwestern University. Everyday, the PC dials the modem at the chapel and connects to the DAS. Using the Somat software, Windows TCE eDAQ v.3.5.1, the test currently running is stopped, data is uploaded, the memory is cleared and another test is reconfigured, and started. This process can be done either remotely or by direct attachment to the DAS. Currently, a program called Automate is employed to induce the PC to automatically control Windows TCE. The program also induces the PC to convert the raw data uploaded from the DAS to text files, for importation into Microsoft Excel.

Currently, the success rate of this automatic process is not very high. Ongoing trials of different automation techniques continue in order to find a self-sufficient program. Meanwhile, uploads continue on a regular basis with the help of ITI staff. Detailed instructions necessary to connect with the DAS and upload data can be found in Table D2.

Displaying the data via the internet

In addition to retrieving data from the DAS, an additional automation process has been employed for this project. Everyday, the following website, http://iti.birl.northwestern.edu/acm/minneapolis/, is updated to reflect the data collected from the DAS. At a designated time, text files (which have been saved from the raw data files) are automatically copied to the ITI webserver and converted to display over the internet via Java programming scripts. Plots of long term weather versus time and crack displacement versus time can be displayed simultaneously on the website. In addition, time histories of dynamic events can be viewed independently or they can be viewed in comparison to long term crack displacement versus time, on the same plot as described in Siebert (2000). The conversion factors used by the webserver to translate the output voltage to preferred units are listed in Table D3.

Table D2. Communicating with Minneapolis Data Acquisition System (Somat eDAQ)

Dialing the modem:

1) Start WinTCE, enter IP address of eDAQ – 192.168.55.55 (Preferences, Communications)
2) From windows start up menu, start Dial-Up Networking
3) Make new connection, pick modem, configure (19200 if possible to connect only at this speed) under connection (defaults) and options
4) Enter phone number for site (Minneapolis Enga Chapel) : 612-827-1184
5) Once new connection created, edit properties:
    a. Server types – PPP, Inter.
    b. Check log on network, and enable software, Only TCP/IP (under settings specify IP address – current 192.168.55.100)
    c. Server assigned – leave two options checked

   Dial with username as 'ppp' and password '123'

Automate commands:

- Open network dialing, click Minneapolis link and dial
- Open TCE and open latest .tce file
- Stop test
- Upload test
- Automate closes TCE and reopens b/c it usually gives a busy command so you have to open again
- End test
- You usually need to purge the disk so I have included the manual way to purge
- Hit F1 (to get the hardware tab, press configure and then purge
- Now initialize test
- Restart test when you know you have gotten any data that exists
- Hang up phone call
- Exit TCE and open Ease (either through TCE or start menu or desktop)
- Open Ease
- Go to view channels (this just sets up ease so that you are focused on the channels, manually this doesn't really make a difference, but if there is left over data on the channels automate needs some direction to clear it)
- Delete anything in Ease that may be remaining by highlighting and pressing the delete key
- Open data file for that which was just uploaded (or anything)
- Automate focuses on Ease again to make sure it continues
- Highlight channels in order and save as text file (with Ease header) in corresponding text file with same naming convention

- Here's where Minneapolis is a little different: you will want to highlight one channel and go to plot and display channel information. When text box shows on screen you can do two different things: either save as text file and save as c:\minneapolis\headers\minH{FORMATDATETIME "YYMMDD"}.txt or copy all text and paste into text file for that data file
- Either way, you will need to open wordpad and open text file for day
- For the first way you need to open the header file and copy and paste it at the top of the text file or you can just paste it in if you are taking it directly from Ease (it is not really important to make sure there is a header file every day, it just is easier for automate to save as and then retrieve the header from a file – There isn't a way to automatically copy and paste from that text window in ease)…You need the header because you need the run date.
- Highlight all channels again and delete to clear ease channels
- Exit Ease

Table D3. Conversion Factors for Sensors in Minneapolis

Air Blast Conversion

1 mB = 500 mV = 0.5 V (Transducer calibration)

dB = $20*\log_{10}(P/P_o)$, where P_o = 20E-6 N/m^2 (Dowding)

Air Pressure in dB = $20*\log_{10}$(input in volts / 1E-7)

LVDT Macrosensors

DC750 Series – Used for Indoor Crack and Null Sensor and Outdoor Null Sensor
7.87E-3 volts/μm

LVDT used for Outside Null Sensor
3.15E-3 volts/μm

Temperature and Humidity Sensor – Vaisala

Temperature
Range - 23° to 131° F
Zero – 23
Scale - 154
Relative Humidity
Range 0 to 100%
Zero – 0
Scale - 10
(Converted in set-up file)

D3. WinTCS Configuration File

```
[Main]
TCEVersion=V3.5.1
FileVersion=1.2
TargetFCS=eDAQ
IdenDefined=1
HardNameEDaq=ENGA
MasterSampleRate=100000
NumHardItems=3
NumChanItems=12
NumSoftItems=16
NumDataItems=2

[IdenInfo]
Prefix=IDSTD
Title=Enga Memorial Chapel, Minneapolis
MN
Operator=Laureen McKenna
Date=06/08/01
NumCommLines=3
CommLine_1=Vibration Monitoring
CommLine_2=
CommLine_3=First .TCE setup file attempt.
ObjectID=0

[HardItem_1]
Prefix=MS_MPB
ID=MPB
Code=v1.9
SN=MSMPB.06-2224
ECNCount=9
ECNNumber_1=001220
ECNeDate_1=020901
ECNNumber_2=001238
ECNeDate_2=020901
ECNNumber_3=001241
ECNeDate_3=020901
ECNNumber_4=001243
ECNeDate_4=020901
ECNNumber_5=001244
ECNeDate_5=020901
ECNNumber_6=001245
ECNeDate_6=020901
ECNNumber_7=001247
ECNeDate_7=020901
ECNNumber_8=001249
ECNeDate_8=020901
ECNNumber_9=001254
ECNeDate_9=020901
PCMCardState=3
PCMModelNum=M-SYSTEMS
PCMSerialNum=None

[HardItem_2]
Prefix=MS_HILEV
ID=HiLev_1
Code=n/a
SN=MSHLA.03-2145
ECNCount=1
ECNNumber_1=001235
ECNeDate_1=011901
BadCharData=0

[HardItem_3]
Prefix=MS_MPBSER
ID=MPBSer
Code=n/a
SN=MSMPB.06-2224
ECNCount=9
ECNNumber_1=001220
ECNeDate_1=020901
ECNNumber_2=001238
ECNeDate_2=020901
ECNNumber_3=001241
ECNeDate_3=020901
ECNNumber_4=001243
ECNeDate_4=020901
ECNNumber_5=001244
ECNeDate_5=020901
ECNNumber_6=001245
ECNeDate_6=020901
ECNNumber_7=001247
ECNeDate_7=020901
ECNNumber_8=001249
ECNeDate_8=020901
ECNNumber_9=001254
ECNeDate_9=020901
FPGAVersion=n/a
NumHardInterfaces=0
```

[ChanItem_1]
Prefix=XDMS_HILEV
NumIDs=1
ID_1=CH_1
Connector=HiLev_1.c01
SampleRate=1000
Description_1=Longitudinal
Type_1=Voltage
Units_1=volts
ChanDataType=784
FS_Min_1=-1.00000000e+000
FS_Max_1=1.00000000e+000
CalDate=06/08/01
CalSlope=1.00000000e+000
CalIntercept=0.00000000e+000
CalExpSpan=0.00000000e+000
CalSteps=2
CalMode_1=Defined Value
CalEngValue_1=-1
CalSigValue_1=-1
CalMode_2=Defined Value
CalEngValue_2=1
CalSigValue_2=1
PrerunZeroMode=Undefined
PrerunZeroValue=
XdcrMode=0
ObjectID=0
TransducerID=0

[ChanItem_2]
Prefix=XDMS_HILEV
NumIDs=1
ID_1=CH_2
Connector=HiLev_1.c02
SampleRate=1000
Description_1=Vertical
Type_1=Voltage
Units_1=volts
ChanDataType=784
FS_Min_1=-1.00000000e+000
FS_Max_1=1.00000000e+000
CalDate=06/08/01
CalSlope=1.00000000e+000
CalIntercept=0.00000000e+000
CalExpSpan=0.00000000e+000
CalSteps=2
CalMode_1=Defined Value
CalEngValue_1=-1
CalSigValue_1=-1
CalMode_2=Defined Value
CalEngValue_2=1
CalSigValue_2=1
PrerunZeroMode=Undefined
PrerunZeroValue=
XdcrMode=0
ObjectID=0
TransducerID=0

[ChanItem_3]
Prefix=XDMS_HILEV
NumIDs=1
ID_1=CH_3
Connector=HiLev_1.c03
SampleRate=1000
Description_1=Transverse
Type_1=Voltage
Units_1=volts
ChanDataType=784
FS_Min_1=-1.00000000e+000
FS_Max_1=1.00000000e+000
CalDate=06/08/01
CalSlope=1.00000000e+000
CalIntercept=0.00000000e+000
CalExpSpan=0.00000000e+000
CalSteps=2
CalMode_1=Defined Value
CalEngValue_1=-1
CalSigValue_1=-1
CalMode_2=Defined Value
CalEngValue_2=1
CalSigValue_2=1
PrerunZeroMode=Undefined
PrerunZeroValue=
XdcrMode=0
ObjectID=0
TransducerID=0

[ChanItem_4]
Prefix=XDMS_HILEV
NumIDs=1
ID_1=CH_4
Connector=HiLev_1.c04

SampleRate=1000
Description_1=Outside Temperature
Type_1=Temperature
Units_1=Deg F
ChanDataType=784
FS_Min_1=2.30000000e+001
FS_Max_1=1.31000000e+002
CalDate=07/06/01
CalSlope=1.08000002e+001
CalIntercept=2.30000000e+001
CalExpSpan=0.00000000e+000
CalSteps=2
CalMode_1=Defined Value
CalEngValue_1=23
CalSigValue_1=0
CalMode_2=Defined Value
CalEngValue_2=131
CalSigValue_2=10
PrerunZeroMode=Undefined
PrerunZeroValue=
XdcrMode=0
ObjectID=0
TransducerID=0

[ChanItem_5]
Prefix=XDMS_HILEV
NumIDs=1
ID_1=CH_5
Connector=HiLev_1.c05
SampleRate=1000
Description_1=Outside Humidity
Type_1=Humidity
Units_1=%RH
ChanDataType=784
FS_Min_1=0.00000000e+000
FS_Max_1=1.30000000e+002
CalDate=06/08/01
CalSlope=1.00000000e+001
CalIntercept=0.00000000e+000
CalExpSpan=0.00000000e+000
CalSteps=2
CalMode_1=Defined Value
CalEngValue_1=0
CalSigValue_1=0
CalMode_2=Defined Value
CalEngValue_2=100
CalSigValue_2=10
PrerunZeroMode=Undefined
PrerunZeroValue=
XdcrMode=1
ObjectID=0
TransducerID=0

[ChanItem_6]
Prefix=XDMS_HILEV
NumIDs=1
ID_1=CH_6
Connector=HiLev_1.c06
SampleRate=1000
Description_1=Outside Crack
Type_1=Voltage
Units_1=volts
ChanDataType=32
FS_Min_1=-1.00000000e+001
FS_Max_1=1.00000000e+001
CalDate=06/08/01
CalSlope=1.00000000e+000
CalIntercept=0.00000000e+000
CalExpSpan=0.00000000e+000
CalSteps=2
CalMode_1=Defined Value
CalEngValue_1=-10
CalSigValue_1=-10
CalMode_2=Defined Value
CalEngValue_2=10
CalSigValue_2=10
PrerunZeroMode=Undefined
PrerunZeroValue=
XdcrMode=0
ObjectID=0
TransducerID=0

[ChanItem_7]
Prefix=XDMS_HILEV
NumIDs=1
ID_1=CH_7
Connector=HiLev_1.c07
SampleRate=1000
Description_1=Outside Null
Type_1=Voltage
Units_1=volts
ChanDataType=784

FS_Min_1=-1.00000000e+001
FS_Max_1=1.00000000e+001
CalDate=06/08/01
CalSlope=1.00000000e+000
CalIntercept=0.00000000e+000
CalExpSpan=0.00000000e+000
CalSteps=2
CalMode_1=Defined Value
CalEngValue_1=-10
CalSigValue_1=-10
CalMode_2=Defined Value
CalEngValue_2=10
CalSigValue_2=10
PrerunZeroMode=Undefined
PrerunZeroValue=
XdcrMode=0
ObjectID=0
TransducerID=0

[ChanItem_8]
Prefix=XDMS_HILEV
NumIDs=1
ID_1=CH_8
Connector=HiLev_1.c13
SampleRate=1000
Description_1=Outside Air
Type_1=Voltage
Units_1=volts
ChanDataType=784
FS_Min_1=-1.00000000e+001
FS_Max_1=1.00000000e+001
CalDate=06/08/01
CalSlope=1.00000000e+000
CalIntercept=0.00000000e+000
CalExpSpan=0.00000000e+000
CalSteps=2
CalMode_1=Defined Value
CalEngValue_1=-10
CalSigValue_1=-10
CalMode_2=Defined Value
CalEngValue_2=10
CalSigValue_2=10
PrerunZeroMode=Undefined
PrerunZeroValue=
XdcrMode=0
ObjectID=0
TransducerID=0

[ChanItem_9]
Prefix=XDMS_HILEV
NumIDs=1
ID_1=CH_9
Connector=HiLev_1.c09
SampleRate=1000
Description_1=Inside Temperature
Type_1=Temperature
Units_1=Deg F
ChanDataType=784
FS_Min_1=2.30000000e+001
FS_Max_1=1.31000000e+002
CalDate=07/06/01
CalSlope=1.08000002e+001
CalIntercept=2.30000000e+001
CalExpSpan=0.00000000e+000
CalSteps=2
CalMode_1=Defined Value
CalEngValue_1=23
CalSigValue_1=0
CalMode_2=Defined Value
CalEngValue_2=131
CalSigValue_2=10
PrerunZeroMode=Undefined
PrerunZeroValue=
XdcrMode=0
ObjectID=0
TransducerID=0

[ChanItem_10]
Prefix=XDMS_HILEV
NumIDs=1
ID_1=CH_10
Connector=HiLev_1.c10
SampleRate=1000
Description_1=Inside Humidity
Type_1=Humidity
Units_1=%RH
ChanDataType=784
FS_Min_1=0.00000000e+000
FS_Max_1=1.30000000e+002
CalDate=06/08/01
CalSlope=1.00000000e+001
CalIntercept=0.00000000e+000

CalExpSpan=0.00000000e+000
CalSteps=2
CalMode_1=Defined Value
CalEngValue_1=0
CalSigValue_1=0
CalMode_2=Defined Value
CalEngValue_2=100
CalSigValue_2=10
PrerunZeroMode=Undefined
PrerunZeroValue=
XdcrMode=1
ObjectID=0
TransducerID=0

[ChanItem_11]
Prefix=XDMS_HILEV
NumIDs=1
ID_1=CH_11
Connector=HiLev_1.c11
SampleRate=1000
Description_1=Inside Crack
Type_1=Voltage
Units_1=volts
ChanDataType=32
FS_Min_1=-1.00000000e+001
FS_Max_1=1.00000000e+001
CalDate=06/08/01
CalSlope=1.00000000e+000
CalIntercept=0.00000000e+000
CalExpSpan=0.00000000e+000
CalSteps=2
CalMode_1=Defined Value
CalEngValue_1=-10
CalSigValue_1=-10
CalMode_2=Defined Value
CalEngValue_2=10
CalSigValue_2=10
PrerunZeroMode=Undefined
PrerunZeroValue=
XdcrMode=0
ObjectID=0
TransducerID=0

[ChanItem_12]
Prefix=XDMS_HILEV
NumIDs=1
ID_1=CH_12
Connector=HiLev_1.c12
SampleRate=1000
Description_1=Inside Null
Type_1=Voltage
Units_1=volts
ChanDataType=784
FS_Min_1=-1.00000000e+001
FS_Max_1=1.00000000e+001
CalDate=06/08/01
CalSlope=1.00000000e+000
CalIntercept=0.00000000e+000
CalExpSpan=0.00000000e+000
CalSteps=2
CalMode_1=Defined Value
CalEngValue_1=-10
CalSigValue_1=-10
CalMode_2=Defined Value
CalEngValue_2=10
CalSigValue_2=10
PrerunZeroMode=Undefined
PrerunZeroValue=
XdcrMode=0
ObjectID=0
TransducerID=0

[SoftItem_1]
Prefix=TRIG_INT
NumIDs=1
ID_1=Int_Trig
Description_1=
Type_1=Logical
Units_1=
ChanDataType=264
FS_Min_1=0
FS_Max_1=0
InputChs=1
InputCh_1=CH_1
TrigIndex=1
TrigInvert=0
ObjectID=0

[SoftItem_2]
Prefix=TIMECHAN
NumIDs=1
ID_1=Elapsed_Time

Description_1=
Type_1=Time
Units_1=sec
ChanDataType=288
FS_Min_1=0
FS_Max_1=604800
InputChs=1
InputCh_1=CH_1
ObjectID=0

[SoftItem_3]
Prefix=SMOOTH
NumIDs=1
ID_1=Avg_L
Description_1=Longitudinal
Type_1=Voltage
Units_1=volts
ChanDataType=784
FS_Min_1=-1
FS_Max_1=1
InputChs=1
InputCh_1=CH_1
TapCount=9
ObjectID=0

[SoftItem_4]
Prefix=SMOOTH
NumIDs=1
ID_1=Avg_V
Description_1=Vertical
Type_1=Voltage
Units_1=volts
ChanDataType=784
FS_Min_1=-1
FS_Max_1=1
InputChs=1
InputCh_1=CH_2
TapCount=9
ObjectID=0

[SoftItem_5]
Prefix=SMOOTH
NumIDs=1
ID_1=Avg_T
Description_1=Transverse
Type_1=Voltage
Units_1=volts
ChanDataType=784
FS_Min_1=-1
FS_Max_1=1
InputChs=1
InputCh_1=CH_3
TapCount=9
ObjectID=0

[SoftItem_6]
Prefix=SMOOTH
NumIDs=1
ID_1=Avg_OT
Description_1=Outside Temperature
Type_1=Temperature
Units_1=Deg F
ChanDataType=784
FS_Min_1=23
FS_Max_1=131
InputChs=1
InputCh_1=CH_4
TapCount=9
ObjectID=0

[SoftItem_7]
Prefix=SMOOTH
NumIDs=1
ID_1=Avg_OH
Description_1=Outside Humidity
Type_1=Humidity
Units_1=%RH
ChanDataType=784
FS_Min_1=0
FS_Max_1=130
InputChs=1
InputCh_1=CH_5
TapCount=9
ObjectID=0

[SoftItem_8]
Prefix=SMOOTH
NumIDs=1
ID_1=Avg_OC
Description_1=Outside Crack
Type_1=Voltage
Units_1=volts

ChanDataType=32
FS_Min_1=-10
FS_Max_1=10
InputChs=1
InputCh_1=CH_6
TapCount=9
ObjectID=0

[SoftItem_9]
Prefix=SMOOTH
NumIDs=1
ID_1=Avg_ON
Description_1=Outside Null
Type_1=Voltage
Units_1=volts
ChanDataType=784
FS_Min_1=-10
FS_Max_1=10
InputChs=1
InputCh_1=CH_7
TapCount=9
ObjectID=0

[SoftItem_10]
Prefix=SMOOTH
NumIDs=1
ID_1=Avg_OA
Description_1=Outside Air
Type_1=Voltage
Units_1=volts
ChanDataType=784
FS_Min_1=-10
FS_Max_1=10
InputChs=1
InputCh_1=CH_8
TapCount=9
ObjectID=0

[SoftItem_11]
Prefix=SMOOTH
NumIDs=1
ID_1=Avg_IT
Description_1=Inside Temperature
Type_1=Temperature
Units_1=Deg F
ChanDataType=784
FS_Min_1=23
FS_Max_1=131
InputChs=1
InputCh_1=CH_9
TapCount=9
ObjectID=0

[SoftItem_12]
Prefix=SMOOTH
NumIDs=1
ID_1=Avg_IH
Description_1=Inside Humidity
Type_1=Humidity
Units_1=%RH
ChanDataType=784
FS_Min_1=0
FS_Max_1=130
InputChs=1
InputCh_1=CH_10
TapCount=9
ObjectID=0

[SoftItem_13]
Prefix=SMOOTH
NumIDs=1
ID_1=Avg_IC
Description_1=Inside Crack
Type_1=Voltage
Units_1=volts
ChanDataType=32
FS_Min_1=-10
FS_Max_1=10
InputChs=1
InputCh_1=CH_11
TapCount=9
ObjectID=0

[SoftItem_14]
Prefix=SMOOTH
NumIDs=1
ID_1=Avg_IN
Description_1=Inside Null
Type_1=Voltage
Units_1=volts
ChanDataType=784
FS_Min_1=-10

FS_Max_1=10
InputChs=1
InputCh_1=CH_12
TapCount=9
ObjectID=0

[SoftItem_15]
Prefix=TRIG_GEN
NumIDs=1
ID_1=Hour_L
Description_1=Hourly data
Type_1=Time
Units_1=units
ChanDataType=264
FS_Min_1=0
FS_Max_1=0
InputChs=1
InputCh_1=CH_1
DelayPeriod=0
OnPeriod=0.001
OffPeriod=3600
ObjectID=0

[SoftItem_16]
Prefix=DESKCALC
NumIDs=1
ID_1=CTrig
Description_1=Crack trigger
Type_1=Logical
Units_1=
ChanDataType=264
FS_Min_1=0
FS_Max_1=255
InputChs=4
InputCh_1=CH_6
InputCh_2=Avg_OC
InputCh_3=CH_11
InputCh_4=Avg_IC
InFixExpr=((CH_6 - Avg_OC) > 0.00315) || ((CH_6 - Avg_OC) < 0.00315) ||

Pretrigger=0.25
Brst=3000
MaxBurstsMode=0
MaxBurstsRefValue=0

((CH_11 - Avg_IC) > 0.00787) || ((CH_11 - Avg_IC) < 0.00787)
ObjectID=0

[DataItem_1]
Prefix=MS_TIMHIS
ID=One_hour
InputChs=8
InputCh_1=Avg_OT
InputCh_2=Avg_OH
InputCh_3=Avg_OC
InputCh_4=Avg_ON
InputCh_5=Avg_IT
InputCh_6=Avg_IH
InputCh_7=Avg_IC
InputCh_8=Avg_IN
Connector=n/a
TrigCond=Gate
TrigChan=Hour_L
DataType=Int16
HaveTimeChan=0
PCMStorage=1
ObjectID=0

[DataItem_2]
Prefix=BRSHIS
ID=Gr_motion
InputChs=8
InputCh_1=Avg_L
InputCh_2=Avg_V
InputCh_3=Avg_T
InputCh_4=Avg_OC
InputCh_5=Avg_ON
InputCh_6=Avg_OA
InputCh_7=Avg_IC
InputCh_8=Avg_IN
Connector=n/a
TrigCond=When True
TrigChan=Int_Trig
DataType=Int16
Posttrigger=2.75
PCMStorage=1
PCMDirectMode=0
ObjectID=0